Evaluation of oxidation-sensitive polymersomes as vaccine nanocarriers to enhance humoral responses against arenavirus envelope glycoproteins

THÈSE N° 8193 (2017)

PRÉSENTÉE LE 8 DÉCEMBRE 2017

PROGRAMME DOCTORAL EN BIOTECHNOLOGIE ET GÉNIE BIOLOGIQUE

ÉCOLE POLYTECHNIQUE FÉDÉRALE DE LAUSANNE

POUR L'OBTENTION DU GRADE DE DOCTEUR ÈS SCIENCES

PAR

Clara GALAN NAVARRO

acceptée sur proposition du jury:

Prof. M. Dal Peraro, président du jury
Prof. S. Kunz, Prof. M. Swartz, directeurs de thèse
Prof. D. Nardelli, rapporteuse
Prof. B. Marsland, rapporteur
Prof. B. Correia, rapporteur

EPFL

ÉCOLE POLYTECHNIQUE
FÉDÉRALE DE LAUSANNE

Suisse
2017

ACKNOWLEDGEMENTS

This thesis was only made possible thanks to the contribution of valuable people who has participated not only granting professional impulse but also providing irreplaceable support and understanding.

First, I would like to thank my supervisor, Stefan Kunz, for his invaluable support during the last years and for always believing in me. I also acknowledge him for the independence and autonomy that I developed along this time thanks to the trust he deposited on me and form whom I learnt countless things. And to Professor Melody Swartz for the great opportunity she offered me accepting me in her team.

I also thank the LLCB lab, specially Dr. Sachiko Hirosue and Dr. Marcela Rincon, for all the help during this collaboration, without which this project wouldn't have been possible.

I am also immensely grateful to all my former colleagues and friends form Stefan's lab; you made long lab days into pleasant journeys.

To my thesis Jury, Professor Matteo Dal Peraro, Professor Denise Nardelli, Professor Benjamin Marsland, and Professor Bruno Correia: many thanks for accepting being part of my committee and taking the time to read and contribute to my thesis.

Finally, to my lovely parents, whose unconditional love and faith in me got me where I am today. And to my brother, whom support and joyful spirit helped me to go through many good and bad moments during my thesis.

ABSTRACT

Vaccines currently represent one of the most effective means to control and prevent infectious diseases affecting humans and animals and have dramatically improved public health, quality of life, and life expectancy. Over the last years several conceptual and technological advances in the field of bioengineering and immunology have allowed the development of new vaccines designs. Expanding novel domains such as structural biology, human monoclonal antibody isolation, high throughput sequencing, and design of new nanocarrier delivery platforms have changed the landscape of vaccinology. These new vaccine formulations allow the design of tailor-made antigens and particulate vehicles which allow better and fine-tuned protective immune responses against known and newly emerging pathogens. Over the past decades emerging human pathogens with the potential to cause severe epidemics have become a major public health problem. The last Ebola and Zika virus epidemics demonstrated in a dramatic manner that there is an urgent need to develop prophylactic and therapeutic approaches against pathogenic emerging viruses.

Most successful vaccines rely on attenuated live microorganisms to induce protective immunity. However, changed demographics and associated safety concerns makes the development of a safer alternative a priority. Subunit vaccines composed of microbial components and proteins have emerged as a suitable alternative, however they are generally less immunogenic. To address this problematic our laboratory works on the development of immunization platforms which allow 1) the development of safe recombinant subunit vaccines and 2) the rapid generation of specific monoclonal antibodies using biosynthetic immunogens without the need for prior isolation and culture of the agent.

The approach evaluated in the present studies is based on a novel polymersome (PS) platform serving as nanocarrier for efficient antigen delivery and the induction of humoral immunity. The potential of PS was assessed in the context of two important human emerging pathogens form the arenavirus family that cause severe hemorrhagic fevers and of which there are neither FDA-approved vaccines not prophylactic treatments: Lassa virus (LASV), endemic in Western Africa, and Machupo virus (MACV), the causative agent of Bolivian hemorrhagic fever. In a first part, we evaluated the PS platform's capacity to enhance humoral immunity against the envelope glycoprotein 1 of LASV, (LASV GP1) that is notorious for its weak immunogenicity and poor antibody response. Immunization of mice with adjuvanted PS (LASV GP1) enhanced the quality of the humoral response to LASV GP1, eliciting antibodies with higher binding affinity to virion GP1, increased levels of polyfunctional anti-viral CD4 T cells, and the frequency of IgG-secreting B cells. PS (LASV GP1) elicited a more diverse epitope repertoire of anti-viral IgG. In a second part, we employed the PS platform in combination with single cell B cell sorting and cloning of

recombinant IgG to generate a first set of species-specific mAbs against MACV. These new mAbs show exquisite specificity and negligible cross-reactivity to closely related arenaviruses in relevant techniques making them a unique and powerful tool for research and diagnostics purposes.

RÉSUMÉ

Les vaccins représentent aujourd'hui le plus effective moyen de contrôler et prévenir les maladies infectieuses et ayant un impact sur la santé publique ainsi que la qualité et l'espérance de vie. Pendant ces dernières années plusieurs innovations technologiques et conceptuels dans les domaines de la bioingénierie et l'immunologie ont permis le développement d'un nouveau genre de vaccin. L'expansion des domaines tels que la biologie structurelle, l'isolation des anticorps monoclonaux humain, le séquençage « high throughput » et le design des nouveaux transports des antigènes par « nanocarrier delivery platforms » ont complètement changé le concept actuel de la vaccination. La nouvelle formulation des vaccins a permis le design des antigènes dit « sur mesure » et des nano-véhicules lesquels ont donné la possibilité d'améliorer et maîtriser la réponse immunitaire contre des pathogènes connus et émergeants. Au cours des dernières années les pathogènes émergeants chez l'homme capables de causer des épidémies sérieuses sont devenu un problème de santé publique majeur. Les récentes épidémies provoquées par les virus Ebola et Zika ont démontré qu'il existe un besoin urgent de développer des mesures prophylactiques et thérapeutiques contre les virus pathogéniques humain.

Les vaccins qui rencontrent le plus de succès jusqu'à présent dépendent principalement de l'immunisation à l'aide de vecteurs vivants atténués. Néanmoins, les problèmes de sécurité associés aux vecteurs vivants atténués font du développent d'alternatives plus sures une priorité. Par conséquent, les vaccins sous-unités, composés d'éléments microbiaux et protéiques, sont apparus comme une solution plus sûre, par contre moins immunogénique. Pour adresser cette problématique notre laboratoire travaille dans le développement des systèmes d'immunisation qui permet à la fois la conception des vaccins recombinants sous-unités et la production rapide des anticorps monoclonaux spécifiques en utilisant que des immunogènes biosynthétiques sans besoin de l'isolation et culture préalable de l'agent pathogène.

La stratégie suivie dans cette thèse est basée sur une nouvelle plateforme de polymersome (PS) comme moyen de cargaison et de livraison de l'antigène pour l'induction d'une réponse immunitaire humorale améliorée. Les caractéristiques des PS ont été investigué à l'aide de deux pathogènes humain appartenant aux arénavirus, le Lassa virus (LASV), endémique dans l'Afrique de l'ouest, et le virus de Machupo (MACV) présent à Bolivie. Ces deux virus sont à l'origine de nombreux cas de fièvres hémorragiques sévères chez l'homme et pour lesquelles il n'existe ni de vaccin ou de traitement disponible approuvés ni d'outils de diagnostic spécifiques.

Dans une première partie nous avons décidé d'étudier la faisabilité d'un vaccin PS pour la livraison de l'antigène du virus Lassa, dont la glycoprotéine 1 (LASV GP1). Cette protéine est connue pour faible antigenicité et une faible réponse humorale. L'immunisation des suries avec

LASV GP1 encapsulée dans des PS enrichie la qualité de la réponse humorale contre LASV GP1 et élicite un répertoire des épitopes IgG plus diverse. Dans une deuxième partie nous avons utilisé la plateforme PS en combinaison avec l'isolation unicellulaire des cellules B et le clonage des IgGs recombinantes pour générer des premiers anticorps monoclonaux contre MACV. Ces nouveaux anticorps ont une haute spécificité pour les protéines de MACV et ont montré une réactivité négligeable contre des virus semblables de la même famille, faisant de ces anticorps des outils uniques pour le développement des techniques de recherche et diagnostique.

En résumé, cette thèse décrit deux études exhaustives, qui ont permis la production rapide d'anticorps spécifiques grâce à l'amélioration des réponses immunitaires adaptatives générées après la l'administration des vaccins basés sur des nano-vecteurs. De plus, les avances scientifiques ici exposées sont immédiatement applicables pour établir de nouvelles lignes directrices pour le design de nouveaux vaccins. On espère que cette thèse peut bénéficier à la communauté afin qu'elle soit mieux préparée pour la prochaine menace pandémique.

Mots-clefs

Nanoparticule, polymersome, anticorps, Lassa, ganglion lymphatique, vaccin, qualité, cellule T CD4+, cellule T CD8+, cellule B, cellule dendritique

TABLE OF CONTENTS

INTRODUCTION

Discovery, classification, and ecology of Arenaviruses

Structure and life cycle of arenaviruses

Structure-function relationships of the LASV and MACV attachment glycoproteins

Pathogenesis and immune response to pathogenic arenaviruses infection

Current diagnostics and therapy against arenaviruses

Status of arenavirus vaccine development

Antiviral antibody responses

Subunit vaccines

Antigen delivery via nanoparticulated platforms

Enhancing the efficacy of subunit vaccines-Adjuvants

OXIDATION-SENSITIVE POLYMERSOMES AS VACCINE NANOCARRIERS ENHANCE HUMORAL RESPONSES AGAINST LASSA VIRUS ENVELOPE GLYCOPROTEIN

LIST OF FIGURES

COMMON ABBREVIATIONS

PS: Polymersome

LCMV: Lymphochoriomeningitis virus

LASV: Lassa Virus

MACV: Machupo Virus

JUNV: Junin virus

LASV GP1: Lassa virus Glycoprotein 1

MACV GP1: Machupo virus Glycoprotein 1

JUNV GP1: Junin virus Glycoprotein 1

LN: Lymph node

DC: Dendritic cell

APC: Antigen presenting cells

Tfh: T follicular helper

CHAPTER 1

INTRODUCTION

Motivation, background and outline of the thesis

INTRODUCTION

MOTIVATION

Over the past decades emerging human pathogens with the potential to cause severe epidemics have become a major public health problem. In 2015, experts from the World Health Organization published a priority list of eight pathogens likely to cause serious outbreaks in the near future. The list includes highly pathogenic viruses like Ebola virus, Middle East respiratory syndrome (MERS), and Lassa virus. Most of these highly contagious viral pathogens are causative agents of severe diseases with high case fatality rates. These emerging pathogens frequently affect poor countries of the developing world, which is exacerbated by the current lack of effective therapies or preventive measures. For these reasons, the development of affordable and reliable diagnostics, efficacious anti-viral drugs, and protective vaccines represents an urgent need.

Arenaviruses belong to a diverse viral family of emerging zoonotic pathogens that are important causative agents of severe hemorrhagic fevers in humans. They are predominately found in the Americas and Africa and are commonly classified as either New or Old World arenaviruses, respectively. The most relevant pathogen among all arenaviruses is Lassa virus (LASV) that currently threatens circa 200 million people living in Western Africa. With several hundred thousand infections per year and over 5,000 deaths annually, LASV represents a serious public health problem in the affected regions [1]. The South American hemorrhagic fever viruses Junin (JUNV), Machupo (MACV), and Guanarito (GTOV) have emerged as causative agents of severe human diseases with high fatality rates in the Americas. Due to their proven transmissibility via aerosol and high lethality, hemorrhagic arenaviruses are considered category A select agents by the Centers for Disease Control and Prevention. Currently, there are no FDA-approved vaccines available for the prevention of arenavirus infection. Treatment options are limited to supportive care and the off-label use of ribavirin, which is effective only when given early during the course of infection and has relevant side effects [2].

The last Ebola virus outbreak in Western Africa 2013-2016 demonstrated in a dramatic manner that there is an urgent need to develop prophylactic and therapeutic approaches against hemorrhagic fever viruses as part of a global preparedness for future epidemics. Vaccines are a major success in modern medicine as a prophylactic measure to reduce the mortality of viral infections. Considering the amount of people affected and the limited public health infrastructure in the regions with high pathogen prevalence, the development of safe and efficacious vaccines and therapeutic approaches against hemorrhagic arenaviruses is of high priority. Antibodies targeting viral attachment proteins play a crucial role in vaccine-mediated protection against many viral infections [3-5] and hold promise for therapeutic approaches [6]. Specific antibodies to emerging viruses are further invaluable tools for diagnostics and biomedical research. Despite successful development of promising experimental life vaccine candidates against some pathogenic arenaviruses, biosafety concerns prevented so far FDA-

approval for human use. Therefore, there is an urgent need to engineer immunization platforms which allow 1) the development of safe recombinant subunit vaccines and 2) the rapid generation of specific monoclonal antibodies using biosynthetic immunogens without the need for prior isolation of the agent. The development of such a platform must combine a state-of-the art bioengineering, protein biochemistry, and viral immunology. The approach evaluated in the present studies is based on a novel polymersome (PS) platform serving as nanocarrier for efficient antigen delivery and the induction of humoral immunity. In a first part, we evaluated the PS platform's capacity to enhance humoral immunity against the envelope glycoprotein of LASV that is notorious for its weak immunogenicity and poor antibody response. In a second part, we employed the PS platform in combination with single cell B cell sorting and cloning of recombinant IgGs to try to generate a first set of species-specific mAbs against MACV.

BACKGROUND

Discovery, classification, and ecology of Arenaviruses

The discovery of arenaviruses dates back to 1933 when the prototypic lymphocytic choriomeningitis virus (LCMV) was isolated by Armstrong and Lillie from brain tissue of a victim of a St. Louis encephalitis epidemic [7, 8]. A few years later, Rivers and Scott isolated a similar virus from a case of aseptic meningitis and found serologic cross-reactivity with the filterable agent previously isolated by Armstrong and Lillie. In sections of electron microscopic images, the virions showed a characteristic "sandy" (Lat. *arenosus*) aspect, due to inclusion of ribosomes. Combined with serological and biochemical evidence, a new virus family, the *Arenaviridae,* was proposed in 1970.

The *Arenaviridae* family has been recently separated by the International Committee on Taxonomy of Viruses into a main genus Mammarenavirus and a novel genus Reptarenavirus [9], the latter including several species of arenaviruses isolated from snakes. Based on phylogenetic analysis and serological data at hand, the Mammarenaviruses are currently divided into two major groups: the Old World and the New World arenavirus complex [10] (Fig. 1). For simplicity, I will henceforth use the classical term "arenaviruses" synonymous for the entire family and members of the Mammarenavirus genus. Where applicable, viruses of the Reptarenavirus genus will be specifically referred to. The Old World arenavirus lineage contains the prototypic LCMV that shows world-wide distribution [11]. The infection of LCMV in the mouse has served as a veritable *Rosetta's Stone* to dissect fundamental mechanisms of viral pathogenesis and immunology leading to fundamental discoveries in viral immunobiology awarded by several Nobel Prizes [8, 12]. In pediatric medicine, LCMV is increasingly recognized as a relevant and under-diagnosed human pathogen and severe infections have been observed in immune-compromised transplant patients [13-15]. The highly pathogenic Lassa virus (LASV) is widely distributed over large areas of Western Africa, where the virus has been endemic for over 1000 years [16, 17]. Lujo virus (LUJV) recently emerged in Southern Africa associated with a cluster of fatal infections, but has remained elusive ever since [18]. The African arenaviruses Mopeia, Mobala, and Ippy virus have until now not been associated with human disease and their pathological potential remains unclear.

The New World arenaviruses are divided into Clades, A, B, C, and D. Clade D corresponds to former Clades A/B or A/rec and may have resulted from recombination events between members of Clade A and B [9]. Viruses of Clade B include all human pathogenic viruses, namely Junin (JUNV), Machupo (MACV), Guanarito (GTOV), Sabia (SABV), and Chapare (CHAV) virus. Interestingly, these viruses do not group within a specific sub-Clade, but cluster phylogenetically with closely related non-pathogenic viruses such as Tacaribe (TCRV) and Amapari virus (AMPV) [19].

Arenaviruses are zoonotic pathogens and a short number of closely related rodent species serve as reservoirs for each arenavirus species in nature [10, 20]. These reservoir hosts are persistently

infected, and show no overt signs and symptoms of disease, resulting in a so-called "carrier" state, characterized by high levels of viral multiplication in all organs and extensive shedding in urine, saliva, and feces [8]. The current phylogenetic diversity among arenaviruses is probably the result of long-term co-evolution between these viruses and their host species. Mechanisms that drive arenavirus diversity are evolutionary radiation of rodent species, vertical and horizontal transfer of viruses within and between populations, as well as recombination and reassortant events [9, 11]. The reservoirs of LASV are semi-domestic rodents of *Mastomys* species [21]. Similar to murine species harboring LCMV (*Mus domesticus* and *Mus musculus*), *M. natalensis* invades human dwellings and index cases of Lassa fever are related to contacts with infected rodents [16]. Reservoir-to-human transmission is the major route of LASV infection in man and occurs mainly via aerosol or close contact with rodent excreta, as well as contamination [17, 22]. Human-to-human transmission of LASV has been reported in nosocomial outbreaks associated with high case fatalities [23]. JUNV causing Argentine haemorrhagic fever (AHF) occurs seasonally with a peak between April and June linked to the dymanics of the feral populations of *Calomys* field voles [24, 25]. Human transmission of JUNV and MACV results from inhalation of contaminated dust or consumption of contaminated food [26]. Abnormally low rainfall, combined and excessive use of insecticide, decimated cats, allowing rapid expansion of MACV-infected *Calomys* rodents. TCRV was initially isolated from bats [7] and has recently been detected in host-seeking *Amblyomma americanum* ticks [27]. It is however unclear if the presence of virus in ticks is the consequence of passive spill-over or active viral replication in arthropod tissues.
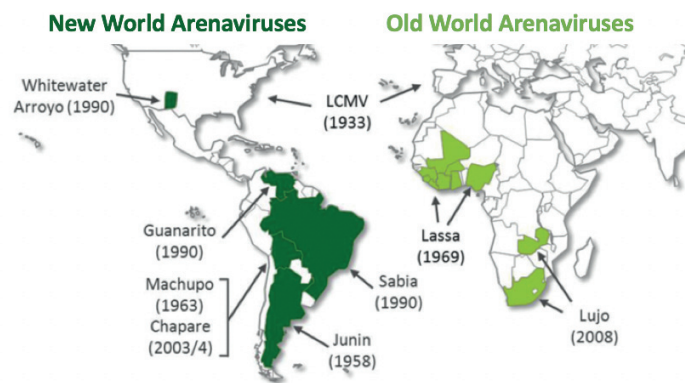
Figure 1. Geographic distribution of human pathogenic arenaviruses. The year of the first description is indicated in brackets.

Structure and life cycle of arenaviruses

The Arenaviruses are enveloped negative-strand RNA viruses that form spherical to pleomorphic particles with diameters of 50–300 nm [28] (Fig. 2). The viral genome is comprised of two RNA segments. The large (L) segment of *ca*. 7.3 kb and the small (S) segment of *ca*. 3.5 kb) contain each two

open reading frames (ORF) in opposite orientation, separated by a noncoding intergenic region with a predicted hairpin structure. The S RNA segment encodes the nucleoprotein (NP) and the envelope glycoprotein precursor (GPC). The L RNA encodes the viral RNA-dependent RNA polymerase L, as well as the viral matrix protein Z. The viral GPC is synthesized as a single polypeptide chain and posttranslationally cleaved by the cellular proteases signal peptidase and subtilisin kexin isozyme-1/site-1 protease (SKI-1/S1P) to yield an unusually stable signal peptide (SSP), the mature virion glycoproteins GP1 and GP2 [29]. The mature SSP/GP1/GP2 complex forms a trimer and represents the functional unit of virus-cell attachment and virus fusion [30]. The N-terminal GP1 engages cellular receptors, and decorates the tip of the virion spike [31, 32]. The C-terminal GP2 resembles fusion-active envelope GPs of other viruses and is implicated in viral fusion [33].
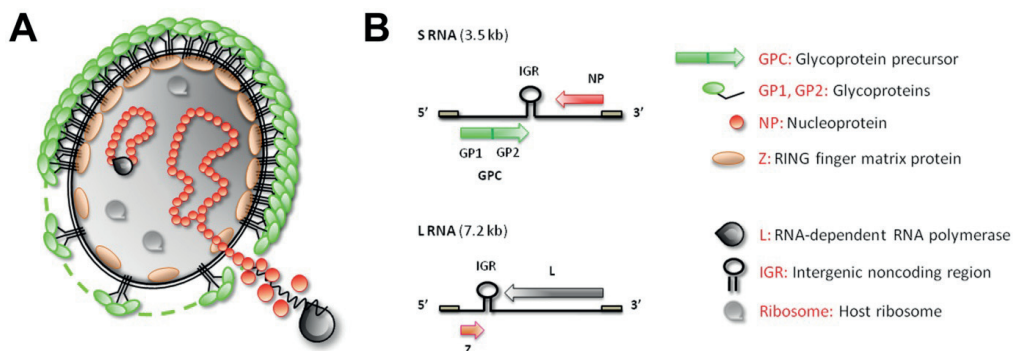
Figure 2: Virion structure (A) and genome organization (B) of Arenaviruses. For details, please see text.

The arenavirus life cycle is non-lytic and confined to the cytoplasm [30, 34-40]. As for every virus, the first step of arenavirus infection requires attachment of the virion to one or more cellular receptor(s) (Fig. 3A). Most Old World arenaviruses, including LCMV and LASV, as well as the Clade C New World viruses Latino and Oliveros use dystroglycan (DG), a ubiquitously expressed receptor for proteins of the extracellular matrix (ECM), as a high affinity receptor (Fig. 3B) [41, 42]. In developing and adult tissues, DG provides a molecular link between the ECM and the actin-based cytoskeleton. Initially encoded as a single polypeptide, DG is cleaved into the extracellular α-DG and membrane anchored β-DG [43]. In mammals, α-DG is subject to complex post-translational modifications that are essential for its function as a receptor for ECM proteins and arenaviruses [44-46]. Unusual protein O-mannosylation of α-DG is followed by synthesis of [Xyl-α1-GlcA-3-β1-3] co-polymers by the dual-specific glycosyltransferase like-acetyl glucosaminyl transferase (LARGE) [47, 48]. The LARGE-derived [Xyl-α1-GlcA-3-β1-3] polysaccharide is nown as "matriglycan" and recognizes ECM proteins and arenavirus GP1 [44, 49, 50]. The recently solved high-resolution X-ray structure of the pre-fusion conformation of LASV GP indicates that multiple residues located at the trimeric interface engage the DG-derived matriglycan polymers with high avidity [32]. The DG core protein is ubiquitously expressed in most mammalian cells similar to house-keeping genes. However, functional glycosylation of DG by

LARGE is subject of tight tissue-specific control [49]. This makes DG appear as a "tunable" receptor, whose virus-binding affinity critically depends on LARGE modification and greatly varies between tissues.

Upon receptor attachement, Old World arenaviruses use an endocytotic pathway resembling macropinocytosis for cell entry [38, 51, 52]. Subsequently, the virus passes through the multivesicular body and reaches the late endosome [53]. At the late endosome, LASV GP1 undergoes a unique "receptor switch". Acidic pH (<5.5) induces major conformational changes in LASV GP1, resulting in dissociation from DG-linked matriglycan. A triad of His residues characteristic of the low pH conformation of LASV GP1 engages the late endosomal/lysosomal protein (LAMP)-1, followed by fusion triggering [54]. Fusion of the viral membrane with the limiting membrane of the late endosome by the fusion-active GP2 creates a "fusion pore". Within the arenaviruses, the dependence on LAMP-1 for cell entry is unique for LASV [55, 56] and represents an interesting analogy to the filoviruses Ebola virus, whose fusion depends on the late endosomal protein Niemann-Pick C1 [57].

New World arenaviruses of Clade B use transferrin receptor (TfR)-1, a highly conserved cargo receptor involved in iron metabolism, and clathrin-mediated endocytosis (CME) for cell entry [58]. The ability of a Clade B New World arenavirus to use the human orthologue of TfR1 is linked to its potential to cause hemorrhagic fever in human [59, 60]. In contrast, non-pathogenic viruses use TfR1 orthologues from other species. More recently, the Tyro3/Axl/Mer (TAM) receptor tyrosine kinases Axl and Tyro3/Dtk, T cell Immunoglobulin Mucin (TIM) proteins 1 and 4, as well as the C-type lectins DC-specific ICAM-3-grabbing nonintegrin (DC-SIGN) and LSECtin have been identified as novel candidate receptors for arenaviruses [61-65], but their exact role is currently unclear.

At the fusion pore, the arenavirus capsid disassembles to free the viral ribonucleoprotein (RNP) by an unknown mechanism of "uncoating". According to the negative-strand genome, the arenavirus RNP is comprised of viral RNA, NP, and the polymerase L, comprising the minimal unit of viral transcription and replication. Viral transcription is initiated by the L polymerase at the incoming RNP, resulting in expression of NP and L. As NP accumulates, the viral polymerase progressively shifts to a replicase mode, generating full-length antigenomic RNA in positive-strand orientation that serves as template for the transcription of GPC and Z as well as synthesis of further copies genomic RNA [66]. Newly synthesized NP assembles the viral replication-transcription complexes (RTC) that become initially apparent as discrete puncta at the light microscopy level that grow in size and progressively coalesce into larger structures distributed throughout the cytosol [67, 68]. Arenavirus RTC are membrane-associated structures that contain cellular lipids and proteins, including translation factors of the eIF4F complex, suggesting the formation of membrane-associated "platforms" for viral transcription and replication [67, 68].

In the final stages of the arenavirus life cycle, progeny particles assemble and are released by budding from the plasma membrane. The key factor in the budding process is the small RING finger Z protein that functions as a *bona fide* matrix protein in arenavirus particle assembly [36, 69]. As with other matrix proteins of enveloped viruses, arenavirus Z interacts with the cytosolic tail of GP2 [70] and specific cellular factors of the endosomal/multiple vesicle body pathway to drive the budding of viral particles from "budding zones" [34, 36, 39, 69].
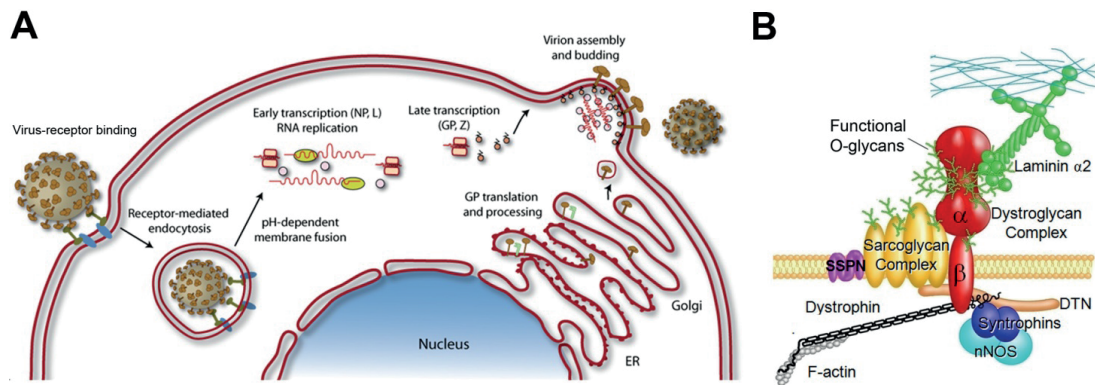
Figure 3: LASV receptor and life cycle. (A) The life cycle of LASV. (B) Schematic representation the LASV receptor DG found in muscle cells associated with the ECM protein laminin (Dr. Renzi Han, Loyola University).

Structure-function relationship of the LASV and MACV attachment glycoproteins

During maturation, processing of the arenavirus GPC precursor by SKI-1/S1P yields the N-terminal GP1, which is implicated in binding to the cellular receptors [71] and the transmembrane GP2 that mediates fusion and resembles class I viral fusion proteins [33, 72, 73] (Fig. 4A). Arenavirus GPC contain a remarkably stable signal peptide (SSP) of 58 amino acids that contains two hydrophobic domains and undergoes myristoylation at its N-terminus [74-77]. In the mature tripartite complex SSP/GP1/GP2 that forms the trimeric virion spike, SSP interacts with the GP2 subunit (Fig. 4B). Examination of LASV particles in electron cryomicroscopy combined with tomography revealed that the trimeric SSP/GP1/GP2 complex undergoes significant changes when exposed to low pH [78].

Resolution of the X-ray structures of the GP1 of LASV, MACV, and JUNV revealed a similar compact α/β fold, despite significant sequence variation [79-81]. High-resolution structures of MACV GP1 in complex with its receptor TfR1 revealed that the GP1 monomer represents the functional unit of receptor recognition and that trimerization is not required for receptor binding [60, 82]. In these studies, MACV GP1 was found to bind to the apical surface of hTfR1 without competing with transferrin binding. More recent crystallographic studies resolved the structure of the pre-fusion conformation of the mature envelope GP of the prototypic Old World arenavirus LCMV [31]. Within the pre-fusion

trimer, LCMV GP1 and GP2 undergo extensive interactions, involving ionic bonds. In contrast to the New World arenaviruses, monomeric LCMV GP1 is unable to bind the receptor DG with high affinity, suggesting that either avidity or the quaternary structure of the pre-fusion trimer is required. Recently, the crystal structure of the ectodomain of LASV GP in its trimeric, pre-fusion conformation was solved in complex with a nAb from a human survivor [32] (Fig. 5). These studies illuminate the structural basis for neutralization of LASV by a nAb that clamps two of the monomers together at the base of the trimer. The nAb may neutralize by blocking conformational changes taking place within the trimer that are required for receptor binding, the late endosomal receptor switch mentioned above, and fusion. In an elegant study, Pinschewer et al, provided evidence for an inherently low immunogenicity of LASV GP1 as a consequence of extensive glycan shielding, [83], which is similar to the situation with other viruses like human immunodeficiency virus (HIV)-1. In line with this, the exposed surfaces at the side and lower portions of the LASV GP trimer are extensively shielded by N-glycans, leaving only a few "cracks in the armor" vulnerable to Ab binding.

Once delivered to the late endosome, low pH sets off a series of conformational changes leading to shedding of GP1, engagement of LAMP-1, and triggering of fusion of the viral and cellular membrane mediated by GP2 (Fig. 4C). The post-fusion conformation of arenavirus GP2 is similar to the six-helix bundle conformation common to a number of class I fusion proteins of enveloped viruses [33, 73]. The SSP is crucial for transport and processing of arenavirus GPC [74-76, 84, 85]. Both N- and C-termini of SSP are located in the cytosol [86] and SSP associates non-covalently with a zinc-binding domain within the cytoplasmic tail of GP2 [87, 88]. The SSP-GP2 interactions critically modulate pH-induced activation of membrane fusion [89, 90] and are targeted by a range of potent arenavirus fusion inhibitors [91, 92], pinpointing this unique feature of arenavirus fusion as a target for the development of anti-viral therapeutics.
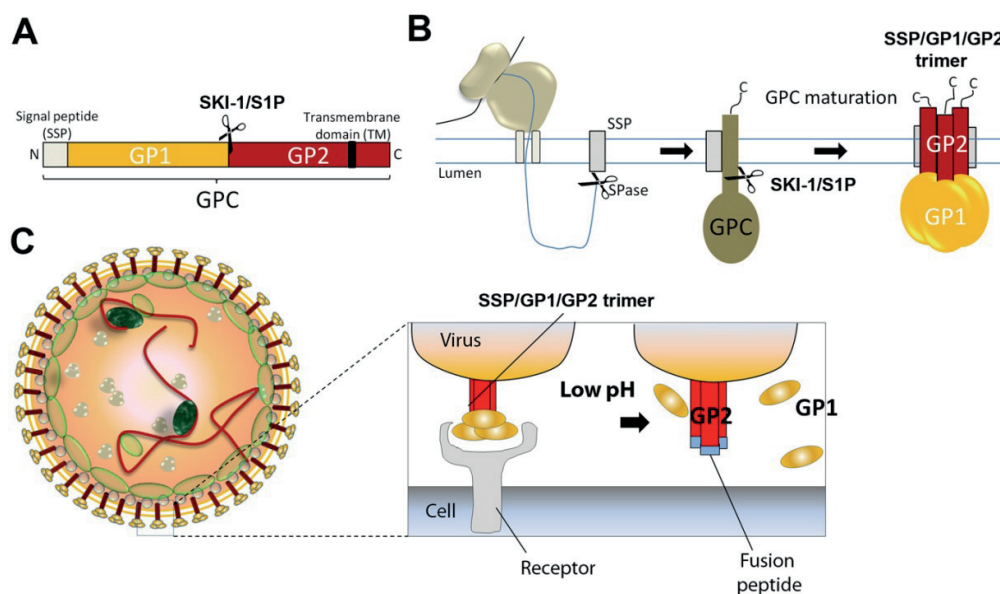
Figure 4. Maturation and trimerization of arenavirus GP. (A) The arenavirus GPC precursor is comprised of the stable signal peptide (SSP), GP1, and GP2. The transmembrane domain and the site of SKI-1/S1P cleavage are indicated (scissors). (B) Sequential processing of arenavirus GPC in the secretory pathway by signal peptidase (SPase) and SKI-1/S1P. The mature tripartite complex SSP/GP1/GP2 forms the mature trimeric GP spike (C) The mature GP trimer decorates the virion surface and engages cellular receptors. Under acidic pH, GP1 dissociates and liberates the fusion peptide of GP2, triggering fusion between the viral and the cellular membrane.
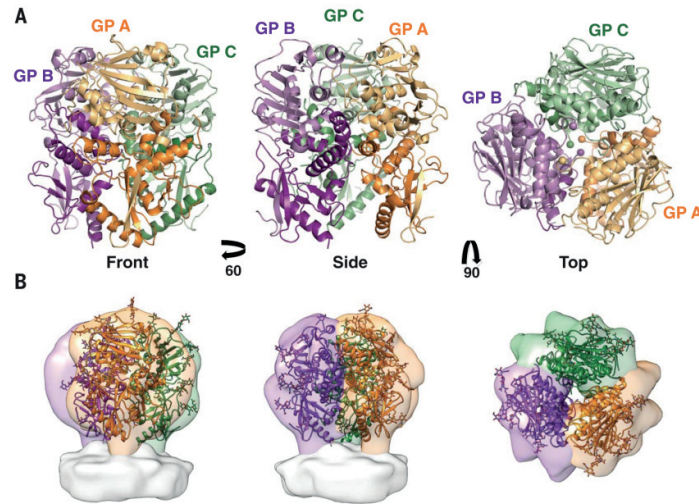
Figure 5: Cartoon representation of the LASV GP extodomain trimer from the front, side, and top [32]. The GP1 subunit of each monomer is in a light shade and the GP2 subunit in a dark shade. In the top view, spheres indicate positions of the C-terminus of GP1 and the N-terminus of GP2 at the trimeric interface. (B) The crystal structure of the LASV GP trimer (cartoon) docked into the tomographic reconstruction of the LASV GPC spike from fixed virions in the same orientations as shown in (A).

Pathogenesis and immune response to pathogenic arenaviruses infection

After an incubation period of 7-18 days Lassa fever manifests initially with non-specific, flu-like signs and symptoms, including fever, weakness and general malaise [16]. Signs of increased vascular permeability such as facial and lung edema, as well as mucosal bleeding are associated with poor prognosis [1, 93, 94]. Contagiousness initiates with the onset of symptoms and increases with disease severity, consistent with the presentation of pharyngeal shedding, vomiting, diarrhea and bleeding, together with high levels of viral load in body fluids. The virus is shed in urine for six weeks and up to six months in semen. In severe cases, patients develop progressive symptoms of shock, accompanied by internal bleeding. Those recovering develop a robust cellular anti-viral immune response during the second week of disease and clear the virus. A highly predictive factor for disease outcome in human Lassa fever is the serum viral load [95]. Patients with fatal disease have higher initial viral loads ($>10^6$ PFU/ml) and are unable to limit viral spread. Survivors have lower initial viremia and control infection

progressively. In contrast to the persistent infection in their rodent reservoir hosts, there is no evidence for persistence of arenaviruses in man and survivors clear the virus completely [25, 96], although there is recent evidence for protracted infections [17].

A widely known particularity of fatal LASV infection is virus-induced suppression of the host's innate defense, in particular the type I interferon (IFN) response, that represents an early and decisive barrier against viral infections. The ability of LASV to efficiently suppress innate immunity is linked to the NP. The NPs of all known arenaviruses contain a 3'-5' exoribonuclease function in their C-terminal domain, which may be involved in degradation of viral RNA, thereby removing the viral "danger signal" recognized by the host cell's pathogen recognition receptors (PRR) of the RIG-I helicase and Toll-like receptor (TLR) family [97]. More recent studies identified the Z protein as an additional IFN-I antagonist that targets RIG-I and prevents IFN-I induction [98, 99]. Interestingly, only Z proteins of human pathogenic viruses, but not non-pathogenic viruses, can bind to human RIG-I, pinpointing Z as a classical virulence factor. Following productive viral infection at the site of entry, the virus rapidly enters the bloodstream to reach lymph nodes, spleen, and liver. In lymphoid organs, LASV efficiently targets antigen presenting cells (APC), in particular dendritic cells (DCs), which represent the most important class of professional APC in *primo* infection. Instead of being recognized and presented as a foreign antigen, LASV establishes productive infection in DCs and perturbs their capacity of antigen presentation [100, 101], contributing to immunosuppression in severe infection. Examination of fatal Lassa fever cases revealed little tissue damage and inflammation, suggesting a weak anti-viral immune response [93, 102]. Considering existing clinical and experimental data, it appears that LASV uses a dual strategy to suppress adaptive immunity on the one hand blocking antigen presentation by DCs and on the other hand promoting exhaustion of anti-viral CD8 T cells. The pathophysiology of the terminal hemorrhagic shock syndrome is largely unknown. Blood loss in Lassa fever is minimal and there is little evidence for a "cytokine storm" observed in classical hemorrhagic fevers [16]. The terminal shock syndrome in Lassa fever may involve functional changes in vascular endothelial cells preceding shock and death, combined with alterations in liver, adrenal gland, and other organs [1, 93]. In survivors, anti-viral CD8 T cells represent a major correlate of protection, indicating a pivotal role of cellular immunity. Neutralizing antibodies to LASV appear only late in convalescence and are frequently of low titers. Their role in protection against re-infection is currently unclear. However, if provided at sufficiently high titers, nAb to LASV proved to be protective in post-exposure prophylaxis in animals [103, 104], and in human cases [105, 106], providing proof-of-concept.

In contrast to LASV that efficiently evades and suppresses the cellular IFN-I and cytokine response, infection with New World arenaviruses like JUNV and MACV results in elevated cytokine levels [107, 108]. Indeed, patients with exacerbated disease consistently show elevated levels of TNF-α and INF-I. To what extend these enhanced cytokine levels reflect simply higher viral loads is currently unknown. In contrast to LASV, JUNV and MACV elicit a robust nAb response in the second week of

disease that correlates with positive disease outcome [24]. The strong nAb responses against New World arenaviruses points out that the viral GP1 is immunogenic and a recombinant vaccine capable of inducing sufficient nAb titers seems feasible. The reasons for the noticeable difference in quality of the antibody response between LASV and JUNV/MACV lie, at least in part, in the differential glycosylation of the GP1 moieties that represent the targets for nAb [83].

Current diagnostics and therapy against arenaviruses

Molecular diagnostics based on real-time quantitative PCR, nucleic acid hybridization, and more recently next generation sequencing (NGS) proved invaluable for etiological diagnostics in the clinic [109-112]. In recent years, highly sensitive PCR-based molecular diagnostics tests for arenaviruses have been developed, including reverse-transcription (RT)-PCR assays for the detection of LASV by targeting conserved regions of the L gene, an improved RT-PCR for Lassa virus amplifying the 5'region of the S RNA, and an RT-PCR assay coupled with oligonucleotide array hybridization [113].With these recent developments, RT-PCR has become the method of choice for the detection of LASV. A recent study performed in Nigeria demonstrated that the establishment of a laboratory routine based on molecular diagnostics significantly improved Lassa fever case management [114]. For the South American viruses, molecular diagnostics is less developed and the design of virus-specific RT-qPCR routines faces the problem of extensive sequence variation between geographic isolates.

Complementary to molecular diagnostics, serology remains crucial for etiological diagnosis and sero-epidemiological studies of human arenavirus infection. Common antibody detection systems used in routine diagnostics include immunofluorescence assay (IFA), enzyme-linked immunosorbent assay (ELISA), and different formats of neutralization tests. Serology by IFA has been the classical method for arenavirus diagnostics for several decades and is still in use today. In this method, infected monolayers of Vero cells are inactivated by ultraviolet (UV) light, treated with acetone, or irradiated with gamma-rays. Drops of cell cultures mounted onto glass slides are then incubated with the patients' serum and a specific antibody reaction is detected by IFA. The threshold is defined as a signal above background at a serum dilution of 1:4, which is difficult to assess. Moreover, the major viral antigen detected within acetone-fixed infected cell specimens is the viral NP, which results in serological cross-reactions in the IFA test, in particular among New World arenaviruses [115, 116]. Greatest cross-reactivity is observed between the closely related MACV and JUNV, followed by TCRV, which represents a major limitation of the method. ELISA using recombinant viral proteins has lately been developed as an alternative to IFA for early and rapid serological diagnosis, but face essentially the same restrictions for New World arenavirus diagnostics [117]. The neutralization test is considered specific for all members of the *Arenaviridae*. However, cross-reactivity was observed with high-titer reference sera between JUNV and MACV, which is a major problem and quantification of neutralizing antibodies (nAb) can therefore vary greatly (*Dr. Delia Enria, personal communication*).

For routine isolation of virus from clinical samples and reservoir rodents in surveillance study, the E6 clone of Vero cells is used as a suitable cell line. However, a cytopathic effect is often difficult to detect, and definitive detection of virus in inoculated cultures requires examination by IFA or ELISA. A major limitation for the detection New World viruses is again the current lack on specific antibodies capable to distinguish in particular MACV from JUNV, which represent the major pathogens among the South American hemorrhagic fever viruses.

Only one licensed drug for treatment of human arenavirus infection is the broad spectrum guanosine analogue ribavirin (Rib) (1-β-D-ribofuranosyl-1,2,4-triazole-3-carboxamide) [118]. Rib reduces both morbidity and mortality in humans associated with LASV infection [119], and experimentally in MACV [120] and JUNV [25] infections, only when administered early during disease. Major problems with Rib are the limited bioavailability and the unwanted side-effects, in particular hemolytic anemia, and restriction of its use in some patient groups, e.g. pregnant women. Several experimental treatments are currently being evaluated for Arenaviruses, including antivirals, molecules targeting host cells and immunomodulators. However, none of these have undergone extended human trials. Due to space limitations, I therefore refer to recent reviews [121, 122]. Immune plasma transfer therapy for JUNV arenaviruses have been prove highly effective [25], but is frequently associated with a self-limiting neurological syndrome [24], whose pathophysiology is currently not understood. These potential complications underscore the need for alternative therapies.

Current status of arenavirus vaccine development

The only existing vaccine for the prevention of Argentine hemorrhagic fever caused by JUNV is the live-attenuated vaccine Candid 1 that was developed in the 1980s [123]. Candid 1 has been used in selected risk groups in Argentine, predominantly agricultural workers, where it turned out to be safe and with high efficiency. When the Argentine National Immunization Plan included the Candid 1 vaccine, morbidity and mortality rates dropped down significantly in the area. However, there are considerable concerns about the safety of the vaccine for the general population and Candid 1 has not yet been approved outside of Argentina. Considering the magnitude of the public health problem and its nature as an endemic disease, an effective LASV vaccine is of urgent need for the general population, healthcare and laboratory workers and military personnel. When in first place early trials with killed LASV vaccines did not succeed at eliciting a protective immune response [124], then, following efforts focused mainly on the development of live vaccines. Initially, in a vaccine called ML29, LASV was attenuated by generating genetic reassortants with the less pathogenic Mopeia virus [125]. This reassortant vaccine, showed efficacy in guinea pigs [126] and small non-human primates [127]. However, despite the attenuation of ML29 and Candid1, the use of these live vaccines in population of the affected areas encounters large limitations due to safety concerns and the prevalence of immunosuppressive conditions, making them not suitable from broad vaccine campaigns. Evaluation of recombinant viral platforms for antigen delivery, including vaccinia virus [128], vesicular stomatitis

virus [129, 130], and the Yellow Fever virus vaccine strain 17D [131] revealed that the solely presence of arenavirus GP was necessary and sufficient to confer protection in different live models. One of the imitations of recombinant viral platforms is the host immunity elicited against the vector backbone and the biosafety concerns related to life replicating agents. A promising safety profile is the most appealing feature of inactivated ('killed') vaccines or other non-replicating vaccine approaches, such as virus-like particles (VLPs), peptide-based, and DNA vaccines. Although these vaccine approaches induced specific immune responses in animal studies, they had in general low immunogenicity and efficacy [132]. Another approach undertaken in LASV vaccine development are epitope-based vaccines. Using computer-assisted algorithms, protective MHCI-restricted CD8 T cell and MHCII-restricted CD4 T cell epitopes have been identified in LASV GP and NP that confer cross-protection against viral challenge with LCMV [133]. However, while application of a peptide vaccine in naive individuals might be safe, administration to individuals previously exposed to the pathogen, may trigger re-activation of memory CD8 and CD4 T cells, which could result in immunopathology. This is of particular concern for LASV due to locally high seroprevalence of up to 40% among adults in some parts of Western Africa [134]. Alphavirus replicon technology is a convenient solution between 'killed' vaccines and replication-competent platforms due to its safety and immunogenicity profiles. Particles derived from alphavirus replicons, while they are unable to spread beyond the first infected cells, they can deliver and transduce the genes of interest in target cells and stimulate similar immune responses as those elicited by alphavirus-vectored vaccines and inactivated vaccines. RNA replicon vectors derived from an attenuated Venezuelan equine encephalitis virus (VEEV) were successfully applied to express LASV GPC and NP proteins, and protect guinea pigs against fatal Lassa fever [135]. Up to this point, the previously presented vaccine platforms haven't been developed any further nor underwent human vaccine trials.

Antiviral antibody responses

Immune control of viruses frequently requires a cooperation of the cellular and humoral responses of the adaptive immune system. In higher vertebrates, the immune response to viral infection includes the production of antibodies capable of recognizing a remarkably diverse array of antigens, including glycoproteins decorating viral particles [5, 136]. The antibody response plays an important role in protection against viral infections and this protection combines virus neutralization and effector-mediated destruction of virions and infected cells, which prevents infection spread and lowers viral load and clinical symptoms. Neutralizing antibodies represent therefore a major immunological correlate of protection in many successful vaccines [136]. Even though neutralization is probably the most powerful function antibodies exert against viruses, the neutralizing activity of a given serum or monoclonal antibody is essentially an operational definition that strongly depends on the assays used. This is illustrated by a very recent collaborative study aiming at the standardization of antibody neutralization tests for Ebola virus to establish an International Reference Reagent through WHO that included to 16

laboratories and 22 different assays [137]. Across the board, quantitative correlation was generally poor, with only five of the 22 assays giving a correlation coefficient of 0.7 or greater. Notably, among the five best assays ranged a VSV pseudotype neutralisation test similar to the one used in my studies. The correlation between neutralizing titers assessed *in vitro* with protection *in vivo* is challenging and requires careful standardization. Moreover, there is evidence from work on LCMV that non-neutralizing antibodies to GP1 can confer some degree of protection, e.g. by preventing persistent viral infection [138]. Mechanistically, protecting activity requires antibodies to be of relativity high affinity/avidity for the exposed structures on the viral surface. If such antibodies cover the virion surface to a sufficient degree, they can prevent viral infectivity by interfering with receptor binding and cell entry. For many viral systems, this simple model proposed by Parren and Burton in 2001 is supported by available experimental data on virus neutralization [3, 139]. Moreover, the process of viral entry may require conformational changes of viral surface proteins and antibody binding can prevent viral entry by interfering with such conformational changes. During co-evolution with their vertebrate reservoir hosts, many viruses developed strategies to evade an effective humoral anti-viral immune response. The envelope glycoproteins of many viruses form oligomers in which a considerable proportion of the monomeric surface of the viral attachment protein is hidden at the inner face of the multimer, limiting antibody accessibility. Enveloped viruses including major pathogens such as HIV-1, Ebola, and LASV, use extensive "glycan shielding" to avoid antibody recognition [136, 140]. The host cell-derived N- and O-glycans present on viral GPs decrease immunogenicity since they are recognized as "self". Mature LASV GP has 11 potential N-linked glycosylation sites on each of the monomers, whereas MACV GPC has only 5 glycosylation sites in total [83]. In addition, other factors can influence the antigenicity of native viral surface including the accessibility of the antibody to the antigenic sites as mentioned above, the structural arrangement of the glycoproteins on the surface and the host's B-cell repertoire specificity for epitopes in the accessible sites (Fig. 6).
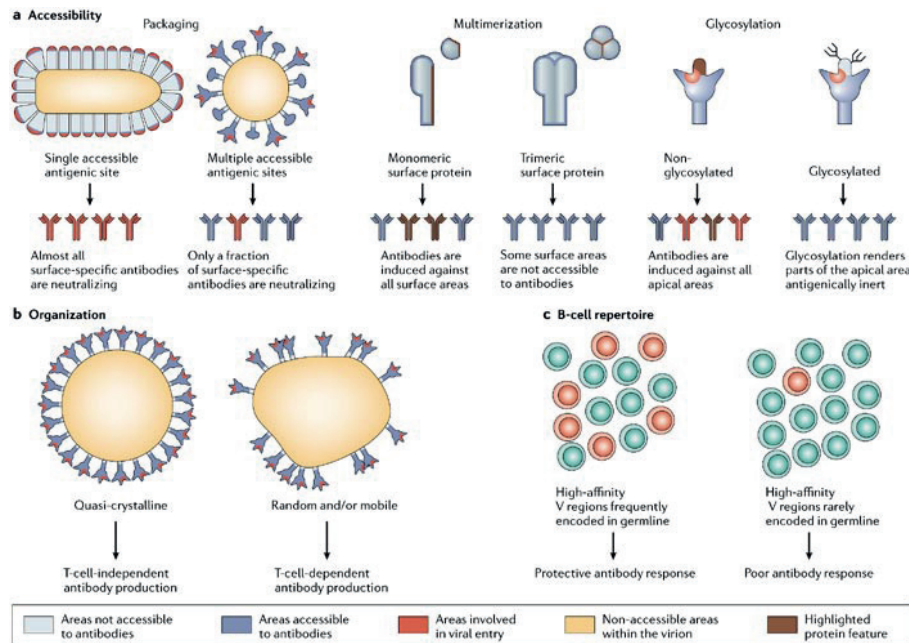
Figure 6: Overview of the factors influencing the immunogenicity of viral surfaces. A) Accessibility of the antigenic site is determinant for the immunogenicity of viral surfaces. B) Organization of antigens in the viral surface can modulate T cell antibody production. C) B-cell repertoire determines the quality of the antibody response. [141].

Subunit vaccines

Increasing knowledge in the field of vaccinology allowed defining the immunogenic components of existing vaccines that are responsible for eliciting protective immune responses. This permits to isolate specific antigenic parts from a pathogen, avoiding the inclusion of virulence factors that could potentially promote disease. Subunit vaccines are formulated based on such synthetic or biosynthetic antigenic components, combined with immunostimulatory compounds (adjuvants) to induce protective immunity. Subunit vaccines have the advantage that they can be reproducibly produced in bulk amounts [142] and lack exogenous materials that are often present in heat- or chemically-inactivated preparations of classical killed vaccines. For this reason, subunit vaccines are *a priori* safer than live-attenuated or killed vaccines and offer a controlled and targeted mode of immunization. A major drawback of recombinant vaccines is their reduced immunogenicity compared to life vaccines, especially in generating robust $CD4^+$ and $CD8^+$ T cell responses and the requirement of several boosts to achieve immunity [143]. To improve the induction of T cell responses, recombinant immunogens can be conjugated to nanocarriers of different chemical composition [144]. Vaccine parameters such as the administration route, delivery method, and adjuvant selection should be carefully chosen in order to enhance not only the magnitude, but also the quality of the immune response to novel subunit vaccine candidates.

The initial step during an immune response is the antigen uptake by APCs, followed by its presentation to T cells. Macrophages, B cells and dendritic cells (DCs) are traditionally known as professional APCs. In particular DCs have the capacity to efficiently present endogenous and exogenous antigen in the context of MHCI and MHCII, respectively, thus playing a crucial role in mounting both CD8 and CD4 T cell responses in primo infections [145-148]. The use of subunit vaccines capable of targeting DCs appears as a promising strategy to enhance their potency. Upon activation, DCs migrate to secondary lymphoid organs such as lymph nodes, where the immune response is initiated by antigen presentation [147, 149] followed by T cell differentiation and B cell class switching and maturation [149]. A widely used method to target subunit vaccines to lymph nodes is intradermal administration. Lymphatic capillaries in the skin take up macromolecules from the periphery, which reach afferent lymphatic vessels that drain into local lymph nodes where subunit vaccines are transported either by migratory DCs or in a cell-independent manner [150].

Antigen delivery via nanoparticulated platforms

Vaccine delivery systems use biomaterials to mimic various properties of pathogens to increase immunogenicity of otherwise weak antigens. This is achieved by the design of vaccines that mimic size, geometry, antigen presentation kinetics, and molecular patterns of viral antigens. Other key feature of these nanocarrier platforms is the ability to protect the antigen from early degradation. Examples of particulate delivery systems include polymeric nanoparticles, micelles, dendrimers, immune stimulating complexes and polymersomes (PS) [151, 152]. Lately, nanoscaled capsules like PS have been successfully developed for entrapment and targeted transport of a broad range of active payloads with sustained controlled release. The regulation of unique features such as mechanical stability, shell permeability, monodispersity, and biocompatibility is key for the successful implementation of these artificial vesicles as sophisticated delivery vehicles for tunable immune responses. The so-called "smart polymersomes" are able to respond to various external stimuli as pH, temperature, redox potential, magnetic fields, or light in order to carry out a controlled release of the payloads. Their chemical nature frequently allows co-delivery of suitable adjuvants that provide the "danger signals" for local innate immune stimulation.

Our laboratory recently developed a new PS nanocarrier systems based on the assembly of an amphiphilic block copolymer composed of polyethylene glycol (PEG) and polypropylene sulfide (PPS) shown in Fig. 7. These PS present several benefits as a vaccine platform. The aqueous interior allows secure transportation of hydrophilic molecules including immunogens and adjuvants avoiding chemical modification of the loaded molecules, while the surrounding membrane of the self-assembled bilayer vesicle can retain hydrophobic molecules [153]. The vesicle-like arrangement is determined by the ratio of the hydrophobic to hydrophilic composition of the block copolymers, and the solely presence of small amounts of oxidation power to oxidize PPS to the sulfoxide in the PS, is required to initiate the

destabilization of the vesicular aggregates into micelles which results in the release of the encapsulated content [154]. Moreover, the aggregates resulting from oxidation are sufficiently small for renal clearance [154].

Recent strategies for developing preventative and therapeutic vaccines have focused on the ability to deliver antigen to DCs in a targeted and prolonged manner. Nanoscale biomaterials loaded with different molecules transit through the lymphatic system and are taken up by DCs localized in draining lymphnodes, processes that are dependent on particle size. Empirically, *in vivo* delivery to lymph node-resident DCs is optimal with nanoparticles with a diameter smaller that 200 nm [155], whereas particles bigger that 45 nm drain most efficiently through the tissue interstitium into the lymphatic system [150] [156]. Nanocarriers with approximately 100 nm diameter, e.g. PS, undergo efficient lymphatic transport followed by rapid endocytosis by DCs. In addition, PS have the ability to enhance CD4 T cell responses, which is beneficial for the induction of antibodies. Lastly, the encapsulation process is a straightforward procedure that does not require any chemical treatment of the protein immunogen, thus preserving its native conformation. In sum, the novel PS platform combines unique features that make it promising for the development of a safe recombinant vaccine and platform for the rapid production of specific monoclonal Abs against pathogenic viruses [157, 158].
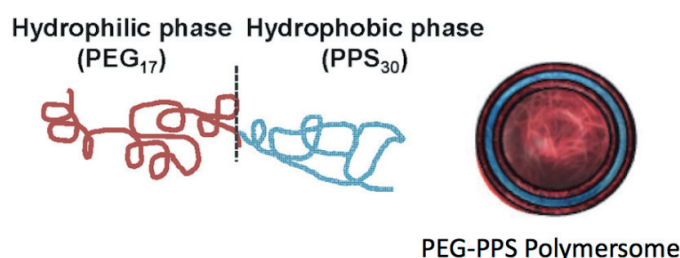
Figure 7. Schematic representation of PEG-*bl*-PPS block copolymers and vesicles. Block copolymers composed of PEG and PPS self-assemble into oxidation-sensitive polymersomes in aqueous solutions. Hydrophobic and hydrophilic regions are shown in blue and red, respectively.

Enhancing the efficacy of subunit vaccines - Adjuvants

In subunit vaccines, recombinant antigens are formulated with adjuvant molecules that mimic pathogen-associated molecular patterns (PAMPs), or "danger signals", that function as agonists for TLRs. Adjuvanted vaccines could potentially offset the lack of stimulation and enhance pathogen-specific responses involved in protection. The first commercially available adjuvant used in order to improve the immunogenicity of vaccine against diphtheria was aluminum-based [159]. Together with aluminum, oil-in-water emulsions were for a long time the sole compounds to be widely accepted. Adjuvants are used as part of a strategy to improve vaccine outcomes through synthetic or endogenous molecules that tune the immune effect which results in an enhanced and prolonged pathogen-specific immune response. In

addition, adjuvants can modulate the nature of the immune response by skewing towards a particular phenotype, favoring certain types of immunoglobulin classes or inducting different types of cytotoxic or T helper cell responses (Th1 vs. Th2). The low immunogenicity of certain antigens can be improved and the type immune response optimized, while reducing the amount of antigen required. Accordingly, succeeding the administration of different adjuvants cytokine responses of different nature can be observed. Generally, addition of TLR agonists to vaccine emulsions tunes the response towards a Th1 phenotype. Small molecule adjuvants (SMA) involve, among others, natural products such as monophosporyl lipid A (MPLA), a derivative of bacterial lipopolysaccharides (LPS), which has a much safer profile than LPS while still retaining its immunomodulatory properties [160]. MPLA is known to be effective at promoting both CD8 and CD4 T cell responses, as well as inducing long-lasting humoral responses [161]. Currently, MPLA is included in several vaccines undergoing phase III clinical trials [162]. SMA also includes synthetic drug-like molecules such as imidazoquinolines, including resiquimod (R-848) [163] and gardiquimod [164], which act as TLR7/8 agonists. CpG-based adjuvants, often synthetic, are other examples of SMAs which act as TLR9 agonists. CpGs are immunostimulatory DNA sequences containing unmethylated CpG dinucleotides found naturally in bacterial DNA that are recognized by TLR9. CpG-B is the most used and best-characterized TLR9 agonists and acts on a broad range of APCs, improving antigen uptake and presentation, as well as cytokine secretion [165, 166].

Preclinical studies in humans have demonstrated that a combination of adjuvants can synergize if united in the same vaccine formulation, making adjuvants more attractive for vaccine development. Innate receptors agonists could potentially become toxic at certain concentrations, thereby they must be administered carefully, in a manner that optimizes immunogeneicity but reduces counteractive local and systemic inflammatory reactions.

OUTLINE OF THE THESIS

In a first part of my thesis described in chapter 2, we evaluated oxidation-sensitive PS for their ability to enhance humoral immunity against the poorly immunogenic GP1 surface antigen of LASV. Based on structural information, we designed a recombinant immunogen derived from LASV GP1 which was successfully encapsulated into the aqueous core of polymersomes and delivered in combination with a well-established adjuvant. Mice immunized with LASV GP1-loaded PS showed enhanced quality of the humoral response, including in particular antibodies binding to GP1 displayed at the surface of intact virion particles. The better quality of the antibody response correlated with an increase in polyfunctional anti-viral CD4 T cells and anti-LASV GP1 IgG-secreting B cells. Peptide array analysis demonstrated a significantly broader epitope range of anti-viral IgG elicited by the polymersomes.

In chapter 3, we applied our findings from chapter 2 to design a novel strategy to rapidly develop specific mAbs against newly emerging viral pathogens without the need of virus isolation or culture. Starting from sequence information only, we provide proof-of-concept by developing a novel panel of "first in class" specific mAb to MACV GP1. The novel specific MACV GP1 mAbs were characterized for their potential use in diagnostics and research using established techniques.

Chapter 4 summarizes structural studies on LASV GP1 that I performed during my stay of three month in the highly respected laboratory of Prof. Erica Ollman Saphire at the Scripps Research Institute in La Jolla, CA. Specifically, I undertook an attempt to obtain the crystal structure of the purified LASV GP1 immunogen and performed antigen binding to a newly isolated human nAb.

Finally, in Chapter 5 we summarize our findings, discuss about the implications of our results and present the future prospects of our studies.

In collaboration with Marcela Rincon-Restrepo, I contributed to the demonstration of the efficacy of a peptide vaccine based on nanoparticles (NPs) to stimulate CD8 T cell responses upon intradermal delivery. Here, we provide evidence that PS loading has a strong impact on the quality of the immune response, skewing memory CD8 T cells to an effector-like memory phenotype.

REFERENCES

1. Geisbert, T.W. and P.B. Jahrling, *Exotic emerging viral diseases: progress and challenges.* Nat Med, 2004. **10**(12 Suppl): p. S110-21.
2. Isa, S.E., et al., *Postexposure prophylaxis for Lassa fever: Experience from a recent outbreak in Nigeria.* Nigerian Medical Journal : Journal of the Nigeria Medical Association, 2016. **57**(4): p. 246-250.
3. Burton, D.R., E.O. Saphire, and P.W. Parren, *A model for neutralization of viruses based on antibody coating of the virion surface.* Curr Top Microbiol Immunol, 2001. **260**: p. 109-43.
4. Parren, P.W. and D.R. Burton, *The antiviral activity of antibodies in vitro and in vivo.* Advances in immunology, 2001. **77**: p. 195-262.
5. Karlsson Hedestam, G.B., et al., *The challenges of eliciting neutralizing antibodies to HIV-1 and to influenza virus.* Nature reviews. Microbiology, 2008. **6**(2): p. 143-55.
6. Zeitlin, L., et al., *Antibody therapeutics for Ebola virus disease.* Curr Opin Virol, 2016. **17**: p. 45-9.
7. Buchmeier, M.J., J.C. de la Torre, and C.J. Peters, *Arenaviridae: the viruses and their replication*, in *Fields Virology*, D.L. Knipe and P.M. Howley, Editors. 2007, Lippincott-Raven: Philadelphia. p. p. 1791-1828.
8. Oldstone, M.B., *Biology and Pathogenesis of Lymphocytic Choriomeningitis Virus Infection*, in *Arenaviruses*, M.B. Oldstone, Editor. 2002. p. 83-118.
9. Radoshitzky, S.R., et al., *Past, present, and future of arenavirus taxonomy.* Arch Virol, 2015. **160**(7): p. 1851-74.
10. Charrel, R.N., X. de Lamballerie, and S. Emonet, *Phylogeny of the genus Arenavirus.* Curr Opin Microbiol, 2008. **11**(4): p. 362-8.
11. Emonet, S.F., et al., *Arenavirus genetic diversity and its biological implications.* Infect Genet Evol, 2009. **9**(4): p. 417-29.
12. Zinkernagel, R.M., *Lymphocytic choriomeningitis virus and immunology.* Curr Top Microbiol Immunol, 2002. **263**: p. 1-5.
13. Bonthius, D.J., *Lymphocytic choriomeningitis virus: a prenatal and postnatal threat.* Advances in pediatrics, 2009. **56**: p. 75-86.
14. Palacios, G., et al., *A new arenavirus in a cluster of fatal transplant-associated diseases.* N Engl J Med, 2008. **358**(10): p. 991-8.
15. Fischer, S.A., et al., *Transmission of lymphocytic choriomeningitis virus by organ transplantation.* N Engl J Med., 2006. **354**(21): p. 2235-49.
16. McCormick, J.B. and S.P. Fisher-Hoch, *Lassa fever.* Curr Top Microbiol Immunol, 2002. **262**: p. 75-109.
17. Andersen, K.G., et al., *Clinical Sequencing Uncovers Origins and Evolution of Lassa Virus.* Cell, 2015. **162**(4): p. 738-50.
18. Briese, T., et al., *Genetic detection and characterization of Lujo virus, a new hemorrhagic fever-associated arenavirus from southern Africa.* PLoS Pathog, 2009. **5**(5): p. e1000455.
19. Choe, H., et al., *Transferrin receptor 1 in the zoonosis and pathogenesis of New World hemorrhagic fever arenaviruses.* Curr Opin Microbiol, 2011. **14**(4): p. 476-82.
20. Clegg, J.C., *Molecular phylogeny of the arenaviruses.* Curr Top Microbiol Immunol, 2002. **262**: p. 1-24.
21. Monath, T.P., et al., *Lassa virus isolation from Mastomys natalensis rodents during an epidemic in Sierra Leone.* Science, 1974. **185**(147): p. 263-5.
22. McCormick, J.B., et al., *A prospective study of the epidemiology and ecology of Lassa fever.* J Infect Dis, 1987. **155**(3): p. 437-44.
23. Fisher-Hoch, S.P., et al., *Review of cases of nosocomial Lassa fever in Nigeria: the high price of poor medical practice.* Bmj, 1995. **311**(7009): p. 857-9.
24. Peters, C.J., *Human infection with arenaviruses in the Americas.* Curr Top Microbiol Immunol, 2002. **262**: p. 65-74.
25. Weissenbacher, M.C., R.P. Laguens, and C.E. Coto, *Argentine hemorrhagic fever.* Curr Top Microbiol Immunol, 1987. **134**: p. 79-116.
26. Kenyon, R.H., et al., *Aerosol infection of rhesus macaques with Junin virus.* Intervirology, 1992. **33**(1): p. 23-31.
27. Sayler, K.A., et al., *Isolation of Tacaribe virus, a Caribbean arenavirus, from host-seeking Amblyomma americanum ticks in Florida.* PLoS One, 2014. **9**(12): p. e115769.
28. de la Torre, J.C., *Molecular and cell biology of the prototypic arenavirus LCMV: implications for understanding and combating hemorrhagic fever arenaviruses.* Ann N Y Acad Sci, 2009. **1171 Suppl 1**: p. E57-64.
29. Burri, D.J., et al., *Envelope glycoprotein of arenaviruses.* Viruses, 2012. **4**(10): p. 2162-81.
30. Nunberg, J.H. and J. York, *The curious case of arenavirus entry, and its inhibition.* Viruses, 2012. **4**(1): p. 83-101.

31.   Hastie, K.M., et al., *Crystal structure of the prefusion surface glycoprotein of the prototypic arenavirus LCMV.* Nat Struct Mol Biol, 2016. **23**(6): p. 513-21.

32.   Hastie, K.M., et al., *Structural basis for antibody-mediated neutralization of Lassa virus.* Science, 2017. **356**(6341): p. 923-928.

33.   Igonet, S., et al., *X-ray structure of the arenavirus glycoprotein GP2 in its postfusion hairpin conformation.* Proc Natl Acad Sci U S A, 2011. **108**(50): p. 19967-72.

34.   Fehling, S.K., F. Lennartz, and T. Strecker, *Multifunctional nature of the arenavirus RING finger protein Z.* Viruses, 2012. **4**(11): p. 2973-3011.

35.   Grant, A., et al., *Junin virus pathogenesis and virus replication.* Viruses, 2012. **4**(10): p. 2317-39.

36.   Urata, S. and J.C. de la Torre, *Arenavirus budding.* Adv Virol, 2011. **2011**: p. 180326.

37.   Emonet, S.E., S. Urata, and J.C. de la Torre, *Arenavirus reverse genetics: new approaches for the investigation of arenavirus biology and development of antiviral strategies.* Virology, 2011. **411**(2): p. 416-25.

38.   Torriani, G., C. Galan-Navarro, and S. Kunz, *Lassa Virus Cell Entry Reveals New Aspects of Virus-Host Cell Interaction.* J Virol, 2017. **91**(4).

39.   Wolff, S., H. Ebihara, and A. Groseth, *Arenavirus budding: a common pathway with mechanistic differences.* Viruses, 2013. **5**(2): p. 528-49.

40.   Loureiro, M.E., et al., *Uncovering viral protein-protein interactions and their role in arenavirus life cycle.* Viruses, 2012. **4**(9): p. 1651-67.

41.   Cao, W., et al., *Identification of alpha-dystroglycan as a receptor for lymphocytic choriomeningitis virus and Lassa fever virus [see comments].* Science, 1998. **282**(5396): p. 2079-81.

42.   Oldstone, M.B. and K.P. Campbell, *Decoding arenavirus pathogenesis: essential roles for alpha-dystroglycan-virus interactions and the immune response.* Virology, 2011. **411**(2): p. 170-9.

43.   Barresi, R. and K.P. Campbell, *Dystroglycan: from biosynthesis to pathogenesis of human disease.* J Cell Sci., 2006. **119**(Pt 2): p. 199-207.

44.   Yoshida-Moriguchi, T. and K.P. Campbell, *Matriglycan: a novel polysaccharide that links dystroglycan to the basement membrane.* Glycobiology, 2015. **25**(7): p. 702-13.

45.   Kunz, S., et al., *Posttranslational modification of alpha-dystroglycan, the cellular receptor for arenaviruses, by the glycosyltransferase LARGE is critical for virus binding.* J Virol, 2005. **79**(22): p. 14282-96.

46.   Rojek, J.M., et al., *Old World and clade C New World arenaviruses mimic the molecular mechanism of receptor recognition used by alpha-dystroglycan's host-derived ligands.* J Virol, 2007. **81**(11): p. 5685-95.

47.   Inamori, K., et al., *Dystroglycan function requires xylosyl- and glucuronyltransferase activities of LARGE.* Science, 2012. **335**(6064): p. 93-6.

48.   Praissman, J.L., et al., *The functional O-mannose glycan on alpha-dystroglycan contains a phospho-ribitol primed for matriglycan addition.* Elife, 2016. **5**.

49.   Goddeeris, M.M., et al., *LARGE glycans on dystroglycan function as a tunable matrix scaffold to prevent dystrophy.* Nature, 2013. **503**(7474): p. 136-40.

50.   Briggs, D.C., et al., *Structural basis of laminin binding to the LARGE glycans on dystroglycan.* Nat Chem Biol, 2016. **12**(10): p. 810-4.

51.   Iwasaki, M., et al., *Cell entry of lymphocytic choriomeningitis virus is restricted in myotubes.* Virology, 2014. **458-459**: p. 22-32.

52.   Oppliger, J., et al., *Lassa virus cell entry via dystroglycan involves an unusual pathway of macropinocytosis.* J Virol, 2016.

53.   Pasqual, G., et al., *Old world arenaviruses enter the host cell via the multivesicular body and depend on the endosomal sorting complex required for transport.* PLoS Pathog, 2011. **7**(9): p. e1002232.

54.   Jae, L.T., et al., *Virus entry. Lassa virus entry requires a trigger-induced receptor switch.* Science, 2014. **344**(6191): p. 1506-10.

55.   Cohen-Dvashi, H., et al., *Role of LAMP1 Binding and pH Sensing by the Spike Complex of Lassa Virus.* J Virol, 2016. **90**(22): p. 10329-10338.

56.   Israeli, H., et al., *Mapping of the Lassa virus LAMP1 binding site reveals unique determinants not shared by other old world arenaviruses.* PLoS Pathog, 2017. **13**(4): p. e1006337.

57.   Jae, L.T. and T.R. Brummelkamp, *Emerging intracellular receptors for hemorrhagic fever viruses.* Trends Microbiol, 2015. **23**(7): p. 392-400.

58.   Radoshitzky, S.R., et al., *Transferrin receptor 1 is a cellular receptor for New World haemorrhagic fever arenaviruses.* Nature., 2007. **446**(7131): p. 92-6. Epub 2007 Feb 7.

59.   Helguera, G., et al., *An antibody recognizing the apical domain of human transferrin receptor 1 efficiently inhibits the entry of all new world hemorrhagic Fever arenaviruses.* J Virol, 2012. **86**(7): p. 4024-8.

60. Radoshitzky, S.R., et al., *Machupo virus glycoprotein determinants for human transferrin receptor 1 binding and cell entry.* PLoS One, 2011. **6**(7): p. e21398.

61. Shimojima, M. and Y. Kawaoka, *Cell surface molecules involved in infection mediated by lymphocytic choriomeningitis virus glycoprotein.* J Vet Med Sci, 2012. **74**(10): p. 1363-6.

62. Shimojima, M., et al., *Identification of cell surface molecules involved in dystroglycan-independent lassa virus cell entry.* J Virol, 2012. **86**(4): p. 2067-78.

63. Jemiolty, S., et al., *TIM-family proteins promote infection of multiple enveloped viruses through virion-associated phosphatidylserine.* PLoS Pathog, 2013. **9**(3): p. e1003232.

64. Goncalves, A.R., et al., *Role of DC-SIGN in Lassa Virus Entry into Human Dendritic Cells.* J Virol, 2013. **87**(21): p. 11504-15.

65. Martinez, M.G., et al., *Utilization of human DC-SIGN and L-SIGN for entry and infection of host cells by the New World arenavirus, Junin virus.* Biochem Biophys Res Commun, 2013. **441**(3): p. 612-7.

66. Perez, M. and J.C. de la Torre, *Characterization of the genomic promoter of the prototypic arenavirus lymphocytic choriomeningitis virus.* J Virol, 2003. **77**(2): p. 1184-94.

67. Baird, N.L., J. York, and J.H. Nunberg, *Arenavirus infection induces discrete cytosolic structures for RNA replication.* J Virol, 2012. **86**(20): p. 11301-10.

68. Knopp, K.A., et al., *Single nucleoprotein residue modulates arenavirus replication complex formation.* MBio, 2015. **6**(3): p. e00524-15.

69. Perez, M., R.C. Craven, and J.C. de la Torre, *The small RING finger protein Z drives arenavirus budding: implications for antiviral strategies.* Proc Natl Acad Sci U S A, 2003. **100**(22): p. 12978-83.

70. Capul, A.A., et al., *Arenavirus Z-glycoprotein association requires Z myristoylation but not functional RING or late domains.* J Virol, 2007. **81**(17): p. 9451-60.

71. Borrow, P. and M.B. Oldstone, *Characterization of lymphocytic choriomeningitis virus-binding protein(s): a candidate cellular receptor for the virus.* J Virol, 1992. **66**(12): p. 7270-81.

72. Eschli, B., et al., *Identification of an N-terminal trimeric coiled-coil core within arenavirus glycoprotein 2 permits assignment to class I viral fusion proteins.* J Virol., 2006. **80**(12): p. 5897-907.

73. Parsy, M.L., et al., *Crystal structure of Venezuelan hemorrhagic fever virus fusion glycoprotein reveals a class 1 postfusion architecture with extensive glycosylation.* J Virol, 2013. **87**(23): p. 13070-5.

74. Eichler, R., et al., *Identification of Lassa virus glycoprotein signal peptide as a trans-acting maturation factor.* EMBO Rep, 2003. **4**(11): p. 1084-8.

75. Eichler, R., et al., *Signal peptide of Lassa virus glycoprotein GP-C exhibits an unusual length.* FEBS Lett, 2003. **538**(1-3): p. 203-6.

76. York, J., et al., *The signal peptide of the Junin arenavirus envelope glycoprotein is myristoylated and forms an essential subunit of the mature G1-G2 complex.* J Virol, 2004. **78**(19): p. 10783-92.

77. Froeschke, M., et al., *Long-lived signal peptide of lymphocytic choriomeningitis virus glycoprotein pGP-C.* J Biol Chem, 2003. **278**(43): p. 41914-20.

78. Li, S., et al., *Acidic pH-Induced Conformations and LAMP1 Binding of the Lassa Virus Glycoprotein Spike.* PLoS Pathog, 2016. **12**(2): p. e1005418.

79. Bowden, T.A., et al., *Unusual molecular architecture of the machupo virus attachment glycoprotein.* Journal of virology, 2009. **83**(16): p. 8259-65.

80. Cohen-Dvashi, H., et al., *Molecular Mechanism for LAMP1 Recognition by Lassa Virus.* J Virol, 2015. **89**(15): p. 7584-92.

81. Mahmutovic, S., et al., *Molecular Basis for Antibody-Mediated Neutralization of New World Hemorrhagic Fever Mammarenaviruses.* Cell Host Microbe, 2015. **18**(6): p. 705-13.

82. Abraham, J., et al., *Structural basis for receptor recognition by New World hemorrhagic fever arenaviruses.* Nat Struct Mol Biol, 2010. **17**(4): p. 438-44.

83. Sommerstein, R., et al., *Arenavirus Glycan Shield Promotes Neutralizing Antibody Evasion and Protracted Infection.* PLoS Pathog, 2015. **11**(11): p. e1005276.

84. Messina, E.L., J. York, and J.H. Nunberg, *Dissection of the role of the stable signal peptide of the arenavirus envelope glycoprotein in membrane fusion.* J Virol, 2012. **86**(11): p. 6138-45.

85. York, J. and J.H. Nunberg, *Distinct requirements for signal peptidase processing and function in the stable signal peptide subunit of the Junin virus envelope glycoprotein.* Virology, 2007. **359**(1): p. 72-81.

86. Agnihothram, S.S., et al., *Bitopic membrane topology of the stable signal peptide in the tripartite Junin virus GP-C envelope glycoprotein complex.* J Virol, 2007. **81**(8): p. 4331-7.

87. Agnihothram, S.S., J. York, and J.H. Nunberg, *Role of the stable signal peptide and cytoplasmic domain of G2 in regulating intracellular transport of the Junin virus envelope glycoprotein complex.* J Virol, 2006. **80**(11): p. 5189-98.

88. Briknarova, K., et al., *Structure of a zinc-binding domain in the Junin virus envelope glycoprotein.* J Biol Chem, 2011. **286**(2): p. 1528-36.

89.   York, J. and J.H. Nunberg, *Intersubunit interactions modulate pH-induced activation of membrane fusion by the Junin virus envelope glycoprotein GPC.* J Virol, 2009. **83**(9): p. 4121-6.

90.   York, J. and J.H. Nunberg, *Role of the stable signal peptide of Junin arenavirus envelope glycoprotein in pH-dependent membrane fusion.* J Virol, 2006. **80**(15): p. 7775-80.

91.   Shankar, S., et al., *Small-Molecule Fusion Inhibitors Bind the pH-Sensing Stable Signal Peptide-GP2 Subunit Interface of the Lassa Virus Envelope Glycoprotein.* J Virol, 2016. **90**(15): p. 6799-807.

92.   York, J., et al., *pH-induced activation of arenavirus membrane fusion is antagonized by small-molecule inhibitors.* J Virol, 2008. **82**(21): p. 10932-9.

93.   Yun, N.E. and D.H. Walker, *Pathogenesis of Lassa fever.* Viruses, 2012. **4**(10): p. 2031-48.

94.   Moraz, M.L. and S. Kunz, *Pathogenesis of arenavirus hemorrhagic fevers.* Expert review of anti-infective therapy, 2011. **9**(1): p. 49-59.

95.   McCormick, J.B., et al., *A case-control study of the clinical diagnosis and course of Lassa fever.* J Infect Dis, 1987. **155**(3): p. 445-55.

96.   Johnson, K.M., et al., *Clinical virology of Lassa fever in hospitalized patients.* J Infect Dis, 1987. **155**(3): p. 456-64.

97.   Hastie, K.M., et al., *Hiding the evidence: two strategies for innate immune evasion by hemorrhagic fever viruses.* Curr Opin Virol, 2012. **2**(2): p. 151-6.

98.   Fan, L., T. Briese, and W.I. Lipkin, *Z proteins of New World arenaviruses bind RIG-I and interfere with type I interferon induction.* J Virol, 2010. **84**(4): p. 1785-91.

99.   Xing, J., H. Ly, and Y. Liang, *The Z proteins of pathogenic but not non-pathogenic arenaviruses inhibit the RIG-i-like receptor (RLR)-dependent interferon production.* J Virol, 2014.

100.   Baize, S., et al., *Lassa virus infection of human dendritic cells and macrophages is productive but fails to activate cells.* J Immunol, 2004. **172**(5): p. 2861-9.

101.   Mahanty, S., et al., *Cutting edge: impairment of dendritic cells and adaptive immunity by Ebola and Lassa viruses.* J Immunol, 2003. **170**(6): p. 2797-801.

102.   Walker, D.H., et al., *Pathologic and virologic study of fatal Lassa fever in man.* Am J Pathol, 1982. **107**(3): p. 349-56.

103.   Jahrling, P.B. and C.J. Peters, *Passive antibody therapy of Lassa fever in cynomolgus monkeys: importance of neutralizing antibody and Lassa virus strain.* Infect Immun, 1984. **44**(2): p. 528-33.

104.   Jahrling, P.B., *Protection of Lassa virus-infected guinea pigs with Lassa-immune plasma of guinea pig, primate, and human origin.* J Med Virol, 1983. **12**(2): p. 93-102.

105.   Leifer, E., D.J. Gocke, and H. Bourne, *Lassa fever, a new virus disease of man from West Africa. II. Report of a laboratory-acquired infection treated with plasma from a person recently recovered from the disease.* Am J Trop Med Hyg, 1970. **19**(4): p. 677-9.

106.   Monath, T.P., et al., *Lassa fever in the Eastern Province of Sierra Leone, 1970-1972. II. Clinical observations and virological studies on selected hospital cases.* Am J Trop Med Hyg, 1974. **23**(6): p. 1140-9.

107.   Huang, C., et al., *Junin virus infection activates the type I interferon pathway in a RIG-I-dependent manner.* PLoS Negl Trop Dis, 2012. **6**(5): p. e1659.

108.   Kolokoltsova, O.A., et al., *RIG-I enhanced interferon independent apoptosis upon Junin virus infection.* PLoS One, 2014. **9**(6): p. e99610.

109.   Lefterova, M.I., et al., *Next-Generation Sequencing for Infectious Disease Diagnosis and Management: A Report of the Association for Molecular Pathology.* J Mol Diagn, 2015. **17**(6): p. 623-34.

110.   Datta, S., et al., *Next-generation sequencing in clinical virology: Discovery of new viruses.* World J Virol, 2015. **4**(3): p. 265-76.

111.   Drosten, C., et al., *Molecular diagnostics of viral hemorrhagic fevers.* Antiviral Res, 2003. **57**(1-2): p. 61-87.

112.   Palacios, G., et al., *Panmicrobial oligonucleotide array for diagnosis of infectious diseases.* Emerg Infect Dis, 2007. **13**(1): p. 73-81.

113.   Ölschläger, S. and S. Günther, *Rapid and Specific Detection of Lassa Virus by Reverse Transcription-PCR Coupled with Oligonucleotide Array Hybridization.* Journal of Clinical Microbiology, 2012. **50**(7): p. 2496-2499.

114.   Ibekwe, T.S., et al., *The sensitivity and specificity of Lassa virus IgM by ELISA as screening tool at early phase of Lassa fever infection.* Nigerian Medical Journal : Journal of the Nigeria Medical Association, 2012. **53**(4): p. 196-199.

115.   Ruo, S.L., et al., *Antigenic relatedness between arenaviruses defined at the epitope level by monoclonal antibodies.* J Gen Virol, 1991. **72 (Pt 3)**: p. 549-55.

116.   Sanchez, A., et al., *Junin virus monoclonal antibodies: characterization and cross-reactivity with other arenaviruses.* J Gen Virol, 1989. **70 (Pt 5)**: p. 1125-32.

117.	Nakauchi, M., et al., *Characterization of monoclonal antibodies to Junin virus nucleocapsid protein and application to the diagnosis of hemorrhagic fever caused by South American arenaviruses.* Clin Vaccine Immunol, 2009. **16**(8): p. 1132-8.

118.	Parker, W.B., *Metabolism and antiviral activity of ribavirin.* Virus Res, 2005. **107**(2): p. 165-71.

119.	McCormick, J.B., et al., *Lassa fever. Effective therapy with ribavirin.* N Engl J Med, 1986. **314**(1): p. 20-6.

120.	Kilgore, P.E., et al., *Prospects for the control of Bolivian hemorrhagic fever.* Emerg Infect Dis, 1995. **1**(3): p. 97-100.

121.	Pasquato, A. and S. Kunz, *Novel drug discovery approaches for treating arenavirus infections.* Expert Opin Drug Discov, 2016. **11**(4): p. 383-93.

122.	Pasquato, A., D.J. Burri, and S. Kunz, *Current drug discovery strategies against arenavirus infections.* Expert Rev Anti Infect Ther, 2012. **10**(11): p. 1297-309.

123.	Enria, D.A. and J.G. Barrera Oro, *Junin virus vaccines.* Curr Top Microbiol Immunol, 2002. **263**: p. 239-61.

124.	McCormick, J.B., et al., *Inactivated Lassa virus elicits a non protective immune response in rhesus monkeys.* J Med Virol, 1992. **37**(1): p. 1-7.

125.	Lukashevich, I.S., et al., *A live attenuated vaccine for Lassa fever made by reassortment of Lassa and Mopeia viruses.* J Virol, 2005. **79**(22): p. 13934-42.

126.	Carrion, R., Jr., et al., *A ML29 reassortant virus protects guinea pigs against a distantly related Nigerian strain of Lassa virus and can provide sterilizing immunity.* Vaccine, 2007. **25**(20): p. 4093-102.

127.	Lukashevich, I.S., et al., *Safety, immunogenicity, and efficacy of the ML29 reassortant vaccine for Lassa fever in small non-human primates.* Vaccine, 2008. **26**(41): p. 5246-54.

128.	Fisher-Hoch, S.P., et al., *Effective vaccine for lassa fever.* J Virol, 2000. **74**(15): p. 6777-83.

129.	Geisbert, T.W., et al., *Development of a new vaccine for the prevention of Lassa fever.* PLoS Med, 2005. **2**(6): p. e183.

130.	Safronetz, D., et al., *A recombinant vesicular stomatitis virus-based Lassa fever vaccine protects guinea pigs and macaques against challenge with geographically and genetically distinct Lassa viruses.* PLoS Negl Trop Dis, 2015. **9**(4): p. e0003736.

131.	Bredenbeek, P.J., et al., *A recombinant Yellow Fever 17D vaccine expressing Lassa virus glycoproteins.* Virology, 2006. **345**(2): p. 299-304.

132.	Olschlager, S. and L. Flatz, *Vaccination strategies against highly pathogenic arenaviruses: the next steps toward clinical trials.* PLoS Pathog, 2013. **9**(4): p. e1003212.

133.	Whitton, J.L., *Designing arenaviral vaccines.* Current topics in microbiology and immunology, 2002. **263**: p. 221-38.

134.	Richmond, J.K. and D.J. Baglole, *Lassa fever: epidemiology, clinical features, and social consequences.* BMJ, 2003. **327**(7426): p. 1271-5.

135.	Pushko, P., et al., *Individual and bivalent vaccines based on alphavirus replicons protect guinea pigs against infection with Lassa and Ebola viruses.* J Virol, 2001. **75**(23): p. 11677-85.

136.	Burton, D.R., et al., *Broadly neutralizing antibodies present new prospects to counter highly antigenically diverse viruses.* Science, 2012. **337**(6091): p. 183-6.

137.	Wilkinson, D.E., et al., *Comparison of platform technologies for assaying antibody to Ebola virus.* Vaccine, 2017. **35**(9): p. 1347-1352.

138.	Bergthaler, A., et al., *Impaired antibody response causes persistence of prototypic T cell-contained virus.* PLoS Biol, 2009. **7**(4): p. e1000080.

139.	Parren, P.W. and D.R. Burton, *The antiviral activity of antibodies in vitro and in vivo.* Adv Immunol, 2001. **77**: p. 195-262.

140.	Burton, D.R. and J.R. Mascola, *Antibody responses to envelope glycoproteins in HIV-1 infection.* Nat Immunol, 2015. **16**(6): p. 571-6.

141.	Hangartner, L., R.M. Zinkernagel, and H. Hengartner, *Antiviral antibody responses: the two extremes of a wide spectrum.* Nat Rev Immunol, 2006. **6**(3): p. 231-43.

142.	Hotaling, N.A., et al., *BIOMATERIAL STRATEGIES FOR IMMUNOMODULATION.* Annual review of biomedical engineering, 2015. **17**: p. 317-349.

143.	Slifka, M.K. and I. Amanna, *How advances in immunology provide insight into improving vaccine efficacy.* Vaccine, 2014. **32**(25): p. 2948-2957.

144.	Hubbell, J.A., S.N. Thomas, and M.A. Swartz, *Materials engineering for immunomodulation.* Nature, 2009. **462**(7272): p. 449-460.

145.	Mildner, A. and S. Jung, *Development and Function of Dendritic Cell Subsets.* Immunity, 2014. **40**(5): p. 642-656.

146.	Vyas, J.M., A.G. Van der Veen, and H.L. Ploegh, *The known unknowns of antigen processing and presentation.* Nature reviews. Immunology, 2008. **8**(8): p. 607-618.

147.   Turley, S.J., A.L. Fletcher, and K.G. Elpek, *The stromal and haematopoietic antigen-presenting cells that reside in secondary lymphoid organs.* Nat Rev Immunol, 2010. **10**(12): p. 813-825.

148.   Kambayashi, T. and T.M. Laufer, *Atypical MHC class II-expressing antigen-presenting cells: can anything replace a dendritic cell?* Nat Rev Immunol, 2014. **14**(11): p. 719-730.

149.   Malhotra, D., A.L. Fletcher, and S.J. Turley, *Stromal and hematopoietic cells in secondary lymphoid organs: partners in immunity.* Immunological reviews, 2013. **251**(1): p. 160-176.

150.   Reddy, S.T., et al., *Exploiting lymphatic transport and complement activation in nanoparticle vaccines.* Nat Biotechnol, 2007. **25**(10): p. 1159-64.

151.   Bramwell, V.W. and Y. Perrie, *Particulate delivery systems for vaccines: what can we expect?* Journal of Pharmacy and Pharmacology, 2006. **58**(6): p. 717-728.

152.   Chadwick, S., C. Kriegel, and M. Amiji, *Nanotechnology solutions for mucosal immunization.* Advanced Drug Delivery Reviews, 2010. **62**(4): p. 394-407.

153.   Ahmed, F., et al., *Biodegradable polymersomes loaded with both paclitaxel and doxorubicin permeate and shrink tumors, inducing apoptosis in proportion to accumulated drug.* Journal of Controlled Release, 2006. **116**(2): p. 150-158.

154.   Cerritelli, S., et al., *Aggregation Behavior of Poly(ethylene glycol-bl-propylene sulfide) Di- and Triblock Copolymers in Aqueous Solution.* Langmuir, 2009. **25**(19): p. 11328-11335.

155.   Bachmann, M.F. and G.T. Jennings, *Vaccine delivery: a matter of size, geometry, kinetics and molecular patterns.* Nat Rev Immunol, 2010. **10**(11): p. 787-796.

156.   Reddy, S.T., et al., *In vivo targeting of dendritic cells in lymph nodes with poly(propylene sulfide) nanoparticles.* Journal of Controlled Release, 2006. **112**(1): p. 26-34.

157.   Stano, A., et al., *Tunable T cell immunity towards a protein antigen using polymersomes vs. solid-core nanoparticles.* Biomaterials, 2013. **34**(17): p. 4339-46.

158.   Scott, E.A., et al., *Dendritic cell activation and T cell priming with adjuvant- and antigen-loaded oxidation-sensitive polymersomes.* Biomaterials, 2012. **33**(26): p. 6211-9.

159.   Marrack, P., A.S. McKee, and M.W. Munks, *Towards an understanding of the adjuvant action of aluminium.* Nature reviews. Immunology, 2009. **9**(4): p. 287-293.

160.   Casella, C.R. and T.C. Mitchell, *Putting endotoxin to work for us: monophosphoryl lipid A as a safe and effective vaccine adjuvant.* Cell Mol Life Sci, 2008. **65**(20): p. 3231-40.

161.   Martins, K.A.O., et al., *Adjuvant-enhanced CD4 T Cell Responses are Critical to Durable Vaccine Immunity.* EBioMedicine, 2016. **3**: p. 67-78.

162.   Pravetoni, M., et al., *Effect of Currently Approved Carriers and Adjuvants on the Pre-Clinical Efficacy of a Conjugate Vaccine against Oxycodone in Mice and Rats.* PLoS ONE, 2014. **9**(5): p. e96547.

163.   Mark, K.E., et al., *Three Phase III Randomized Controlled Trials of Topical Resiquimod 0.01-Percent Gel To Reduce Anogenital Herpes Recurrences.* Antimicrobial Agents and Chemotherapy, 2014. **58**(9): p. 5016-5023.

164.   Ma, F., et al., *The TLR7 agonists imiquimod and gardiquimod improve DC-based immunotherapy for melanoma in mice.* Cellular and Molecular Immunology, 2010. **7**(5): p. 381-388.

165.   Kasturi, S.P., et al., *Programming the magnitude and persistence of antibody responses with innate immunity.* Nature, 2011. **470**(7335): p. 543-547.

166.   Steinhagen, F., et al., *TLR-based immune adjuvants.* Vaccine, 2011. **29**(17): p. 3341-55.

CHAPTER 2

Oxidation-sensitive polymersomes as vaccine nanocarriers enhance humoral responses against Lassa virus envelope glycoprotein

Clara Galan-Navarro[2], Marcela Rincon-Restrepo[2], Gert Zimmer[3] Erica Ollmann-Saphire[4], Jeffrey A. Hubbell[2,5,] Sachiko Hirosue[2*], Melody A. Swartz[2,5*], and Stefan Kunz[1*]

[1] Institute of Microbiology, Lausanne University Hospital. Lausanne, Switzerland
[2] Laboratory of Lymphatic and Cancer Bioengineering, Institute of Bioengineering, École Polytechnique Féderal de Lausanne (EPFL) 1015 Lausanne, Switzerland
[3] Division of Virology, Institute of Virology and Immunology, 3147 Mittelhäusern, Switzerland
[4] Department of Immunology and Microbiology, The Scripps Research Institute, La Jolla, California, United States of America. Skaggs Institute for Chemical Biology, The Scripps Research Institute, La Jolla, California, United States of America
[5] Institute for Molecular Engineering and Ben May Department of Cancer Research, University of Chicago, IL, United States of America

* Corresponding authors. Mailing address: Institute of Microbiology, University Hospital Center and University of Lausanne, Lausanne CH-1011, Switzerland. Phone: +41-21 314 7743, Fax: +41-21 314 4060. E-mail: Stefan Kunz, Stefan.Kunz@chuv.ch; Sachiko Hirosue, sach@alum.mit.edu; Melody Swartz, melodyswartz@uchicago.edu.

Abstract: 150 words

--In press—

ABSTRACT

Lassa virus (LASV) causes severe hemorrhagic fever with high mortality, yet no vaccine currently exists. Antibodies targeting viral attachment proteins are crucial for protection against many viral infections. However, the envelope glycoprotein (GP)-1 of LASV elicits weak antibody responses due to extensive glycan shielding. Here, we explored a novel vaccine strategy to enhance humoral immunity against LASV GP1. Using structural information, we designed a recombinant GP1 immunogen, and then encapsulated it into oxidation-sensitive polymersomes (PS) as nanocarriers that promote intracellular MHCII loading. Mice immunized with adjuvanted PS (LASV GP1) showed superior humoral responses than free LASV GP1, including antibodies with higher binding affinity to virion GP1, increased levels of polyfunctional anti-viral CD4 T cells, and IgG-secreting B cells. PS (LASV GP1) elicited a more diverse epitope repertoire of anti-viral IgG. Together, these data demonstrate the potential of our nanocarrier vaccine platform for generating virus-specific antibodies against weakly immunogenic viral antigens.

INTRODUCTION

Lassa virus (LASV) is an Old World arenavirus that causes a severe viral hemorrhagic fever with high mortality in humans [1, 2] and is currently considered one of the most important emerging pathogens by WHO [3]. Endemic in Western Africa from Senegal to Cameroon, LASV causes several hundred thousand infections per year with thousands of deaths. In nature, LASV is carried by persistent infection of reservoir rodent host of *Mastomys* species, semi-domestic rodents that invade human dwellings [1]. Reservoir-to-human transmission represents a major route of human infection [4] and human-to-human transmission has been reported in nosocomial outbreaks [5]. Due to its transmissibility via aerosol [6] and high lethality, LASV is further considered a category A select agent by the Centers of Disease Control [7]. There is currently no licensed vaccine available and the standard of care is limited to supportive measures and the use of ribavirin, which reduces mortality when delivered early in infection [8]. Severe Lassa fever in humans is characterized by extensive viral replication and spread, resulting in high viremia and progressive signs and symptoms of shock. Viral load early in disease is predictive for fatal disease outcome, indicating competition between viral spread and replication and the patient's immune system [9]. Control of primary LASV infection in survivors seems mainly mediated by the anti-viral CD8 T-cell response, whereas neutralizing antibodies appear late during convalescence and are generally of low titers [10].

Antibodies represent a major immunological correlate of protection in many successful vaccines. These protective antibodies control the initial burst of viral replication by neutralizing free virus, thus limiting viral spread. The consequent reduction in viral load provides the host's immune system a window of opportunity to develop a timely adaptive response capable of controlling the pathogen [11]. Studies in numerous viral systems demonstrated that antibodies targeting viral attachment proteins are of particular importance, as they can neutralize free virus by preventing host cell attachment and entry [12-14]. Recently, recombinant monoclonal antibodies (mAb) targeting viral attachment proteins showed promise for protection in prophylactic, post-exposure, and therapeutic settings, as illustrated in groundbreaking studies with recombinant antibody cocktails against Ebola virus [15]. Specific antibodies to viral surface proteins are further of great importance in viral serology diagnostics and epidemiology, in particular in the context of newly emerging or re-emerging pathogens.

Initial trials with killed LASV vaccines failed to elicit protective immunity [16], and the development of a safe and efficacious LASV subunit vaccine capable of inducing robust antibodies titers remains an unsolved problem [17]. A major challenge is the low immunogenicity of the LASV envelope GP1 which decorates the virion spikes, is involved in host cell attachment, and represents the main target for protective antibodies [18-20]. A recent elegant study in a mouse model demonstrated that the inherently low immunogenicity of LASV GP1 is a consequence of extensive epitope shielding by N-linked glycans [21]. This is reminiscent of the surface GPs of other major human pathogens, including human immunodeficiency virus (HIV)-1 and hepatitis C virus (HCV) [11, 22].

29

To enhance immunogenicity of subunit vaccines, a range of antigen nanocarriers have been developed, including polymer-based nanoparticles, liposomes, polymersomes, dendrimers, cyclodextrin-containing polymers, carbon nanotubes, and gold nanoparticles [23]. We recently developed a novel watery-core polymersome (PS) nanocarrier system designed to efficiently deliver antigen to lymph nodes, enhance uptake by dendritic cells (DCs), and promote antigen presentation [24, 25]. Polymersomes are stable vesicles composed of self-assembling oxidation-sensitive block co-polymers, in particular hydrophobic polypropylene sulfide (PPS) in combination with hydrophilic polyethylene glycol (PEG) [25]. Hydrophilic molecules such as soluble recombinant protein antigens and some adjuvants can be incorporated into the watery core of PEG-*bl*-PPS PS, whereas hydrophobic molecules can associate with the leaflet of the membrane bilayer. Previous studies demonstrated that incorporation of model protein antigens into the aqueous core of PS enhances antigen presentation by dendritic cells *in vitro* [25]. *In vivo*, PS induced robust T cell immunity against protein antigens with enhanced frequencies of antigen-specific CD4 T cells [24].

In our present study, we evaluated a new vaccine, consisting of our PS nanocarrier platform in combination with a newly developed immunogen, for its ability to enhance the humoral immune response to the weakly immunogenic LASV GP1 in a mouse model.

RESULTS

Immunogen design, production, and characterization

The LASV glycoprotein precursor GPC is initially synthesized as a single polypeptide that is proteolytically processed into the peripheral GP1 and the membrane-associated GP2 (Fig. 1A). The N-terminal GP1 decorates the tips of the trimeric virion spike and is implicated in receptor binding [26], whereas the transmembrane GP2 resembles fusion-active class I envelope proteins of other viruses [27]. LASV GP1 represents an independent fold with a globular structure [28]. Based on available structural information, we engineered a stable, soluble LASV GP1 fragment comprised of amino acids 92-256, spanning the putative receptor binding sites [28, 29] and known neutralizing epitopes [20] (Fig. 1A). Removal of the 33 N-terminal amino acids of GP1 markedly enhanced expression without affecting the overall fold of the protein [30]. To ensure high expression levels and proper folding, recombinant LASV GP1 was expressed in mammalian cells as a C-terminal fusion protein with the Fc moiety of human IgG1 [31]. To allow efficient removal of the human Fc part after purification, an enterokinase (EK) cleavage site was inserted following the C-terminus of LASV GP1, resulting in the construct LASVGP1-EK-Fc (Fig. 1A). Western blot of the recombinant protein expressed in HEK293E cells revealed the expected apparent molecular masses of the GP1-Fc fusion protein that formed the expected dimer (Fig. 1B).

Large-scale protein expression was carried out in high-density suspension cultures under serum-free conditions, followed by the purification strategy outlined in Fig. 1C. Briefly, conditioned cell culture supernatant was subjected to protein A affinity chromatography, followed by EK cleavage performed on the column, allowing selective elution of LASV GP1 under physiological conditions. Eluted LASV GP1 was further purified by ion exchange chromatography followed by gel filtration, resulting in > 98% pure protein with the expected apparent molecular mass (Fig. 1D). Our construct design resulted in formation of an intermolecular disulfide bond via C230. Accordingly, SDS-PAGE under non-reducing conditions revealed that LASV GP1 formed a dimer (Fig. 1E). To further confirm the expected molecular mass and dimerization of LASV GP1, we combined size-exclusion chromatography with multi angle light scattering (SEC-MALS) (Fig. S1). From the detected molecular mass of the LASV GP1 dimer of 56.1 kDa, only 30.5 kDa corresponded to the predicted polypeptide, indicating extensive post-translational modifications, mainly N-glycosylation, in line with previous studies [29, 32]. Examination of the glycosylation pattern of LASV GP1 revealed the presence of high mannose N-glycans (Fig. S2), similar to GP1 derived from authentic virus [33] and recombinant full-length GP1 [32]. To assess the correct conformation of our recombinant LASV GP1, we tested binding of a panel of previously described conformation-sensitive anti-GP1 mAbs [20] in ELISA. As shown in Fig. S3, all mAb tested recognized our LASV GP1. Together, the data suggest that our LASV GP1 retains at least part of its native conformation and displays a glycosylation pattern similar to GP1 from authentic virus, making it a suitable immunogen for our studies.

Preparation of polymersomes loaded with LASV GP1 antigen

PEG-*bl*-PPS PS (Fig. 2A) were synthesized as outlined in Fig. 2B and described in Materials and Methods [24, 25]. To monitor efficiency of immunogen encapsulation, recombinant purified LASV GP1 was fluorescence labeled with the fluorophore AF594. Considering the small molecule nature of the fluorophore, we did not expect a significant impact on the physicochemical nature of our recombinant immunogen. After 48 h incubation at 4°C, PS were extruded and purified by gel filtration chromatography. A significant proportion of LASV GP1 co-eluted with the PS fraction, indicating efficient antigen loading (Fig. 2C). To validate the integrity of the encapsulated antigen, loaded PS were lysed with 0.5% Triton-X 100 and analyzed by SDS-PAGE. The antigen recovered from PS migrated similar to the input, indicating conservation of the dimeric from during the encapsulation process (Fig. 2D). Remaining free LASV GP1 was removed by size exclusion chromatography. Nanoparticles in the 100 nm range ensure efficient lymphatic transport and delivery to antigen-presenting cells in lymph nodes upon intradermal or subcutaneous immunization [24]. The resulting PS (LASV GP1) displayed an average size range of 163 ±7 nm, with a polydispersity index of 0.1 ± 0.05 (Fig. 2E), which was suitable for our immunization studies.

Delivery of LASV GP1 via PS enhances the quality of the antibody response

To evaluate the capacity of PS to induce an anti-LASV GP1 antibody response, age- and sex-matched groups of five adult C57BL/6 mice each were immunized with 10 ᶍg of antigen as PS (LASV GP1) or free LASV GP1, in combination with 10 ᶍg monophosphoryl lipid A (MPLA), an adjuvant that represents a detoxified lipopolysaccharide derivative [34]. As a ligand for Toll-like receptor (TLR)-4, MPLA is capable of enhancing cellular and humoral immune responses and is included in several vaccines undergoing phase III clinical trials. Mice received a prime-boost immunization three weeks apart with the same immunogen formulation (Fig. 3A). When compared to free antigen, mice that had received PS (LASV GP1) showed similar to mildly enhanced titers of anti-LASV GP1-specific IgG on days 28, 60, and 105 after immunization, as assessed by ELISA (Fig. 3B). Analysis of the IgG isotypes revealed similar trends to those observed with total IgG. On day 28, both groups had high titers of anti-LASV GP1 IgG2a and IgG2c and robust levels of antigen-specific IgG1, whereas titers of IgG3 were generally low (Fig. 3B). As expected, immunization with empty PS did not elicit detectable titers of LASV GP1-specific antibodies (data not shown).

A major immunological correlate of protection in viral infection and anti-viral vaccines are antibodies binding with high affinity to the viral attachment protein in its native conformation [11]. To detect such virus-binding anti-LASV GP1 antibodies in sera of immunized mice, we employed a solid-phase virus-binding assay (Fig. 3C). Since LASV is classified as a biosafety level (BSL)-4 agent work with live virus is restricted to high containment laboratories. To detect LASV-binding antibodies, we used recombinant lymphocytic choriomeningitis virus expressing LASV GP (rLCMV-LASVGP) that

has been widely used as a BSL2 model for the characterization of LASV tropism and entry *in vitro* [35-38] and *in vivo* [39, 40]. Previous studies revealed that GP1 of rLCMV-LASVGP closely resembles authentic LASV [33], making the chimera a suitable tool to detect virus-binding antibodies. The rLCMV-LASVGP was produced in BHK-21 cells, followed by purification via ultracentrifugation over a renografin gradient as described [41]. Purified virus was immobilized in microtiter plates and incubated with serial dilutions of sera derived from vaccinated and control mice. Virus-bound antibodies were detected via a secondary antibody in a color reaction. Sera of mice immunized with free antigen contained only low titers of virus-binding antibodies (Fig. 3D). In contrast, animals immunized with PS (LASV GP1) consistently developed higher titers of virus-binding antibodies that became detectable after day 28 and stayed high by day 60 and 105 (Fig. 3D).

To assess the neutralizing capacity of sera immunized with PS (LASV GP1), we employed a well-established pseudotype assay based on recombinant replication-deficient vesicular stomatitis virus (VSV) containing a luciferase reporter [42] displaying full-length LASV GP (Fig. S2A). The rVSV-LASVGP pseudotypes were mixed with sera in presence or absence of complement for one hour at 37°C. The mix of pseudotypes and antibodies was added to fresh monolayers of A549 cells and infection detected by luciferase assay as described [43]. Despite robust titers of virus-binding anti-LASV GP1 antibodies present in serum of PS (LASV GP1)-immunized mice, we failed to detect significant neutralizing activity under our assay conditions on days 28, 60, and 106 (Fig. S2B). This suggests that the virus-binding LASV GP1 antibodies were either non-neutralizing or present at insufficient concentrations to allow neutralization.

Encapsulation of LASV GP1 antigen in PS enhances follicular helper CD4 T cells, polyfunctional CD4 T cells, and antigen-specific B cells.

Next, we investigated if the increased virus-specific antibody titers in PS (LASV GP1)-immunized mice correlated with enhanced CD4 T cell and B cell responses. To this end, we immunized groups of mice as shown in Fig. 3A. After 28 d, spleens and draining lymph nodes (LN) were collected and the CD4 T cell responses evaluated by *ex vivo* re-stimulation assay, using purified LASV GP1 antigen. As a control, we used purified human Fc to assure that the CD4 T cell responses were indeed directed to the viral protein and not remaining traces of Fc. No response was induced upon re-stimulation with human-Fc (data not shown), confirming specificity to the LASV GP1 antigen. First, we evaluated whether immunization with PS (LASV GP1) enhanced the frequency of antigen-specific CD4 T follicular helper (Tfh) cells using the markers CXCR5 and PD1 in flow cytometry [44]. The percentage of CD4 Tfh cells was significantly enhanced in LN, but not in spleen of PS (LASV GP1)-immunized animals (Fig. 4A). Next, we assessed the surface phenotype of total CD4 T cells using the markers CD25 and CD44 [45] and observed a significant increase in the expression of both markers in LN and spleens of mice immunized with PS (LASV GP1), suggesting enhanced CD4 T cell activation upon PS immunization

(Fig. 4B). Virus-specific CD4 T cells isolated from spleens and LN of PS (LASV GP1)-immunized animals secreted significantly higher amounts of IFNγ compared to the group that had received protein only (Fig. 4C). Immunization with PS (LASV GP1) likewise enhanced the frequency of TNFα-producing CD4 T cells, whereas the increase in spleen was not significant (Fig. 3C). Moreover, we observed significantly enhanced frequencies of polyfunctional IFNγ/TNFα-secreting CD4 T cells in LN, but not in spleen (Fig. 4C). Next we sought to investigate possible effects of our PS delivery system on the frequencies of antigen-specific IgG-secreting B cells. For this purpose we performed ELISpot assays using our LASV GP1 as antigen. As shown in Fig 4D, we observed a marked increase in the frequency of antigen-specific IgG secreting B cells derived from LN and spleens isolated from mice immunized with PS (LASV GP1).

Polymersome-delivery broadens the epitope-range of anti-LASV GP1 antibodies

The detection of robust titers of virus-binding antibodies (Fig. 2D) and enhanced frequencies of antigen-specific B cells in animals immunized with PS (LASV GP1) but not free antigen (Fig. 4D), indicated a marked effect of PS-delivery on the quality of the antibody response. To quantitatively compare the breadth of the anti-LASV GP1 antibody response induced by PS (LASV GP1) *vs*. free antigen, we employed peptide arrays. The custom-made array format consisted of glass slides displaying 20mer peptides covering the entire sequence of our antigen with an off-set of one amino acid (Fig. 5A). This type of array has been widely used to study the epitope specificity of antibody responses in a reliable and quantitative manner [46]. The presentation of linear synthetic peptides may not recapitulate some conformational epitopes present on LASV GP1, which is a limitation of the system. In line with the detection of important differences in the specific antibody responses towards PS (LASV GP1) compared to free antigen, our peptide arrays revealed a significantly broader epitope range of antibodies present in sera derived from mice immunized with PS (LASV GP1) (Fig. 5A-C). Based on recently determined high-resolution X-ray structures of LASV GP1 [28] and the GP1 of the structurally and genetically closely related LCMV [47], we made a first attempt to localize the epitopes recognized by the antibodies elicited in our immunization studies (Fig. 5D). Immunization with free antigen induced antibodies that bound predominantly to the N-terminal (epitope L95-S111) and C-terminal part (epitope P236-I239) of LASV GP1. In contrast, antigen delivery by PS resulted in the generation of antibodies capable to bind the core of LASV GP1. Some of the structures recognized were located in the upper face of GP1 that is exposed in the context of the mature GP1/GP2 trimer at the viral surface (Fig. 5D). Specifically, epitope N114-N119 was located upstream of α-helix 1, while epitope S139-N148 was located within a link region between α-helix 1 and the β-3 domain. Epitope N185-N191 mapped to the α-3 domain. Overall, the data corroborates that our PS platform enhanced the quality of the immune response to LASV GP1 by broadening the epitope range of the induced anti-viral antibodies.

34

DISCUSSION

In the present study, we evaluated a PS-based nanocarrier platform for its ability to improve the antibody response against the poorly immunogenic surface antigen of LASV. Delivery of a recombinant LASV GP1-derived immunogen via PS enhanced the magnitude and the quality of the antibody response, inducing robust titers of virus-binding antibodies. Immunization with PS further enhanced the quality of the CD4 T cell and B cell response, resulting in a broader epitope range.

A large body of clinical and experimental evidence indicates that primary LASV infection in humans and animals is controlled mainly via the anti-viral CD8 T cell response, whereas anti-GP1 antibodies appear only late in convalescence and are generally of low titer [48]. Recent studies in a murine model revealed an inherent lack of immunogenicity of LASV GP1 [21], a characteristic shared by envelope GPs of other important human pathogenic viruses [14, 22, 49]. The poorly immunogenic LASV GP1 was therefore ideally suited as a relevant and well-characterized example for the evaluation of our PS platform in a mouse model *in vivo*, setting the bar rather high. Based on recent structural studies, we successfully generated a suitable recombinant LASV GP1-derived immunogen containing major antigenic sites involved in receptor binding and neutralization. When expressed in mammalian cells, the LASV GP1 fragment retained conformational epitopes and displayed an N-glycosylation pattern consistent with the authentic virus-derived antigen [29, 32]. Encapsulation of the immunogen into the watery core of PEG-*bl*-PPS PS was efficiently carried out under physiological pH and ionic strength. This mild encapsulation conditions avoided any chemical modification of the protein, ensuring conservation of the native conformation.

Employing a murine model that has been extensively used to study antibody responses to arenaviruses, we investigated the impact of PS encapsulation on the immunogenicity of our LASV GP1 antigen. Antigen encapsulation into PS enhanced overall LASV GP1-specific antibody titers and markedly increased virus-binding antibodies, capable of recognizing GP1 in the context of the authentic virion spike. Using a well-established assay based on pseudotypes, similar to the one employed in recent studies on human neutralizing mAb to LASV [20], we were however unable to detect significant neutralization (Fig S2B). This resembles the situation in human patients and experimental infection in non-human primates, where convalescent sera contain generally low titers of neutralizing antibodies [50]. In our system, neutralizing antibodies may be present in the serum, albeit at too low titers to be detected in our assay. Alternatively, the virus-binding anti-LASV GP1 antibodies may be non-neutralizing. Interestingly, studies with the closely related LCMV revealed that the generation of non-neutralizing antibodies directed towards GP1 could contribute to protection *in vivo* [51]. However, since rLCMV-LASVGP infection in the mouse, even at high dose, results in only transient low-level viremia [39], this challenge model appears not suitable for viral challenge studies in our context.

Delivery of LASV GP1 via PS resulted in higher frequencies of follicular helper CD4 T cells, which represent a unique subset of CD4 T cell providing help to B cells within germinal centers,

promoting affinity maturation, class switch, plasma cell differentiation, and memory formation. Encapsulation of the antigen in PS increased the numbers of antigen-specific CD4 T cells and the frequency of polyfunctional IFN-γ /TNF-α secreting CD4 T cells. The higher frequency of antigen-specific IgG-secreting B cells in spleens of PS immunized mice was in line with the observed increase of the humoral response in terms of both magnitude and quality.

Screening with peptide arrays provided first evidence that the PS-delivered antigen improved the humoral immune response by broadening the epitope range. In contrast to free protein, PS (LASV GP1) induced the formation of antibodies reactive with the epitopes N114-N119, S139-N148 and N185-N191. Earlier studies on the related LCMV identified the sequence N114-N119 as a site for neutralization [52][189][189][189]. Recently, Robinson *et al*. characterized a panel of mAbs isolated from human Lassa fever survivors and found neutralizing antibodies directed against the GP1 subunit, specifically against GP1-A and GP1-B binding sites, that involve amino acids present in N114-N119 [20]. In a proof-of-concept study performed in a guinea pig model of Lassa fever, these mAb conferred protection in post-exposure prophylaxis [53]. One of the most relevant epitopes identified in this study in the LASV GP1 region, is the S139-N148 epitope, which is highly conserved among different LASV isolates and Old World arenaviruses and has been proved to be implicated in the interaction of LCMV and LASV GP1 with the cellular receptor dystroglycan [47]. The abovementioned epitope locates to the interface of the GP1 trimer which is involved in receptor binding. The N185-N191 LASV GP1 peptide is likewise highly conserved among Old World arenaviruses [47]. In conclusion, our studies demonstrated that PS encapsulation markedly increased the quality and magnitude of the antibody response to our newly designed LASV GP1-derived immunogen, including the generation of virus-binding antibodies. If the augmentation of the specific antibody response observed in our study with the poorly immunogenic LASV GP1 is a general feature of our platform is at this point unclear and more work including envelope glycoproteins from other viruses will be needed to confirm this.

The very recently solved structure of the pre-fusion conformation of the LASV GP1/GP2 trimer spike highlights the relevance of quaternary structures and the GP1/GP2 interface for receptor binding and antibody neutralization [54]. It is at this point unclear if the conformational differences between monomeric LASV GP1 crystallized at low pH [28] and GP1 in the context of the mature GP1/GP2 trimeric spike [54] are due to the different pH, GP1 trimerization, or the presence of GP2. It is therefore possible that our LASV GP1 at neutral pH at least in part resembles the conformation within the trimer. This is indeed suggested by binding of a panel of conformation-sensitive mAb, as well as the observed induction of virus-binding anti-LASV GP1 antibodies by our PS platform. In any case, the novel structural insights into the structure of the mature LASV GP virion spike provide novel and promising leads for the development of a next generation of improved LASV vaccine immunogens. Candidates may then be tested in the context of our platform in order to elicit an optimal neutralizing antibody response. Improved vaccine immunogens may further allow a simplified vaccination approach, ideally

a "single shot" instead of the prime-boost described here. This would be a decisive advantage for vaccine campaigns in remote areas with suboptimal health care infrastructure.

The advent of powerful next-generation sequencing technologies has greatly accelerated the discovery of novel pathogenic viruses [55, 56]. However, such viruses can frequently not be isolated and the limited number of clinical cases makes isolation of B cell clones from survivors challenging. A decisive advantage of our PS platform in the context of emerging viruses is the use of recombinant immunogens that can be designed and produced biosynthetically based on available sequence information. The versatile immunization scaffold of PS combined with the antigen production and efficient encapsulation method that we present here allows rapid production of specific antibodies. Our PS platform may thus allow the development of a "pipeline" to generate recombinant mAb via immunization, followed by B cell sorting and cloning of specific IgG using established methodology [57] within a few months. Such mAb could be rapidly tested for neutralization and evaluated for therapeutic potential. In addition, the availability of specific mAb against novel pathogenic viruses will be invaluable for diagnostic purposes to track epidemics.

MATERIALS AND METHODS

Animals

C57BL/6 female mice, aged 8-12 weeks, were purchased from Harlan (Gannat, France). All animal experiments were performed under the approval from the Veterinary Authority of the Canton of Vaud (Switzerland) according to Swiss regulations of animal welfare (animal protocol number 2502.1 and 2235.1).

Cells and viruses

Human lung carcinoma epithelial (A549) cells were cultured in Dulbecco modified Eagle medium (DMEM) containing10% (vol/vol) fetal bovine serum (FBS), supplemented with glutamine and penicillin-streptomycin (Pen/Strep). The generation, growth, and purification of recombinant lymphocytic choriomeningitis virus expressing the LASV glycoprotein (rLCMV-LASVGP) has been described elsewhere [35]. According to the institutional biosafety guidelines of the Lausanne University Hospital, the chimera rLCMV-LASVGP has been classified as a biosafety level (BSL) 2 pathogen for use in cell culture. For viral quantification, a previously described immunofocus assay (IFA) was performed [58].

Construction of the expression construct LASVGP1Δ33-EK-huFc

For the construction of the expression construct LASVGP1Δ33-EK-huFc pcDNA3.1 IntA, cDNA fragments coding for the a LASVGP1 fragment from which residues 58-92 (not starting from the SSP) were removed from the N terminal part, were amplified by PCR introducing a 5'-HindIII restriction site and a C-terminal enterokinase (EK) recognition sequence (DDDDKI) followed by a 3' BamHI restriction site using the primer sequences 5'-CGC AAG CTT ATG GAG ACA GAC ACA CTC CTG CTA-3' Rev: 5'-ATA AGG ATC CCC GAT CTT GTC ATC GTC ATC GCT TAT GTA GAT GTC ACG GGT GCG-3'. The PCR product was then digested with HindIII and BamHI and inserted into the expression vector pcDNA3.1 IntA (kindly provided by Dr. Robert Garry, Tulane University) together with a cDNA fragment coding for human IgG1 Fc, obtained from the construct DGFc5 pcDNA3 described previously [59], via digestion with BamHI and XhoI. The final construct was verified by DNA sequencing.

Recombinant protein expression and purification

Suspension-adapted HEK-293E cells were maintained in serum-free ExCell 293 medium (SAFC Biosciences, St. Louis, MO), supplemented with 4 mM glutamine. On the day before transfection, cells were seeded in fresh medium at a density of 10^6 cells/ml. After 16-14 h, the cells were harvested, separated by centrifugation for 5 min and 2 x 10^7 cells re-suspended in 50 ml of RPMI 1640 containing 0.1% pluronic F68 (SABiosciences, Qiagen AG, Hombrechtikon, Switzerland) in a 250 ml glass bottle. Plasmid DNA of the LASVGP1Δ33-EK-huFc construct (1.5 mg) and 3 mg of linear 25 kDa

polyethylenimine (Polysciences, Eppenheim, Germany) in a solution of 1 mg/ml in water were sequentially added to the culture and mixed. The culture was agitated by orbital shaking at 110 rpm in an ISF-4-W incubator (Kühner AG, Birsfelden, Switzerland) at 37°C in the presence of 5% CO_2. After 60 min, the 50 ml transfection mix was transferred into a 2 l glass bottle containing 450 ml of FreeStyle medium (Invitrogen, California) supplemented with 4 mM glutamine and 3.75 mM valproic acid. The culture was transferred to an incubator shaker at 37°C with 5% CO_2 with agitation at 110 rpm. At 7 days post-transfection, cell culture medium was recovered by centrifugation at 2,500 rpm for 10 min and filtered through a 0.22 μm membrane.

Conditioned supernatant containing recombinant LASVGP1Δ33-EK-huFc protein was loaded onto a protein A sepharose 4B affinity chromatography column (5 ml matrix volume) at a rate of 0.5ml/min at 4°C. After washing with 40 volumes of PBS, the column was equilibrated with 10 volumes of enterokinase (EK) buffer (20 mM Tris/HCl, 50 mM NaCl, 2 mM $CaCl_2$, pH 7.5). Enterokinase (New England Biolabs, MA) was diluted in EK cleavage buffer (0.32μg purified enzyme in 5ml) and loaded onto the protein A column containing bound LASVGP1Δ33-EK-huFc protein. Cleavage was performed at RT for 6 h, followed by elution with EK buffer. Remaining EK in the eluate was inactivated by adding trypsin inhibitor conjugated to agarose beads (New England Biolabs, MA). The absence of residual human IgG1 Fc from eluates was verified by Western blot analysis as described [59].

For ion exchange chromatography (IEC), the most concentrated factions obtained from the EK cleavage above were diluted 20 x with binding buffer (20 mM Tris/HCl, pH 8.0) and loaded onto a 4.7 ml HiScreen Q-sepharose high performance (HP) column at a flow rate of 1 ml/min. Unbound protein was removed by washing with 10 volumes of binding buffer and bound protein eluted with a linear gradient (20 volumes) from 0 to 100% elution buffer (20 mM Tris/HCl, pH 8.0, 1 M NaCl) at a flow rate of 1 ml/min. Fractions of 2 ml were collected and analyzed by SDS–PAGE and Coomassie blue staining. The fractions containing LASVGP1Δ33, henceforth referred to as LASVGP1, were pooled and concentrated to 2 ml in an Amicon Ultra-15 centrifugation concentrator with a cut-off of 10 kDa (Millipore, Darmstadt, Germany).

For subsequent size exclusion chromatography, the concentrated pool from the IEC was loaded onto a 121 ml HiLoad S200 16/60 Prep Grade Superdex-200 column pre-equilibrated in PBS at a flow rate of 1 ml/min. Fractions of 2 ml were collected and analyzed by SDS-PAGE and Coomassie blue staining. Fractions containing LASV GP1 were pooled and concentrated in an Amicon Ultra-15 centrifugation concentrator (10 kDa cut-off), followed by and sterile filtration through a Millipore 0.22 μm Millex-GP membrane. Overall protein yields were 5 mg/l of starting material and purity was >98%.

Block-copolymer synthesis and polymersome preparation

All chemical reagents were reagent grade and purchased from Sigma-Aldrich, MO, unless otherwise stated. Polymerosomes (PS) were prepared as described [25]. Briefly, block-copolymers were

synthesized using benzyl mercaptan to start the living polymerization of propylene sulfide (PPS). The terminal thiolates were capped with PEG-mesylate. For purification, the co-polymers were precipitated two times in cold methanol. The purity and length of the PPS chain were confirmed by gel chromatography and NMR. Chains of PEG_{17}-bl-$PPS_{x,}$ containing between x=26-32 PPS units were used to form PS. An amount of 30-50 mg was re-suspended in dichloromethane and placed in piranha-etched glass vials to desiccate overnight. For the formation of PS with LASV GP1, a thin film of copolymer was rehydrated with a solution of 500 μl of LASV-GP1 or fluorescence-labeled LASV-GP1 (2 mg/ml) in 50 mM sodium phosphate buffer, and rotated for 48 h at 4°C. Next, the solution was extruded at least four times through a 0.2 μm nucleopore track-etched membrane (Whatman, Maidstone, UK) to obtain PS ranging between 150-170 nm with polydispersity values < 0.2. Purification of the PS loaded with LASV GP1 immunogen from free protein was achieved by size exclusion chromatography through a Sepharose CL-6B column. Fractions containing PS were pooled and further concentrated though an Ultra-centrifugation filter (Amicon Millipore, Darmstadt, Germany) with a cut-off of 100 kDa. Efficiency of LASV GP1 loading into PS was 430 μg/ml calculated by subtracting the amount of the unloaded protein from the starting material used. The size of PS was determined by dynamic light scattering with a Nano Zs Zetasizer (Malvern Instruments, Malvern, UK). PS were controlled for their size and polydispersity, as well as endotoxin levels using the HEK-Blue^TM TLR4 cells and QUANTI-Blue (inVivogen) with endotoxin standard (E-Toxate Endotoxin standard E8029-1VL Sigma-Aldrich) for every batch produced.

SEC-MALS analysis of LASV GP1

For size exclusion chromatography coupled with multiangle light scattering (SEC-MALS), purified LASV GP1 protein was separated on a Superose6 gel filtration column (GE Healthcare, Little Chalfont, UK) pre-equilibrated with 20 mM Tris, 150 mM NaCl, pH 7.5 coupled in-line with a mini DAWN Treos followed by an Optilab T-rEX refractometer (Wyatt Technologies, CA). Data processing and absolute molecular mass calculations were performed using ASTRA software (Wyatt Technologies, CA).

Western blot

Protein Samples were mixed 1:1 with 2x SDS-polyacrylamide gel electrophoresis (PAGE) sample buffer containing 100 mM DTT and boiled (5 min at 95°C). Samples were separated by SDS-PAGE and blotted to nitrocellulose membranes. Membranes were blocked in 3% (w/v) skim milk in PBS and proteins detected with primary antibody after overnight incubation at 4°C using HRP-conjugated secondary antibodies as described [60]. Monoclonal antibody to human IgG1 Fc (Abcam, Cambridge, UK) was used in the dilution 1: 5,000 and polyclonal rabbit anti-mouse-HRP at 1: 3,000. Membranes were developed using enhanced chemiluminescence (ECL) using Amersham ECL Prime Western Blotting Detection Reagent (GE Healthcare lifesciences Little Chalfont, UK). Signal acquisition was performed with ImageQuant LAS 4000Mini (GE Healthcare lifesciences Little Chalfont, UK).

Immunization protocol

All immunizations were administered intra-dermal (i.d.) into the four footpads, under isofluorane anesthesia. For all formulations, 10 μg of LASV GP1 was injected per animal, together with 10 μg of MPLA (Salmonella minnesota R595, AvantiLipids). All PS and proteins batches were tested negatively for endotoxin using a Toll-like receptor activation assay based on HEK-Blue reporter cell lines (Invivogen, CA).

Enzyme-linked immunosorbent assay (ELISA)

For the detection of antigen-specific antibodies in ELISA, 96-well Nunc MaxiSorp® plates were coated with 5 μg/mL of LASV GP1 overnight at 4°C. Plates were washed three times with PBS/ 0.02% (wt/vol) Tween-20 and blocked with 2.5% (wt/vol) casein solution in PBS for 2 h at room temperature (RT). Serial dilutions of serum in 2.5% (wt/vol) casein/PBS were added and incubated for 2 h at RT. Plates were washed four times, following by incubation with HRP-conjugated secondary antibodies specific for and IgG1, IgG2a,c, IgG3 or total IgG (Southern Biotech, Birmingham, AL). After incubation for 1 h at RT, plates were washed four times and developed using 50 μl of 3,3',5,5'-tetramethylbenzidine (eBiosciences, MA). The signal was stopped by adding 20 μl of 2 M H_2SO_4. Plates were analyzed using a plate reader spectrophotometer (Tecan, Mannedorf, Switzerland) by measuring the absorbance at 450 nm with correction at 570 nm. Specific signals were calculated by subtraction of absorbance obtained with samples containing the blocking casein only (background control).

Virus binding assay

For the detection of virus-binding specific antibodies, 96-well Nunc MaxiSorp® plates were coated with Renografin purified and UV-inactivated rLCMV-LASVGP (10^7 PFU/ml in PBS) prepared as described [61] overnight at 4°C. Plates were washed three times with PBS and blocked for 2 h with a 2.5% (wt/vol) casein solution in PBS. Serial dilutions of serum in 2.5% (wt/vol) casein/PBS were added and incubated for 2 h at RT. Plates were washed four times, followed by incubation with HRP-conjugated secondary antibodies against total IgG (Southern Biotech Birmingham, AL). After incubation for 1 h at RT, plates were washed four times and developed and read as described above.

Preparation of cell suspensions and *ex vivo* restimulation

Preparation of cell suspensions and *ex vivo* restimulation was performed as described [24]. Briefly, lymph nodes were digested with collagenase D in DMEM supplemented with 1.2 mM $CaCl_2$, 2% (vol/vol) FBS, Pen/Strep (500μg/ml). After digestion, lymph node cell suspensions were pressed through a 70 μm nylon cell strainer. For spleens, single cell suspensions were prepared by mechanical disruption through a 70 μm nylon cell strainer. Splenocytes were further treated with hypotonic ammonium chloride potassium bicarbonate buffer (150 mM NH_4Cl, 10 mM $KHCO_3$, 0.1 mM EDTA) to lyze red blood cells. For *ex vivo* restimulation, 3 x 10^6 cells were plated in 96-well plates and cultured

in DMEM supplemented with 10% (vol/vol) FBS, Pen/Strep (500μg/ml) for 2 h at 37°C in the presence of 200 μg/ml of purified LASV GP1. As a negative control, cells were restimulated with the Fc portion of human IgG. For detection of intracellular cytokines, 5 μg/ml of Brefeldin A was added to the culture and left for 3 h, followed by washing in cold PBS.

Flow cytometry

Three million cells were plated in cone-shaped 96 well plates, washed once with HBSS, and stained with live/dead fixable cell viability reagent (Life technologies, CA). For surface staining, cells were washed once with HBSS supplemented with 0.5% (wt/vol) BSA (Sigma) (staining buffer) and resuspended in an antibody cocktail using the panel of mAb listed in Supplementary Table 1. For intracellular staining, cells were fixed and permeabilized with the Foxp3/Transcription Factor Fixation/Permeabilization kit (eBiosciences, MA) according to the manufacturer's instructions. Cells were stained in permeabilization buffer with the mAb cocktail described in Supplementary Table 1. After staining, cells were resuspended in staining buffer for analysis by flow cytometry. Flow cytometry was performed using a CyAnTM ADP (Beckman Coulter) and data were analyzed with FlowJo software package (Ashland, OR).

Enzyme-linked immunospot assay (ELISPOT)

B cell ELISPOT assays were performed using the IgG kit (Mabtech, Nacka Strand, Sweden) according to the manufacturer's instructions. Briefly, serial dilutions of cells derived from lymph nodes were plated in duplicates overnight in LASV GP1 coated PVDF 96-well plates (Millipore, Darmstadt, Germany). Unbound cells were removed and wells incubated for 2 h with biotinylated anti-mouse total IgG in PBS. After several washes, wells were incubated with streptavidin conjugated to alkaline phosphatase (AP) for 1 hour. Spots were revealed using 5-bromo-4-chloro-3-indolyl-phosphate/nitro blue tetrazolium (BCIP/NBT), and counted with an automatic reader (Bioreader 2000; BioSys GmbH). Results were represented as number of spots corresponding to antibody-secreting cells per 10^6 total lymph node cells and splenocytes.

Peptide array (CelluspotsTM)

CelluspotsTM (Intavis AG, Cologne, Germany) were designed based on the LASV GP1 sequence spanning from amino acids 92-250 and were comprised of 20mer peptides with an offset of one amino acid. Slides were blocked with blocking buffer, followed by 2 h incubation at RT with sera at 1:200 dilution in blocking buffer. Slides were further washed 3 times with PBS/ 0.02% (wt/vol) Tween-20 and incubated with goat anti mouse IgG conjugated to IR dye 800cw (1:10000) from Li-COR Biotechnology (Lincoln, NE) in blocking buffer for 1 h. Finally, slides were washed 3 times with PBS/ 0.02% (wt/vol) Tween-20. Signals were visualized using the LI-COR Odyssey Infrared Imaging System (LI-COR, Inc., Lincoln, NE).

Pseudovirion neutralization assay

Recombinant propagation-defective vesicular stomatitis virus (VSV) encoding the two reporter proteins green fluorescent protein (GFP) and firefly luciferase (Luc) was generated as described [42]. Recombinant VSV pseudotypes bearing the envelope GP of LASV Josiah were generated as reported earlier [62]. For the pseudovirion neutralization assay, sera were diluted 1:20 in complete MEM, followed by two-fold serial dilutions. For each well (quadruplicates), serum dilutions (50 μl) were mixed with an equal volume of complete MEM containing 4,000 infectious units (IU) of rVSV-LASV GP and incubated for 1 h at 37 °C. Following this incubation, the mixture was added to fresh monolayers of A549 cells cultured in clear bottom white-walled 96-well plates (Costar). After 1 h, the inoculum was removed by washing and fresh medium added. After 20 h at 37 °C and 5% (vol/vol) CO_2, luciferase reporter activity was detected using the Luciferase Assay System (Promega, WI). A GloMax (Promega, WI) microplate reader was used for signal acquisition.

Statistical Analysis

One-way ANOVA followed by a Bonferroni post-test was used to assess statistical differences between the groups with a p-value < 0.05 was used as criterion of statistical significance. All data was analyzed using the GraphPad Prism 5 Software (GraphPad Software Inc., La Jolla, CA). All data presented as bar graphs represent the mean ± standard deviation (SD).
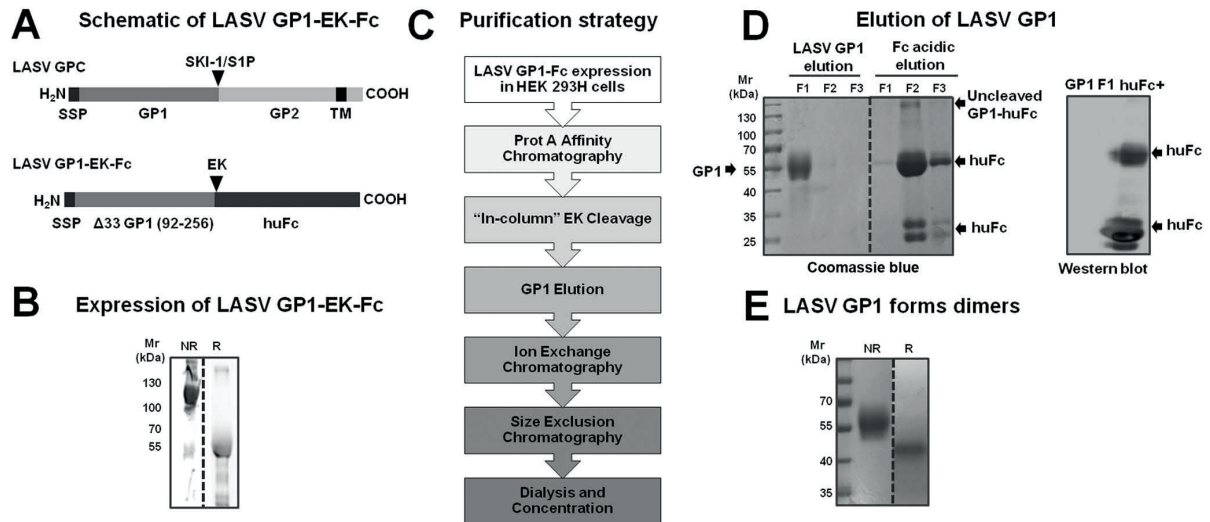
Figure 1. LASV GP1 antigen design, production and characterization. A) Schematic representation of arenavirus GPC and LASV GP1-Fc: The N-terminal receptor-binding GP1 subunit, the C-terminal GP2, the transmembrane domain, and the stable signal peptide (SSP) are indicated, as well as the EK cleavage site and the human Fc moiety. B) Detection of LASV GP1-EK-Fc in Western blot. LASV GP1-EK-Fc was expressed in HEK293T cells by transient transfection. Conditioned supernatants were collected, total protein precipitated, separated by SDS-PAGE under non-reducing (NR) or reducing (R) conditions, and blotted to nitrocellulose. Blots were probed with a human IgG Fc-specific antibody combined with an HRP-conjugated secondary antibody and enhanced chemiluminescence (ECL). Relative molecular masses are indicated. C) Schematic of the purification process. LASV GP1-EK-Fc was expressed in high-density suspension cultures of HEK293H cells in serum-free medium. Cleared conditioned supernatants were subjected to protein A affinity chromatography. Elution of LASV GP1 antigen was performed by EK cleavage of bound LASV GP1-EK-Fc on the column under neutral pH. After subsequent ion exchange and size exclusion chromatography, purified protein were dialyzed against PBS and concentrated. D) Elution of LASV GP1 by EK cleavage. Protein A-bound LASV GP1-EK-Fc was incubated with EK, followed by elution under neutral pH. Fractions were analyzed by SDS-PAGE under non-reducing conditions. Fractions LASV GP1 F1-3 correspond to the eluate and fractions Fc to the IgG Fc moiety eluted under acidic conditions, stained by Coomassie blue. The absence of IgG Fc from LASV GP1 eluate (F1) was verified by Western blot. Purified human IgG1 Fc was included as a positive control. Relative molecular masses are indicated. E) LASV GP1 forms a dimer. LASV GP1 purified as in (C) was separated by SDS-PAGE under reducing (R) and non-reducing (NR) conditions.
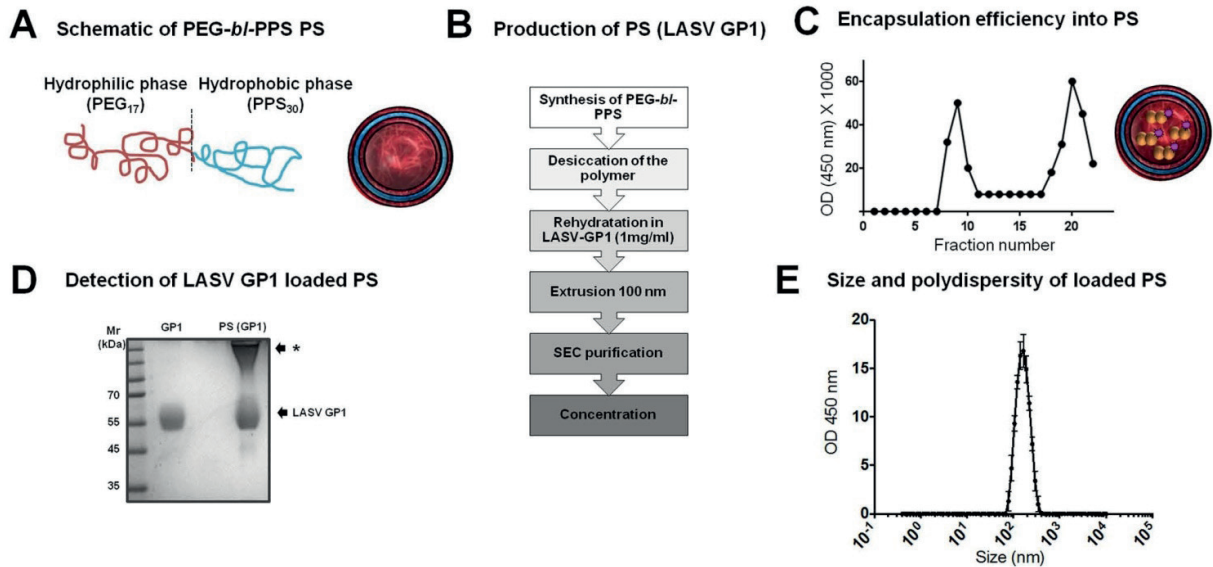
Figure 2. LASV GP1 polymersomes production and purification. A) Schematic representation of PEG-*bl*-PPS block copolymers and vesicles. Block copolymers composed of PEG and PPS self-assemble into oxidation-sensitive polymersomes in aqueous solutions. Hydrophobic and hydrophilic regions are shown in blue and red, respectively. B) Flow sheet of the encapsulation process. After chemical synthesis, the PEG-PPS polymers were desicated and rehydratated in an aqueous solution of LASV GP1. The newly formed PEG-*bl*-PPS PS were then extruded at 100 nm, purified by size exclusion chromatography, and concentrated. C) Encapsulation efficiency into polymersomes. Elution of fluorescent-labeled LASV GP1 after mixing with the PEG-PPS block-copolymers from a size-exclusion column. PS-associated protein (orange spheres) appeared in fractions 7-10, whereas free protein eluteed in fractions 18-22. Fraction numbers are plotted against arbitraty raw absorbance units (RAU). D) Encapsulated protein was recovered from PS by detergent treatment, followed by SDS-PAGE under non-reducing conditions. Recovered protein (PS (GP1)) was compared to reference free protein (GP1). The band corresponding to dimeric LASV GP1 is indicated. The signal corresponding to the apparent high molercular mass aggregates (*) was likely the result of a loading artifact of PS-recovered material that we consistently observed. E) Size and polydispersity of loaded polymersomes were determined as described in Material and Methods. Data shown represent absorbance plotted against paricle diameter. The maximum peak corresponds to 163 ±7 nm.
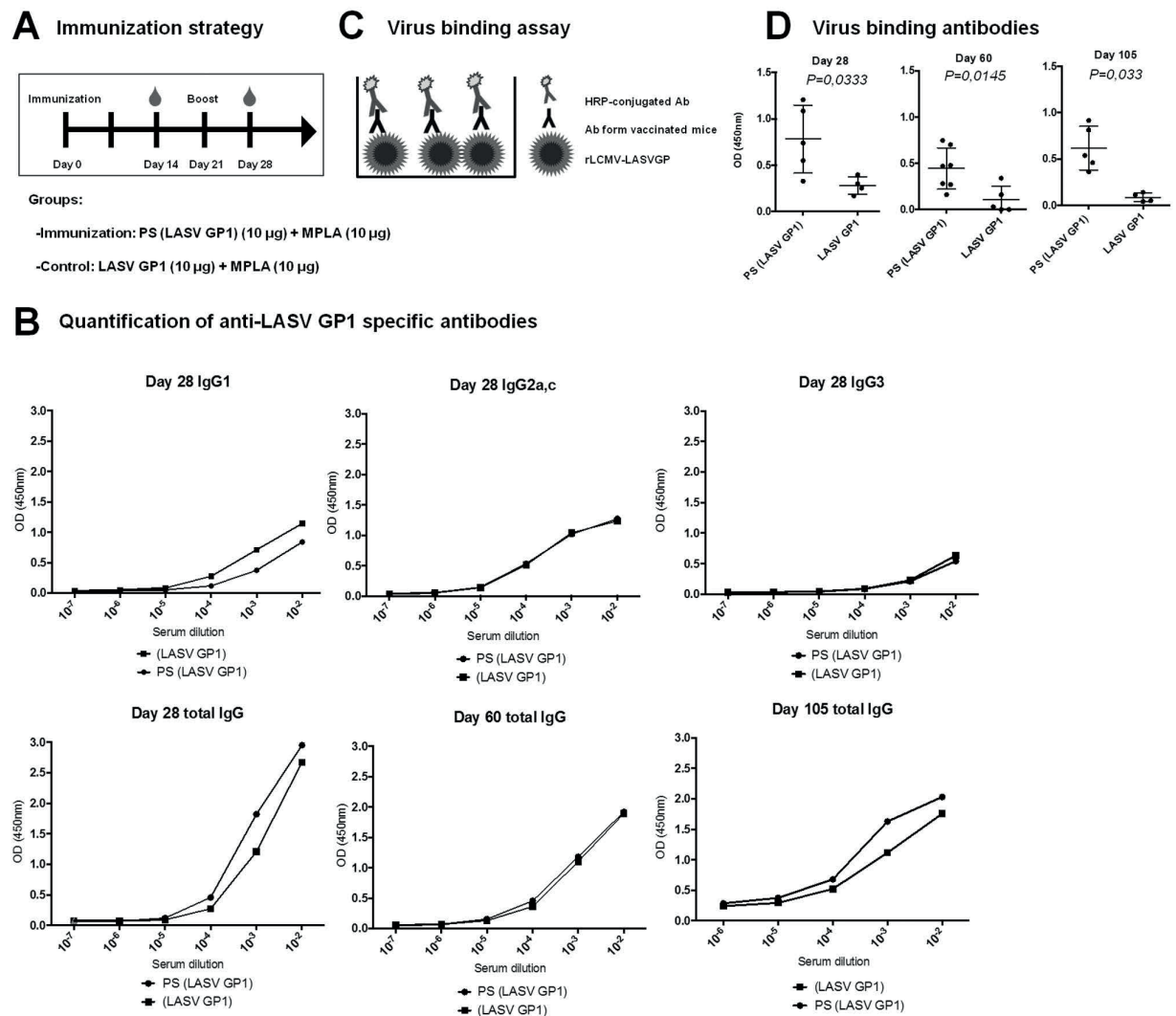
Figure 3. Polymersomes induce virus-binding anti-LASV GP1 antibodies. A) Schedule of immunization, blood draws, and composition of the immunization cocktail. B) Detection of anti-LASV GP1 specific IgG in ELISA. Microtiter plates were coated with purified LASV GP1 antigen. After blocking, plates were incubated with sera in 10-fold serial dilutions for 2 h at RT. For the detection of LASV GP1-specifig IgG, bound primary antibodies were detected by HRP-conjugated secondary antibodies to total IgG and the indicated IgG isotypes in a color reaction. Data are OD 450 nm (n = 5± SD). C) Schematic of the virus-binding assay. For details, please see text. D) Detection of virus-binding anti-LASV GP1 antibodies. Microtiter plates were coated with the purified rLCMV-LASV GP, followed by blocking and incubation with sera as in (B). Virus-bound total IgG was detected with a HRP-conjugated secondary antibody in a color reaction. Data represent individual animals. One out of three independent experiments is shown.
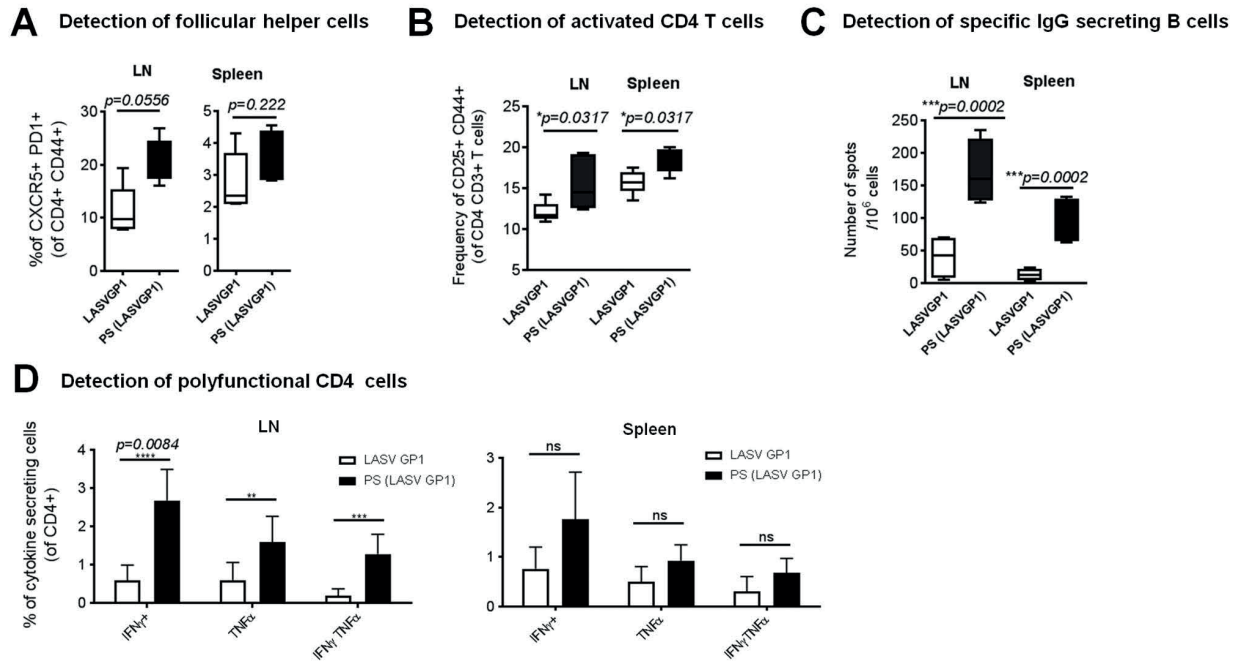
Figure 4. LASV GP1 antigen delivery via PS enhances antigen-specific follicular helper CD4 T cells, polyfunctional CD4 T cells, and IgG secreting B cells. Mice were immunized as in (3A) with PS (LASVGP1) or free LASV GP1 combined with MPLA. One week after the last immunization, lymph node cells (LN) and splenocytes (spleen) were isolated and restimulated *ex vivo* using LASV GP1 antigen. The percentage of follicular dendritic CD4 T cells among total CD4 T cells was detected using the markers CXCR5 and PD1 in flow cytometry (A) and the frequency of activated CD4 T cells assessed by staining for CD25 and CD44 (B). Data are from one out of two independent experiments, n = 5± SD. P-values are indicated, ns = not significant. C) Detection of IFNγ-producing and polyfunctional IFNγ/TNFα-secreting CD4 T cells by intracellular cytokine staining after *ex vivo* restimulation with 200 μg of LASV GP1 in the presence of Brefeldin A. Data are from one of two independent experiments, n = 5± SD. P-values are indicated, ns = not significant. D) Detection of specific IgG secreting B cells assessed by ELISpot as detailed in Materials and Methods. Data are from one of two independent experiments, n = 5± SD. with p-values indicated.
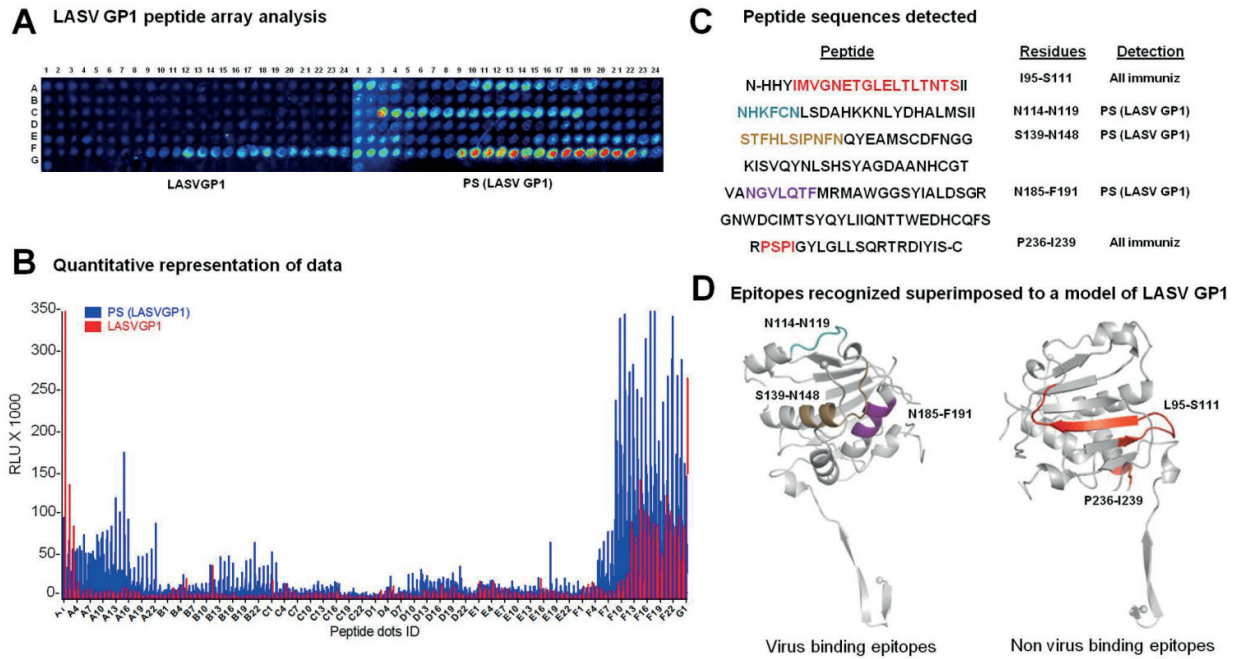
Figure 5. Polymersomes enhance the epitope-range of the anti-LASVGP1 antibody response. A) LASV GP1 peptide array analysis. The peptide array consists of spots of 20mer peptides spanning the entire LASV GP1 sequence (off-set of one amino acid) starting from the N terminus (A1) and ending with the C-terminal peptide (G1). Peptide arrays were probed with sera at a dilution of 1:200, follwed by detection with a HRP-conjugated secondary antibody to total IgG. Slides were developed using ECL. Displayed is a represenative LASV GP1 and PS (LASV GP1) example with luminescence signal intesities shown in false colors with red representing the more intense and light blue the less intense signals. B) Data from (A) plotted as relative intensity (*y* axis) of each spot (PS (LASV GP1) blue bars and control LASV GP1 (red bars) in the array with its position relative to the protein sequence (*x* axis). C) The peptide sequences corresponding to the spots detected in (A). D) Identified peptide sequences recognized by LASV GP1 antibodies in PS (LASV GP1) vaccinated mice in (A) superimposed on a structural model of LASV GP1 taken from (44).

48

SUPPLEMENTARY INFORMATION
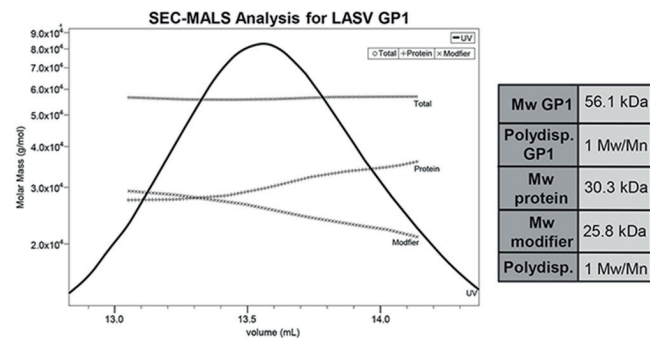
Figure S1. The elution profile of purified LASV GP1 was determined by size exclusion chromatography coupled with multiangle light scattering (SEC-MALS) as detailed in Materials and Methods. The horizontal line corresponds to the calculated mass for LASV GP1, 56.1 kDa, of which, only 30.5 kDa corresponded to the predicted polypeptide, indicating extensive post-translational modifications.
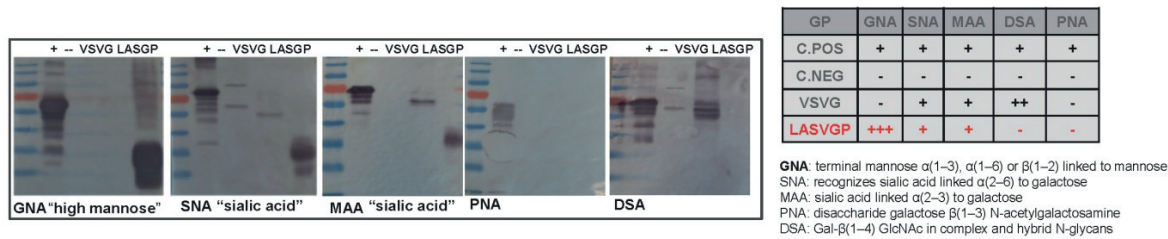
Figure S2. Analysis of the glycosylation pattern of recombinant LASV GP1. The glycosylation pattern of LASV GP1 was examined using the DIG glycan differentiation kit (Roche, Switzerland) according to the manufacturer's instruction. Briefly, purified LASV GP1 and internal controls supplied with the kit were separated using 10% SDS–PAGE and transferred to PVDF membranes. The membranes were blocked in 20 ml of blocking solution supplied by the manufacturer for 30 min. After two washes with PBS, membranes were incubated with digoxigenin-labeled lectins *Galanthus nivalis* agglutinin (GNA), *Sambucus nigra* agglutinin SNA), *Datura stramonium* agglutinin (DSA), *Maackia amurensis* agglutinin (MAA), and peanut agglutinin (PNA) for 1 h. After two washes with PBS, the lectin binding pattern was visualized with an AP-conjugated anti-digoxigenin antibody using ECL according to the manufacturer's instructions.

LASV GP1 coated ELISA

OD (450nm) — y-axis (0 to 3)

x-axis (LASVGP1 mAb): 10.4B* 19.7E* 18.5D 9.9F 21.5F 3.3B 4.2F 19.5A 5.6H
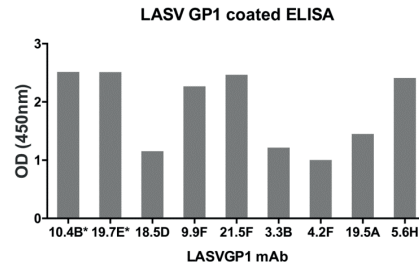
Figure S3. **Purified LASV GP1 binds to different LASV GP1 mAbs.** Binding to different LASV GP1 mAb isolated from human LASV survivors [33] was tested by ELISA. Microtiter plates were coated with 5 µg/ml of purified LASV GP1 followed by incubation with 5 µg/ml of purified mAbs. Bound primary antibody was detected with a HRP-conjugated secondary antibody in a color reaction. Data is optic density (OD) at wavelength 540 nm.

A

-N-P-M-GFP - Luc-L- rVSVΔG*-VSVG

-N-P-M-GFP - Luc-L- rVSVΔG*-LASVGP

B

Sample	Neutralization
Positive control Rep 9	+++
Naïve serum	-
PS (LASV GP1) serum	-
LASV GP1 serum	-
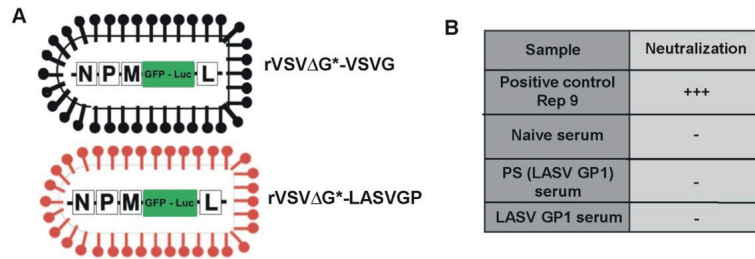
Figure S4. Detection of neutralizing anti-LASV GP1 antibodies in a pseudotype neutralization assay. A) Schematic representation of recombinant VSV pseudotypes. The replication-deficient rVSVΔG*-GFP-Luc lacking the endogenous glycoprotein (G) protein was pseudotyped by *trans*-complementation with either the cognate VSV G glycoprotein (rVSVΔG*-VSVG) or full-length LASV GP Josiah (rVSVΔG*-LASVG). Sera were diluted 1:20 (quadruplicates) and mixed with an equal volume of complete MEM containing VSV pseudotypes at 4,000 infectious units (IU) per well of a 96-well plate in presence and absence of complement. As a positive control we used the DNA aptamer Rep9 that targets arenavirus GP and acts like a neutralizing antibody [63]. This mixture was incubated for 1 h at 37 °C and added to fresh monolayers of A549 cells. Luciferase reporter activity was detected after 48 h. Only the samples treated with the poitive control aptamers showed marked neutralization, whereas neutralization in serum-treated samples did not reach statistical significance.

PANEL Thf		CD-4 activation		B CELL activation	
antibody	dilution	antibody	dilution	antibody	dilution
CD4	1:150	CD62_L	1:150	CD86	1:200
BCl-6	1:50	CD25	1:100	B220	1:200
B220	1:200	B220	1:200	IgM	1:200
PD-1	1:50	CD8	1:100	LD aqua	1:500
LD aqua	1:500	CD4	1:100	MHCII IA/IE	1:200
CXCR5biotin	1:40	LD aqua	1:500		
		CD3	1:100		
		CD44	1:200		

Supplementary table 1. Antibodies used for the FACS staining as detailed in Materials and Methods.

REFERENCES

1.   McCormick, J.B. and S.P. Fisher-Hoch, *Lassa fever*. Curr Top Microbiol Immunol, 2002. **262**: p. 75-109.
2.   Geisbert, T.W. and P.B. Jahrling, *Exotic emerging viral diseases: progress and challenges*. Nat Med, 2004. **10**(12 Suppl): p. S110-21.
3.   Sweileh, W.M., *Global research trends of World Health Organization's top eight emerging pathogens*. Global Health, 2017. **13**(1): p. 9.
4.   Andersen, K.G., et al., *Clinical Sequencing Uncovers Origins and Evolution of Lassa Virus*. Cell, 2015. **162**(4): p. 738-50.
5.   Fisher-Hoch, S.P., et al., *Review of cases of nosocomial Lassa fever in Nigeria: the high price of poor medical practice*. Bmj, 1995. **311**(7009): p. 857-9.
6.   Stephenson, E.H., E.W. Larson, and J.W. Dominik, *Effect of environmental factors on aerosol-induced Lassa virus infection*. J Med Virol, 1984. **14**(4): p. 295-303.
7.   Borio, L., et al., *Hemorrhagic fever viruses as biological weapons: medical and public health management*. Jama, 2002. **287**(18): p. 2391-405.
8.   McCormick, J.B., et al., *Lassa fever. Effective therapy with ribavirin*. N Engl J Med, 1986. **314**(1): p. 20-6.
9.   McCormick, J.B., et al., *A case-control study of the clinical diagnosis and course of Lassa fever*. J Infect Dis, 1987. **155**(3): p. 445-55.
10. Prescott, J.B., et al., *Immunobiology of Ebola and Lassa virus infections*. Nat Rev Immunol, 2017.
11. Burton, D.R., et al., *Broadly neutralizing antibodies present new prospects to counter highly antigenically diverse viruses*. Science, 2012. **337**(6091): p. 183-6.
12. Burton, D.R., E.O. Saphire, and P.W. Parren, *A model for neutralization of viruses based on antibody coating of the virion surface*. Curr Top Microbiol Immunol, 2001. **260**: p. 109-43.
13. Parren, P.W. and D.R. Burton, *The antiviral activity of antibodies in vitro and in vivo*. Advances in immunology, 2001. **77**: p. 195-262.
14. Karlsson Hedestam, G.B., et al., *The challenges of eliciting neutralizing antibodies to HIV-1 and to influenza virus*. Nature reviews. Microbiology, 2008. **6**(2): p. 143-55.
15. Zeitlin, L., et al., *Antibody therapeutics for Ebola virus disease*. Curr Opin Virol, 2016. **17**: p. 45-9.
16. McCormick, J.B., et al., *Inactivated Lassa virus elicits a non protective immune response in rhesus monkeys*. J Med Virol, 1992. **37**(1): p. 1-7.
17. Olschlager, S. and L. Flatz, *Vaccination strategies against highly pathogenic arenaviruses: the next steps toward clinical trials*. PLoS Pathog, 2013. **9**(4): p. e1003212.
18. Borrow, P. and M.B. Oldstone, *Characterization of lymphocytic choriomeningitis virus-binding protein(s): a candidate cellular receptor for the virus*. J Virol, 1992. **66**(12): p. 7270-81.
19. Sanchez, A., et al., *Junin virus monoclonal antibodies: characterization and cross-reactivity with other arenaviruses*. J Gen Virol, 1989. **70**(Pt 5)): p. 1125-32.
20. Robinson, J.E., et al., *Most neutralizing human monoclonal antibodies target novel epitopes requiring both Lassa virus glycoprotein subunits*. Nat Commun, 2016. **7**: p. 11544.
21. Sommerstein, R., et al., *Arenavirus Glycan Shield Promotes Neutralizing Antibody Evasion and Protracted Infection*. PLoS Pathog, 2015. **11**(11): p. e1005276.
22. Burton, D.R. and J.R. Mascola, *Antibody responses to envelope glycoproteins in HIV-1 infection*. Nat Immunol, 2015. **16**(6): p. 571-6.
23. Webster, D.M., P. Sundaram, and M.E. Byrne, *Injectable nanomaterials for drug delivery: carriers, targeting moieties, and therapeutics*. Eur J Pharm Biopharm, 2013. **84**(1): p. 1-20.
24. Stano, A., et al., *Tunable T cell immunity towards a protein antigen using polymersomes vs. solid-core nanoparticles*. Biomaterials, 2013. **34**(17): p. 4339-46.
25. Scott, E.A., et al., *Dendritic cell activation and T cell priming with adjuvant- and antigen-loaded oxidation-sensitive polymersomes*. Biomaterials, 2012. **33**(26): p. 6211-9.
26. Li, S., et al., *Acidic pH-Induced Conformations and LAMP1 Binding of the Lassa Virus Glycoprotein Spike*. PLoS Pathog, 2016. **12**(2): p. e1005418.
27. Igonet, S., et al., *X-ray structure of the arenavirus glycoprotein GP2 in its postfusion hairpin conformation*. Proc Natl Acad Sci U S A, 2011. **108**(50): p. 19967-72.
28. Cohen-Dvashi, H., et al., *Molecular Mechanism for LAMP1 Recognition by Lassa Virus*. J Virol, 2015. **89**(15): p. 7584-92.
29. Illick, M.M., et al., *Uncoupling GP1 and GP2 expression in the Lassa virus glycoprotein complex: implications for GP1 ectodomain shedding*. Virol J, 2008. **5**: p. 161.
30. Bowden, T.A., et al., *Unusual molecular architecture of the machupo virus attachment glycoprotein*. J Virol, 2009. **83**(16): p. 8259-65.
31. Radoshitzky, S.R., et al., *Transferrin receptor 1 is a cellular receptor for New World haemorrhagic fever arenaviruses*. Nature., 2007. **446**(7131): p. 92-6. Epub 2007 Feb 7.

32.   Branco, L.M., et al., *Lassa virus-like particles displaying all major immunological determinants as a vaccine candidate for Lassa hemorrhagic fever.* Virol J, 2010. **7**: p. 279.

33.   Goncalves, A.R., et al., *Role of DC-SIGN in Lassa Virus Entry into Human Dendritic Cells.* J Virol, 2013. **87**(21): p. 11504-15.

34.   Casella, C.R. and T.C. Mitchell, *Putting endotoxin to work for us: monophosphoryl lipid A as a safe and effective vaccine adjuvant.* Cell Mol Life Sci, 2008. **65**(20): p. 3231-40.

35.   Rojek, J.M., et al., *Different mechanisms of cell entry by human-pathogenic Old World and New World arenaviruses.* J Virol, 2008. **82**(15): p. 7677-87.

36.   Pasqual, G., et al., *Old world arenaviruses enter the host cell via the multivesicular body and depend on the endosomal sorting complex required for transport.* PLoS Pathog, 2011. **7**(9): p. e1002232.

37.   Moraz, M.L., et al., *Cell entry of Lassa virus induces tyrosine phosphorylation of dystroglycan.* Cell Microbiol, 2013. **15**(5): p. 689-700.

38.   Rojek, J.M., et al., *Binding of Lassa virus perturbs extracellular matrix-induced signal transduction via dystroglycan.* Cell Microbiol, 2012. **14**(7): p. 1122-34.

39.   Lee, A.M., et al., *Pathogenesis of Lassa fever virus infection: I. Susceptibility of mice to recombinant Lassa Gp/LCMV chimeric virus.* Virology, 2013.

40.   Sommerstein, R., et al., *Evolution of recombinant lymphocytic choriomeningitis virus/Lassa virus in vivo highlights the importance of the GPC cytosolic tail in viral fitness.* J Virol, 2014. **88**(15): p. 8340-8.

41.   Dutko, F.J. and M.B. Oldstone, *Genomic and biological variation among commonly used lymphocytic choriomeningitis virus strains.* J Gen Virol, 1983. **64 (Pt 8)**: p. 1689-98.

42.   Berger Rentsch, M. and G. Zimmer, *A vesicular stomatitis virus replicon-based bioassay for the rapid and sensitive determination of multi-species type I interferon.* PLoS One, 2011. **6**(10): p. e25858.

43.   Moeschler, S., et al., *Quantification of Lyssavirus-Neutralizing Antibodies Using Vesicular Stomatitis Virus Pseudotype Particles.* Viruses, 2016. **8**(9).

44.   Baumjohann, D. and K.M. Ansel, *Tracking early T follicular helper cell differentiation in vivo.* Methods Mol Biol, 2015. **1291**: p. 27-38.

45.   Fazekas de St Groth, B., A.L. Smith, and C.A. Higgins, *T cell activation: in vivo veritas.* Immunol Cell Biol, 2004. **82**(3): p. 260-8.

46.   Viskovska, M., et al., *Probing the sites of interactions of rotaviral proteins involved in replication.* J Virol, 2014. **88**(21): p. 12866-81.

47.   Hastie, K.M., et al., *Crystal structure of the prefusion surface glycoprotein of the prototypic arenavirus LCMV.* Nat Struct Mol Biol, 2016. **23**(6): p. 513-21.

48.   Yun, N.E. and D.H. Walker, *Pathogenesis of Lassa fever.* Viruses, 2012. **4**(10): p. 2031-48.

49.   Walker, L.M. and D.R. Burton, *Rational antibody-based HIV-1 vaccine design: current approaches and future directions.* Current opinion in immunology, 2010. **22**(3): p. 358-66.

50.   Johnson, K.M., et al., *Clinical virology of Lassa fever in hospitalized patients.* J Infect Dis, 1987. **155**(3): p. 456-64.

51.   Bergthaler, A., et al., *Impaired antibody response causes persistence of prototypic T cell-contained virus.* PLoS Biol, 2009. **7**(4): p. e1000080.

52.   *<._4536.full.pdf>*.

53.   Cross, R.W., et al., *Treatment of Lassa virus infection in outbred guinea pigs with first-in-class human monoclonal antibodies.* Antiviral Res, 2016. **133**: p. 218-22.

54.   Hastie, K.M., et al., *Structural basis for antibody-mediated neutralization of Lassa virus.* Science, 2017. **356**(6341): p. 923-928.

55.   Lefterova, M.I., et al., *Next-Generation Sequencing for Infectious Disease Diagnosis and Management: A Report of the Association for Molecular Pathology.* J Mol Diagn, 2015. **17**(6): p. 623-34.

56.   Datta, S., et al., *Next-generation sequencing in clinical virology: Discovery of new viruses.* World J Virol, 2015. **4**(3): p. 265-76.

57.   Tiller, T., C.E. Busse, and H. Wardemann, *Cloning and expression of murine Ig genes from single B cells.* J Immunol Methods, 2009. **350**(1-2): p. 183-93.

58.   Oppliger, J., et al., *Lassa virus cell entry via dystroglycan involves an unusual pathway of macropinocytosis.* J Virol, 2016.

59.   Kunz, S., et al., *Molecular analysis of the interaction of LCMV with its cellular receptor [alpha]-dystroglycan.* J Cell Biol, 2001. **155**(2): p. 301-10.

60.   Kunz, S., et al., *Mechanisms for lymphocytic choriomeningitis virus glycoprotein cleavage, transport, and incorporation into virions.* Virology, 2003. **314**(1): p. 168-78.

61.   Kunz, S., et al., *Use of alternative receptors different than alpha-dystroglycan by selected isolates of lymphocytic choriomeningitis virus.* Virology, 2004. **325**(2): p. 432-45.

62.   Kunz, S., et al., *Characterization of the interaction of lassa fever virus with its cellular receptor alpha-dystroglycan.* J Virol, 2005. **79**(10): p. 5979-87.

63.   Lee, A.M., et al., *Inhibition of cellular entry of lymphocytic choriomeningitis virus by amphipathic DNA polymers.* Virology, 2008. **372**(1): p. 107-17.

CHAPTER 3

A novel strategy for the generation of monoclonal antibodies to emerging viruses

Clara Galan-Navarro[1,2], Antra Zeltina[3], Marcela Rincon-Restrepo[2], Sachiko Hirosue[2], Melody A. Swartz[2,5], Katie Doores[4*], Thomas Bowden[3*] and Stefan Kunz[1*]

[1] Institute of Microbiology, Lausanne University Hospital. Lausanne, Switzerland

[2] Laboratory of Lymphatic and Cancer Bioengineering,Institute of Bioengineering, École Polytechnique Féderal de Lausanne (EPFL) 1015 Lausanne, Switzerland

[3] Division of Structural Biology, Welcome Trust Centre for human Genetics, University of Oxford, Roosevelt Drive, Oxford OX3 7BN, UK

[4] Department of Infectious Diseases, King's College London SE1 9RT, UK

[5] Institute for Molecular Engineering and Ben May Department of Cancer Research, University of Chicago, IL, United States of America

* Corresponding authors. Mailing address: Institute of Microbiology, University Hospital Center and University of Lausanne, Lausanne CH-1011, Switzerland. Phone: +41-21 314 7743, Fax: +41-21 314 4060. E-mail: Stefan Kunz, Stefan.Kunz@chuv.ch Thomas A. Bowden, email: thomas.bowden@strubi.ox.ac.uk Katie J. Doores, katie.doores@kcl.ac.uk.

Keywords: Polymersomes, nanocarrier, Machupo virus, monoclonal antibodies.

Abstract: 247 words

--Article in preparation—

ABSTRACT

The advent of powerful next-generation sequencing greatly accelerated the discovery of novel pathogenic emerging viruses. Virus-specific monoclonal antibodies (mAb) represent crucial tools for research and diagnostics on such novel pathogens. However, lack of suitable culture systems and limited numbers of clinical cases frequently prevent isolation of the live virus or of virus-specific B cell clones from convalescent individuals for mAb production. Here we describe a novel approach for the generation of virus-specific mAb using biosynthetic immunogens based only on sequence information using the New World arenavirus Machupo (MACV) that causes Bolivian hemorrhagic fever as an example. Despite several efforts, the generation of mAb specific for MACV remains an unmet challenge. We produced a suitable recombinant immunogen derived from the MACV envelope glycoprotein that was encapsulated into oxidation-sensitive polymersomes serving as nanocarriers for antigen delivery. This versatile immunization scaffold facilitates intracellular MHCII loading and promotes a potent antibody response. Mice were immunized with adjuvanted antigen-loaded polymersomes in a prime-boost scheme and individual antigen-specific memory B cells isolated by single cell sorting. Pairs of mouse immunoglobulin heavy and light chains were PCR amplified and inserted into expression vectors, followed by expression in mammalian cells. Using this approach, we identified a novel set of MACV-specific mAb that show exquisite specificity in ELISA, Western blot, immunofluorescence assay, and flow cytometry. Their negligible cross-reactivity even with closely related New World arenaviruses makes these new mAb unique and powerful tools for research and diagnostics on this important and largely understudied emerging human pathogen.

INTRODUCTION

Over the past decades, emerging or re-emerging viral infectious diseases have caused numerous serious outbreaks. The majority of emerging human pathogenic viruses are zoonotic pathogens. Current climate changes affecting reservoir population dynamics, urbanization, and almost unrestricted global trade promote human contacts with novel and unknown animal species, increasing the risks of zoonotic infections. The successful control of epidemics caused by novel pathogens critically depends on the availability of rapid and sensitive diagnostic methods to detect, identify, and trace the agent in the clinic, at the community level, and in the environment. Molecular diagnostics based on real-time quantitative PCR, nucleic acid hybridization, and more recently next generation sequencing (NGS) proved invaluable for the discovery of novel pathogens, routine clinical diagnostics, and outbreak control [1, 2]. As a second pillar, serology is crucial for both etiological diagnosis and seroepidemiological studies. Antibody detection systems include immunofluorescence assay (IFA), enzyme-linked immunosorbent assay (ELISA), and different formats of neutralization tests. Virus-specific monoclonal antibodies (mAb) are of great importance for detection of viral antigens and examination of antigenic relationships of emerging viruses in research and diagnostics. However, lack of suitable cell culture systems and the often limited numbers of clinical cases occurring in remote areas frequently prevent isolation of the virus or of virus-specific B cell clones from convalescent individuals. Moreover, close structural relationship to other viruses sometimes prevented the generation of species-specific mAbs. In our present study, we developed a novel strategy for the rapid, efficient, and cost-effective production of recombinant mAb using biosynthetic immunogens designed "from scratch" based exclusively on available sequence information. To assess feasibility of our approach, we performed a proof-of-concept study taking the highly pathogenic New World arenavirus *Machupo* (MACV), as an example.

The arenaviruses are a large and diverse family of emerging viruses that include causative agents of severe viral hemorrhagic fevers (VHF) in humans and represent important public health problems [3]. Based on their geographical distribution, mammalian arenaviruses are divided into Old World and New World viruses that are carried mainly by rodents [4]. Since the 1950s, the Clade B New World arenaviruses MACV, Junin (JUNV), Guanarito (GTOV), Sabia (SABV), and Chapare virus (CHAV) have emerged as causative agents of severe VHF in the Americas with case fatality rates of 30-50% [5]. Currently, there are no FDA approved vaccines available and treatment options are limited. In their reservoir species, the viruses are maintained by persistence and human infection occurs mainly by zoonotic transmission through inhalation of contaminated rodent excreta [6, 7]. After an incubation period of 1-3 weeks, patients initially develop flu-like symptoms followed by gastrointestinal manifestations, mucosal bleeding, and in some cases neurological problems. The varied and non-specific early clinical signs and symptoms of the South American VHF render clinical diagnosis often difficult [6]. Rapid pathogen detection is therefore imperative to prevent the risk of human-to-human transmission, in particular in nosocomial settings. Although MACV has been discovered in the 1960s,

all attempts to generate specific mAb have failed so far, severely limiting research and development of diagnostic tests [8-10]. In our proof-of-concept study, we tried to close this gap, generating a first set of MACV-specific mAb for use in diagnostics, research, and development. Our novel approach, outlined schematically in Figure 1 is based on newly developed polymersomes (PS) used as antigen nanocarrier for the enhancement of humoral immunity. Our PS are non-infectious, stable vesicles composed of biopolymers which can efficiently deliver antigen to lymph nodes, enhance uptake, and promote antigen presentation. Soluble biosynthetic immunogens combined with suitable adjuvants can be incorporated into the watery core without further modification. Following immunization with the PS nanocarrier, single antigen-binding B cells are isolated from spleen of immunized mice by flow cytometry (FACS). Single-cell RNA is extracted, reversely transcribed, and paired heavy and light chains amplified by PCR using specific primer sets. The resulting amplicons are cloned into expression vectors, allowing recombinant IgG production in mammalian cells. Using this approach, we were able to isolate a set of "first-in-class", species-specific recombinant mAb against MACV.

RESULTS

Generation of polymersome nanocarriers delivering the MACV GP1 immunogen

Among New World arenavirus proteins, GP1, decorating the tips of the virion spike, shows the least conservation and represents therefore the most promising candidate for the development of species-specific mAb. Available structural data reveal that MACV GP1 represents an independent fold with a globular structure (Fig. 2A) [11]. The GP1 monomer is necessary and sufficient for binding to the cellular receptor human transferrin receptor (TfR1) [20, 21] and represents the target for neutralizing antibodies [6]. The co-crystal structure of MACV GP1 with hTfR1 revealed that the interaction between GP1 and TfR1 involves several contacts via extended GP1 loops and extensive hydrogen-bonding networks [20]. The soluble recombinant MACV GP1 fragment used as immunogen in our study is comprised of amino acids 87-257, spanning the known receptor binding sites, as well as neutralizing epitopes.

For antigen delivery, we chose PEG-*bl*-PPS (Fig. 2C), capable of enhancing CD4 T cell responses [22] and humoral responses to weakly immunogenic viral surface antigens (Galan et al, 2017 in press). Polymersomes were synthesized and loaded with immunogen as described in detail in Materials and Methods [13, 22]. Nanoparticles with diameters in the 100 nm ensure efficient lymphatic transport and delivery to antigen-presenting cells in lymph nodes upon intradermal or subcutaneous immunization [22]. The resulting PS (MACV GP1) displayed an average size range of 150 nm, with a polydispersity index of 0.1. (Fig. 2D), making them suitable for our purposes. Our previous studies identified the Toll-like receptor (TLR)-4 ligand monophosphoryl lipid A (MPLA) [23] as a suitable adjuvant capable of enhancing the humoral response to PS loaded with a poorly immunogenic viral surface antigen (Galan et al., 2017). Age- and sex-matched C57BL/6 mice were immunized with PS (MACV GP1) in combination with 10 μg MPLA. Mice received a prime-boost immunization three weeks apart with the immunogen formulations indicated in Fig. 3A. All immunized mice showed robust titers of anti-MACV GP1-specific IgG on day 60 after immunization, as assessed by ELISA using our recombinant MACV GP1 as antigen, (Fig. 3B).

Sorting of single antigen-specific memory B cells and cloning of anti-MACV GP1-specific IgGs

Next, we sought to isolate antigen specific memory B cells form immunized mice. For this purpose, the 5 mice showing the highest anti-MACV GP1 IgG titers, as assessed by ELISA (Fig. 3B) were selected and boosted with the PS (MACV GP1) + MPLA formulation. After 10 days, serum titers of anti-MACV GP1 were again measured and animals that reached a 1:1,000,000 endpoint dilution in ELISA were sacrificed. Total splenocytes were obtained and IgG expressing B cells isolated as outlined in Fig. 4A. To ensure specificity of B cells to MACV GP1 and minimize cross-reactivity, IgG expressing B cells were sorted after binding to fluorescence labeled recombinant MACV GP1 and the GP1 of the closely related JUNV that is notorious for cross-reactivity. Using flow cytometry, we separated MACV GP1-

specific IgG1 producing B from cross-reactive cells. Out of the 960 single cells that were sorted, 384 cells were selected for total RNA extraction and cDNA synthesis, by reverse transcriptase using random hexamer priming. Then, 17 pairs of mouse Ig heavy and light chains were amplified with primers chosen based on previous publications [16]. The variable heavy- and light-chain domains were then amplified by nested PCR. The first PCR uses a primer mix that anneals to the V(D)J leader sequences and an Ig constant region reverse primer. The second PCR is performed with primers annealing to the 5′ end of the variable (V) genes and a nested reverse primer to an Ig constant region. The PCR products were then purified, sequenced, and inserted into eukaryotic expression vectors, followed by transient co-transfection in HEK293T cells. Recombinant IgG from conditioned supernatants were purified by protein G affinity chromatography. Finally, 14 purified candidate mAb were tested for their ability to bind MACV GP1 in ELISA, resulting in the identification of 6 MACV GP1binding mAb, 10G7, 7C11, 8F4, 8B9, 8G8, and 8B7 (Fig. 5A).

Characterization of the recombinant anti-MACV GP1 mAb

In a first step to characterize the newly obtained candidate mAb to MACV GP1, we defined their IgG isotype in ELISA using isotype-specific secondary antibodies. All candidate antibodies belonged to class IgG1 (Fig. 5B). A major goal of our study was to identify species-specific anti-MACV GP antibodies. To validate their specificity for MACV GP1, we performed ELISA using analogous recombinant GPs fragments of the related New World arenaviruses JUNV, GTOV, and OECV (Ocozocoautla de Espinosa virus) antigens. As a negative control, we included the GP1 of the only distantly related Old World arenavirus Lassa (LASV). All candidate mAbs were highly specific for MACV GP1 with negligible cross-reactivity to the other GP1s (Fig. 5A), providing fist evidence of species-specificity of our mAb.

The GP1 of MACV represents a compact globular fold that is stabilized by intramolecular disulfide-bonds. To probe possible conformation-dependence of our candidate mAb, we heated our recombinant MACV GP1 in presence or absence of 100 mM DTT, followed by SDS-PAGE under denaturing conditions. Proteins were blotted to nitrocellulose and probed with our candidate mAb in Western blot. All mAb recognized MACV GP1 in Western blot performed under reducing-denaturing conditions (Fig. 6A), suggesting that intact disulfide bonds are not required for binding. Although we cannot exclude the possibility of some re-folding of the immobilized protein, the observed strong binding in reducing Western blot suggests that our mAb may recognize non-conformational epitopes.

A major application of species-specific mAb in diagnostics and research will be IFA. Since MACV and most of the closely related Clade B New World arenaviruses, in particular JUNV and GTOV, are BSL4 pathogens, work with live viruses is restricted. To assess specificity of our mAb in IFA we therefore tested them against recombinant full-length GPC expressed in mammalian cells. First, a plasmid expressing MACV GPC-Flag was transfected into HEK 293T cells. After 48 h, cells were

fixed with paraformaldehyde and either permeabilized with saponin or left untreated. Cells were then stained with our candidate mAb in combination with a fluorophore-conjugated secondary antibody. The mAbs 10G7, 7C11, 8F4, and 8B9 gave a characteristic cell-surface staining on non-permeabilized cells well above background (Fig. 7A), whereas mAbs 8D8 and 8D7 gave weaker staining and were not further pursued (data not shown). To verify the specificity of mAbs 10G7, 7C11, 8F4, and 8B9 in IFA, they were tested against the full-length GPC of the closely related JUNV. In line with our ELISA and Western blots, the mAbs proved to be specific for MACV GP1 with no detectable cross-reactivity for the GP1 of related viruses under our assay conditions (Fig. 7B).

In addition to IFA, we verified reactivity and specificity of our mAbs in flow cytometry. To this end, HEK 293T cells were transfected with a plasmid expressing MACV GPC-Flag. Live non-permeabilized cells were stained with mAbs 10G7, 7C11, 8F4, and 8B9 in staining buffer containing sodium azide in order to prevent internalization of GPC. After fixation, bound mAbs were detected with a florescence-labeled secondary antibody. Analysis by flow cytometry revealed robust and specific staining in MACV GPC transfected cells, but not mock-transfected controls (Fig. 8).

Our initial characterization revealed that our mAb 10G7, 7C11, 8F4, and 8B9 were highly specific for MACV GP1 with possible applications in ELISA, Western blot, IFA, and flow cytometry, making them valuable tools for research and diagnostics. In a next step, we assessed neutralizing activity of the mAbs, employing a well-established pseudotype assay based on recombinant replication-competent, propagation-deficient vesicular stomatitis virus (VSV) lacking the G protein (VSVΔG) containing a luciferase reporter [18] displaying full-length mature MACV GP (Fig. S1A). Briefly, VSVΔG-MACVGP pseudotypes were mixed with mAb at 20 μg/ml for one hour at 37°C. The mixture of pseudotypes and antibodies was added to fresh monolayers of VeroE6 cells and infection detected by luciferase or GFP assay as described [24]. Despite robust binding to MACV GP1, none of the mAbs achieved significant neutralizing activity under our assay conditions, whereas soluble hTfR1 included as a positive control lead efficiently blocked infection (Fig. S1B).

DISCUSSION

Hemorrhagic arenaviruses are classified as BSL4 pathogens and high containment facilities are required to handle live virus samples for diagnostic purposes. To circumvent these restrictions, serological assays based on recombinant viral antigens have been developed, including direct IgG-ELISA, IFA, and capture-ELISA [8, 25, 26]. These serological assays are highly sensitive and specific for LASV [26] and JUNV [8]. However, the current lack of specific mAb to MACV [8-10] so far prevented the development of specific tests for MACV, severely restricting research and development. The current lack of mAb to MACV is likely explained by the high antigenic relatedness in particular to JUNV, which shows higher prevalence. Examination of available sequences revealed that the GP1 moiety involved in host cell attachment shows the largest variation, possible reflecting selective pressure exerted by the humoral immune response of the host [27, 28]. However, several lines of evidence support the notion that the arenavirus GP1 are inherently weak antigens due to glycan shielding [29], similar to the envelope GPs of other human pathogens, such as human immunodeficiency virus (HIV)-1 or hepatitis C virus (HCV) [30-32]. Using a recombinant receptor-binding fragment of the GP1 of the Old World arenavirus LASV, we recently showed that mice immunized with adjuvanted PS (LASV GP1) showed superior humoral responses than free antigen, including antibodies with higher binding affinity (Galan-Navarro et al., 2017). This was reflected by increased levels of polyfunctional anti-viral CD4 T cells and IgG-secreting B cells, as well as a more diverse epitope repertoire of anti-viral IgG. Considering the extensive glycosylation found of envelope GPs of major families of emerging viruses, including filoviruses, Bunyaviruses, and arenaviruses, we employed our PS platform for antigen delivery. Recombinant MACV GP1 was synthesized based on the available sequence information [33] and encapsulated into PS. For immunization, PS (MACV GP1) were applied following a prime-boost protocol, which induced robust anti-MACV GP1 IgG responses. Using purified recombinant immunogen, we achieved isolation of 960 single antigen-specific B cells. Total RNA was extracted from 384 cells, followed by cDNA synthesis. Amplification using specific primers and subsequent filtering of data resulted in the identification of 17 pairs of mouse immunoglobulin heavy and light chains. Expression in HEK293T cells yielded 14 recombinant IgG that were screened for antigen specificity using ELISA. Six mAb were selected based on their specificity and high binding affinity in ELISA.

Since research and diagnostic applications involve a range of techniques, we validated the sensitivity and specificity of our mAb in ELISA, Western blot, IFA, and flow cytometry. Examination in ELISA against a panel of recombinant arenavirus GP1, including the closely related Clade B viruses JUNV and GTOV revealed exquisite sensitivity. Examination of mAb in Western blot under reducing conditions revealed strong binding of our mAb to denatured antigen, making them suitable for the examination of fixed specimens that had undergone virus inactivation, which would be a decisive advantage considering the requirement of BSL4 to handle unfixed native samples. Since IFA remains a major diagnostic technique and is widely used in research, we validated specificity of our anti-MACV

GP1 mAb using the full-length GPC of MACV and the closely related JUNV. In contrast to all mAb isolated so far [9, 10], our set of mAb was highly specific for MACV GP1 in fixed cell specimens. Staining of non-permeabilized cells revealed the characteristic cell surface staining associated with the expression of full length GPC in infected or transfected cells. Lastly, examination of our mAb in flow cytometry performed on live, non-permeabilized cells confirmed the high specificity for MACV GP1 over JUNV GP1. Initial examination of our mAb in a neutralization test based on pseudotypes of vesicular stomatitis virus (VSV) [18, 24] revealed little neutralizing activity (Sup. Figure 1). Combined with the observed ability of our mAb to strongly bind reduced denatured MACV GP1 in Western blot, this suggests that they are directed against, non-conformational epitopes, possibly located at the non-neutralizing face of the protein. We are currently screening a larger number of antigen-specific B cells in order to isolate neutralizing mAb.

Despite some sequence variation, MACV and JUNV have a nearly identical overall GPC architecture and share the host cell receptor TfR1uisng a conserved binding mode. The capacity of our polymersomes to induce specific mAb against MACV GP1 is therefore unprecedented and demonstrates the potential of this versatile immunization scaffold. As previously shown in our studies on the notoriously weakly immunogenic LASV GP1, the platform may further promote the quality of antibody responses against otherwise poor antigens. This may enhance the probability of successful mAb isolation, removing an important bottleneck. Considering that the clinical signs and symptoms of Bolivian VHF caused by MACV in humans are virtually indistinguishable from those of classical Argentine VHF associated with JUNV, our virus-specific mAb may be useful for the direct detection of the virus in tissue specimens using IFA. In addition, we are currently developing a capture-ELISA format for the rapid and sensitive detection of MACV antigen in serum and CSF samples. In sum, we used a versatile PS-based immunization scaffold to rapidly generate recombinant mAb to MACV GP1 that show exquisite specificity in ELISA, IFA, Western blot and flow cytometry. These mAb represent valuable tools for research and development for the biomedical research comunity and clinical diagnostics.

ACKNOWLEDGEMENTS

MATERIALS AND METHODS

Animals

C57BL/6 female mice, aged 8-12 weeks, were purchased from Harlan (Gannat, France). All animal experiments were performed under the approval from the Veterinary Authority of the Canton of Vaud (Switzerland) according to Swiss regulations of animal welfare (animal protocol number 2502.1 and 2235.1).

Recombinant MACV GP1

Purified recombinant MACV GP1 was obtained as described [11]. The globular domain of MACV GP1 glycoprotein responsible for attachment to human transferrin receptor 1 (residues 87 to 257 from the complete mature GP; GenBank accession number AAS77647.1) was cloned into the pHLsec vector containing the chicken RPTP signal sequence (5). MACV GP1 was expressed in HEK 293T cells transfected with 2 mg DNA/liter of cell culture in the presence of 5 M kifunensine, which prevents extension of N-glycans, resulting in protein bearing oligomannose-type glycans. MACV GP1 protein was purified from the cell supernatant by using immobilized metal affinity chromatography (IMAC) followed by size-exclusion chromatography (SEC). Protein yields were 2.0 mg MACV GP1/liter of cell culture at purity of >98%. LASV GP1 (residues 58-92) and JUNV GP1 (residues 87–231) antigens used here were described in previous studies in Galan-Navarro et al. 2017 and [12].

Block-copolymer synthesis and polymersome preparation

All chemical reagents were reagent grade and purchased from Sigma-Aldrich, MO, unless otherwise stated. Polymersomes (PS) were prepared as described [13]. Briefly, block-copolymers were synthesized using benzyl mercaptan to start the living polymerization of propylene sulfide (PPS). The terminal thiolates were capped with PEG-mesylate. For purification, the co-polymers were precipitated two times in cold methanol. The purity and length of the PPS chain were confirmed by gel chromatography and NMR. Chains of PEG_{17}-bl-PPS_x, containing between x=26-32 PPS units were used to form PS. An amount of 30-50 mg was re-suspended in dichloromethane and placed in piranha-etched glass vials to desiccate overnight. For the formation of PS with MACV GP1, a thin film of copolymer was rehydrated with a solution of 500 μl of MACV GP1 or fluorescence-labeled MACV GP1 (2 mg/ml) in 50 mM sodium phosphate buffer, and rotated for 48 h at 4°C. Next, the solution was extruded at least four times through a 0.2 μm nucleopore track-etched membrane (Whatman, Maidstone, UK) to obtain PS ranging between 150-170 nm with polydispersity values < 0.2. Purification of the PS loaded with MACV GP1 immunogen from free protein was achieved by SEC through a Sepharose CL-6B column. Fractions containing PS were pooled and further concentrated though an ultra-centrifugation filter (Amicon Millipore, Darmstadt, Germany) with a cut-off of 100 kDa. Efficiency of MACV GP1 loading into PS was 430 μg/ml calculated by subtracting the amount of the unloaded protein from the starting material used. The size of PS was determined by dynamic light scattering with a Nano Zs Zetasizer

(Malvern Instruments, Malvern, UK). PS were controlled for their size and polydispersity, as well as endotoxin levels using the HEK-Blue™ TLR4 cells and QUANTI-Blue (inVivogen) with endotoxin standard (E-Toxate Endotoxin standard E8029-1VL Sigma-Aldrich) for every batch produced.

Western-blot

Protein Samples were mixed 1:1 with 2x SDS-polyacrylamide gel electrophoresis (PAGE) sample buffer containing 100 mM DTT and boiled (5 min at 95°C). Samples (1μg of purified MACV GP1) were separated by SDS-PAGE and blotted to nitrocellulose membranes. Membranes were blocked in 3% (w/v) skim milk in PBS and proteins detected with primary antibody after overnight incubation at 4°C using HRP-conjugated secondary antibodies as described [14]. Monoclonal antibodies to MACV GP1 were used at 1 μg/ml and polyclonal rabbit anti-mouse-HRP at 1: 3,000. Membranes were developed using enhanced chemiluminescence (ECL) using Amersham ECL Prime Western Blotting Detection Reagent (GE Healthcare lifesciences Little Chalfont, UK). Signal acquisition was performed with ImageQuant LAS 4000Mini (GE Healthcare lifesciences Little Chalfont, UK).

Immunization protocol

All immunizations were administered intra-dermal (i.d.) into the four footpads, under isofluorane anesthesia. For all formulations, 10 μg of MACV GP1 was injected per animal, together with 10 μg of MPLA (Salmonella minnesota R595, AvantiLipids). All PS and proteins batches were tested negatively for endotoxin using a Toll-like receptor activation assay based on HEK-Blue reporter cell lines (Invivogen, CA).

Enzyme-linked immunosorbent assay (ELISA)

For the detection of antigen-specific antibodies in ELISA, 96-well Nunc MaxiSorp® plates were coated with 5 μg/mL of MACV GP1 overnight at 4°C. Plates were washed three times with PBS/ 0.02% (wt/vol) Tween-20 and blocked with 2.5% (wt/vol) casein solution in PBS for 2 h at room temperature (RT). Serial dilutions of serum in 2.5% (wt/vol) casein/PBS were added and incubated for 2 hrs at RT. Plates were washed four times, following by incubation with HRP-conjugated secondary antibodies specific for and IgG1, IgG2a,c, IgG3 or total IgG (Southern Biotech, Birmingham, AL). After incubation for 1 h at RT, plates were washed four times and developed using 50 μl of 3,3',5,5'-tetramethylbenzidine (eBiosciences, MA). The signal was stopped by adding 20 μl of 2 M H$_2$SO$_4$. Plates were analyzed using a plate reader spectrophotometer (Tecan, Mannedorf, Switzerland) by measuring the absorbance at 450 nm with correction at 570 nm. Specific signals were calculated by subtraction of absorbance obtained with samples containing the blocking casein only (background control).

Flow cytometry

For detection of full-length MACV GP on transfected HEK293T cells, 3x10^6 cells were plated in cone-shaped 96 well plates, washed once with HBSS, and stained with live/dead fixable cell viability reagent

(Life technologies, CA). For surface staining, cells were washed once with HBSS supplemented with 0.5% (wt/vol) BSA (Sigma) and resuspended in HBSS, 0.5% (wt/vol) BSA containing primary antibodies at the indicated concentrations. Bound primary antibodies were detected with a phycoerythrine (PE)-conjugated goat anti-mouse IgG secondary antibodies (1:100) in HBSS, 0.5% (wt/vol) BSA. After staining, cells were resuspended in staining buffer for analysis by flow cytometry. Flow cytometry was performed using a CyAnTM ADP (Beckman Coulter) and data were analyzed with FlowJo software package (Ashland, OR).

Single memory B cell sorting

Staining and single-cell sorting of memory B cells was performed as described [15]. Briefly, mice were sacrificed and fresh total splenocytes harvested were sequentially incubated with different specific antibodies (Supplementary table 1). For antigen specific-staining Streptavidin fluorescent proves were used (Alexa488-SA: 53370D, Alexa647-SA: 54050D and PE-SA). Then, Washed cells were subjected to single cell sorting to isolate CD4−, CD8−, Gr-1−, F4/80−, B220+, CD38−, IgM−, IgG+, and MACV GP1$^+$ memory B cells into 96-well plates using a FACSAria III sorter (Becton Dickinson) according to von Boehmer et al., 2016 detailed descrition. The cells were then lysed with 4 μl lysis buffer containing RNASin (Promega) 40 U/μl (0,3 μl), DPBS (Dulbecco) 10 x (0.2 μl), DTT (Invitrogen) 100 mM (0.4 μl) and nuclease-free water (3.1 μl). The sorted plates were stored at −80 °C until further processing.

Cloning and expression of Ig genes as a recombinant antibody

Cloning of recombinant IgGs was performed as reported earlier [16]. Briefly, total RNA of each antigen-specific sorted B cell was extracted and cDNA synthesized using reverse transcription (RT) with random hexamer primining. IgH and IgK or Igλ light chain genes were amplified in separate nested PCR reactions using cDNA as a template and water as a negative control. The PCR products were sequenced and subjected to IGBLAST to determine the V and J region of IgH and IgK or Igλ, respectively. Specific primers of V and J genes with restriction sites were used to amplify and clone the specific products into corresponding expression vectors. Vectors to express variable heavy chain and light chain of the antibody were transfected into HEK293T cells. Cell supernatant were collected after 48 h of transfection.

Immunofluorescence assay (IFA)

The immunofluorescence assay was described previously [17] . Briefly, A549 cells were seeded in a 96-well plate (3×10^4 cells/well). After 19 h, cells were transiently transfected with expression constructs for the indicated full-length arenavirus GPC and lipofectamine. At 48 h postransfection, cells were fixed with 4% paraformaldehyde (PFA). The cells were permeabilized with 0.01% (wt/vol) saponin in PBS containing 3% (wt/vol) BSA] and reacted first with each MACV GP1 mAb, followed by an Alexa Fluor 568-labeled (green) or rhodamine (red) anti-mouse secondary antibodies and counterstaining of nuclei (DAPI, blue). Specimens were examined by FLoid Cell imaging station form Life Sciences, CA.

Pseudovirion neutralization assay

Pseudotyped propagation-defective vesicular stomatitis virus (VSV) encoding the two reporter proteins green fluorescent protein (GFP) and firefly luciferase (Luc) was generated as described [18]. VSV pseudotypes bearing the envelope GP of MACV were generated as reported earlier [19]. For the pseudovirion neutralization assay, sera were diluted 1:20 in complete MEM, followed by two-fold serial dilutions. For each well (quadruplicates), serum dilutions (50 μl) were mixed with an equal volume of complete MEM containing 4,000 infectious units (IU) of VSV-MACV GP and incubated for 1 h at 37 °C. Following this incubation, the mixture was added to fresh monolayers of A549 cells cultured in clear bottom white-walled 96-well plates (Costar). After 1 h, the inoculum was removed by washing and fresh medium added. After 20 h at 37 °C and 5% (vol/vol) CO_2, luciferase reporter activity was detected using the Luciferase Assay System (Promega, WI). A GloMax (Promega, WI) microplate reader was used for signal acquisition.

Data collection and Statistical Analysis

1-way ANOVA (analysis of variance) followed by a Bonferroni post-test was used to assess statistical differences between the groups with a p-value < 0.05 was used as criterion of statistical significance. All data was analyzed using the GraphPad Prism 5 Software (GraphPad Software Inc., La Jolla, CA). All data presented as bar graphs represent the mean ± standard deviation (SD).

FIGURES
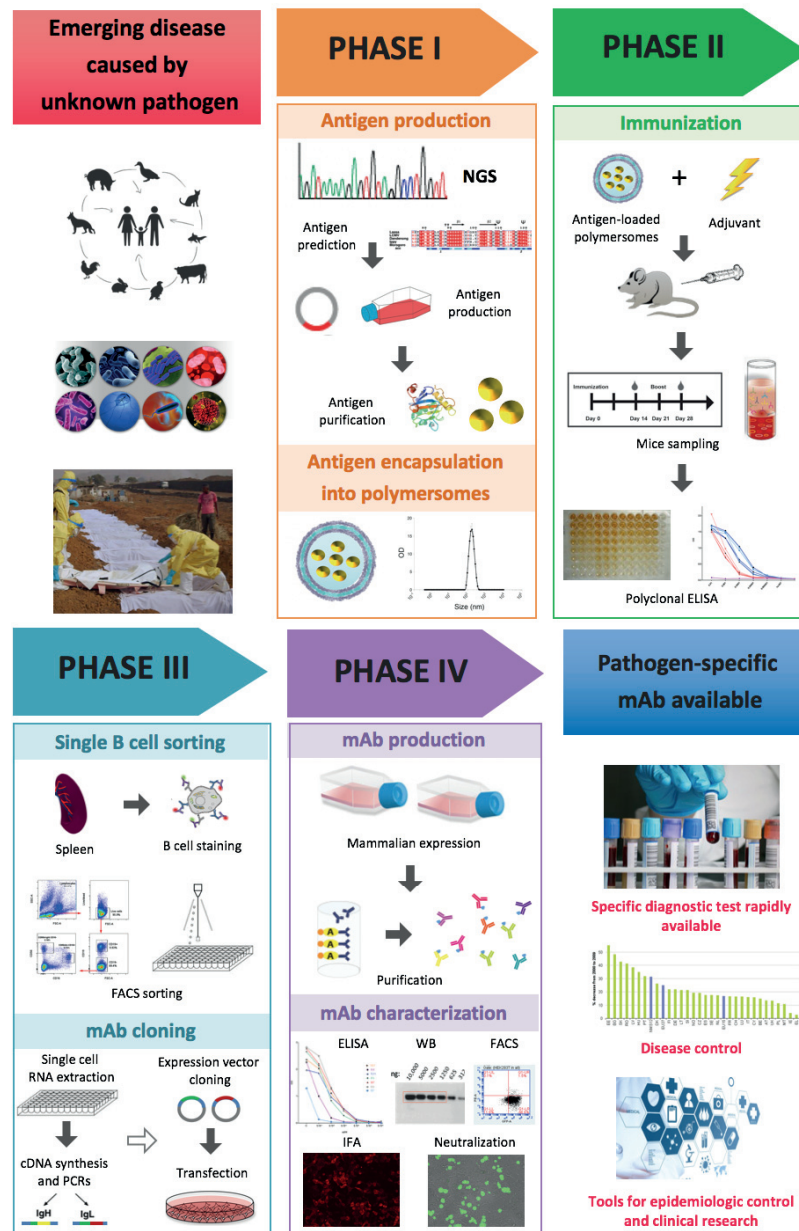
Figure 1. Workflow of our approach developed to rapidly produce recombinant mAb against newly emerging pathogens. When a disease caused by an unknown pathogen emerges, subtractive NGS approaches can be used to determine the nucleotide sequence of the pathogen's genetic material without the need to isolate the agent. Biocomputational analysis frequently allows the classification of the novel agent and the identification of putative ORFs coding for its structural and non-structural proteins that represent possible targets for antibodies. Based on this information, new candidate antigens can be *de novo* synthesized or produced in recombinant form based on cDNA sequences and purified. These antigens can then be encapsulated into PS nanocarriers (PHASE I). Antigen loaded PS combined with

a suitable predetermined adjuvant formulation can be used to immunize mice and obtain an enhanced polyclonal antigen-specific humoral immune response (PHASE II). Upon immunization following a prime-boost scheme, splenocytes are isolated form responding animals, followed by sorting of antigen-specific B cells using recombinant antigen as a bait in flow cytometry. Total RNA is extracted from individual antigen-specific B cells and specific primers used to amplify corresponding heavy and light IgG chains. Paired heavy and light chains are inserted into a mammalian expression vector in order to produce the recombinant monoclonal Abs (PHASE III). Finally, the candidates recombinant mAbs can be characterized in order to use them as therapeutic or diagnostic tools (PHASE IV).
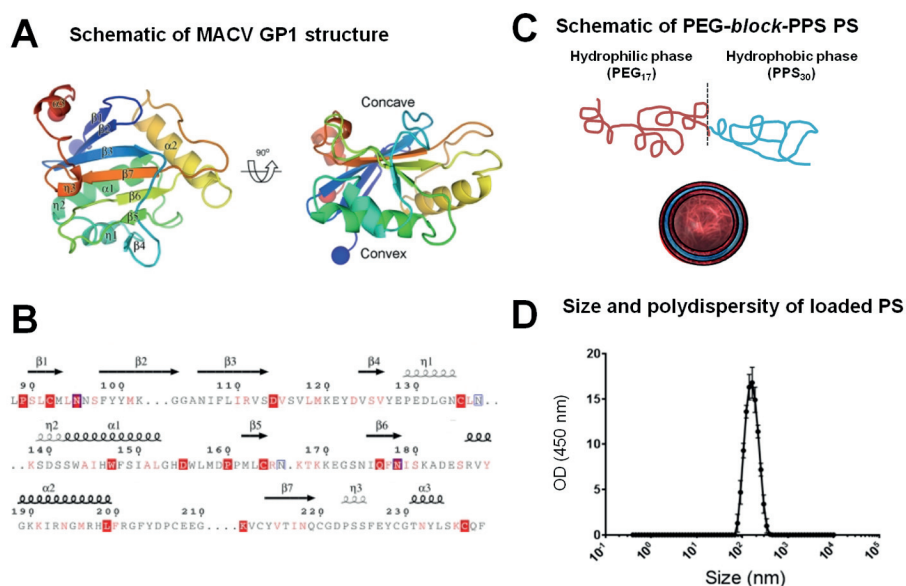
Figure 2. MACV GP1 antigen structure and PS (MACV GP1) production and immunization. A) Structure of MACV GP1. Left panel with cartoon diagram of MACV GP1 colored as a rainbow with the N terminus shown in blue and the C terminus in red. The N and C-termini are marked with blue and red spheres, respectively. Right panel with view of MACV GP1 rotated by 90° [33]. B) Sequence alignment of residues observed in the MACV GP1 crystal structure. Secondary structure elements are shown with an arrow and helices are shown as spirals, with α-helices shown in bold. Residues which are highlighted red are fully conserved with other related NW arenavirus GP1, residues which are colored red are partially conserved, and residues which are black are not conserved. Amino acids which correspond to predicted N-linked glycosylation sites are marked with blue boxes. C) Schematic representation of PEG-*bl*-PPS block copolymers and vesicles. Block copolymers composed of PEG and PPS self-assemble into oxidation-sensitive PS in aqueous solutions. Hydrophobic and hydrophilic regions are shown in red and blue, respectively. D) Size and polydispersity of loaded PS were

determined as described in Material and Methods. Data shown represent absorbance plotted against particle diameter. Maximum peak corresponds to 163 ±7 nm.
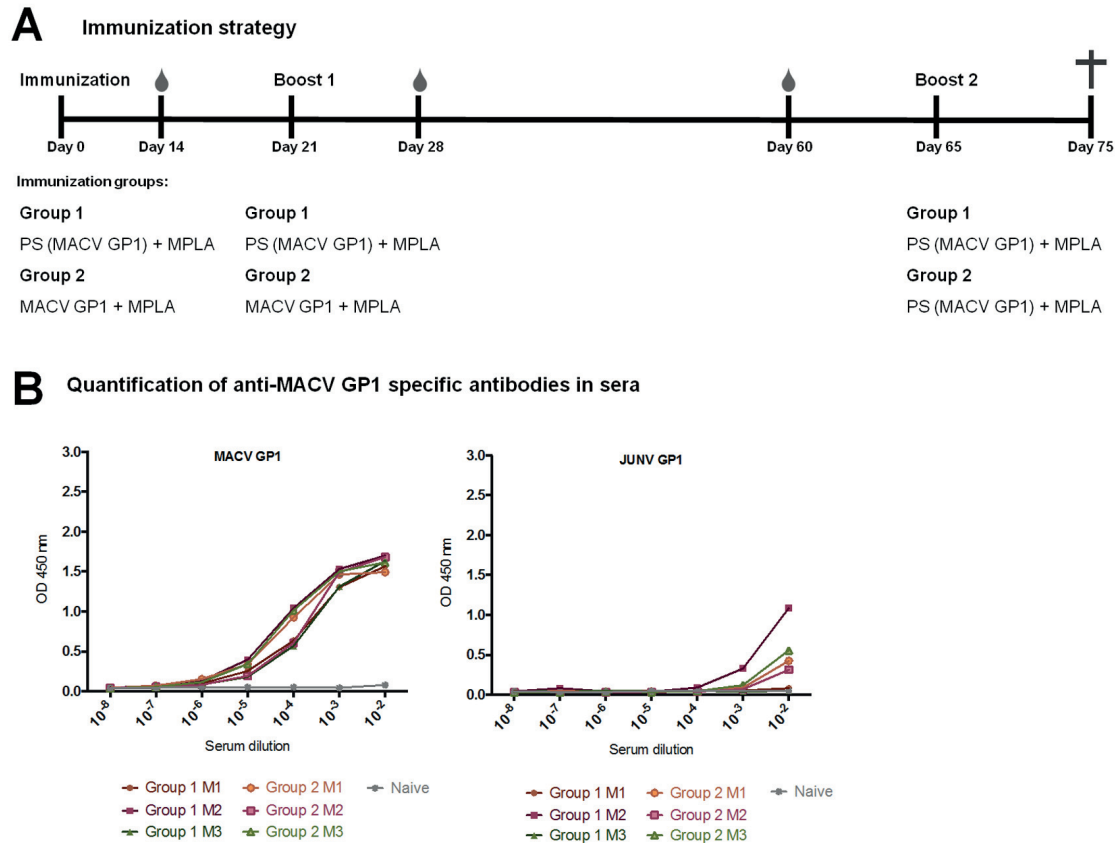
Figure 3. Immunization with PS (MACV GP1) induces a humoral response against MACV GP1. A) Schedule of immunization, blood draws, and composition of the immunization cocktail. Mice were immunized with either 10 μg of PS (MACV GP1) or 10 μg of MACV GP1. 10 μg of MPLA were constantly provided in the formulation. Mice were boosted 21 days after prime immunization and bleed on days 14 and 28 after prime immunization and every two weeks onwards. B) Detection of polyclonal anti-MACV GP1 and anti-JUNV GP1 specific IgG present in mice serum 60 days post immunization with specific ELISA test. Plates were coated with 5 μg of purified MACV GP1 or JUNV GP1 respectively. Data are OD 450 nm (n = 5± SD).

A Strategy of antigen-specific B cell sorting

Population selection:
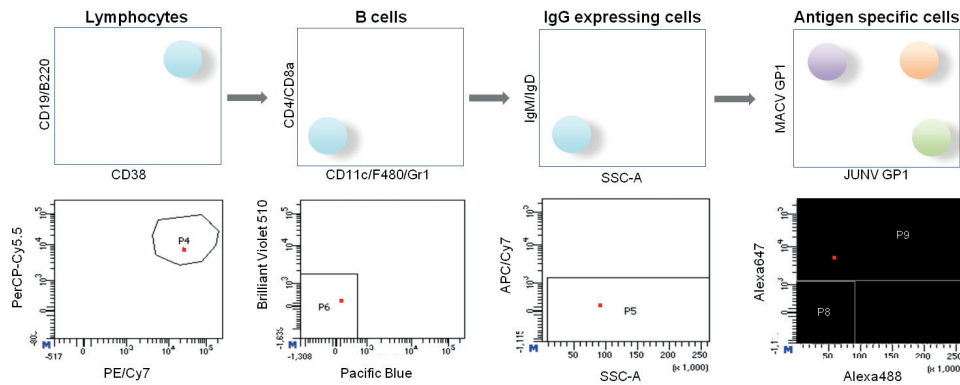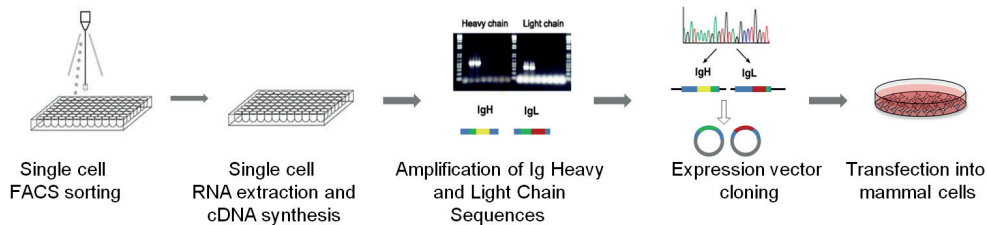
Figure 4. Sorting of single antigen-specific B cells and cloning of anti-MACV GP1-specific IgGs.
A) Gating strategy for isolation of antigen-specific single B cells. Antigen-specific IgG memory B cells are obtained by gating for $B220^+$, $CD38^+$, IgG^+IgM^- cells excluding cells expressing CD8, F4/80, CD4 and Gr-1 (DUMP). Gating for antigen-binding cells yielded three different populations, MACV GP1 specific (purple), JUNV GP1 specific (green) and cross-reactive MACV-JUNV GP1 specific B cells (orange). B) Work flow of the strategy followed for the cloning and expression of antigen specific IgG. Briefly, after single memory B cell isolation, V(D)J transcripts were amplified by RT-PCR. Fragments were then combined with linearized expression vectors, assembled *in vitro* as part of a sequence- and ligation-independent cloning reaction and then transformed into *Escherichia coli*. Purified vectors were then used to transfect HEK293 suspension cells and produce and isolate mAb.

Figure 5. The mAbs 10G7, 8G8, 7C11, 8F4, 8B7, and 8B9 are specific for MACV GP1. A) Microtiter plates were coated with purified MACV, JUNV, GTOV, OECV and LASV GP1s purified antigens. After blocking, plates were incubated with each MACV GP1 mAb in 10-fold serial dilutions for 2 hrs at RT. For the detection, bound primary antibodies were detected by HRP-conjugated secondary antibodies to total IgG. B) IgG isotype determination of MACV GP1 mAb in a color reaction. Data are OD 450 nm (n = 5± SD).
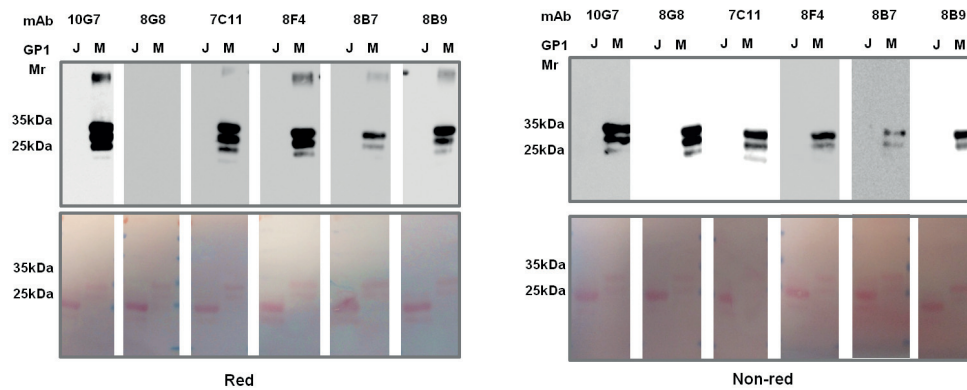
Figure 6. Specificity of MACV GP1 mAbs to MACV GP1 in Western Blot. A) The mAbs 10G7, 8G8, 7C11, 8F4, 8B7, and 8B9 recognize MACV GP1 in Western blot under reducing/denaturing conditions. For Western blotting, purified MACV GP1 and JUNV GP1 protein were subjected to SDS-PAGE under reducing and not reducing conditions, and the separated proteins transferred to a nitrocellulose membrane. After blocking, the membrane was incubated with each of the mAbs, followed by incubation with HRP-conjugated secondary antibody and development by ECL. Molecular mass markers are indicated.
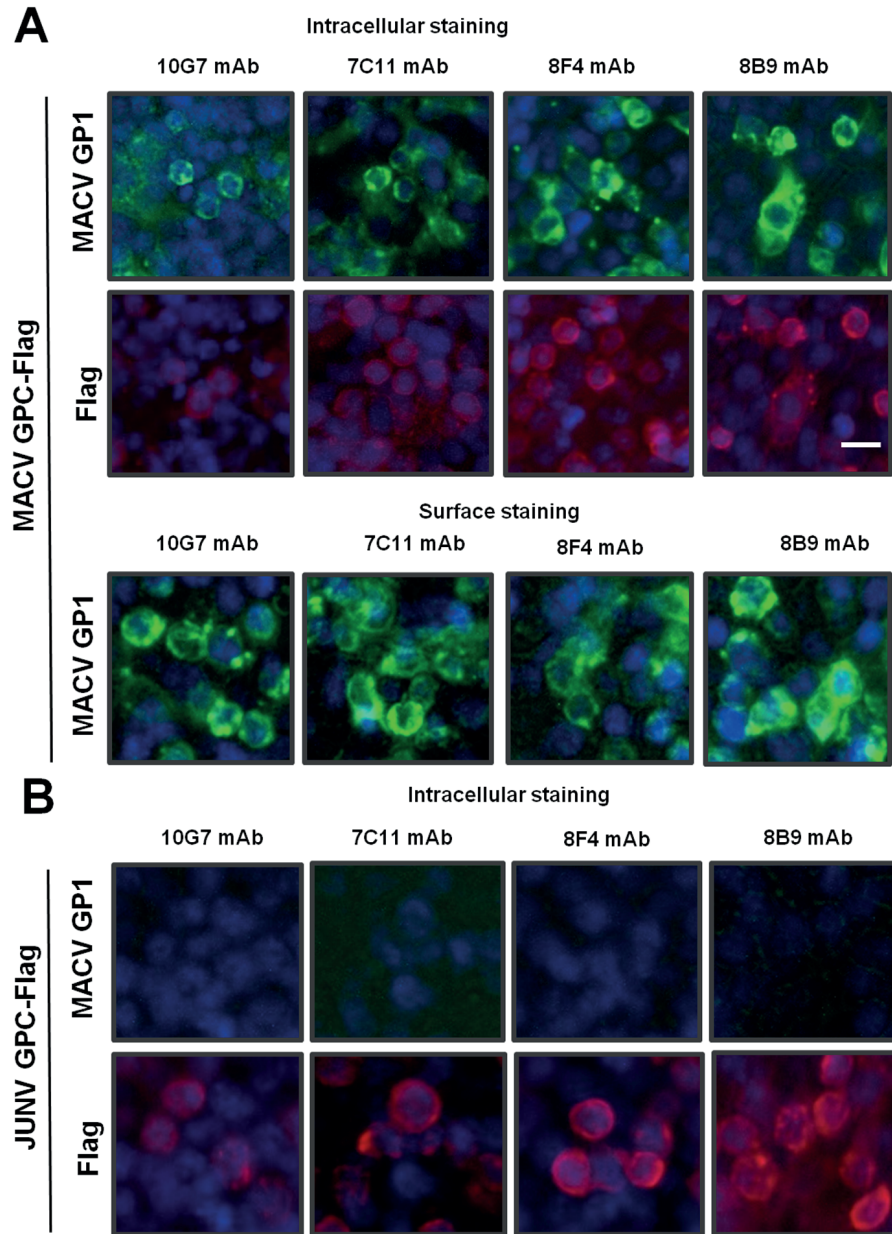
Figure 7. mAbs 10G7, 7C11, 8F4, and 8B9 are specific for MACV GP1 in IFA. Immunofluorescence assay with mAbs 10G7, 7C11, 8F4, and 8B9. HEK293T cells were transfected with MACV GPC-Flag, (A) JUNV GPC-Flag (B) or mock transfected, cells fixed and then treated with saponin for permeabilization (intracellular staining) or left untreated (surface staining) and incubated with the indicated mAbs. Bound mAbs were detected with a secondary antibody conjugated to GFP and the flag tag was detected with a secondary antibody conjugated to rhodamine-red. Bar = 10 μm.

Surface staining of MACV GPC expressing cells with MACV GP1 mAb
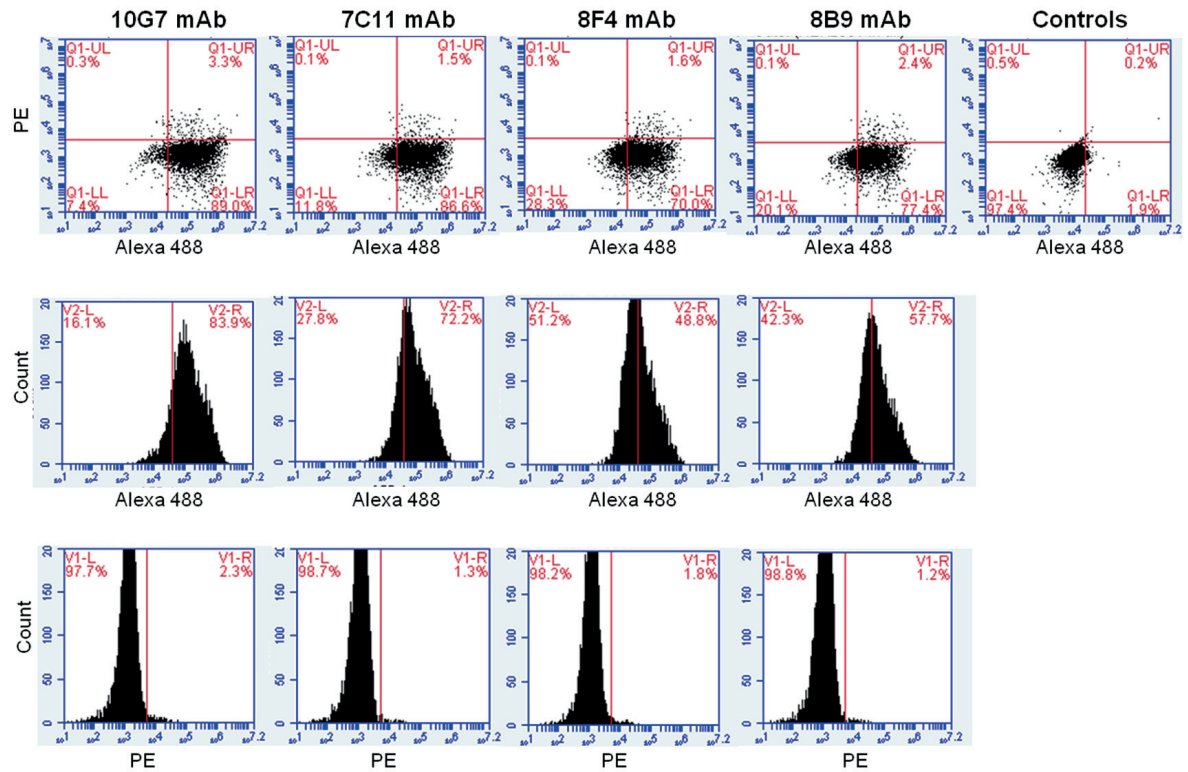
Figure 8. MACV GP1 mAbs bind to MACV GP1 in live cells. A) Detection of MACV GP1 on live non-permeabilized cells in flow cytometry. HEK 293T cells were transfected with MACV GPC-Flag and live, non-permeabilized cells stained with the indicated mAbs. After fixation, bound primary antibodies were detected in flow cytometry using PE-conjugated or Alexa 488 secondary antibodies.
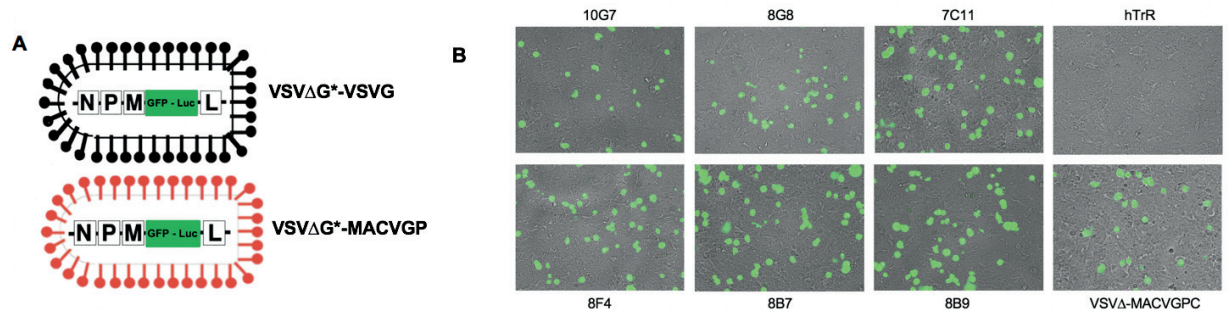
Fig S1. Detection of neutralizing anti-MACV GP1 antibodies in a pseudotype neutralization assay. **A)** Schematic representation of VSV pseudotypes. The replication-deficient VSVΔG*-GFP-Luc lacking the endogenous glycoprotein (G) protein was pseudotyped by *trans*-complementation with either the cognate VSV G glycoprotein (VSVΔG*-VSVG) or full-length MACV GP (VSVΔG*-MACVG). mAbs were diluted up to 20μg/ml (quadruplicates) and mixed with an equal volume of complete MEM containing VSV pseudotypes at 4,000 infectious units (IU) per well of a 96-well plate in presence and absence of complement. As a positive control we used purified hTfR1 which acts like a neutralizing antibody [34]. This mixture was incubated for 1 h at 37 °C and added to fresh monolayers of A549 cells. Luciferase/GFP reporter activity was detected after 48 h. Only the samples treated with the poitive control showed marked neutralization, whereas neutralization in antibody-treated samples did not reach statistical significance.

Distributor	ref	Ab
eBioscience	45-0452-80	Anti-Human/Mouse CD45R (B220) PerCP-Cy5.5 25 ug
eBioscience	45-0193-80	Anti-Mouse CD19 PerCP-Cy5.5 25 ug
Biolegend	102717	PE/Cy7 anti-mouse CD38 Antibody [Clone: 90]
Biolegend	405715	APC/Cy7 anti-mouse IgD Antibody [Clone: 11-26c.2a]
Biolegend	406515	APC/Cy7 anti-mouse IgM Antibody [Clone: RMM-1]
Biolegend	100751	Brilliant Violet 510™ anti-mouse CD8a Antibody [Clone: 53-6.7]
Biolegend	100553	Brilliant Violet 510™ anti-mouse CD4 Antibody [Clone: RM4-5]
eBioscience	48-5931-80	Anti-Mouse Ly-6G (Gr-1) eFluor® 450 25 ug
eBioscience	48-0114-80	Anti-Mouse CD11c eFluor® 450 25 ug
Biolegend	123123	Pacific Blue™ anti-mouse F4/80 Antibody [Clone: BM8]
Insight Biotechnology	553142	Rat anti-Mouse CD16/CD32 (FcBlock), 0.5mg

Supplementary table 1. Antibodies used for the B cell sorting staining as detailed in Materials and Methods.

REFERENCES

1. Lefterova, M.I., et al., *Next-Generation Sequencing for Infectious Disease Diagnosis and Management: A Report of the Association for Molecular Pathology*. J Mol Diagn, 2015. **17**(6): p. 623-34.
2. Datta, S., et al., *Next-generation sequencing in clinical virology: Discovery of new viruses*. World J Virol, 2015. **4**(3): p. 265-76.
3. Buchmeier, M.J., J.C. de la Torre, and C.J. Peters, *Arenaviridae: the viruses and their replication*, in *Fields Virology*, D.L. Knipe and P.M. Howley, Editors. 2007, Lippincott-Raven: Philadelphia. p. p. 1791-1828.
4. Radoshitzky, S.R., et al., *Past, present, and future of arenavirus taxonomy*. Arch Virol, 2015. **160**(7): p. 1851-74.
5. Charrel, R.N., et al., *Arenaviruses and hantaviruses: from epidemiology and genomics to antivirals*. Antiviral Res, 2011. **90**(2): p. 102-14.
6. Peters, C.J., *Human infection with arenaviruses in the Americas*. Curr Top Microbiol Immunol, 2002. **262**: p. 65-74.
7. McCormick, J.B. and S.P. Fisher-Hoch, *Lassa fever*. Curr Top Microbiol Immunol, 2002. **262**: p. 75-109.
8. Nakauchi, M., et al., *Characterization of monoclonal antibodies to Junin virus nucleocapsid protein and application to the diagnosis of hemorrhagic fever caused by South American arenaviruses*. Clin Vaccine Immunol, 2009. **16**(8): p. 1132-8.
9. Sanchez, A., et al., *Junin virus monoclonal antibodies: characterization and cross-reactivity with other arenaviruses*. J Gen Virol, 1989. **70 (Pt 5)**: p. 1125-32.
10. Ruo, S.L., et al., *Antigenic relatedness between arenaviruses defined at the epitope level by monoclonal antibodies*. J Gen Virol, 1991. **72 (Pt 3)**: p. 549-55.
11. Bowden, T.A., et al., *Unusual molecular architecture of the machupo virus attachment glycoprotein*. Journal of virology, 2009. **83**(16): p. 8259-65.
12. Zeltina, A., et al., *Convergent immunological solutions to Argentine hemorrhagic fever virus neutralization*. Proc Natl Acad Sci U S A, 2017. **114**(27): p. 7031-7036.
13. Scott, E.A., et al., *Dendritic cell activation and T cell priming with adjuvant- and antigen-loaded oxidation-sensitive polymersomes*. Biomaterials, 2012. **33**(26): p. 6211-9.
14. Kunz, S., et al., *Mechanisms for lymphocytic choriomeningitis virus glycoprotein cleavage, transport, and incorporation into virions*. Virology, 2003. **314**(1): p. 168-78.
15. Tiller, T., C.E. Busse, and H. Wardemann, *Cloning and expression of murine Ig genes from single B cells*. J Immunol Methods, 2009. **350**(1-2): p. 183-93.
16. von Boehmer, L., et al., *Sequencing and cloning of antigen-specific antibodies from mouse memory B cells*. Nat Protoc, 2016. **11**(10): p. 1908-1923.
17. Rojek, J.M., et al., *Old World Arenavirus Infection Interferes with the Expression of Functional {alpha}-Dystroglycan in the Host Cell*. Mol Biol Cell, 2007. **29**: p. 29.
18. Berger Rentsch, M. and G. Zimmer, *A vesicular stomatitis virus replicon-based bioassay for the rapid and sensitive determination of multi-species type I interferon*. PLoS One, 2011. **6**(10): p. e25858.
19. Kunz, S., et al., *Characterization of the interaction of lassa fever virus with its cellular receptor alpha-dystroglycan*. J Virol, 2005. **79**(10): p. 5979-87.
20. Abraham, J., et al., *Structural basis for receptor recognition by New World hemorrhagic fever arenaviruses*. Nat Struct Mol Biol, 2010. **17**(4): p. 438-44.
21. Radoshitzky, S.R., et al., *Transferrin receptor 1 is a cellular receptor for New World haemorrhagic fever arenaviruses*. Nature., 2007. **446**(7131): p. 92-6. Epub 2007 Feb 7.
22. Stano, A., et al., *Tunable T cell immunity towards a protein antigen using polymersomes vs. solid-core nanoparticles*. Biomaterials, 2013. **34**(17): p. 4339-46.
23. Casella, C.R. and T.C. Mitchell, *Putting endotoxin to work for us: monophosphoryl lipid A as a safe and effective vaccine adjuvant*. Cell Mol Life Sci, 2008. **65**(20): p. 3231-40.
24. Moeschler, S., et al., *Quantification of Lyssavirus-Neutralizing Antibodies Using Vesicular Stomatitis Virus Pseudotype Particles*. Viruses, 2016. **8**(9).
25. Fukushi, S., et al., *Serological assays based on recombinant viral proteins for the diagnosis of arenavirus hemorrhagic fevers*. Viruses, 2012. **4**(10): p. 2097-114.
26. Saijo, M., et al., *Development of recombinant nucleoprotein-based diagnostic systems for Lassa fever*. Clinical and vaccine immunology : CVI, 2007. **14**(9): p. 1182-9.
27. Emonet, S.F., et al., *Arenavirus genetic diversity and its biological implications*. Infect Genet Evol, 2009. **9**(4): p. 417-29.
28. Charrel, R.N., X. de Lamballerie, and S. Emonet, *Phylogeny of the genus Arenavirus*. Curr Opin Microbiol, 2008. **11**(4): p. 362-8.

29. Sommerstein, R., et al., *Arenavirus Glycan Shield Promotes Neutralizing Antibody Evasion and Protracted Infection*. PLoS Pathog, 2015. **11**(11): p. e1005276.

30. Burton, D.R. and J.R. Mascola, *Antibody responses to envelope glycoproteins in HIV-1 infection*. Nat Immunol, 2015. **16**(6): p. 571-6.

31. Burton, D.R., et al., *Broadly neutralizing antibodies present new prospects to counter highly antigenically diverse viruses*. Science, 2012. **337**(6091): p. 183-6.

32. Walker, L.M. and D.R. Burton, *Rational antibody-based HIV-1 vaccine design: current approaches and future directions*. Current opinion in immunology, 2010. **22**(3): p. 358-66.

33. Bowden, T.A., et al., *Unusual molecular architecture of the machupo virus attachment glycoprotein*. J Virol, 2009. **83**(16): p. 8259-65.

34. Lee, A.M., et al., *Inhibition of cellular entry of lymphocytic choriomeningitis virus by amphipathic DNA polymers*. Virology, 2008. **372**(1): p. 107-17.

CHAPTER 4

Conclusions, implications and future directions

CONCLUSIONS

In the first part of my thesis a PS-based nanocarrier platform was evaluated for its ability to improve the antibody response against the poorly immunogenic surface antigen GP1 of LASV. We were able to demonstrate that antigen encapsulation into PS enhanced overall LASV GP1-specific antibody titers and markedly increased virus-binding antibodies, capable of recognizing GP1 in the context of the authentic virion spike. Delivery of the poorly immunogenic LASV GP1 via PS resulted in higher frequencies of follicular helper CD4 T cells, increased the numbers of antigen-specific CD4 T cells and the frequency of polyfunctional IFN-γ /TNF-α secreting CD4 T cells. An enhanced frequency of antigen-specific IgG-secreting B cells correlated with a broadened epitope-range. Together, the data indicate that PS encapsulation enhanced the humoral response in terms of both magnitude and quality.

During the second part of my studies, we took an additional step and applied the obtained knowledge to develop a novel approach for the rapid production of antigen-specific recombinant mAb using biosynthetic antigens that can be generated based on sequence information only. In a proof-of-concept study, we combined our PS platform with single B cell sorting and molecular cloning of recombinant IgGs, to generate a unique panel of "first in class" mAb specific to MACV GP1 which showed exquisite selectivity for MACV in ELISA, Western blot, IFA, and flow cytometry. These novel mAbs will be invaluable for research and development of novel diagnostic tests against this devastating and understudied emerging pathogen.

IMPLICATIONS AND FUTURE DIRECTONS

Towards a new vaccine against Lassa virus

Lassa virus currently causes several hundred thousand infections per year with thousands of deaths, affecting some of the poorest countries in the World. Incomplete knowledge of the virus and the disease, the requirement for BSL4 facilities to work with live virus, and lack of suitable platforms prevented so far the development of an efficient and safe vaccine. The limited therapeutic options, overall weak public health infrastructure in affected regions, and the rapid geographical spread of this hemorrhagic fever-causing virus, makes progress in the field indispensable and of immediate importance. A series of recent reports emphasized the promise of protective antibodies in treatment and prevention of Lassa fever and provided novel insights into the mechanisms of antibody-mediated neutralization of LASV [1-4]. Research on the fundamental virology of Lassa virus further shed light on the molecular mechanisms of viral attachment and entry that are the key targets for protective antibodies [5-10]. Compilation of these published studies with our work presented here and studies that I contributed to (Fedeli et al., manuscript attached) could pave the way for the development of a protective LASV vaccine as well as novel immunotherapeutics.

A major drawback of our current PS (LASV GP1) vaccine formulation is its apparent inability to elicit potent neutralizing antibodies (nAb) defined operationally by our VSV-pseudotype-based in vitro neutralization test. Notably, the same neutralization test format proved to be very powerful in recent applications for the Ebola vaccine development [11], suggesting an inherent limitation in our vaccine system rather than an experimental artefact. Novel insights into the molecular mechanisms of antibody-mediated neutralization of LASV provide a possible explanation for this. Examination of a large panel of nAb isolated from Lassa fever survivors revealed specificity for conformational epitopes that frequently depended on GP1/GP2 quaternary structures [1]. The very recently reported high resolution structure of LASV GP in its pre-fusion conformation bound to one of these newly isolated nAb further highlighted the relevance of quaternary structures during immunization, emphasizing that the GP1/GP2 interface is essential for receptor binding and antibody neutralization [2]. To experimentally address this issue, I propose to design a new improved LASV immunogen retaining key structural elements of the quaternary structure of the prefusion GP trimer, in particular features of the GP1/GP1 trimer and GP1/GP2 heterodimer interface. A major challenge will be the stabilization of the trimeric structure of the LASV GP ectodomain in absence of the membrane anchor. In their structural studies, Hastie et al. achieved this stabilization by "clamping" the soluble LASV GP ectodomain into its trimeric form with an antibody [2]. Similar stabilization of the trimeric ectodomain of a trimeric class I viral fusion protein was achieved with a smaller biosynthetic trimerization domain used in studies on the influenza A virus 1918 hemagglutinin [12]. We expect that delivery of an immunogen containing at least parts of the crucial molecular interfaces of the trimer via our PS platform would markedly increase the probability to obtain nAb.

Many nAb target viral envelope GPs in their pre-fusion conformation and interfere with binding to receptors or co-receptors [13, 14]. This would be the case for at least some of the nAb elicited by the newly improved antigen derived from the LASV GP prefusion trimer outlined above. Interestingly, upon entry via its cellular receptor DG, LASV is rapidly delivered to the late endosome, where the virus undergoes a "receptor switch" and engages the late endosomal/lysosomal resident protein LAMP-1 that is essential for efficient fusion [5, 7, 8]. Although most Old World arenaviruses can use DG as a receptor, the ability to hijack LAMP-1 as a late endosomal entry factor is unique for LASV [9]. Our unpublished data further show that LASV entry via the alternative receptor Axl likewise depends of LAMP-1, suggesting convergence at the level of the late endosomal entry factor (Fedeli et al., manuscript attached). The use of an essential intracellular entry factor by LASV is shared by the filovirus Ebola that hijacks the late endosomal protein Niemann-Pick1 (NPC1) to penetrate the limiting endosomal membrane [15]. A current model of the sequence of events during this late endosomal receptor switch is presented in Fig. 1. Please note that the dissociation from the cell surface receptor is followed by a lag-phase during which the free LASV GP undergoes protonation, preventing fusion until it engages LAMP1 that provides the fusion-triggering signal. Very recent experimental studies performed in our laboratory by my colleague Dr. Chiara Fedeli revealed a duration of this lag-phase of circa 5-10 min. Considering the fast on-rates of high affinity nAb, pre-loading of cells with nAb targeting the specific conformation of LASV GP1 required for LAMP-1 binding appears as a promising "second hit" strategy to prevent viral fusion at the level of the late endosome. Recent cryo-tomography studies on authentic LASV particles indicated drastic conformational changes of LASV GP1 under acidic pH (< 5.5) [16]. Performing crystallization of LASV GP1 under acidic pH, the structure of the low pH conformation was resolved [7]. As expected this stable low energy conformation of LASV GP1 bound LAMP-1 with high affinity, but was unable to recognize the cell surface receptor DG. Since the low pH conformation of LASV GP1 represents an attractive second target for anti-viral nAb, I propose to deliver both, LASV GP in its pre-fusion conformation and the low pH form of GP1 in a combined PS-based vaccine. The resulting antibody response would include "classical" nAb targeting LASV GP in its pre-fusion conformation, thus preventing host cell attachment, and a second type of nAb that would enter the scene once the virus has overcome the barrier of the plasma membrane and reaches the late endosomal compartment in search for its entry factor LAMP-1. As all RNA viruses, LASV has a high mutation rate, rendering this pathogen highly plastic. A major concern of recombinant LASV vaccines based on biosynthetic immunogens is the possibility of the virus to escape nAb by acquisition of specific mutations in immunodominant B cell epitopes. Targeting in addition the secondary endosomal receptor binding would still block such putative escape variants, reducing the risk of vaccine failure. Moreover, LASV enters human cells via macropinocytosis [10], which is the major pathway of bulk liquid transport. As a consequence, both virion and nAb would reach the same cellular compartment, the late endosomes, where viral fusion takes place. Conceptually, a similar strategy is currently explored against Ebola virus targeting NPC1 at the level of the late endosome.
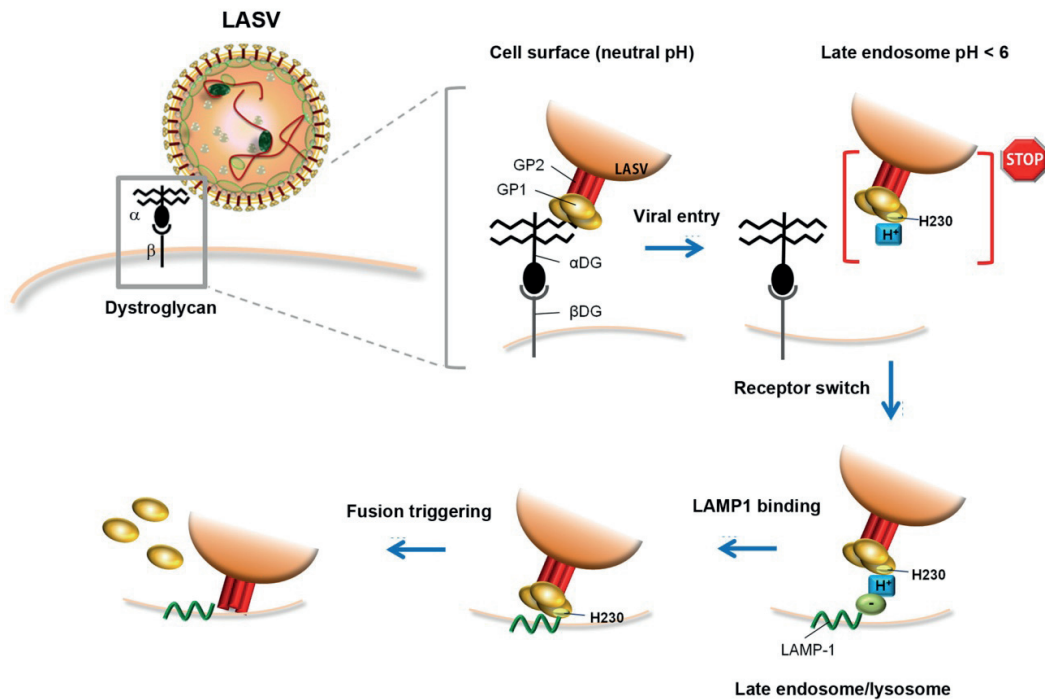
Figure 1. Current model for the late endosomal "receptor switch" of LASV. At the cell surface, LASV GP1 engages the O-linked matriglycan polysaccharides displayed by α-DG, followed by endocytosis via an unusual pathway related to macropinocytosis. Progressive acidification of late endosomes induces a structural change in LASV GP1, which dissociates from DG and adapts a low pH conformation displaying a histidine-triad. Protonation of residue H230 "locks" GP1 in the pre-fusion state, preventing premature fusion. Engagement of LAMP1 neutralizes the positive charge on H230 of GP1 and triggers efficient fusion with the limiting membrane of the late endosome/lysosome. Taken from [17].

A novel approach for the production of mAb against novel emerging human pathogens

Regarding pathogenic novel emerging viruses their classification as BSL3 or BSL4 pathogens frequently limits diagnostics, in particular in remote areas with limited public heath infrastructure. Reliable, specific, inexpensive, rapid, and high-throughput, point-of-care, virus-free serology assays, are critical tools for the decision-making process during the initial steps of an emerging health crisis in order to contain the outbreak. The necessity for sensitive and specific diagnostic tests for the detection of emerging and re-emerging pathogens is dramatically illustrated by the ongoing outbreak of Zika virus. The only transient viremia in individuals infected with Zika virus limits the positive predictive value of RT-PCR and other molecular diagnostic tests. The lack of a specific serological test for Zika caused extensive misdiagnosis of early cases that were erroneously taken for Dengue, a very abundant pathogen in many of the affected countries. Due to the persisting cross-reactivity with multiple flavivirus antigens and the lack of specific serology-based assays, laboratory diagnosis of Zika virus still relies on laborious and time-consuming virus isolation or RNA detection techniques with the abovementioned limitations. As more structural information becomes available on the E proteins of Zika and other relevant flaviviruses, the design of candidate biosynthetic antigens that may be capable of eliciting specific mAb to Zika becomes feasible. Our novel approach would allow rapid testing of panels of biosynthetic immunogen candidates using our PS platform. In case a specific response is obtained, B cells could be isolated, followed by cloning and production of recombinant mAb. Such mAb could then be directly used in etiological diagnostics in the clinic, e.g. IFA of infected tissue specimens or sandwich-ELISA for direct pathogen detection, as well as references for seroepidemiological studies. An example for such an assay is a highly specific sandwich-ELISA based on mAbs developed for the detection of JUNV currently used in Argentina in endemic regions [18, 19]. The advent of powerful next-generation sequencing technologies has greatly accelerated the discovery of novel pathogens, but their isolation is frequently not possible. Another decisive advantage of our novel approach based on the PS platform in the context of emerging pathogens is the use of recombinant biosynthetic immunogens that can be designed and produced based on available sequence information only. In our proof-of-concept study, we showed that the versatile immunization scaffold of PS allows rapid production of specific antibodies via immunization, followed by B cell sorting, and cloning of specific IgG within a few months. Such mAb can be rapidly tested for specificity and evaluated for diagnostic as well as therapeutic potential.

REFERENCES

1. Robinson, J.E., et al., *Most neutralizing human monoclonal antibodies target novel epitopes requiring both Lassa virus glycoprotein subunits.* Nat Commun, 2016. **7**: p. 11544.
2. Hastie, K.M., et al., *Structural basis for antibody-mediated neutralization of Lassa virus.* Science, 2017. **356**(6341): p. 923-928.
3. Cross, R.W., et al., *Treatment of Lassa virus infection in outbred guinea pigs with first-in-class human monoclonal antibodies.* Antiviral Res, 2016. **133**: p. 218-22.
4. Mire, C.E., et al., *Human-monoclonal-antibody therapy protects nonhuman primates against advanced Lassa fever.* Nat Med, 2017.
5. Jae, L.T., et al., *Virus entry. Lassa virus entry requires a trigger-induced receptor switch.* Science, 2014. **344**(6191): p. 1506-10.
6. Jae, L.T., et al., *Deciphering the glycosylome of dystroglycanopathies using haploid screens for lassa virus entry.* Science, 2013. **340**(6131): p. 479-83.
7. Cohen-Dvashi, H., et al., *Molecular Mechanism for LAMP1 Recognition by Lassa Virus.* J Virol, 2015. **89**(15): p. 7584-92.
8. Cohen-Dvashi, H., et al., *Role of LAMP1 Binding and pH Sensing by the Spike Complex of Lassa Virus.* J Virol, 2016. **90**(22): p. 10329-10338.
9. Israeli, H., et al., *Mapping of the Lassa virus LAMP1 binding site reveals unique determinants not shared by other old world arenaviruses.* PLoS Pathog, 2017. **13**(4): p. e1006337.
10. Oppliger, J., et al., *Lassa virus cell entry via dystroglycan involves an unusual pathway of macropinocytosis.* J Virol, 2016.
11. Wilkinson, D.E., et al., *Comparison of platform technologies for assaying antibody to Ebola virus.* Vaccine, 2017. **35**(9): p. 1347-1352.
12. Stevens, J., et al., *Structure of the uncleaved human H1 hemagglutinin from the extinct 1918 influenza virus.* Science, 2004. **303**(5665): p. 1866-70.
13. Burton, D.R. and J.R. Mascola, *Antibody responses to envelope glycoproteins in HIV-1 infection.* Nat Immunol, 2015. **16**(6): p. 571-6.
14. Burton, D.R., et al., *Broadly neutralizing antibodies present new prospects to counter highly antigenically diverse viruses.* Science, 2012. **337**(6091): p. 183-6.
15. Jae, L.T. and T.R. Brummelkamp, *Emerging intracellular receptors for hemorrhagic fever viruses.* Trends Microbiol, 2015. **23**(7): p. 392-400.
16. Li, S., et al., *Acidic pH-Induced Conformations and LAMP1 Binding of the Lassa Virus Glycoprotein Spike.* PLoS Pathog, 2016. **12**(2): p. e1005418.
17. Torriani, G., C. Galan-Navarro, and S. Kunz, *Lassa Virus Cell Entry Reveals New Aspects of Virus-Host Cell Interaction.* J Virol, 2017. **91**(4).
18. Nakauchi, M., et al., *Characterization of monoclonal antibodies to Junin virus nucleocapsid protein and application to the diagnosis of hemorrhagic fever caused by South American arenaviruses.* Clin Vaccine Immunol, 2009. **16**(8): p. 1132-8.
19. Fukushi, S., et al., *Serological assays based on recombinant viral proteins for the diagnosis of arenavirus hemorrhagic fevers.* Viruses, 2012. **4**(10): p. 2097-114.

APPENDIX

Structural studies of LASV GP1 antigen

Articles & manuscripts as co-author

-Lassa virus cell entry reveals new aspects of virus-host cell interaction

-Antigen persistence promoted by nanoparticle-carrier vaccine induces protective CD8 T cells with an effector memory phenotype

-Different roles of Axl in cell entry of Lassa virus

Contribution to manuscripts:

Review Torriani et al. JVI

In this invited Gem review article of the Journal of Virology, I participated in the discussions, the development of concepts, and writing of the article.

Manuscript Fedeli et al., JVI

This manuscript is currently under revision at the *Journal of Virology*.

In this project, I developed the specific protocols for virus production and purification that were instrumental for the study, specifically experiments shown in Fig. 2, 4, 6, and 7. I further optimized existing experimental protocols for IFA detection and quantification of virus used throughout the study.

Manuscript Rincon-Estrepo et al.,

In this manuscript I have amplified and quantified the LCMV virus for the challenge experiments. I have helped with performance of the animal work in mice, both in during immunization and during i.v challenge with the virus. I have also collaborated in the bleeding and organ collection of mice throughout the experiments. I participated in the discussions, the development of concepts exposed in the article.

STRUCTURAL STUDIES ON LASV GP1 ANTIGEN

BACKGROUND AND MOTIVATION

During the first years of my doctoral thesis I evaluated a novel vaccine platform based on polymersomes (PS) coupled with biosynthetic antigens for its potential to elicit a protective antibody response against Arenaviruses. For this purpose, a LASV immunogen derived from the receptor-binding domain of the viral envelope glycoprotein (GP) 1 was engineered. To achieve sufficient expression levels and to ensure proper folding, LASV GP1 was expressed as a C-terminal fusion with human IgG1 containing an enterokinase processing site, allowing cleavage of the protein. When expressed in human cells, the LASV GP1 immunogen showed an N-glycosylation pattern similar to authentic LASV GP1 present on the virus. Using a solid-phase binding assay previously developed to assess LASV-receptor binding [1], we observed binding to the LASV receptor DG. These features and the high purity of the protein obtained, in addition to the fact that it can be produced in high amounts in mammalian cells, made this antigen an interesting candidate to obtain structural information on LASV GP1 in its putative pre-fusion conformation that represents the primary target for nAb. Structural data at atomic resolution for viral proteins is key for understanding their function at the molecular level and can facilitate novel avenues for combating viral infections. A detailed structure of an antigen or a complex of an antigen with specific antibodies could give insight not only into viral entry mechanisms, but as well provide information about antibody neutralization or protection, information which could provide a template for vaccine design.

The only known high-resolution structure of LASV GP1 up to beginning of 2017 was obtained from a truncated, underglycosylated variant produced in insect cells that crystallized under low pH (5.0) [2]. This form of LASV GP was unable to bind to dystroglycan but recognized the late endosomal resident protein LAMP-1 that represents an intracellular receptor for LASV.

During 2016, I spent three months as a visiting graduate student in Prof. Erica Ollmann Saphire's laboratory, one of the world's leading structural biologist working on emerging viruses and who has made crucial advances in the field of hemorrhagic fever viruses such Ebola virus and arenaviruses. An important goal in Prof. Saphires laboratory was the structural characterization of the LASV GP1 antigen via crystallization of LASV GP1 protein. Since crystallization of the heavy glycosylated viral antigen in its native conformation is sometimes challenging, the viral GP was complexed with Fab fragments isolated from human LASV survivors [3] that bind conformation-dependent epitopes. These can stabilize GP1's conformation and therefore facilitate the formation of regular crystals that show sufficient X-ray diffraction patterns to obtain robust datasets and predict protein structure. Among the experiments performed during this internship, the first was to further characterize the purified LASV GP1 antigen using Size Exclusion Chromatography with Multi-Angle Light Scattering Detection (SEC-MALS). Static Light Scattering (SLS) is an optical technique that measures the intensity of the scattered light in dependence of the scattering angle to obtain information

on the scattering source. A typical application is the determination of the average molecular weight of a macromolecule such as a polymer or a protein. Performing MALS experiments on LASV GP1 helped us to determine the protein fraction of the sample in comparison with the modifier, (the glycans) and gave us information about the polydispersity of both, the protein fraction and the modifier (Figure 1A).

A panel of different LASV GP1 human mAb was isolated from patients surviving Lassa fever, including three neutralizing mAb against LASV GP1 [3]. A first screen to confirm binding of Fab fragments of some of these mAb to LASV GP1 protein was performed by direct ELISA (Figure 1 B). The six best binding Fab candidates were used to generate LASV GP1-Fab complexes, namely 10.4B, 19.5E, 5.6H, 19.5A, 2.4F and 3.3B. After the Fabs were produced and purified, complexes with LASV GP1 protein were made (Figure 1C left panel) and SEC purified (Figure 1C right panel), followed by crystallization with different conditions suitable for the formation of protein crystals. The method used was always the vapor diffusion-sitting drop technique in 96 well plates (Figure 1 D). For the trays setup, an automated microseeding apparatus (Orwex) was used to seed exact drop ratios within a tray. All complexes were then tested with four commercial screening 96 well trays, including TOP 96, Index, PEG-ION and PEG II. Initial hits were followed up by optimization of the initial leading condition. In order to obtain bigger crystals of better diffracting quality, parameters like precipitant concentration, pH, complex concentration, drop ratio well/complex solution, PEG concentration and other conditions were tested.

OPTIMIZATION PROCEDURE FOR LASV GP1-10.4B FAB COMPLEX CRYSTALS

The most promising hit was obtained with the nAb 10.4B. The leading condition (0.1 M sodium malonate, pH 6, 12% PEG 3350) was optimized by varying parameters as precipitant concentration, pH, drop protein: mother liquor solution ratio, PEG- or complex concentration (Figure 1 D). Crystals were also transferred to bigger drops in 24 well trays. First optimization consisted in a small variation of the salt concentration between 0.1 and 0.15 M sodium malonate, increasing the percentage of PEG 3350 (10-14%), different pH (5, 6 and 7) and two different complex concentrations (5/10 mg/ml). First optimization revealed that the pH was a critical factor as crystals only grew at pH 7. High concentration of PEG 3350 resulted in too high nucleation which resulted in an undesired microcrystal shower. Crystals in 0.1 M sodium malonate grew also better. The drop ratio between the well condition and the protein solution is an important factor that could be determining. Hence, two different drop ratios were tested (0.15:0.15 and 0.22:0.22) which gave similar crystals. It is crucial that the selected conditions are both reproducible and allow crystal stability, preventing the crystal to melt over time. The next step for the optimization was to obtain bigger crystals by translating the conditions from 96 well plates to 24 well plates using the hanging drop technique. Translation to bigger crystals could be a critical step to improve diffraction. However, some crystals resist to the translation and do not grow using a different

technique than the initial leading one. Fortunately, crystals translated well to bigger drops and bigger crystals were grown. Next, different concentrations of complex (5, 10 and 6.8 mg/ml) were tested. As expected, crystals grew faster with higher complex concentrations. In order to speed up the crystal growth, new drops were seeded with previously grown crystals. LASV GP1-10.4B Fab complexes seeds were collected from 0.1 M sodium malonate 12% PEG 3350 condition and diluted into 0.12 M sodium malonate 13.2% PEG 3350. After crystals were mechanically crushed, the solution was diluted 10^{-4} times and used as seeds for new crystals.

Several initial hits were sent to the Stanford Synchrotron Radiation Laboratory (SSRL) for an initial X-ray diffraction analysis (Figure 1E left panel) while others leading hits were condition-optimized to get better diffracting patterns. In order to avoid ice at the crystal surface and protect the crystal form changing temperatures, crystals were frozen in the leading solution with different concentrations of additives cryoprotectants as PEG 400, glycerol, ethylene-glycol and mineral oil since different cryoprotectant compounds could affect the quality of the crystal during the freezing process. Diffraction patterns obtained confirmed to be protein crystals and moreover we could confirm that the protein crystallized was the complex GP1-Fab and not only the Fab fraction since both proteins would have distinct unit cells volumes. However, the resolution obtained was only 10-15 Å. Indexing into the correct space group was therefore not possible at this point and further optimization will be needed (Figure 1 F). The next step towards the optimization would be an additive screening where single components are added to the leading optimized condition in order to improve in the quality of the crystal.

FIGURES
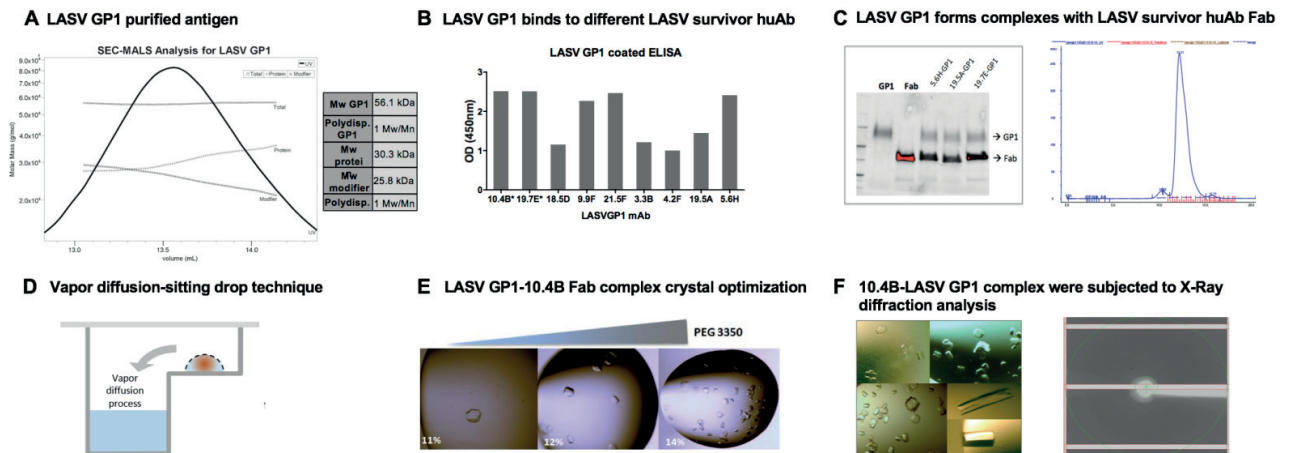
Figure 1. Structural studies of LASV GP1 antigen. A) LASV GP1 antigen characterization. The elution profile of LASV GP1 was determined by SEC-MALS. The horizontal line corresponds to the calculated mass for LASV GP1, of 56.1 kDa. B) Purified LASV GP1 binds to different LASV GP1 mAbs. Binding to different LASV GP1 mAb isolated from human LASV survivors was tested by ELISA. Microtiter plates were plated with 5 µg/ml of purified LASV GP1 followed by incubation with 5 µg/ml of purified mAbs. Bound mAb were detected with a HRP-conjugated secondary antibody in a color reaction. Data are optical densities, means, n = 2. C) LASV GP1 antigen forms complexes with the Fab of nAb 10.4B that recognizes a conformational epitope [3]. In left panel, free stain blot to analyze LASV GP1-Fab complexes of different Ab Fab fragments. In the right panel, one LASV GP1-Fab complex is purified through SEC. D) Schematic of the vapor diffusion-sitting drop technique for protein crystallization. Image adapted from http://www.douglas.co.uk E) Example of crystals obtained during the process of optimization of crystallization conditions for the LASV GP1-10.4B Fab complex with different PEG 3350 concentrations. F) Crystals of LASV GP1-10.4B Fab complex analyzed by X-ray diffraction in the Stanford Synchrotron Radiation Laboratory (SSRL) (left panel). X-ray diffraction panel obtained from LASV GP1-10.4B Fab complex crystal. Cell dimensions: a, b, c (Å): 142.06 195.39 234.71 α, β, γ (°): 90.093 90.091 90.686. Resolution (Å): ≈10. Outer green ring is ~6.5Å. (right panel).

REFERENCES

1. Kunz, S., et al., *Posttranslational modification of alpha-dystroglycan, the cellular receptor for arenaviruses, by the glycosyltransferase LARGE is critical for virus binding.* J Virol, 2005. **79**(22): p. 14282-96.
2. Cohen-Dvashi, H., et al., *Molecular Mechanism for LAMP1 Recognition by Lassa Virus.* J Virol, 2015. **89**(15): p. 7584-92.
3. Robinson, J.E., et al., *Most neutralizing human monoclonal antibodies target novel epitopes requiring both Lassa virus glycoprotein subunits.* Nat Commun, 2016. **7**: p. 11544.

Lassa virus cell entry reveals new aspects of virus-host cell interaction

Giulia Torriani[1], Clara Galan-Navarro[1], and Stefan Kunz[1§]

[1] Institute of Microbiology, Lausanne University Hospital and University of Lausanne

Lausanne, Switzerland

§ Corresponding author.

Mailing address: Institute of Microbiology, University Hospital Center and University of Lausanne, Lausanne CH-1011, Switzerland. Phone: +41-21 314 7743, Fax: +41-21 314 4060, E-mail Stefan.Kunz@chuv.ch.

Abstract: 75 words

Text: 2687 words

Running title: Lassa virus cell entry

ABSTRACT

Viral entry represents the first step of every viral infection and is a determinant for the host-range and disease potential of a virus. Here we review the latest developments on cell entry of the highly pathogenic Old World arenavirus Lassa, providing novel insights into the complex host cell interaction of this important human pathogen. We will cover new discoveries on the molecular mechanisms of receptor recognition, endocytosis, and the use of late endosomal entry factors.

Lassa virus is a significant human pathogen

Among the arenaviruses, Lassa virus (LASV) represents the most prevalent human pathogen with several hundred thousand infections per year [1]. Carried by persistent infection of the reservoir rodent host *Mastomys natalensis*, LASV is endemic in large parts of Western Africa. Arenaviruses are enveloped negative-strand RNA viruses with a non-lytic life cycle confined to the cytosol. The arenavirus genome is comprised of a small (S) RNA segment encoding the envelope glycoprotein precursor (GPC) and the nucleoprotein (NP), and an L segment coding for the matrix protein (Z) as well as the viral polymerase (L) [2]. The GPC is synthesized as a single polypeptide and undergoes processing yielding a stable signal peptide (SSP), the N-terminal GP1, and the transmembrane GP2. The GP1 binds to cellular receptors, whereas GP2 mediates viral fusion and structurally resembles class I viral fusion proteins.Upon receptor binding, LASV enters the host cell via receptor-mediated endocytosis with subsequent transport to late endosomal compartments, where fusion occurs at low pH [3, 4]. Arenavirus fusion has been covered by an excellent recent review [5] and will therefore not be detailed here. By an unknown mechanism of "uncoating", the viral ribonucleoprotein is released into the cytosol where viral transcription and replication takes place. The assembly and release of arenavirus infectious progeny is orchestrated by the matrix protein Z, which recruit ESCRT proteins that are crucial for virion budding.

Human LASV infection occurs mainly via reservoir-to-human transmission [6] that likely involves inhalation of contaminated aerosolized rodent excreta and ingestion of contaminated food [1]. Following early viral multiplication at the site of entry, the virus disseminates via the bloodstream reaching lymph nodes, spleen, and liver, where productive infection is established. A predictive factor for disease outcome is the viral load early in infection, indicating a close competition between viral spread and replication and the patient's immune system [7]. The pathophysiology of the fatal shock syndrome is not well understood and may involve functional changes in vascular endothelial cells, liver, adrenal gland, and other organs [8]. Current treatment is limited to supportive care and the antiviral drug ribavirin that reduces mortality when given early in disease [9]. Due to its proven transmissibility via aerosol [10] and high lethality, LASV is considered a Category A agent by the Centers of Disease Control [11]. The lack of a licensed vaccine and limited treatment options make the development of novel therapeutic strategies against LASV an urgent need. Anti-viral drugs capable of reducing multiplication and spread of LASV may provide the patient's immune system a window of opportunity to develop an anti-viral immune response. A major challenge for the development of drugs against LASV is however the limited structural information available on the pathogen. As all viruses, LASV critically depends on the molecular machinery of the host cell for its multiplication. Targeting viral entry appears further as a promising strategy for therapeutic intervention as it allows blocking the pathogen before it can take control over the host cell. The identification of cellular factors required for productive LASV entry and their evaluation as possible targets for therapeutic anti-viral intervention is therefore of great interest.

Lassa virus shows complex receptor use

The first LASV receptor was identified as dystroglycan (DG), a ubiquitously expressed conserved cellular receptor for extracellular matrix (ECM) proteins [12]. In mammals, DG is found in most tissues, where it provides a molecular link between the ECM and the actin cytoskeleton. Apart from LASV, DG can serve as a receptor for most isolates of the prototypic arenavirus lymphocytic choriomeningitis virus (LCMV), the African arenaviruses Mopeia and Mobala, as well as Clade C New World arenaviruses [12, 13]. The DG core protein is initially synthesized as a single polypeptide chain that undergoes autoprocessing, yielding the peripheral α-DG interacting with ECM proteins and the transmembrane β-DG. At the cytosolic face, β-DG associates with the cytoskeletal adaptor proteins dystrophin and utrophin, anchoring the DG complex to the actin cytoskeleton [14]. During biosynthesis, α-DG undergoes remarkably complex O-glycosylation that is essential for its biological function [15]. The functional glycosylation of α-DG starts with the biosynthesis of the unusual O-linked trisaccharide [O-Man-β1-4-GlcNAc-β1-3GalNAc] that undergoes phosphorylation at the O-mannosyl residue [16]. A ribitol moiety links the trisaccharide to [Xyl-α1-GlcA-3-β1-3] co-polymers synthesized by the dual-specific glycosyltransferase like-acetylglucosaminyltransferase (LARGE) [17, 18]. The LARGE-derived [Xyl-α1-GlcA-3-β1-3] polysaccharide is called "matriglycan" and recognizes LG domains of ECM proteins via an unusual lectin-type binding [15, 19, 20]. Modification of DG by LARGE is also crucial for arenavirus binding [21, 22] and a recent elegant haploid screen revealed that LASV GP1 strikingly mimics the mechanisms of receptor recognition of host-derived ECM proteins [23]. While the DG core protein is ubiquitously expressed in most mammalian cells, functional glycosylation by LARGE is under tight tissue-specific control [19]. Dystroglycan therefore appears as a "tunable" receptor [19], whose virus-binding affinity is influenced by the length of the LARGE-derived glycans [21]. Genome-wide association studies in human populations revealed positive selection for specific LARGE alleles in populations from Western African [6, 24, 25]. Although the exact role of the selected LARGE alleles in LASV susceptibility of carriers is not yet clear, the data suggest a role of DG's post-translational modifications in virus-host co-evolution.

Binding of viruses to their receptor(s) frequently induces signaling that functions as a "knock on the door" to facilitate entry [26]. The cytosolic domain of β-DG can associate with signaling molecules, including the adaptor Grb2 [27], MAP kinases MEK and ERK [28], and focal adhesion kinase [29]. Engagement of cellular α-DG by LASV GP induced tyrosine phosphorylation of β-DG's cytosolic domain, resulting in dissociation from the cytoskeletal adaptor utrophin, which may promote internalization of the virus-receptor complex [30]. Virus-receptor binding further affected signaling cross-talk of DG with α6β1 integrins, another widely expressed family of ECM receptors that can functionally cooperate with DG [31, 32]. However, since β1 integrins are dispensable for LASV entry, the role of this phenomenon for viral infection is currently unclear.

More recently, the Tyro3/Axl/Mer (TAM) receptor tyrosine kinases Axl and Tyro3/Dtk, as well as the C-type lectins DC-specific ICAM-3-grabbing nonintegrin (DC-SIGN) and LSECtin have been

identified as novel candidate receptors for LASV and LCMV [33, 34]. Tyro3 and Axl are broadly expressed receptors for the phoshatidylserine (PS)-binding serum proteins Gas6 and protein S and are involved in removal of apoptotic cells [35, 36]. Over the past years, TAM kinases have been implicated in viral entry by "apoptotic mimicry", which involves recognition of PS displayed in the viral lipid envelope by cellular PS receptors and is used by a broad range of enveloped viruses [37-42]. The co-expression of DG with TAM receptors in tissues infected by LASV suggests complex receptor use. However, conflicting data have been reported on the roles of TAM receptors in Old World arenavirus infection. A role for Axl and Tyro3 in LASV entry was initially discovered by expression cloning using a LASV pseudotype platform [34]. Antibody perturbation experiments supported a contribution of Axl to LASV entry into cells lacking functional DG [34]. However, other studies found no enhancement of LASV or LCMV entry by over-expression of TAM kinases and the authors concluded that these PS receptors are unable to mediate productive infection [43]. Notably, mice deficient in Axl remained highly susceptible to LCMV infection *in vivo* [44]. More work will be needed to define the exact roles of TAM kinases in LASV entry into specific human target cells and their role *in vivo*.

Based on their more restricted expression patterns, DC-SIGN and LSECtin may contribute to LASV entry into specific cell types, including dendritic cells (DC) that represent important early targets during infection [45]. *In vitro* studies on monocyte-derived human DC revealed that high mannose N-glycans displayed on LASV GP1 could engage DC-SIGN during attachment [46]. However, DC-SIGN seemed dispensable for subsequent viral entry. This seems in stark contrast to arthropod-borne Phleboviruses and Dengue virus [40, 47] that use DC-SIGN as true entry receptor in DC. However, the candidate receptor expression pattern of monocyte-derived DC *in vitro* may differ from authentic DC populations *in vivo* putting limitation to this model.

Dystroglycan-mediated LASV entry involves an unusual pathway of macropinocytosis

Initial studies suggested that Old World arenaviruses enter via an unknown clathrin- and dynamin-independent pathway [48-50]. More recent genome-wide RNA interference silencing screens identified sodium hydrogen exchangers (NHE) as host factors involved in the multiplication of LCMV [51]. Based on these findings, de la Torre and colleagues validated NHE as entry factors for LCMV and LASV and demonstrated for the first time a link between arenavirus entry and macropinocytosis [52]. Employing a panel of "diagnostic inhibitors" for macropinocytosis proposed by Mercer and Helenius [53, 54], LASV entry into human epithelial cells was investigated. In line with earlier studies, functionally glycosylated DG served as the main receptor for LASV in epithelia, whereas other candidate receptors were either absent or dispensable [55]. Consistent with previous studies [52], LASV entry was independent of dynamin, dependent on NHE, and required the dynamics of the actin cytoskeleton. The small GTPase Cdc42 and its downstream effectors PAK1 and N-Wasp were required for the regulation of LASV entry, whereas Rac1, RhoA, the Arp2/3 complex, myosin II, and myosin light chain kinase seemed dispensable in the cell types tested. The identification of PAK1 as a LASV entry factor was

further in line with a recent screen for anti-LASV drugs that identified the PAK1 inhibitor OSU-03012 as a hit [56].

Macropinocytosis is a major pathway of cell entry used by >20 different viruses and the pathogens seem to recruit specific sets of regulatory proteins according to their needs [54, 57]. In line with this, LASV entry requires a limited subset of the known regulators of "classical" macropinocytosis. In most cells, macropinocytosis is not constitutively active, but needs to be activated [53]. A series of classical studies on other viruses, including the poxvirus vaccinia (VACV), respiratory syncytial virus, influenza A virus, Echovirus 1 [58], and African swine fever virus revealed that the pathogens are able to activate the pathway [42, 58-61]. As a consequence, virus attachment to the plasma membrane induces membrane "blebbing", triggers actin-depolymerization, and increases bulk fluid uptake. In contrast, LASV entry only minimally affected the host cell's membrane- and actin-dynamics, [55], possibly due to distinct receptor use and/or differences in virion size. Several kinases implicated in macropinocytosis are required for LASV entry, including protein kinase C (PKC), phosphoinositol 3 kinase (PI3K), epithelial growth factor receptor (EGFR), and hepatocyte growth factor receptor (HGFR) [55, 56]. The data at hand suggest that DG can link LASV to a pathway related to macropinocytosis that causes only minimal perturbation of the host cell, which may be a required for its non-lytic life cycle and the ability to persist in its rodent reservoir.

LAMP-1 is a late endosomal entry factor for LASV that facilitates viral fusion

Similar to other early endosomal compartments, early macropinosomes undergo maturation [62]. Recent studies revealed that macropinosome maturation is crucial for productive VACV entry [63], but it is unknown to what extent this applies for LASV. Moreover, the fate of late macropinosomes is unclear and may involve fusion with classical late endosomes and lysosomes. Since LASV passes through late endosomes and depends on the endosomal sorting complex required for transport for entry [49], it will be of interest to see if and at which point incoming LASV "merges" into the classical late endosomal route. Using an unbiased haploid screening approach, Jae et al. identified the lysosome-associated membrane protein (LAMP) 1 as a late endosomal entry factor required by LASV [64]. Under the acidic conditions of the late endosome, the virus dissociated from its high affinity receptor DG and engaged LAMP1, which triggered efficient fusion. Recent structural analysis of LASV GP1 combined with functional studies provided insights into the mechanisms underlying this "receptor switch" (Fig. 1). X-ray analysis revealed the existence of a stable low pH conformation of LASV GP1 displaying a triad of histidine residues that form a binding site for LAMP1 and is conserved among Old World arenaviruses [65]. Recent electron cryotomography studies on authentic LASV particles revealed conformational changes in GP1 to occur under pH 5, in line with the X-ray data [66]. Although LAMP1 is crucial for productive LASV entry [64], LAMP1 binding is not strictly required for fusion *per se*, evidenced by mutations within the histidine-triad that were still able to undergo fusion albeit at lower pH [67]. Elegant functional studies demonstrated that residue H230 within the histidine-triad on LASV GP1 undergoes

protonation around pH 5.5, when GP1 starts dissociating from DG (Fig. 1). A positive charge at residue H230 had an inhibitory effect on LASV GP fusion activity, preventing premature fusion. Engagement of GP1 protonated at H230 with LAMP1 may neutralize the positive charge via a countercharge provided by LAMP1, promoting fusion triggering [67] (Fig. 1). These studies reveal a remarkable role of the histidine-triad in orchestrating fusion activity of LASV GP with the timing and location of the receptor switch from DG to LAMP1. This scenario further suggests a division of labor between DG and LAMP1 in LASV entry. Functional DG appears to serve as a high affinity receptor that efficiently captures free virus at the cell surface via its matrigylcan polysaccharides that likely reach above the gylcocalyx, followed by rapid endocytosis. Whether DG requires assistance by other yet unknown co-receptor(s) for virus internalization is currently unknown. Engagement of the late endosomal receptor LAMP1 likely guarantees optimal spatial conditions for fusion in proximity to the limiting membrane of the late endosome. The use of late endosomal entry factors by LASV has further interesting parallels to filoviruses and may reflect a more common strategy of late-penetrating viruses, as discussed in an excellent recent review [68].

Perspectives and challenges

Recent developments on LASV entry provided novel insights into the complex interaction of this pathogen with the host cell. At the same time new questions arose that need to be addressed. As pointed out above, several lines of evidence support the notion that DG's function as a LASV receptor critically depends on post translational modification. However, the tissue tropism of the virus does not always correlate with the extent of DG's functional glycosylation. This is illustrated by skeletal muscle that expresses DG with long matriglycan chains and high LASV binding affinity [19], but seems largely resistant to infection by LCMV [69] and LASV [70, 71]. Recent studies revealed that the resistance of differentiated myotubes against LCMV lies at the level of viral entry [72], suggesting that expression of functionally glycosylated DG *per se* is insufficient for productive infection. Considering the complex interaction pattern of DG with cellular proteins, cell-type specific DG complexes likely represent the "functional units" of virus entry. Pre-existing "steady-state" interactions of DG with specific cellular factors may thus influence DG's ability to function as a viral receptor. Moreover, some data at hand suggest that virus binding to DG induces receptor signaling and affects the molecular composition of the complex. It is therefore conceivable that virus engagement of the receptor induces a dynamic pattern of protein-protein interactions involved in the entry process, as recently illustrated in a ground-breaking study on hepatitis C virus entry [73]. The advent of unbiased "shotgun" proteomics approaches, including sensitive label-free quantification, provides new and powerful techniques to address these questions [74].

Cell entry of LASV critically depends on cellular kinases [55, 56], indicating a role of signaling in LASV entry. The virus may actively induce cellular signaling to promote entry, as well as to "prime" the host cell to facilitate subsequent steps of infection. Since viruses are opportunistic and may "create"

their own pathways by re-shuffling cellular factors according to their needs, focusing on specific signaling pathways may face some limitations. Recently, quantitative phosphoproteomics was successfully used to dissect the complex signaling events following attachment of human immunodeficiency virus-1 [75], paving the way for similar studies on emerging viruses. Candidate signaling pathways involved in productive LASV entry could be integrated into a "LASV entry network" allowing the identification of promising drug targets. Since candidate signaling molecules may represent already known drug targets in other human disorders, clinically approved drugs or drug candidates in advanced stages of development may be "re-purposed" to combat this important human pathogen.

FIGURE 1
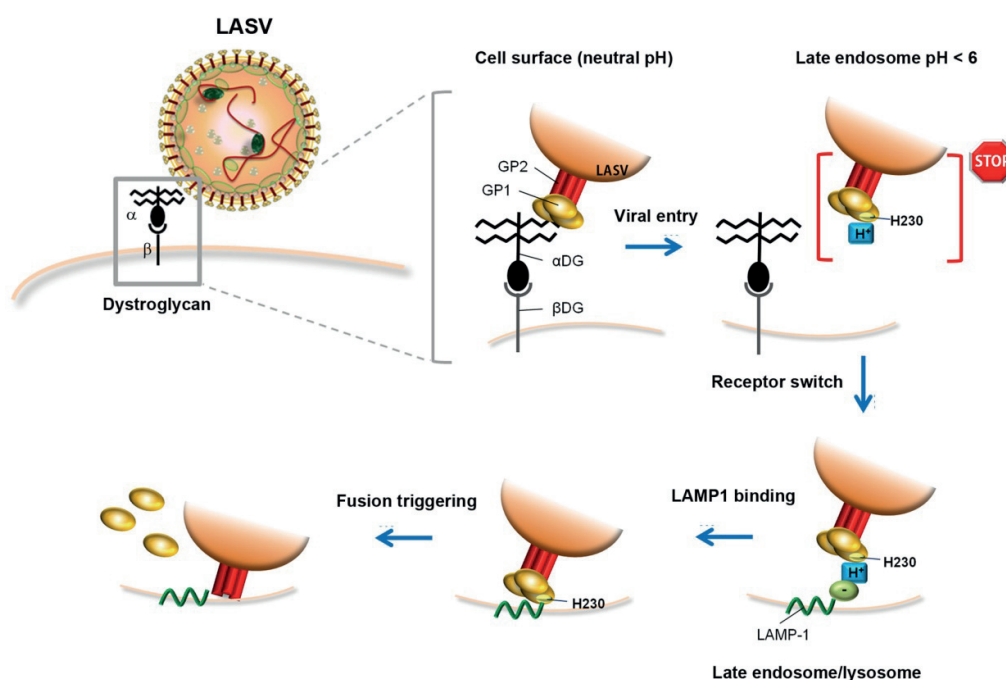
Current model for receptor use, cell entry, and late endosomal "receptor switch" of LASV [64, 65, 67]. At the cell surface, LASV GP1 engages the O-linked matriglycan polysaccarides displayed by α-DG, followed by endocytosis via an unusual pathway related to macropinocytosis. Progressive acidification of late endosomes induces a structural change in LASV GP1, which dissociates from DG and adapts a low pH conformation displaying a histidine-triad. Protonation of residue H230 "locks" GP1

in the pre-fusion state, preventing premature fusion. Engagement of LAMP1 neutralizes the positive charge on H230 of GP1 and triggers efficient fusion with the limiting membrane of the late endosome/lysosome (for details, please see text

REFERENCES

1. **McCormick JB, Fisher-Hoch SP.** 2002. Lassa fever. Curr Top Microbiol Immunol **262:**75-109.
2. **Buchmeier MJ, de la Torre JC, Peters CJ.** 2007. Arenaviridae: the viruses and their replication, p. p. 1791-1828. *In* Knipe DL, Howley PM (ed.), Fields Virology, 4th ed. Lippincott-Raven, Philadelphia.
3. **Cosset FL, Marianneau P, Verney G, Gallais F, Tordo N, Pecheur EI, ter Meulen J, Deubel V, Bartosch B.** 2009. Characterization of Lassa virus cell entry and neutralization with Lassa virus pseudoparticles. J Virol **83:**3228-3237.
4. **Klewitz C, Klenk HD, ter Meulen J.** 2007. Amino acids from both N-terminal hydrophobic regions of the Lassa virus envelope glycoprotein GP-2 are critical for pH-dependent membrane fusion and infectivity. J Gen Virol. **88:**2320-2328.
5. **Nunberg JH, York J.** 2012. The curious case of arenavirus entry, and its inhibition. Viruses **4:**83-101.
6. **Andersen KG, Shapiro BJ, Matranga CB, Sealfon R, Lin AE, Moses LM, Folarin OA, Goba A, Odia I, Ehiane PE, Momoh M, England EM, Winnicki S, Branco LM, Gire SK, Phelan E, Tariyal R, Tewhey R, Omoniwa O, Fullah M, Fonnie R, Fonnie M, Kanneh L, Jalloh S, Gbakie M, Saffa S, Karbo K, Gladden AD, Qu J, Stremlau M, Nekoui M, Finucane HK, Tabrizi S, Vitti JJ, Birren B, Fitzgerald M, McCowan C, Ireland A, Berlin AM, Bochicchio J, Tazon-Vega B, Lennon NJ, Ryan EM, Bjornson Z, Milner DA, Jr., Lukens AK, Broodie N, Rowland M, Heinrich M, Akdag M, Schieffelin JS, Levy D, Akpan H, Bausch DG, Rubins K, McCormick JB, Lander ES, Gunther S, Hensley L, Okogbenin S, Viral Hemorrhagic Fever C, Schaffner SF, Okokhere PO, Khan SH, Grant DS, Akpede GO, Asogun DA, Gnirke A, Levin JZ, Happi CT, Garry RF, Sabeti PC.** 2015. Clinical Sequencing Uncovers Origins and Evolution of Lassa Virus. Cell **162:**738-750.
7. **McCormick JB, King IJ, Webb PA, Johnson KM, O'Sullivan R, Smith ES, Trippel S, Tong TC.** 1987. A case-control study of the clinical diagnosis and course of Lassa fever. The Journal of infectious diseases **155:**445-455.
8. **Geisbert TW, Jahrling PB.** 2004. Exotic emerging viral diseases: progress and challenges. Nature medicine **10:**S110-121.
9. **McCormick JB, King IJ, Webb PA, Scribner CL, Craven RB, Johnson KM, Elliott LH, Belmont-Williams R.** 1986. Lassa fever. Effective therapy with ribavirin. N Engl J Med **314:**20-26.
10. **Stephenson EH, Larson EW, Dominik JW.** 1984. Effect of environmental factors on aerosol-induced Lassa virus infection. J Med Virol **14:**295-303.
11. **Borio L, Inglesby T, Peters CJ, Schmaljohn AL, Hughes JM, Jahrling PB, Ksiazek T, Johnson KM, Meyerhoff A, O'Toole T, Ascher MS, Bartlett J, Breman JG, Eitzen EM, Jr., Hamburg M, Hauer J, Henderson DA, Johnson RT, Kwik G, Layton M, Lillibridge S, Nabel GJ, Osterholm MT, Perl TM, Russell P, Tonat K.** 2002. Hemorrhagic fever viruses as biological weapons: medical and public health management. Jama **287:**2391-2405.
12. **Cao W, Henry MD, Borrow P, Yamada H, Elder JH, Ravkov EV, Nichol ST, Compans RW, Campbell KP, Oldstone MB.** 1998. Identification of alpha-dystroglycan as a receptor for lymphocytic choriomeningitis virus and Lassa fever virus [see comments]. Science **282:**2079-2081.
13. **Spiropoulou CF, Kunz S, Rollin PE, Campbell KP, Oldstone MB.** 2002. New World arenavirus clade C, but not clade A and B viruses, utilizes alpha-dystroglycan as its major receptor. J Virol **76:**5140-5146.
14. **Barresi R, Campbell KP.** 2006. Dystroglycan: from biosynthesis to pathogenesis of human disease. J Cell Sci. **119:**199-207.
15. **Yoshida-Moriguchi T, Campbell KP.** 2015. Matriglycan: a novel polysaccharide that links dystroglycan to the basement membrane. Glycobiology **25:**702-713.
16. **Yoshida-Moriguchi T, Willer T, Anderson ME, Venzke D, Whyte T, Muntoni F, Lee H, Nelson SF, Yu L, Campbell KP.** 2013. SGK196 is a glycosylation-specific O-mannose kinase required for dystroglycan function. Science **341:**896-899.
17. **Inamori K, Yoshida-Moriguchi T, Hara Y, Anderson ME, Yu L, Campbell KP.** 2012. Dystroglycan function requires xylosyl- and glucuronyltransferase activities of LARGE. Science **335:**93-96.
18. **Praissman JL, Willer T, Sheikh MO, Toi A, Chitayat D, Lin YY, Lee H, Stalnaker SH, Wang S, Prabhakar PK, Nelson SF, Stemple DL, Moore SA, Moremen KW, Campbell KP, Wells L.** 2016. The functional O-mannose glycan on alpha-dystroglycan contains a phospho-ribitol primed for matriglycan addition. eLife **5**.

19. **Goddeeris MM, Wu B, Venzke D, Yoshida-Moriguchi T, Saito F, Matsumura K, Moore SA, Campbell KP.** 2013. LARGE glycans on dystroglycan function as a tunable matrix scaffold to prevent dystrophy. Nature **503:**136-140.

20. **Briggs DC, Yoshida-Moriguchi T, Zheng T, Venzke D, Anderson ME, Strazzulli A, Moracci M, Yu L, Hohenester E, Campbell KP.** 2016. Structural basis of laminin binding to the LARGE glycans on dystroglycan. Nat Chem Biol **12:**810-814.

21. **Kunz S, Rojek JM, Kanagawa M, Spiropoulou CF, Barresi R, Campbell KP, Oldstone MB.** 2005. Posttranslational modification of alpha-dystroglycan, the cellular receptor for arenaviruses, by the glycosyltransferase LARGE is critical for virus binding. J Virol **79:**14282-14296.

22. **Rojek JM, Spiropoulou CF, Campbell KP, Kunz S.** 2007. Old World and clade C New World arenaviruses mimic the molecular mechanism of receptor recognition used by alpha-dystroglycan's host-derived ligands. J Virol **81:**5685-5695.

23. **Jae LT, Raaben M, Riemersma M, van Beusekom E, Blomen VA, Velds A, Kerkhoven RM, Carette JE, Topaloglu H, Meinecke P, Wessels MW, Lefeber DJ, Whelan SP, van Bokhoven H, Brummelkamp TR.** 2013. Deciphering the glycosylome of dystroglycanopathies using haploid screens for lassa virus entry. Science **340:**479-483.

24. **Sabeti PC, Varilly P, Fry B, Lohmueller J, Hostetter E, Cotsapas C, Xie X, Byrne EH, McCarroll SA, Gaudet R, Schaffner SF, Lander ES, Frazer KA, Ballinger DG, Cox DR, Hinds DA, Stuve LL, Gibbs RA, Belmont JW, Boudreau A, Hardenbol P, Leal SM, Pasternak S, Wheeler DA, Willis TD, Yu F, Yang H, Zeng C, Gao Y, Hu H, Hu W, Li C, Lin W, Liu S, Pan H, Tang X, Wang J, Wang W, Yu J, Zhang B, Zhang Q, Zhao H, Zhou J, Gabriel SB, Barry R, Blumenstiel B, Camargo A, Defelice M, Faggart M, Goyette M, Gupta S, Moore J, Nguyen H, Onofrio RC, Parkin M, Roy J, Stahl E, Winchester E, Ziaugra L, Altshuler D, Shen Y, Yao Z, Huang W, Chu X, He Y, Jin L, Liu Y, Sun W, Wang H, Wang Y, Xiong X, Xu L, Waye MM, Tsui SK, Xue H, Wong JT, Galver LM, Fan JB, Gunderson K, Murray SS, Oliphant AR, Chee MS, Montpetit A, Chagnon F, Ferretti V, Leboeuf M, Olivier JF, Phillips MS, Roumy S, Sallee C, Verner A, Hudson TJ, Kwok PY, Cai D, Koboldt DC, Miller RD, Pawlikowska L, Taillon-Miller P, Xiao M, Tsui LC, Mak W, Song YQ, Tam PK, Nakamura Y, Kawaguchi T, Kitamoto T, Morizono T, Nagashima A, Ohnishi Y, Sekine A, Tanaka T, Tsunoda T, Deloukas P, Bird CP, Delgado M, Dermitzakis ET, Gwilliam R, Hunt S, Morrison J, Powell D, Stranger BE, Whittaker P, Bentley DR, Daly MJ, de Bakker PI, Barrett J, Chretien YR, Maller J, McCarroll S, Patterson N, Pe'er I, Price A, Purcell S, Richter DJ, Sabeti P, Saxena R, Sham PC, Stein LD, Krishnan L, Smith AV, Tello-Ruiz MK, Thorisson GA, Chakravarti A, Chen PE, Cutler DJ, Kashuk CS, Lin S, Abecasis GR, Guan W, Li Y, Munro HM, Qin ZS, Thomas DJ, McVean G, Auton A, Bottolo L, Cardin N, Eyheramendy S, Freeman C, Marchini J, Myers S, Spencer C, Stephens M, Donnelly P, Cardon LR, Clarke G, Evans DM, Morris AP, Weir BS, Johnson TA, Mullikin JC, Sherry ST, Feolo M, Skol A, Zhang H, Matsuda I, Fukushima Y, Macer DR, Suda E, Rotimi CN, Adebamowo CA, Ajayi I, Aniagwu T, Marshall PA, Nkwodimmah C, Royal CD, Leppert MF, Dixon M, Peiffer A, Qiu R, Kent A, Kato K, Niikawa N, Adewole IF, Knoppers BM, Foster MW, Clayton EW, Watkin J, Muzny D, Nazareth L, Sodergren E, Weinstock GM, Yakub I, Birren BW, Wilson RK, Fulton LL, Rogers J, Burton J, Carter NP, Clee CM, Griffiths M, Jones MC, McLay K, Plumb RW, Ross MT, Sims SK, Willey DL, Chen Z, Han H, Kang L, Godbout M, Wallenburg JC, L'Archeveque P, Bellemare G, Saeki K, An D, Fu H, Li Q, Wang Z, Wang R, Holden AL, Brooks LD, McEwen JE, Guyer MS, Wang VO, Peterson JL, Shi M, Spiegel J, Sung LM, Zacharia LF, Collins FS, Kennedy K, Jamieson R, Stewart J.** 2007. Genome-wide detection and characterization of positive selection in human populations. Nature **449:**913-918.

25. **Andersen KG, Shylakhter I, Tabrizi S, Grossman SR, Happi CT, Sabeti PC.** 2012. Genome-wide scans provide evidence for positive selection of genes implicated in Lassa fever. Philosophical transactions of the Royal Society of London. Series B, Biological sciences **367:**868-877.

26. **Grove J, Marsh M.** 2011. The cell biology of receptor-mediated virus entry. J Cell Biol **195:**1071-1082.

27. **Yang B, Jung D, Motto D, Meyer J, Koretzky G, Campbell KP.** 1995. SH3 domain-mediated interaction of dystroglycan and Grb2. J Biol Chem **270:**11711-11714.

28. **Spence HJ, Dhillon AS, James M, Winder SJ.** 2004. Dystroglycan, a scaffold for the ERK-MAP kinase cascade. EMBO Rep.

29. **Cavaldesi M, Macchia G, Barca S, Defilippi P, Tarone G, Petrucci TC.** 1999. Association of the dystroglycan complex isolated from bovine brain synaptosomes with proteins involved in signal transduction. J Neurochem **72:**1648-1655.

30. **Moraz ML, Pythoud C, Turk R, Rothenberger S, Pasquato A, Campbell KP, Kunz S.** 2013. Cell entry of Lassa virus induces tyrosine phosphorylation of dystroglycan. Cell Microbiol **15:**689-700.

31. **Ferletta M, Kikkawa Y, Yu H, Talts JF, Durbeej M, Sonnenberg A, Timpl R, Campbell KP, Ekblom P, Genersch E.** 2003. Opposing roles of integrin alpha6Abeta1 and dystroglycan in laminin-mediated extracellular signal-regulated kinase activation. Mol Biol Cell **14:**2088-2103.

32. **Rojek JM, Moraz ML, Pythoud C, Rothenberger S, Van der Goot FG, Campbell KP, Kunz S.** 2012. Binding of Lassa virus perturbs extracellular matrix-induced signal transduction via dystroglycan. Cell Microbiol **14:**1122-1134.

33. **Shimojima M, Kawaoka Y.** 2012. Cell surface molecules involved in infection mediated by lymphocytic choriomeningitis virus glycoprotein. The Journal of veterinary medical science / the Japanese Society of Veterinary Science **74:**1363-1366.

34. **Shimojima M, Stroher U, Ebihara H, Feldmann H, Kawaoka Y.** 2012. Identification of cell surface molecules involved in dystroglycan-independent lassa virus cell entry. J Virol **86:**2067-2078.

35. **Lemke G, Burstyn-Cohen T.** 2010. TAM receptors and the clearance of apoptotic cells. Ann N Y Acad Sci **1209:**23-29.

36. **Lemke G, Rothlin CV.** 2008. Immunobiology of the TAM receptors. Nat Rev Immunol **8:**327-336.

37. **Amara A, Mercer J.** 2015. Viral apoptotic mimicry. Nature reviews. Microbiology **13:**461-469.

38. **Morizono K, Chen IS.** 2014. Role of phosphatidylserine receptors in enveloped virus infection. J Virol **88:**4275-4290.

39. **Morizono K, Xie Y, Olafsen T, Lee B, Dasgupta A, Wu AM, Chen IS.** 2011. The soluble serum protein Gas6 bridges virion envelope phosphatidylserine to the TAM receptor tyrosine kinase Axl to mediate viral entry. Cell Host Microbe **9:**286-298.

40. **Meertens L, Carnec X, Lecoin MP, Ramdasi R, Guivel-Benhassine F, Lew E, Lemke G, Schwartz O, Amara A.** 2012. The TIM and TAM families of phosphatidylserine receptors mediate dengue virus entry. Cell Host Microbe **12:**544-557.

41. **Frei AP, Jeon OY, Kilcher S, Moest H, Henning LM, Jost C, Pluckthun A, Mercer J, Aebersold R, Carreira EM, Wollscheid B.** 2012. Direct identification of ligand-receptor interactions on living cells and tissues. Nature biotechnology **30:**997-1001.

42. **Mercer J, Helenius A.** 2008. Vaccinia virus uses macropinocytosis and apoptotic mimicry to enter host cells. Science **320:**531-535.

43. **Jemielity S, Wang JJ, Chan YK, Ahmed AA, Li W, Monahan S, Bu X, Farzan M, Freeman GJ, Umetsu DT, Dekruyff RH, Choe H.** 2013. TIM-family proteins promote infection of multiple enveloped viruses through virion-associated phosphatidylserine. PLoS Pathog **9:**e1003232.

44. **Sullivan BM, Welch MJ, Lemke G, Oldstone MB.** 2013. Is the TAM receptor Axl a receptor for lymphocytic choriomeningitis virus? J Virol **87:**4071-4074.

45. **Van Breedam W, Pohlmann S, Favoreel HW, de Groot RJ, Nauwynck HJ.** 2014. Bitter-sweet symphony: glycan-lectin interactions in virus biology. FEMS microbiology reviews **38:**598-632.

46. **Goncalves AR, Moraz ML, Pasquato A, Helenius A, Lozach PY, Kunz S.** 2013. Role of DC-SIGN in Lassa Virus Entry into Human Dendritic Cells. J Virol **87:**11504-11515.

47. **Lozach PY, Kuhbacher A, Meier R, Mancini R, Bitto D, Bouloy M, Helenius A.** 2011. DC-SIGN as a receptor for phleboviruses. Cell Host Microbe **10:**75-88.

48. **Rojek JM, Sanchez AB, Nguyen NT, de la Torre JC, Kunz S.** 2008. Different mechanisms of cell entry by human-pathogenic Old World and New World arenaviruses. J Virol **82:**7677-7687.

49. **Pasqual G, Rojek JM, Masin M, Chatton JY, Kunz S.** 2011. Old world arenaviruses enter the host cell via the multivesicular body and depend on the endosomal sorting complex required for transport. PLoS Pathog **7:**e1002232.

50. **Quirin K, Eschli B, Scheu I, Poort L, Kartenbeck J, Helenius A.** 2008. Lymphocytic choriomeningitis virus uses a novel endocytic pathway for infectious entry via late endosomes. Virology **378:**21-33.

51. **Panda D, Das A, Dinh PX, Subramaniam S, Nayak D, Barrows NJ, Pearson JL, Thompson J, Kelly DL, Ladunga I, Pattnaik AK.** 2011. RNAi screening reveals requirement for host cell secretory pathway in infection by diverse families of negative-strand RNA viruses. Proc Natl Acad Sci U S A **108:**19036-19041.

52. **Iwasaki M, Ngo N, de la Torre JC.** 2014. Sodium hydrogen exchangers contribute to arenavirus cell entry. J Virol **88:**643-654.

53. **Mercer J, Schelhaas M, Helenius A.** 2010. Virus entry by endocytosis. Annu Rev Biochem **79:**803-833.

54. **Mercer J, Helenius A.** 2012. Gulping rather than sipping: macropinocytosis as a way of virus entry. Curr Opin Microbiol **15:**490-499.

55. **Oppliger J, Torriani G, Herrador A, Kunz S.** 2016. Lassa virus cell entry via dystroglycan involves an unusual pathway of macropinocytosis. J Virol.

56. **Mohr EL, McMullan LK, Lo MK, Spengler JR, Bergeron E, Albarino CG, Shrivastava-Ranjan P, Chiang CF, Nichol ST, Spiropoulou CF, Flint M.** 2015. Inhibitors of cellular kinases with broad-spectrum antiviral activity for hemorrhagic fever viruses. Antiviral Res **120:**40-47.

57. **Mercer J, Helenius A.** 2009. Virus entry by macropinocytosis. Nat Cell Biol **11:**510-520.

58. **Krieger SE, Kim C, Zhang L, Marjomaki V, Bergelson JM.** 2013. Echovirus 1 entry into polarized Caco-2 cells depends on dynamin, cholesterol, and cellular factors associated with macropinocytosis. J Virol **87:**8884-8895.

59. **Krzyzaniak MA, Zumstein MT, Gerez JA, Picotti P, Helenius A.** 2013. Host cell entry of respiratory syncytial virus involves macropinocytosis followed by proteolytic activation of the F protein. PLoS Pathog **9:**e1003309.

60. **de Vries E, Tscherne DM, Wienholts MJ, Cobos-Jimenez V, Scholte F, Garcia-Sastre A, Rottier PJ, de Haan CA.** 2011. Dissection of the influenza A virus endocytic routes reveals macropinocytosis as an alternative entry pathway. PLoS Pathog **7:**e1001329.

61. **Sanchez EG, Quintas A, Perez-Nunez D, Nogal M, Barroso S, Carrascosa AL, Revilla Y.** 2012. African swine fever virus uses macropinocytosis to enter host cells. PLoS Pathog **8:**e1002754.

62. **Scott CC, Vacca F, Gruenberg J.** 2014. Endosome maturation, transport and functions. Seminars in cell & developmental biology **31:**2-10.

63. **Rizopoulos Z, Balistreri G, Kilcher S, Martin CK, Syedbasha M, Helenius A, Mercer J.** 2015. Vaccinia Virus Infection Requires Maturation of Macropinosomes. Traffic **16:**814-831.

64. **Jae LT, Raaben M, Herbert AS, Kuehne AI, Wirchnianski AS, Soh TK, Stubbs SH, Janssen H, Damme M, Saftig P, Whelan SP, Dye JM, Brummelkamp TR.** 2014. Virus entry. Lassa virus entry requires a trigger-induced receptor switch. Science **344:**1506-1510.

65. **Cohen-Dvashi H, Cohen N, Israeli H, Diskin R.** 2015. Molecular Mechanism for LAMP1 Recognition by Lassa Virus. J Virol **89:**7584-7592.

66. **Li S, Sun Z, Pryce R, Parsy ML, Fehling SK, Schlie K, Siebert CA, Garten W, Bowden TA, Strecker T, Huiskonen JT.** 2016. Acidic pH-Induced Conformations and LAMP1 Binding of the Lassa Virus Glycoprotein Spike. PLoS Pathog **12:**e1005418.

67. **Cohen-Dvashi H, Israeli H, Shani O, Katz A, Diskin R.** 2016. Role of LAMP1 Binding and pH Sensing by the Spike Complex of Lassa Virus. J Virol **90:**10329-10338.

68. **Jae LT, Brummelkamp TR.** 2015. Emerging intracellular receptors for hemorrhagic fever viruses. Trends in microbiology **23:**392-400.

69. **Fazakerley JK, Southern P, Bloom F, Buchmeier MJ.** 1991. High resolution in situ hybridization to determine the cellular distribution of lymphocytic choriomeningitis virus RNA in the tissues of persistently infected mice: relevance to arenavirus disease and mechanisms of viral persistence. J Gen Virol **72:**1611-1625.

70. **Walker DH, McCormick JB, Johnson KM, Webb PA, Komba-Kono G, Elliott LH, Gardner JJ.** 1982. Pathologic and virologic study of fatal Lassa fever in man. The American journal of pathology **107:**349-356.

71. **Yun NE, Walker DH.** 2012. Pathogenesis of Lassa fever. Viruses **4:**2031-2048.

72. **Iwasaki M, Urata S, Cho Y, Ngo N, de la Torre JC.** 2014. Cell entry of lymphocytic choriomeningitis virus is restricted in myotubes. Virology **458-459:**22-32.

73. **Gerold G, Meissner F, Bruening J, Welsch K, Perin PM, Baumert TF, Vondran FW, Kaderali L, Marcotrigiano J, Khan AG, Mann M, Rice CM, Pietschmann T.** 2015. Quantitative Proteomics Identifies Serum Response Factor Binding Protein 1 as a Host Factor for Hepatitis C Virus Entry. Cell reports **12:**864-878.

74. **Gerold G, Bruening J, Pietschmann T.** 2015. Decoding protein networks during virus entry by quantitative proteomics. Virus Res.

75. **Wojcechowskyj JA, Didigu CA, Lee JY, Parrish NF, Sinha R, Hahn BH, Bushman FD, Jensen ST, Seeholzer SH, Doms RW.** 2013. Quantitative phosphoproteomics reveals extensive cellular reprogramming during HIV-1 entry. Cell Host Microbe **13:**613-623.

Antigen persistence promoted by nanoparticle-carrier vaccine induces protective CD8 T cells with an effector memory phenotype

Marcela Rincon-Restrepo[a], Clara Galan[a,b], Ana Rita Goncalvez[b], , Efthymia Vokali[a], Shann Yu[a], Patricia Corthésy-Henrioud[a], Stefan Kunz[b], Jeffrey A. Hubbell [a,c], Sachiko Hirosue[a] and Melody A. Swartz[a,c]

[a] Institute of Bioengineering, École Polytechnique Fédérale de Lausanne, Lausanne, Switzerland

[b] Institute of Microbiology, Lausanne University Hospital, Lausanne, Switzerland

[c] Institute for Molecular Engineering, University of Chicago, Chicago, USA

*Corresponding Author, melodyswartz@uchicago.edu

ABSTRACT

The induction of protective T cell immunity is a major goal of many prophylactic and especially therapeutic vaccines. We describe a nanoparticle (NP) vaccine for delivery of a synthetic peptide representing the MHCI-restricted epitope GP_{33-41} derived from lymphochoriomeningitis virus (LCMV) and show their superior efficacy in eliciting CD8 T cell responses following a prime-boost immunization. NP vaccination in combination with a Toll-like receptor 9 adjuvant promoted generation of a robust pool of memory CD8 T cells with an effector-like phenotype, characterized by high expression of killer cell lectin-like receptor G1 (KLRG1) and low expression of CD43, CD27, CD127, and CD62L. These T effector memory (Tem) cells displayed protective and proliferative capability against a later LCMV challenge, in a comparable manner to T memory cells induced by a dendritic cell-based vaccination with T central memory traits. Moreover, we show the importance of antigen retention promoted by the NP carrier in shaping the differentiation of CD8 T cells. These studies demonstrate that the peptide conjugate NP vaccine can be exploited for inducing robust and long-lasting CD8 T memory cells, emphasizing the importance of the antigen carrier for tuning the quality and the magnitude of the immune response.

INTRODUCTION

In recent years, there has been an increasing interest in the use of synthetic vaccines able to induce protective cellular immunity[1–3]. Particularly, nanoparticles have proved to be promising delivery platforms for low molecular weight subunit components, such as peptides, as these carriers are able to amplify the immunogenicity of such small compounds, thus augmenting antigen (Ag)-specific cellular immune responses[4–8]. Along those lines, our laboratory has developed a platform based on ultra-small synthetic nanoparticles, 25-40 nm in size, composed of propylene sulfide (PPS) cores surrounded by a polyethylene glycol (PEG) corona (herein referred to as NP)[9,10]. We have previously demonstrated that conjugating Ag through a disulfide bond to the PEG corona of the NP can promote induction of high numbers of polyfunctional and cytotoxic CD8 T cells. Mechanistically, our NP design allows for endosomal escape of the Ag into the cytoplasm, enhancing cross-presentation[7,8,11–13].

The development of efficacious recombinant vaccines requires generation of long-lasting memory responses[14,15]. The CD8 T cell memory compartment is heterogeneous, composed of cell populations that differ in their trafficking properties and functionality[15]. Currently, there is growing interest in the T effector memory (Tem) subset, as this subpopulation shows enhanced ability to circulate compared to T central memory (Tcm) cells, which reside in lymphoid organs, thus demonstrating enhanced protection against systemic infections[16–20]. Moreover, there is evidence that differentiation of CD8 T cells into Tem cells occurs during protracted or chronic viral infections that involve persistent levels of antigen in lymphoid organs, maintaining T cells in a effector differentiation state[21–23]. Indeed, during chronic viral infections with the immunosuppressive lymphocytic choriomeningitis virus (LCMV) isolate clone-13 or cytomegalovirus, the levels of antigen stimulation are strongly correlated with the frequency of cells that display high expression of killer cell lectin-like receptor G1 (KLRG1) and low expression of CD62L, characteristics of the Tem subset[24,25]. Similarly, Tem biased differentiation has been reported following vaccination with viral vectors and synthetic carriers that promote antigen retention at the sites of immunization[16–20,26,27]. Since particulate carriers are suggested to enhance cellular immunity by augmenting antigen retention in lymphoid organs[28–30], we set out to evaluate the impact of NP antigen delivery on the differentiation state of memory CD8 T cells, including surface-receptor expression, effector function and anatomical localization.

To this end, we conjugated the well-characterized MHCI H-2D^b-restricted GP$_{33-41}$ epitope derived from the envelope glycoprotein (GP) of LCMV to our NP. Infection of LCMV in the mouse represents one of the most powerful experimental models to study anti-viral T cell immunobiology and has provided insight and fundamental concepts applicable to other viruses and pathogens[31,32]. We employed as adjuvant a well-studied TLR9 ligand, CpG-B, which has been shown to augment protective CD8 T cell immunity to subunit vaccinations[12,33,34].

To benchmark the NP formulation, we included a well-established peptide vaccine that uses dendritic cells (DC) as a vehicle[35–37], to qualitatively compare T cell memory differentiation upon the two regimes of immunization. In contrast to soluble peptides, our NP platform significantly enhanced the magnitude of CD8 T cell responses. Delivery of the LCMV GP_{33-41} epitope by NP increased Ag persistence in lymphoid organs and promoted the survival of a robust population of CD8 memory T cells. These cells adopted an effector-like phenotype, characterized by the expression of KLRG-1, and lack of CD62L, CD43 and CD27. When compared on a per-cell basis with memory T cells induced by a well-established DC vaccination, which display central memory-like characteristics, we show that both types of cells have similar abilities to respond to a viral challenge, and prevent the establishment of viral persistence. Our data further demonstrates that promotion of antigen retention is crucial for the establishment of effector memory cells, and suggests that ultra-small PPS-PEG-based NP are a promising platform for establishing proliferative and protective effector memory responses similar to those observed with vaccination strategies promoting T central memory differentiation.

RESULTS

Nanoparticles enhance cytotoxic and polyfunctional responses to the GP$_{33}$ epitope compared to the soluble form

First, we sought to determine the extent to which the NP carrier enhances cellular responses to the soluble GP$_{33-41}$, the MHC class I H-2D^b-restricted GP$_{33-41}$ epitope derived from the envelope glycoprotein (GP) of LCMV. For this purpose, groups of age- and sex-matched C57BL/6 mice were immunized with a prime-boost immunization regime (Fig. S1a) previously employed in our group, which has shown to be efficient in potentiating CD8 T cell immunity[8,12,34]. The GP$_{33}$ peptide (2 μg) was given either in soluble form or conjugated onto NP (NP-GP$_{33}$) via a disulfide link, which is labeled in the endosome. For both formulations, we used 10 μg of the TLR9 ligand CpG-B, which has proven to enhance cellular immunity in combination with our platform[8,11,34]. Five days after the booster immunization given at day 14, we evaluated the Ag-specific CD8 T cell response by *ex vivo* re-stimulation with 1 μM of GP$_{33}$ peptide.

In skin-draining lymph nodes (dLNs), the NP-GP$_{33}$ immunization induced at least 2-fold higher percentages of IFN-a expressing Ag-specific CD8 T cells and IFN-a /TNF bi-functional CD8 T cells (6.5±0.4 and 1.4±0.1) compared to the soluble peptide (1.9±0.6 and 0.7±0.2). Frequencies of cells simultaneously secreting IFN-a TNF and IL-2 remained low following both immunization regimens (Fig.S1b,c). In the spleen, the NP-GP$_{33}$ immunization likewise induced significantly higher frequencies of Ag-specific CD8 T cells producing either IFN-a or IFN-a/TNF (Fig.S1b,c) Moreover, we noticed an increase in the frequency of degranulating CD8 T cells, characterized by the expression of CD107a, a surrogate marker of cytotoxic activity (Fig.S1b,d). Together, this data confirmed that the NP platform substantially augments the frequencies of cytotoxic T cells to the peptide Ag.
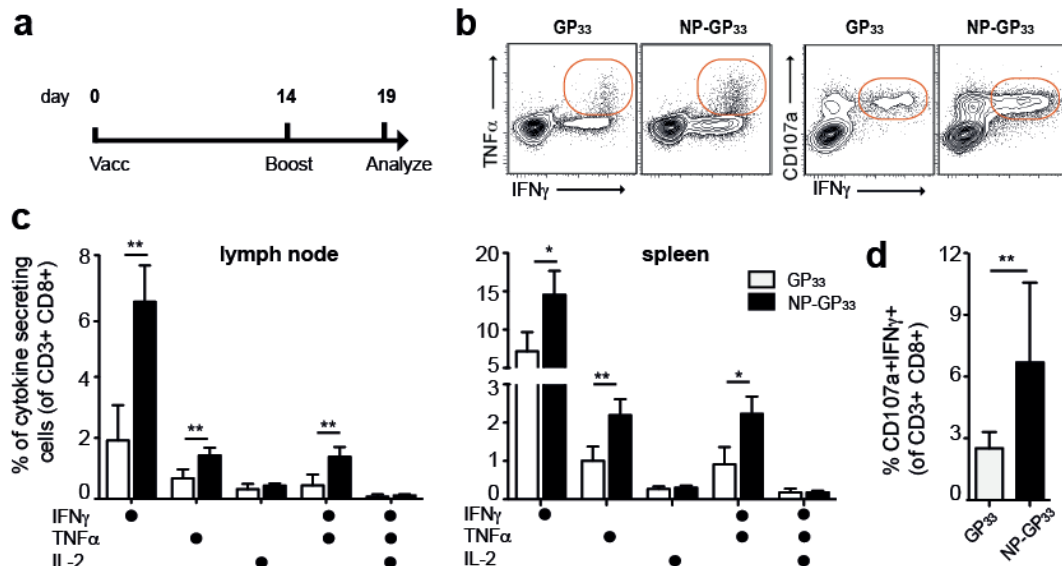
Figure S1. Intradermal immunization with NP-GP$_{33}$ conjugates enhances polyfunctional and cytotoxic CD8 T cells responses to the GP$_{33}$ epitope

a) Mice were immunized twice two weeks apart with NP-GP$_{33}$ or GP$_{33}$ intradermally (i.d.) together with 10 μg CpG-B. Draining lymph nodes and spleen were collected five days after a prime boost immunization for analysis by flow cytometry. b) Representative flow cytometry plots of cytokine-secreting CD8 T cells (*left*) and degranulating CD8 T cells (*right*) in lymph nodes at day 19, after *ex vivo* restimulation with GP$_{33}$ peptide. Cytokine expression was assessed by intracellular staining c) Frequency of endogenous cytokine-secreting CD8 T cells in lymph node and spleen d) Frequency of endogenous cytotoxic CD8 T cells in spleen. Data are representative of three independent experiments with at least n=4 per group. *: p< 0.05; **p<0.01. Mann-Whitney U test.

Nanoparticles promote Ag persistence in secondary lymphoid organs

Ag persistence has important implications for T cell memory differentiation[18,38–40]; hence, we next investigated the ability of NPs to promote Ag retention in lymphoid organs. We performed a side-by-side comparison with a vaccination based on DCs as Ag carriers, for the reason that, similar to the NP formulation, the DC vaccine can be administered i.d., together with a selected adjuvant[35–37]. The dose of antigen used for pulsing DCs and DC numbers were selected based on the ability to promote a similar expansion of P14 cells in spleen upon a single immunization compared to an immunization with NP-GP$_{33}$ (2 ꞏ g) (Fig.S2). The unformulated Ag was used as a negative control as relatively low retention in dLNs was expected at the time points studied.
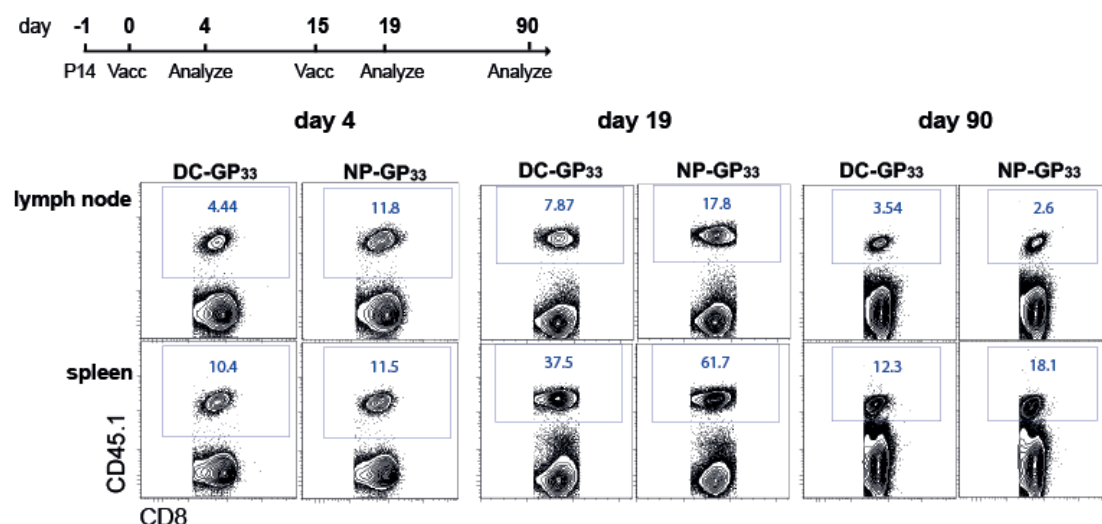
Figure S2. Frequency of P14 cells in lymph nodes and spleen after a prime or a prime boost immunization with NP-GP33 or DC-GP33

Naïve CD45.1 P14 CD8 T cells (5×10^4) were adoptively transferred into host mice and the following day, mice were immunized with NP-GP$_{33}$ (2μg) or DC-GP$_{33}$ (2×10^6 cells), together with $10\ \mu$g of CpG-B. At day 5, 19 or 90 after immunization, lymphocytes retrieved from draining lymph nodes (dLNs) and spleen were collected and analyzed for the frequency of CD45.1 P14 in total CD8 T cells. Data are representative of two independent experiments for days 4 and 19, and three independent experiments for day 90, with at least n=3 per group

Mice were immunized once with NP-GP$_{33}$, DC-loaded with GP$_{33}$ (DC-GP$_{33}$) or soluble GP$_{33}$, in each case combined with CpG-B. One or three weeks after vaccination, we adoptively transferred CFSE-labeled Ag-specific CD45.1 P14 CD8 T cells derived from mice transgenic for the LCMV T cell receptor (TCR), which recognizes the GP$_{33}$ epitope in the context of H-2D^b. Three days after, P14 CD8 T cells were retrieved from dLNs, and the dilution of the CFSE dye was assessed as a means to detect stored Ag in dLNs (Fig.1a). We consistently found higher frequencies of P14 CD8 T cells upon NP-GP$_{33}$ immunization at both time points of analysis (Fig.1b), with corresponding levels of cell proliferation. The percentage of dividing cells was significantly enhanced in mice that had received NP-GP$_{33}$ over the DC-GP$_{33}$ and GP$_{33}$ peptide-only groups (Fig.1c), suggesting that the Ag was retained for longer periods of time (> 3 weeks) when delivered via NP.

Next, we wanted to determine the cells within the dLN within which Ag is retained upon immunization. We administered fluorescently labeled GP$_{33}$ loaded on NP or delivered via DC. To normalize for the amount of Ag, the level of fluorescence of peptide was matched before vaccination between both groups. Ten days after i.d. immunization, animals of the NP-GP$_{33}$ group displayed a higher percentage of Ag$^+$ cells when compared to mice immunized with DC-GP$_{33}$ (Fig.1d). The frequency of CD45^{hi}

hematopoietic cells within the Ag$^+$ fraction was comparable in both groups. The Ag was mainly distributed within major lymphocyte populations (T cells, B cells), and to a lesser extent in LN resident DCs, monocytes, or macrophages (Fig.1e-f).

Interestingly, there were striking differences in Ag retention within the stromal cell (CD45^{low}) compartment, where the NP vaccination displayed a considerably higher frequency of Ag$^+$ cells (Fig.1e). To define the CD45^{low} subpopulations that were associated with GP$_{33}$, we employed a gating strategy based on PECAM-1 (CD31) and podoplanin (gp38) staining, as described previously[41], allowing us to differentiate fibroblastic reticular cells (FRCs, CD31^{low}gp38^{hi}), lymphatic endothelial cells (LECs, CD31^{hi}gp38^{hi}), blood endothelial cells (BECs, CD31^{hi} gp38^{low}), and double negative cells (DN, CD31^{low}gp38^{low}). Analysis of these populations revealed that NP-GP$_{33}$ was specifically retained within LECs, in agreement with previous reports using protein Ag[42,43].Conversely, Ag was not detected in any of the stromal subsets when delivered via DCs (Fig.1g). These data indicate that Ag delivered by NP localizes to both hematopoietic and non-hematopoietic cells in regional dLNs.
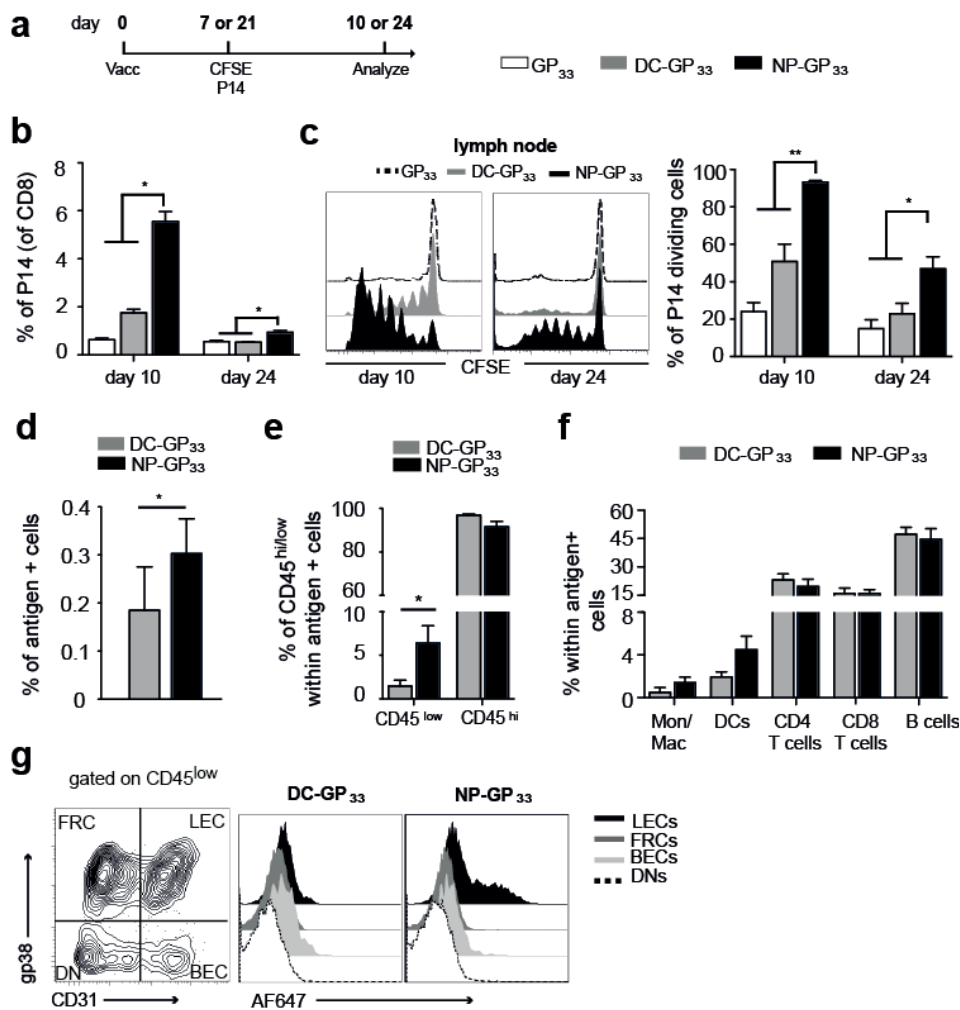
Figure 1. Nanoparticles promote enhanced antigen retention in draining lymph nodes compared to dendritic cell vaccination

a) Naïve C57BL6 mice were immunized with NP-GP$_{33}$ (2 μg) or DC-GP$_{33}$ (2x10^6 cells), together with 10 μg of CpG-B. At day 7 or day 21 post immunization, mice received 1x10^6 CD45.1 P14 CD8 T cells that were CFSE labeled. Three days after the transfer, splenocytes were isolated and proliferation of P14 cells was assessed by CFSE dilution. b) Percent of P14 cells in lymph nodes 3 days after i.v. transfer. c) *Left*, representative histograms; *Right*, percent of dividing P14 cells, calculated as the frequency of CD8 T cells that dilute CFSE compared to the initial population (the non-divided P14 cells). (d-g) Naïve mice were immunized with 2 μg of fluorescently labeled GP$_{33}$ as either soluble, or delivered in NPs or DCs, together with 10 μg of CpG-B. At day 10, lymph nodes cells were retrieved and analyzed by flow cytometry. (d) Percent of GP$_{33}$ positive cells in total lymph node cells. e) Percent of CD45^{hi} and CD45^{low} populations within the GP$_{33}$$^+$ cells. f) Percent of hematopoietic populations within GP$_{33}$$^+$ cells. g) *Left*, gating strategy based on the expression of gp38 (podoplanin) and CD31 (PECAM-1) for the identification of stromal cell subsets. Fibroblastic reticular cells (FRCs), CD31^{low}gp38^{hi}; lymphatic endothelial cells (LECs), CD31^{hi}gp38^{hi}; blood endothelial cells (BECs), CD31^{hi} gp38^{low}); and double negative cells (DNs), CD31^{low}gp38^{low}. *Right,* antigen positive cells within stromal cell subsets. Data is representative of two independent experiments with at least n=3 per group*: $p < 0.05$; **$p<0.01$. b-c) One way ANOVA, d-f) Mann-Whitney U test*.

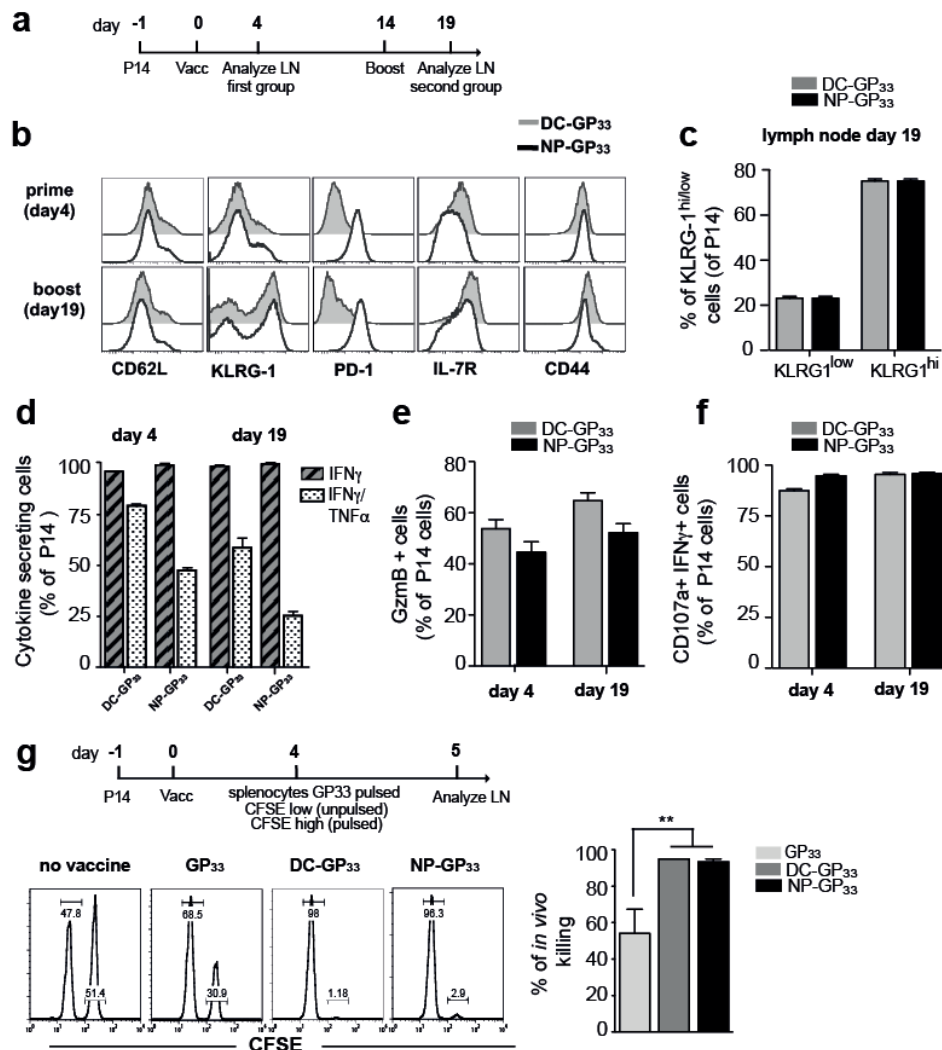**NP-GP$_{33}$ vaccination promotes effector T cells with a different phenotype but comparable cytolytic ability relative to DC-GP$_{33}$**

Because antigen retention kinetics due to NP vaccination was distinct from DC vaccination, we hypothesized this would generate phenotypically and functionally distinct antigen-specific CD8 T cells. Thus, we wanted to investigate how memory CD8 T cells differ between the two immunization regimens with respect to functionality, surface phenotype and trafficking properties. For this purpose, we adoptively transferred 5x10^4 congenically marked P14 CD8 T cells into naïve C57BL6 mice. The following day, animals were immunized i.d. with 2 ǐ g of Ag administered as NP -GP$_{33}$ or DC-GP$_{33}$. All formulations were combined with 10 ǐ g of CpG-B (Fig.2a).

Initially, we sought to evaluate P14 CD8 T cells in dLNs during the effector phase after a prime or a prime-boost immunization. Surface expression phenotype of effector cells at both times of analysis (day 4 and 19) indicated differences in activation upon NP or DC vaccination (Fig.2b). There were consistent differences in the expression of IL-7R, with the DC-vaccinated group maintaining a higher percentage of IL-7R^{hi} cells (83% and 55% at days 4 and 19) compared to the NP counterpart (32% and 21% at days 4 and 19), in line with previous observations of accelerated central memory differentiation when employing DCs as Ag carriers[35,44]. Intriguingly, we also found that P14 CD8 T cell from mice vaccinated

with NP, but not the DC vaccine, expressed the inhibitory receptor programmed cell death protein (PD)-1. Instead, L-selectin (CD62L) expression was downregulated and CD44 and KLRG1 were upregulated in the majority of the P14 CD8 T cells, regardless of the immunization. In particular, KLRG1 expression was considerably higher in both groups after the boost (Fig.2c). This was in agreement with previous reports that demonstrated that multiple immunizations augment the expression of effector-like markers in responsive CD8 T cells[19,45,46] (Fig.2b).

To determine whether cytokine production and degranulation capability varied between both immunizations, we re-stimulated LN cells *ex vivo* for 5 h with 1 ꭐ M of GP$_{33}$. There was a considerable high expression of CD107a and IFN-a in both groups, whereas the levels of TNF ✔ and Granzyme B (GzmB) were lower after NP vaccination. (Fig.2d-f). Nevertheless, effector cells in both groups displayed similar cytotoxic activity, as assessed by the ability of primed CD8 T cells to kill splenocytes that were previously pulsed with the GP$_{33}$ peptide in an *in vivo* killing assay (Fig.2g). The data suggested that, despite phenotypical differences, both immunizations drove functional effector CD8 T cells.

Figure 2. NP-GP$_{33}$ and DC-GP$_{33}$ vaccination promote effector cell subsets that differ in surface expression and cytokine secretion, but exhibit comparable killing activity

a) Naïve CD45.1 P14 CD8 T cells (5×10^4) were adoptively transferred into host mice. The following day, mice were immunized with NP-GP$_{33}$ ($2\,\mu$g) or DC-GP$_{33}$ (2×10^6 cells), together with $10\,\mu$g of CpG-B. At day 4 or 19 after immunization, lymphocytes retrieved from draining lymph nodes (dLNs) were collected and analyzed. b) Expression of various surface markers in P14 cells in dLNs after a prime or a prime boost immunization with DC-GP$_{33}$ or NP-GP$_{33}$. c) Percent of KLRG1^{hi} P14 cells after a prime-boost immunization in DC-GP$_{33}$ and NP-GP$_{33}$ immunized mice. d) Percent of IFN-a IFN-a/TNFα^+, and e) GzmB secreting P14 cells in dLNs, following *ex vivo* restimulation with GP$_{33}$. f) Percent of CD107a$^+$IFN-a cells following *ex vivo* restimulation with GP$_{33}$. g) *In vivo* cytotoxic assay; GP$_{33}$-pulsed (CFSE^{high}) and untreated/unpulsed (CFSE^{low}) splenocytes were transferred intravenously (i.v.) into mice previously vaccinated with DC-GP$_{33}$ and NP-GP$_{33}$, as described above. As a control, mice were vaccinated with soluble 2μg of GP$_{33}$ or were untreated. After 6 h, the frequency of CFSE^{low} and CFSE^{high} cells were assessed by flow cytometry, and the percent of *in vivo* killing calculated. Data is representative of two independent experiments with at least n=3 per group. *: p< 0.05; **p<0.01. *Mann-Whitney U test*.

NP-GP$_{33}$ vaccination induces long-lasting memory CD8 T cells with an effector memory phenotype

In order to assess the evolution in surface phenotype of P14 CD8 T cells, we performed a longitudinal analysis in blood, examining the expression of CD62L and IL-7R. Based on these two markers, three major sub-populations of memory CD8 T cells can be distinguished: T central memory (Tcm, IL-7R^{hi} CD62L^{hi}), T effector memory (Tem, IL-7R^{hi} CD62L^{low}), and T effectors (Teff, IL-7R^{low} CD62L^{low})[47,48]. The latter sub-population has been proposed to represent recently activated CD8 T cells and has been consistently observed upon long-term Ag retention[18,47]. At day five after prime or a prime-boost immunization, circulating memory cells in both groups reflected closely the pattern of expression of IL7-R observed in dLNs (Fig.3a). Meanwhile, at later times (day 90) the majority of NP-GP$_{33}$-induced P14 CD8 T cells consisted of Tem (43±2), followed by Teff (32±2) and Tcm (21±1). The maintenance of the Teff subset further supports that Ag persisted for long periods of time upon NP vaccination. On the contrary, DC vaccination favored generation of P14 memory cells with Tcm characteristics (61±4), while the Tem and Teff subsets were less prevalent (26±3, 3±1) (Fig.3a).

The striking differences in CD8 T cell phenotype between the two vaccine regimens on day 90 prompted us to investigate whether the phenotype of memory P14 CD8 T cells in other organs (liver, spleen, LN, lung) resemble those observed in blood. In LNs the majority of GP$_{33}$-specific CD8 T cells displayed a CD62L^{hi} Tcm phenotype. In contrast, in spleen and peripheral organs such as liver and lung, the memory compartment reflected the phenotype of circulating Ag-specific CD8 T, as similar frequencies of Tcm, Tem and Teff cells were observed when compared to blood (Fig.3b). We also evaluated memory cells

based on a prototypic gating strategy involving KLRG1 and IL-7R[21] as well as CD27 and CD43[49]. Employing these gating schemes further illustrated that NP promoted predominantly Tem cells, based on the prevalence of KLRG1^{hi} IL-7R and CD43^{low} CD27^{low} populations (Fig.S3a-b).

We turned to our previous analysis based on CD62L and IL-7R and assessed how markers such as KLRG-1, CD43 and CD27 were expressed within the three subsets of memory cells (Tcm, Tem, Teff). As expected, the presence of KLRG1 was almost exclusively found in Tem and Teff populations, but not in the Tcm subset. On the contrary, CD43 and CD27 varied to some degree within the individual populations, with CD43^{hi} and CD27^{hi} being detected exclusively in the Tcm subset, while Teff cells displayed low levels of both markers. In comparison, the Tem exhibited heterogeneous expression of CD43, and intermediate-to-low expression levels of CD27 (Fig.3c). In summary, P14 cells from NP-vaccinated mice were prevalently KLRG1^{hi} and CD43^{low}CD27^{low}, which is consistent with a Tem phenotype based on multiple definitions of the phenotype.

Notably, the PD-1 expression observed in Ag-specific CD8 T cells earlier during the effector phase in NP vaccinated mice was also observed at the memory stage (Fig.3d). This suggests that upregulation of PD-1 in our system does not represent a transient phenomenon, but may be an "imprinted" characteristic of CD8 T cells upon activation in the NP vaccination paradigm.

Successively, we were interested in the effector functions of memory CD8 T cells in LNs and spleen and how it may differ from our earlier observations in the early effector phase. As seen previously, the memory CD8 T cells in the NP-vaccinated animals displayed a comparable capacity to express IFN-a and CD107a than with those cells in DC-immunized mice, although TNF ✔ levels were lower, as observed earlier (Fig.3f-g). The frequency of GzmB cells in spleen was also similar between the two groups, with a tendency to be higher in the LNs of NP-GP$_{33}$ treated mice (Fig.3g).

Finally, we evaluated the cellular homing characteristics of these memory CD8 T cells. Previous studies have shown that Tcm cells preferentially reside in the spleen parenchyma, while Tem cell are located mainly in the red pulp[50]. To differentiate between cells located in the splenic red pulp and white pulp, we employed an intravascular staining strategy[51], consisting of an intravenous injection of an anti-CD8 antibody (Ab). This technique discriminates between the red and white pulp based on the staining level by the injected Ab. Congruent with the other functional analyses, we observed that NP-derived memory CD8 T cells with a Tem phenotype were predominantly located in the red pulp. Instead, DC-primed CD8 T cells were enriched in the spleen white pulp, as seen by the lack of staining with the injected Ab (Fig.3h). Altogether, these data suggest that the NP vaccination preferentially promotes the differentiation of CD8 into T cell with characteristics of T effector memory cells.
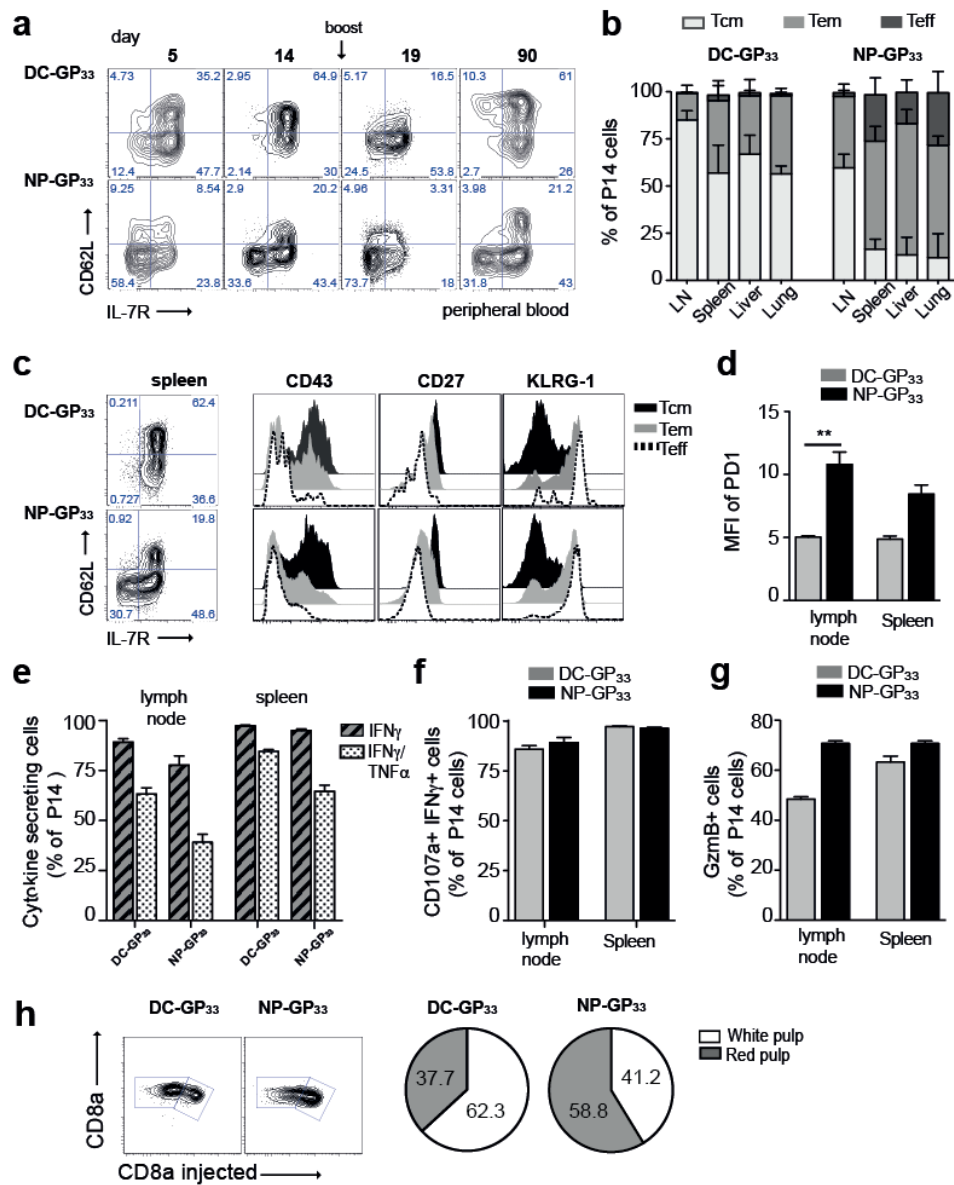
Figure 3. NP-GP$_{33}$ induce the differentiation of antigen specific T cells into T effector memory

Naïve CD45.1 P14 CD8 T cells (5x10^4) were adoptively transferred into host mice and the following day immunized with NP-GP$_{33}$ (2 μg) or DC-GP$_{33}$ (2x10^6 cells), together with 10 μg of CpG-B. At day 90, lymphocytes from lymphoid and peripheral organs were retrieved and analyzed. a) Phenotype of P14 cells in peripheral blood, based on the expression of CD62L and IL-7R expression. **b)** Percent of T central memory (Tcm, CD62L^{hi} IL-7R^{hi}), T effector memory (Tem, CD62L^{low} IL-7R^{hi}) and T effector (Teff, CD62L^{low} IL-7R^{low}) within CD45.1 P14 cells at day 90 in spleen. **c)** Surface expression of CD43, CD27, KLRG-1 within the Tcm, Tem and Teff memory subsets in the DC-GP$_{33}$ and NP-GP$_{33}$ vaccinated mice. **d)** Mean Fluorescence Intensity (MFI) of PD-1 in P14 cells. **e)** Percent of IFN-a, IFN-a/TNFα^+, and **f)** GzmB secreting P14 cells in spleen at day 90, following *ex vivo* restimulation with GP$_{33}$. **g)** Percent of CD107a$^+$IFN-a cells following *ex vivo* restimulation with GP$_{33}$. **h)** Discrimination of memory P14 cells within the red pulp or white pulp by intravital staining with the injection of anti-CD8a i.v. *Right*, pie charts displaying the distribution of memory P14 cells within the spleen after immunization with DC-GP$_{33}$ or NP-GP$_{33}$. Data is representative of three independent experiments with n=3-4 per group, *: p< 0.05; **p<0.01. Mann-Whitney U test.*
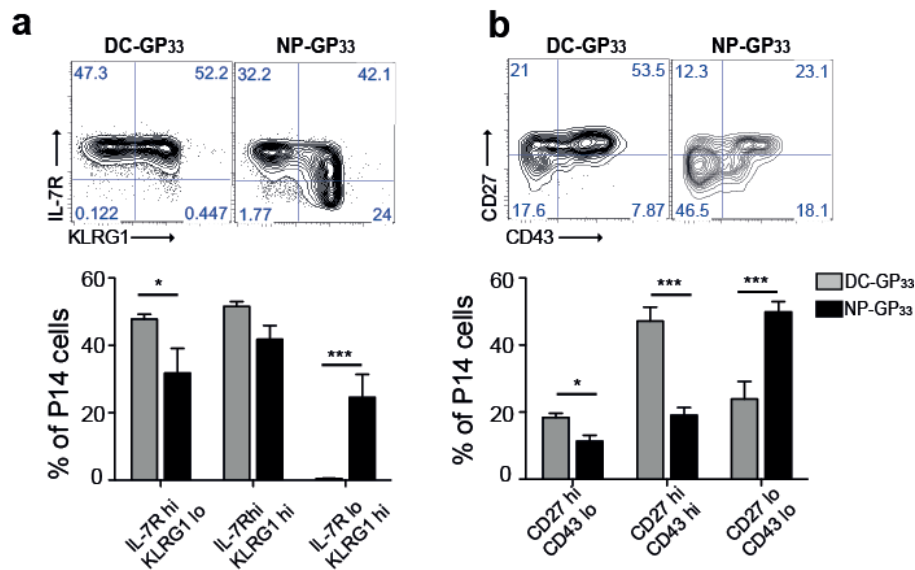
Figure S3. Memory differentiation of antigen specific P14 cell upon vaccination with NP-GP$_{33}$ and DC-GP$_{33}$

Naïve CD45.1 P14 CD8 T cells (5x10^4) were adoptively transferred into host mice and the following day immunized with NP-GP$_{33}$ (2μg) or DC-GP$_{33}$ (2x10^6 cells), together with 10 μg of CpG-B. At day 90, lymphocytes from lymphoid and peripheral organs were retrieved and analyzed. Phenotype of P14 cells in spleen was analyzed based on the expression of a) KLRG1 and IL-7R, or b) based on the expression of CD27 and CD43. Graph bars represent the percent from CD45.1 P14 cells. Data are

representative of three independent experiments with at least n=4 per group*: *p<0.05; **p<0.01, ***: p<0.001. 2way ANOVA with Bonferroni post-test.*

Memory cells induced by NP vaccination respond as robustly to viral and bacterial challenges as those induced by DC vaccination

Next, we evaluated the ability of memory CD8 T cells induced by NP-GP_{33} or DC-GP_{33} vaccination to respond to pathogen challenge. To evaluate protection from viral challenge, we employed the stringent LCMV ARM53-variant clone-13 (Cl-13) infection model, which causes persistent infection associated with generalized T cell exhaustion and immune suppression[52-55]. Briefly, three months post vaccination we sorted and adoptively transferred $5x10^4$ CD45.1 memory CD8 T cells into age-matched CD45.2 naïve hosts. The following day, mice were challenged i.v. with $2x10^6$ PFU LCMV Cl-13. After 14 days, we assessed the numbers of CD45.1 cells present in the spleen and the viral load in kidneys (Fig4.a). Analysis of cell numbers in spleen showed similar frequencies of GP_{33}-specific CD45.1 cells in both groups, indicating that transferred memory T cells deriving from both vaccination schemes proliferated extensively upon viral challenge (Fig.4b). Consequently, we measured the viral titers in the kidneys of infected mice. We found that both groups were able to significantly reduce the virus titers in this organ, compared to the infection control group, which did not receive any cell transfer. Remarkably, there was no difference in virus titers between the two groups, suggesting that cells induced by NP-GP_{33} or DC-GP_{33} vaccination controlled the infection with LCMV Cl-13 to a similar extent (Fig.4c).

Similar results were observed using a bacterial challenge model involving *Listeria monocytogenes expressing ovalbumin* (OVA; *Lm-OVA*) in mice vaccinated with $OVA_{257-264}$ (SIINFEKL), a MHC class I H-2K^b-restricted peptide delivered on the two platforms: NP-SIINFEKL and DC-SIINFEKL (Fig.S4).

Cytokine secretion analysis in the CD45.1 CD8 T cell subset upon LCMV Cl-13 infection demonstrated a polyfunctional phenotype present to a comparable degree in both vaccine schemes (Fig.4d). Interestingly, when we analyzed the expression of PD-1 at day 14 after challenge, we observed that the levels of this marker on the surface of memory CD8 T cells at day 14 after challenge resembled those observed before the infection. This was in contrast to the typical high levels of PD-1 seen in the endogenous CD8 T cells, a hallmark of functional exhaustion after challenge with Cl-13. This suggests that the transferred cells maintained their PD-1 pattern acquired at earlier times (Fig.4e). Collectively, the data demonstrate that memory CD8 T cells derived from NP and DC vaccination, despite their surface marker and homing differences, were able to respond actively to a pathogenic Ag challenge.
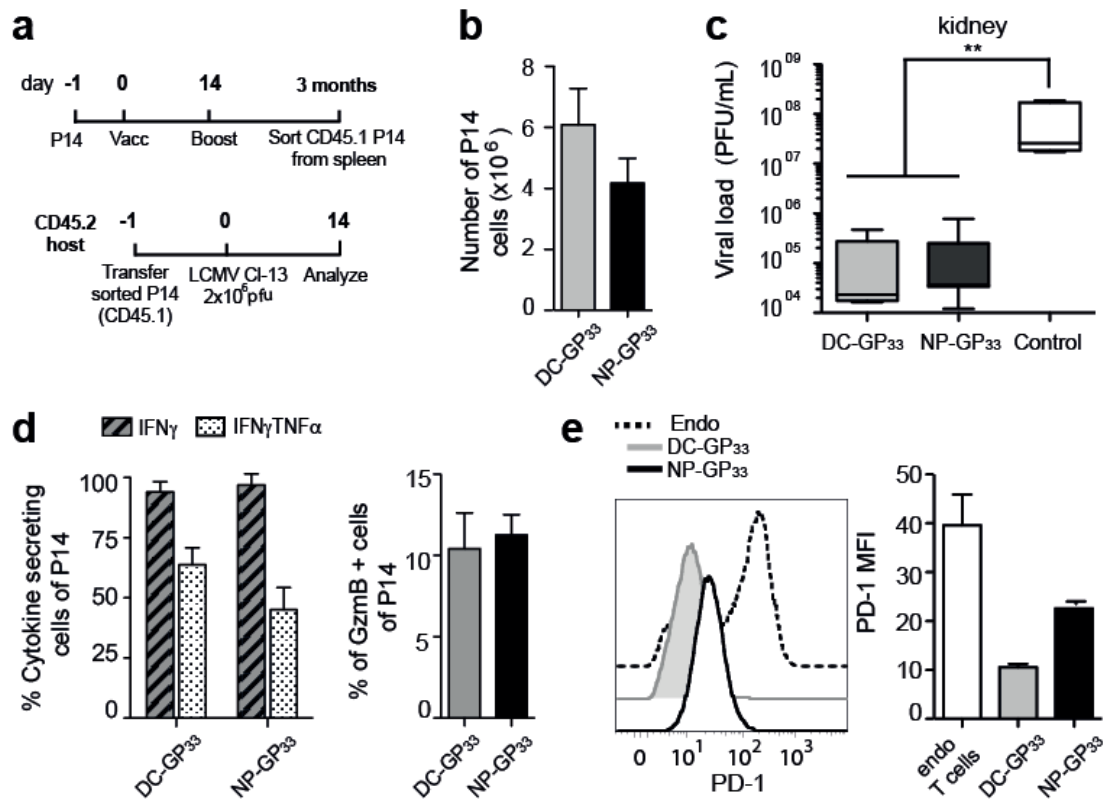
Figure 4. CD8 T memory cells generated following NP-GP$_{33}$ and DC-GP$_{33}$ vaccination display similar protective capacity when challenged with LCMV Cl-13

a) 5×10^4 memory CD45.1 P14 CD8 T cells sorted from splenocytes of DC-GP$_{33}$ or NP-GP$_{33}$ vaccinated mice were transferred into age-matched, CD45.2$^+$ naïve hosts. One day after, mice were challenged i.v. with 2×10^6 PFU. of LCMV Cl-13. **b)** Two weeks post infection (p.i.), whole spleens were analyzed and assessed for the number of CD45.1 P14 cells. **c)** Viral titers in kidney were assessed by qPCR. d) Cytokine secretion (IFN-a, IFN-a/TNFα, *left* and GzmB, *right*) by P14 cells at day 14 p.i. was assessed by intracellular staining, after *ex vivo* restimulation with GP$_{33.}$ **e)** *Left*, representative histograms; right, Mean Fluorescence Intensity (MFI) of PD-1 in transferred P14 cells and endogenous CD8 T cells at day 14 p.i. Data are representative of two independent experiments with n=4 per group. *: p< 0.05; **p<0.01. Mann-Whitney U test*.
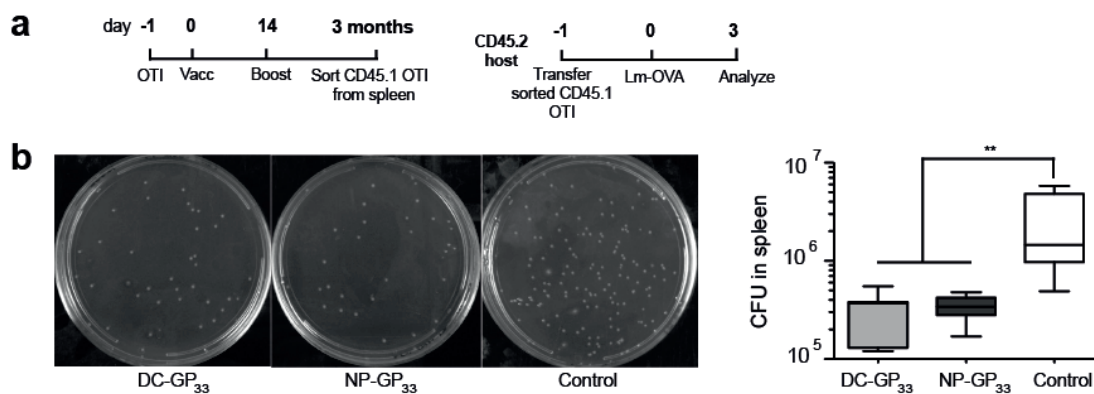
Figure S4. Tem and Tcm cells induced by NP and DC vaccination promote protection to a bacterial challenge

a) Naïve CD45.1 OTI CD8 T cells (5×10^4) were adoptively transferred into host mice and the following day immunized with NP-SIINFEKL (2μg) or DC-SIINFEKL(2×10^6 cells), together with 10 μg of CpG-B. At day 90, 1×10^4 CD45.1 OTI cells were sorted from spleens and adoptively transferred into naïve C57BL6 mice. One day later, mice were challenged i.v. with 1×10^5 CFU of *Listeria-monocytogenes expressing Ovalbumin* (LM-OVA). **b)** Determination of protection by quantification of CFU in spleens of infected mice three days post infection. Data are representative of a single experiment with n=7-8 per group. ***p<0.01. Mann-Whitney U test.*

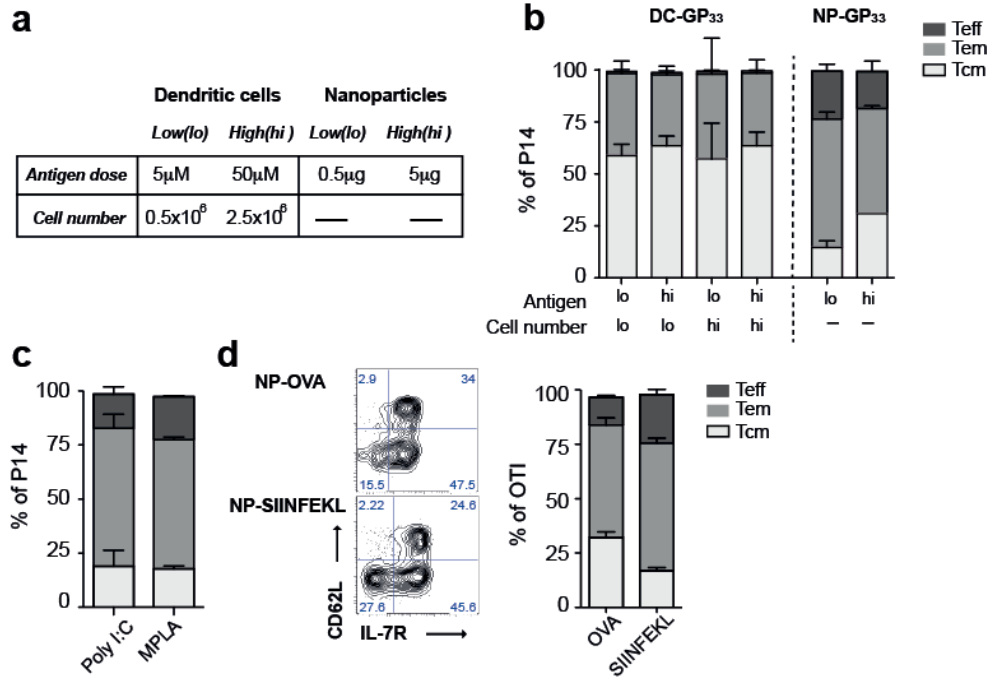**Differentiation into Tem is not affected by antigen dose or TLR identity**

The notable differences in the effector phenotypes between our vaccination paradigms prompted us to evaluate factors that might instruct CD8 T cells towards a certain phenotype. Specifically, we focused on antigen load[37,56–58], adjuvant selection[36,59,60], and the presence of CD4 T cell help during T cell activation[48,61–64].

Antigen does direct the differentiation of CD8 T cells, and thus competition for the antigen by the responding cells may play an important role. To test how early antigen availability impacted T cell memory differentiation upon DC and NP vaccination, we immunized naïve mice previously adoptively transferred with CD45.1 P14 cells with a high and a low dose of peptide (0.5 μg and 5 μg) conjugated onto NP. For the DC vaccine we varied the concentration of peptide delivered to them *in vitro* or the number of DCs used for immunization, keeping the amount of pulsing peptide constant (Fig.5a). We then evaluated the phenotype of the CD8 T cell memory pool generated under these conditions in the spleen. Interestingly, none of the doses tested appeared to have a significant effect on the phenotype, as similar frequencies of Tcm, Tem and Teff where obtained under the doses tested (Fig.5b).

Further, we assessed whether the main Tem differentiation upon NP vaccination was restricted to the use of the TLR9 ligand, CpG-B, as adjuvant, or whether this phenotype was observed when employing other TLR agonists (Fig.5c). We vaccinated mice as detailed above, but instead of CpG-B we used either 10 μg of the TLR4 adjuvant MPLA or 20 μg of the TLR3 ligand Poly I:C. However, P14 CD8 memory T cells consistently displayed a T effector memory phenotype, irrespective of the adjuvant administered.

It has also been proposed that lack of CD4 T cell help can lead to the generation of memory CD8 T cells with effector-like phenotype, similar to what we observed in the NP vaccination[61,65]. Therefore, we evaluated whether vaccination with a full protein (containing MHCII epitopes) could modulate the Tem phenotype observed upon NP-MHCI vaccination. We analyzed at day 90 memory CD8 T cells from mice that received an adoptive transfer of naïve OTI CD8 T cells (5×10^4), which were vaccinated with SIINFEKL or the protein OVA, loaded onto NPs (NP-SIINFEKL or NP-OVA). Mice immunized with NP-SIINFEKL displayed equivalent percentage distributions of Tcm, Tem and Teff to those seen in NP-

GP$_{33}$. Meanwhile, mice that received OVA displayed enhanced numbers of the Tcm population, although Tem cells were still the predominant population at the time of the analysis. Similarly, Teff cells were reduced in the NP-OVA group, but were maintained at considerable frequencies in the memory phase (Fig.5d). These data indicate that CD4 T cell help certainly has an effect on the differentiation of CD8 T cells, as observed in earlier studies [48,61,62]. However, the predominant presence of Tem cells during NP-OVA vaccination suggests that the unhelped memory differentiation is not the main cause of the observed phenotype in NP educated memory T cells.

Figure 5. Differentiation into Tem is not affected by antigen dose or TLR identity. Mice that were adoptively transferred with 5x10^4 naïve CD45.1 P14 CD8 T cells were immunized with NP-GP$_{33}$ or DC-GP$_{33}$, together with 10 μg of CpG-B, 20 μg of Poly I:C or 10 μg of MPLA. At day 90, lymphocytes retrieved from spleen were isolated for analysis by flow cytometry. a) Mice were vaccinated with varying doses of peptide loaded on NPs, with DCs loaded with varying doses of peptide, or varying numbers of DCs. b-c) The phenotype of P14 cells was determined based on the expression of CD62L and IL-7R as T central memory (Tcm, CD62L^{hi} IL-7R^{hi}), T effector memory (Tem, CD62L^{low} IL-7R^{hi}) and T effector (Teff, CD62L^{low} IL-7R^{low}) b) Frequency of CD45.1 P14 cells in spleen at day 90. c) Phenotype of P14 T cells upon vaccination with NP-GP$_{33}$ or DC-GP$_{33}$ adjuvanted with Poly I:C or MPLA. d) Memory phenotype of CD45.1 OT-I memory cells upon immunization with NP-SIINFEKL (2 μg) and NP-OVA (2 μg) together with 10 μg of CpG-B. Data are representative of two independent experiments with n=3-4 per group.

DISCUSSION

Subunit vaccines delivered as synthetic particles have attracted significant attention in the vaccine field due to their capacity to enhance cellular immunity over unformulated antigens. Motivated by this, we have designed a PEG-PPS-based nanoparticle vaccine (NP) and evaluated the impact of NP-conjugation on the activation of CD8 T cells against the LCMV GP antigen, GP_{33}.

Using GP_{33} as model Ag, we confirmed that intradermal immunization with a NP peptide conjugate augmented the frequency of polyfunctional and cytotoxic CD8 T cells compared to the soluble GP_{33} peptide, as evidenced by the increase in multiple cytokine secreting CD8 T cells, and enhanced expression of CD107a, a surrogate marker of cytotoxicity. This is in agreement with previous studies using PEG-PPS NP[7,8,11,12,34], underscoring the potential of this platform to augment quantitatively and qualitatively cellular immune responses in clinically relevant scenarios.

The development of successful T cells vaccines relies on the ability to generate long-lasting memory responses. To have a more comprehensive understanding of the differentiation of memory CD8 T cells upon NP vaccination, we benchmarked our NP platform to a DC-based vaccine, which has proven to be an effective immunization approach for promoting protective CD8 T cell memory responses[35,36]. We show that NP promoted a CD8 T cell memory pool with a bias towards an effector memory phenotype, characterized by high expression of IL-7R, KLRG-1 and a low/intermediate expression of CD43, CD27 and CD62L. These cells were polyfunctional (secreted IFN-a TNF-b simultaneously), had higher circulatory capability and displayed recall potential to viral (with LCMV Cl-13) and bacterial (with *Lm-OVA*) challenges similar to those induced by the DC-based vaccine. Moreover, we demonstrated that NP promoted Ag retention in dLNs when compared to the unformulated peptide or the DC vaccine, potentially allowing the proliferation of newly arrived naïve CD8 T cells over an extended period. In an effort to define the cells in which Ag is retained, we labeled the GP_{33} peptide and showed that Ag was retained mainly in hematopoietic cells in lymph nodes. Additionally, we also observed antigen associated with LECs, in accordance to a previous report with fluorescently labeled protein antigen[42], indicating that Ag delivered by our synthetic nanoparticles can promote retention in this stromal cell subset.

The importance of Ag persistence on memory differentiation has been extensively described during chronic viral infections[24]. In the context of LCMV Cl-13, high loads of antigen primarily in non-lymphoid organs drive CD8 T cells towards functional exhaustion and deletion[22,39,66,67]. These cells are characterized by a high expression of the surface marker KLRG1 and their partially or fully impaired capability to secrete effector molecules[22]. Based on this evidence, KLRG1 has been described as a correlative marker of senescence[68]. Nevertheless, in our system we showed that NP-educated memory T cells, in their majority expressing KLRG1, proliferated upon antigen encounter and displayed cytotoxic capability. Our data supports previous studies that demonstrated the protective efficacy of the

Tem subset[17-20,69]. For instance, Olson *et al*[19] reported that a Tem population with similar traits to the Tem subset generated by the NP vaccine displayed better protective capability to *Listeria monocytogenes* than Tcm cells, despite a lower proliferation recall capacity. Our results are also in accordance with those of Reyes-Sandoval *et al*[18] who demonstrated that frequency of blood-circulating Tem promoted by antigen-delivery via an adenovirus vector correlated with the level of protection against a sporozoite challenge in a malaria model of vaccination.

In addition to Ag persistence as the main factor promoting Tem differentiation, we wanted to understand the contribution of other factors that favor differentiation into Tem cells, such as antigen dose, adjuvant selection and CD4 T cell help. We excluded the possibility that the observed phenotype was caused by drastic differences in Ag dose between the two vaccination regimes, since tuning peptide doses or DC cell numbers did not have an impact in the differentiation of memory CD8 T cells. We further addressed if lack of CD4 T cell help during the immunization could be also responsible for the observed strong effector-like phenotype after NP immunization. Studies in MHCII knockout mice or CD4-deficient mice reported that unhelped memory CD8 T cells display a similar phenotype as the one we observed with NP, characterized by the low expression of CD62L, IL-7R and CD27; and high levels of KLRG1[48,61,70]. We showed that vaccination with the model antigen OVA delivered as a full protein conjugated onto NP promoted a moderate increase in the frequencies of Tcm cells. However, the majority of cells still displayed the Tem phenotype observed with the immunization with the MHCI-restricted NP-SIINFEKL, indicating that the lack of CD4 T cell help is not the main responsible factor for the Tem-biased differentiation. Similarly, modulation of the inflammatory environment using different TLR-based adjuvants promoted little phenotypic change in memory T cells. Consistent with our hypothesis, our data highlights that Ag persistence is a key factor for the generation of Tem cells.

Interestingly, we observed an increase in PD-1 expression on NP-primed memory CD8 T cells, but not other inhibitory receptors, such as LAG-3 (data not shown). Although it is generally believed that not all PD-1^{hi} T cells are exhausted, there are few studies addressing the role of this receptor in memory differentiation[71,72]. Hokey *et al*[72] showed that peptide vaccination in macaques also drives the generation of fully active PD-1^{hi} cells, indicating that rather than representing an exhaustion marker, PD-1 expression may define T cell activation during a primary immune response.

Future studies should address whether protection by this subset arises by a faster response owing to the extra-lymphoid localization and enhanced circulatory potential of this subset. Since it is unlikely that a single phenotype is generated by a vaccine regime, it would be important to elucidate how the different memory subsets synergize to provide protection against pathogens.

In summary, we have shown that NP-vaccination and a benchmark DC vaccination each drives a distinct memory differentiation; PEG-PPS NP-GP$_{33}$ vaccination results in Tem differentiation, while, DC vaccines preferentially promote Tcm cells. Antigen retention in both hematopoietic cells and LECs in

the dLN appears to be key in inducing the Tem bias. Both NP-educated and DC-educated CD8 T cells display protective capacity against viral and bacterial challenge, establishing the NP vector as a promising platform for peptide-based T cells vaccines aiming at promoting protective immunity. Moreover, these studies highlight the importance of vaccine design in tailoring the quality of the immune response.

ACKNOWLEDGMENTS

MATERIALS AND METHODS

Animals

C57BL/6 female mice, age between 8-12 weeks, were purchased from Harlan (France). CD45.1 P14 mice, which encode for a T cell receptor that is specific for the LCMV MCHI epitope GP_{33-41}, were obtained from the group of Pedro Romero at CHUV. All animal experiments were performed under the approval from the Veterinary Authority of the Canton of Vaud (Switzerland) according to Swiss Law (protocols VD2502, VD2235.1 ,VD2954 and VD 2992)

Infections

Mice were infected intravenously (i.v.) with 2.0×10^6 PFU of LCMV-Cl13 virus to establish a chronic infection. Virus was obtained from the group of Dietmar Zehn, University of Lausanne. Viral titers in peripheral organs were measure by qPCR as described by Crotty *et al* [73]. For *Listeria monocytogenes expressing OVA (Lm-OVA)* studies, mice vaccinated with NP-SIINFEKL and DC-SIINFEKL were infected at day 90 post immunization with 1×10^5 colony forming units (CFU) intravenously (i.v.). Three days after, the spleen was harvested and homogenized. Various dilutions of the spleen were plated on brain heart infusion (BHI) (Sigma-Aldrich) agar plates and incubated overnight at $37^{\circ}C$. The following day, CFUs were counted and the amounts of *Lm*-OVA were calculated with respect to the relative dilutions.

Peptide activation

GP$_{33-41}$ (KAVYNFATC) and SIINFEKL peptides were purchased from Thermo Scientific with a purity of >95%. Peptides were activated by adding a 2-pyridylthiol group (Sigma-Aldrich) to the cysteine residue [7]. Peptide purity and activation was confirmed by analytical HPLC/MS.

Nanoparticle preparation

All chemical reagents were reagent grade and purchased from Sigma-Aldrich unless otherwise stated. PPS-PEG nanoparticles (NP) were synthesized as detailed previously [9,10], with some modifications to allow for protein loading into the PEG corona. Briefly, OH-PEG (NP-OH, peptide loading) or a mixture of 1:3 COOH-PEG / OH-PEG (for NP-COOH, protein loading) were used to prepared the emulsion polymerization to form NP. NP-OH were immediately purified by dialysis against MQ H$_2$O for 36 h at room temperature, and passed through a filter with a 0.22 ᶙm pore size (Millipore Corporation). For NP-COOH, the remaining thiolates were quenched by the addition of 45 mg of iodoacetamide and stirred for 15 min. To functionalize the COOH groups on the NP surface, sulfo-NHS (Life Technologies), pyridyl disulfide cysteamine (synthesized in house) and 1ethyl-3-(3-dimethylaminopropyl) (EDC) were added to the mixture and let to react for 24 h. Subsequently, NP were purified and filter as detailed above. The concentration of the loaded pyridyl disulfide was determined by measuring the absorbance at 340 nm after adding TCEP (ThermoScientific) to the NP solution.

Peptide conjugation was achieved by mixing NP-OH with activated peptide for 16 h at room temperature. The concentration of loaded peptide was assessed by measuring the absorbance at 340 nm, which represents the release of pyridyl thione from the peptide as it reacts with free thiols on the NP core. For OVA conjugation, functionalized NP were mixed with guanidine hydrochloride (GndHCl) to achieve a final concentration of 6 M of GndHCl. The solution was filtered through a 0.22 ᶙm membrane (Millipore Corporation) and mixed with OVA for 16 h at room temperature. Non-conjugated peptides and protein were purified by size exclusion chromatography through a Sepharose CL-6B column equilibrated in 0.9% saline solution (Braun). The concentration of loaded protein in the fractions obtained after purification was determined by a BCA assay following the manufacturer's instructions (ThermoScientific).

Before and after the coupling, the size of NPs was determined by dynamic light scattering with a Nano Zs Zetasizer (Malvern Instruments). The diameter of NPs varied between 25 nm - 40 nm.

Generation of bone marrow derived DCs (BMDCs)

Bone marrow derived CD11c+ dendritic cells (BMDCs) were generated by adapting the protocol described by Lutz et al [74]. Briefly, BM cells were cultured for 8-9 days in the presence of 20 ng/mL of GM-CSF, changing the medium every 3 days. After this time, CD11c$^+$ cells constitute the 70-85% of the non-adherent population.

Immunizations

All vaccines were administered intradermally (i.d.) into the four limbs. For peptide-loaded NP and free peptide immunization, a total of 2 μg of Ag and 10 μg of the TLR-9 agonist CpG-B (Microsynth) were injected per mouse. All NP and peptide batches were tested for endotoxin levels using a TLR activation assay based on HEK-Blue reporter cell lines (Invivogen) before immunization. For DC immunizations, BMDCs from day 8-9 were activated overnight with 20 ng/mL of LPS. Afterwards, cells were washed with full medium and pulsed with 10 μM of peptide for 1 h at 37°C. To be sure no free peptide remained during the immunization, cells were washed extensively (3x) and finally resuspended in physiological saline solution at the desired concentration. Shortly before the immunization, the cell slurry was mixed with CpG-B. In total, with the exception of the dosing study, each mouse received a total of $2x10^6$ cells, together with 10 μg of CpG-B. The dose of antigen used for BMDC pulsing and BMDC numbers were selected based on the ability to promote a similar expansion of P14 cells in spleen upon a single immunization compared to an immunization with NP-peptide (2 μg) (Fig.S1).

Adoptive transfers and cell sorting

For adoptive transfers of naive antigen specific CD8 T cells, single cell suspensions were prepared from spleens of CD45.1 P14 mice. CD8 T cells were isolated using the EasySep™ Mouse T Cell Isolation Kit (Stemcell Technologies). Immediately after isolation, $5x10^4$ cells were adoptively transferred i.v. into naïve host mice. For viral challenge experiments, CD45.1 P14 CD8 memory T cells were isolated by flow cytometry-assisted cell sorting. $5x10^4$ cells were adoptively transferred into naïve mice.

***In vivo* cytotoxicity assay**

For *in vivo* cytotoxicity studies, CD45.1 P14 cells were adoptively transferred into wild type naïve mice, and one day after mice were immunized with soluble Ag, NP-GP$_{33}$, or DC-GP$_{33}$, as described above. Four days after the immunization, splenocytes from naïve mice (target cells) were divided in two groups: one group was left untreated, while the second group was pulsed with 10 μM of GP$_{33-41}$ for 40 min at 37°C, and then washed two times in PBS to remove any free peptide. Following this step, the half that was left untreated was stained with 0.4 μM of CFSE (low), while the half that was pulsed with peptide was stained with 4 μM of CFSE (high). Cells were mixed at 1:1 ratio, and a total of $2x10^7$ cells were injected i.v. into previously immunized mice. The following day, spleens were harvested and the percentage of in vivo killing was calculated by the following formula: [1 − ([CFSE^{high}/CFSE^{low} for experimental]/[CFSE^{high}/CFSE^{low} for untreated)] × 100.

Antigen persistence studies

Mice were vaccinated with soluble Ag, NP-GP$_{33}$, or DC-GP$_{33}$ as described above. After either 7 or 21 days, $1x10^6$ CD45.1 P14 cells labeled with 2 μM of CFSE were adoptively transferred into immunized mice, and 3 days after, lymph nodes and spleen were harvested for assessing CD8 T cell proliferation.

For the evaluation of antigen persistence in various cell compartments, mice were vaccinated with a peptide labeled with AF-647 either soluble or loaded in nanoparticles. After 7 days, LNs cells were assessed for the presence of AF-647 signal by flow cytometry.

Cell preparation

Lymph nodes were harvested and opened with needles and first digested in DMEM (1.2 mM CaCl$_2$, 2% FBS, Pen/Strep) containing collagenase IV (1 mg/mL) and DNAse I (40 μg/ml) to isolate lymphocytes. A second digestion step with DMEM and collagenase D (1mg/mL) and DNAse I (40 μg/ml) was performed. Splenocytes were smashed through a 70 μm filter, and red blood cells were lysed with ACK buffer. The resulting cells were resuspended in PBS and stained for flow cytometry.

Ex vivo **restimulation**

Up to 3x10^6 cells from tissue isolated lymphocytes were plated in 96-well plates and cultured in 10%FBS -DMEM medium for 2 h at 37°C in the presence 1 μM of GP$_{33-41}$. Following this step, a final concentration of 5 μg/mL of Brefeldin A was added to the culture and left for 3 additional h. For CD107a staining, cells were cultured together with the monoclonal antibody against CD107a and with Monensin at 2 μg/mL for 5 hrs. Finally, cells were washed in PBS prior to staining for flow cytometry.

Flow cytometry.

Isolated lymphocytes were stained with a live/dead fixable dye (Life technologies) to assess cell viability, and stained for surface markers with a cocktail of monoclonal antibodies from Biolegend and eBiosciences. For intracellular staining, cells were fixed and permeabilized with the Foxp3/Transcription Factor Fixation/Permeabilization kit (eBiosciences) according to the manufacturer's instructions. Cells were stained in permeabilization buffer with a cocktail of monoclonal antibodies. After staining, cells were resuspended in staining buffer and samples acquired using a CyAn^{TM} ADP (Beckman Coulter) or LSRII (BD biosciences) flow cytometer

Data analysis

Samples were analyzed using FlowJo (Tree Star) software and GraphPad Prism 5 Software (GraphPad Software Inc.). Statistically significant differences between the experimental groups were determine by a one-way ANOVA followed by Bonferroni *post-hoc* test correction when more than 2 groups were compared, and by a non-parametric Mann-Whitney U test when two groups were compared. Significance was determine for P values <0.05 ($^*P < 0.05$, $^{**}P < 0.01$, $^{***}P < 0.001$ and n.s.= no symbol). All error bars represent the mean ± standard error.

REFERENCES

1. Smith, D. M., Simon, J. K. & Baker, J. R. Applications of nanotechnology for immunology. *Nat. Rev. Immunol.* **13,** 592–605 (2013).
2. Irvine, D. J., Swartz, M. A. & Szeto, G. L. Engineering synthetic vaccines using cues from natural immunity. *Nat. Mater.* **12,** 978–990 (2013).
3. De Temmerman, M. L. *et al.* Particulate vaccines: On the quest for optimal delivery and immune response. *Drug Discov. Today* **16,** 569–582 (2011).
4. Xu, Z. *et al.* Multifunctional nanoparticles co-delivering Trp2 peptide and CpG adjuvant induce potent cytotoxic T-lymphocyte response against melanoma and its lung metastasis. *J. Control. Release* **172,** 259–265 (2013).
5. Hanson, M. C. *et al.* Nanoparticulate STING agonists are potent lymph node – targeted vaccine adjuvants. **125,** 2532–2546 (2015).
6. Takagi, A. *et al.* Highly efficient antiviral CD8+ T-cell induction by peptides coupled to the surfaces of liposomes. *Clin. Vaccine Immunol.* **16,** 1383–1392 (2009).
7. Hirosue, S., Kourtis, I. C., Van der Vlies, A. J., Hubbell, J. A. & Swartz, M. A. Antigen delivery to dendritic cells by poly(propylene sulfide) nanoparticles with disulfide conjugated peptides: Cross-presentation and T cell activation. *Vaccine* **28,** 7897–906 (2010).
8. Jeanbart, L., Ballester, M., Titta, A. De & Swartz, M. A. Enhancing Efficacy of Anticancer Vaccines by Targeted Delivery to Tumor-Draining Lymph Nodes. *Cancer Immunol Res* **6,** 436–447 (2014).
9. Rehor, A., Hubbell, J. A. & Tirelli, N. Oxidation-sensitive polymeric nanoparticles. *Langmuir* **21,** 411–417 (2005).
10. Van Der Vlies, A. J., Oneil, C. P., Hasegawa, U., Hammond, N. & Hubbell, J. A. Synthesis of pyridyl disulfide-functionalized nanoparticles for conjugating thiol-containing small molecules, peptides, and proteins. *Bioconjug. Chem.* **21,** 653–662 (2010).
11. de Titta, A. *et al.* Nanoparticle conjugation of CpG enhances adjuvancy for cellular immunity and memory recall at low dose. *Proc. Natl. Acad. Sci. U. S. A.* **110,** 19902–19907 (2013).
12. Nembrini, C. *et al.* Nanoparticle conjugation of antigen enhances cytotoxic T-cell responses in pulmonary vaccination. *Proc. Natl. Acad. Sci. U. S. A.* **108,** E989–E997 (2011).
13. Rincon-Restrepo, M. *et al.* Vaccine nanocarriers: Coupling intracellular pathways and cellular biodistribution to control CD4 vs CD8 T cell responses. *Biomaterials* **132,** 48–58 (2017).
14. Seder, R. A., Darrah, P. A. & Roederer, M. T-cell quality in memory and protection: implications for vaccine design. *Nat. Rev. Immunol.* **8,** 247–258 (2008).
15. Kaech, S. M., Wherry, E. & Ahmed, R. Effector and memory T-cell differentiation: implications for vaccine development. *Nat. Rev. Immunol.* **2,** 251–262 (2002).
16. Demento, S. L. *et al.* Role of sustained antigen release from nanoparticle vaccines in shaping the T cell memory phenotype. *Biomaterials* **33,** 4957–4964 (2012).
17. Li, A. V. *et al.* Generation of effector memory T cell-based mucosal and systemic immunity with pulmonary nanoparticle vaccination. *Sci. Transl. Med.* **5,** 204ra130 (2013).
18. Reyes-Sandoval, A. *et al.* CD8+ T effector memory cells protect against liver-stage malaria. *J. Immunol.* **187,** 1347–1357 (2011).
19. Olson, J., McDonald-Hyman, C., Jameson, S. & Hamilton, S. Effector-like CD8+ T Cells in the Memory Population Mediate Potent Protective Immunity. *Immunity* **38,** 1250–1260 (2013).
20. Hansen, S. G. *et al.* Effector memory T cell responses are associated with protection of rhesus monkeys from mucosal simian immunodeficiency virus challenge. *Nat. Med.* **15,** 293–299 (2009).
21. Joshi, N. S. *et al.* Inflammation Directs Memory Precursor and Short-Lived Effector CD8+ T Cell Fates via the Graded Expression of T-bet Transcription Factor. *Immunity* **27,** 281–295 (2007).
22. Wherry, E. J. *et al.* Molecular signature of CD8+ T cell exhaustion during chronic viral infection. *Immunity* **27,** 670–684 (2007).
23. Koup, R. a, Graham, B. S. & Douek, D. C. The quest for a T cell-based immune correlate of protection against HIV: a story of trials and errors. *Nat. Rev. Immunol.* **11,** 65–70 (2011).
24. Wherry, E. J. & Kurachi, M. Molecular and cellular insights into T cell exhaustion. *Nat. Rev. Immunol.* **15,** 486–499 (2015).
25. Thimme, R. *et al.* Determinants of viral clearance and persistence during acute hepatitis C virus infection. *J. Exp. Med.* **194,** 1395–1406 (2001).
26. Martin, D. L. & Tarleton, R. L. Antigen-Specific T Cells Maintain an Effector Memory Phenotype during Persistent Trypanosoma cruzi Infection. **174,** 1594–1601 (2016).
27. Knudsen, M. L. *et al.* Kinetic and phenotypic analysis of CD8+ T cell responses after priming with alphavirus replicons and homologous or heterologous booster immunizations. *J. Virol.* **88,** 12438–12451 (2014).

28.   Irvine, D. J., Hanson, M. C., Rakhra, K. & Tokatlian, T. Synthetic Nanoparticles for Vaccines and Immunotherapy. **115,** 11109–11146 (2015).

29.   Reddy, S. T., Swartz, M. A. & Hubbell, J. A. Targeting dendritic cells with biomaterials: developing the next generation of vaccines. *Trends Immunol.* **27,** 573–579 (2006).

30.   Kourtis, I. C. *et al.* Peripherally Administered Nanoparticles Target Monocytic Myeloid Cells, Secondary Lymphoid Organs and Tumors in Mice. *PLoS One* **8,** e61646 (2013).

31.   Zinkernagel, R. M. in *Arenaviruses II: The Molecular Pathogenesis of Arenavirus Infections* (ed. Oldstone, M. B. A.) 1–5 (Springer Berlin Heidelberg, 2002). doi:10.1007/978-3-642-56055-2_1

32.   Oldstone, M. B. A. in *Arenaviruses II: The Molecular Pathogenesis of Arenavirus Infections* (ed. Oldstone, M. B. A.) 83–117 (Springer Berlin Heidelberg, 2002). doi:10.1007/978-3-642-56055-2_6

33.   Overstreet, M. G. *et al.* CpG-enhanced CD8 + T-cell responses to peptide immunization are severely inhibited by B cells. *Eur. J. Immunol.* **40,** 124–133 (2010).

34.   Ballester, M. *et al.* Nanoparticle conjugation and pulmonary delivery enhance the protective efficacy of Ag85B and CpG against tuberculosis. *Vaccine* **29,** 6959–6966 (2011).

35.   Badovinac, V. P., Messingham, K. A. N., Jabbari, A., Haring, J. S. & Harty, J. T. Accelerated CD8+ T-cell memory and prime-boost response after dendritic-cell vaccination. *Nat. Med.* **11,** 748–756 (2005).

36.   Cui, W. *et al.* TLR4 Ligands Lipopolysaccharide and Monophosphoryl Lipid A Differentially Regulate Effector and Memory CD8+ T Cell Differentiation. *J. Immunol.* **192,** 4221–4232 (2014).

37.   Henrickson, S. E. *et al.* Antigen availability determines CD8+ T cell-dendritic cell interaction kinetics and memory fate decisions. *Immunity* **39,** 496–507 (2013).

38.   Chu, H. H. *et al.* Continuous Effector CD8(+) T Cell Production in a Controlled Persistent Infection Is Sustained by a Proliferative Intermediate Population. *Immunity* **45,** 159–171 (2016).

39.   Wherry, E. J., Blattman, J. N., Murali-Krishna, K., van der Most, R. & Ahmed, R. Viral persistence alters CD8 T-cell immunodominance and tissue distribution and results in distinct stages of functional impairment. *J. Virol.* **77,** 4911–4927 (2003).

40.   Kim, T. S., Hufford, M. M., Sun, J., Fu, Y.-X. & Braciale, T. J. Antigen persistence and the control of local T cell memory by migrant respiratory dendritic cells after acute virus infection. *J. Exp. Med.* **207,** 1161–1172 (2010).

41.   Link, A. *et al.* Fibroblastic reticular cells in lymph nodes regulate the homeostasis of naive T cells. *Nat. Immunol.* **8,** 1255–1265 (2007).

42.   Tamburini, B. A., Burchill, M. A. & Kedl, R. M. Antigen capture and archiving by lymphatic endothelial cells following vaccination or viral infection. *Nat. Commun.* **5,** 3989 (2014).

43.   Hirosue, S. *et al.* Steady-State Antigen Scavenging, Cross-Presentation, and CD8+ T Cell Priming: A New Role for Lymphatic Endothelial Cells. *J. Immunol.* **192,** 5002–5011 (2014).

44.   Pham, N.-L. L., Badovinac, V. P. & Harty, J. T. A default pathway of memory CD8 T cell differentiation after dendritic cell immunization is deflected by encounter with inflammatory cytokines during antigen-driven proliferation. *J. Immunol.* **183,** 2337–2348 (2009).

45.   Masopust, D., Ha, S.-J., Vezys, V. & Ahmed, R. Stimulation history dictates memory CD8 T cell phenotype: implications for prime-boost vaccination. *J. Immunol.* **177,** 831–839 (2006).

46.   Nolz, J. C. & Harty, J. T. Protective capacity of memory CD8+ T cells is dictated by antigen exposure history and nature of the infection. *Immunity* **34,** 781–793 (2011).

47.   Bachmann, M. F., Wolint, P., Schwarz, K., Jäger, P. & Oxenius, A. Functional properties and lineage relationship of CD8+ T cell subsets identified by expression of IL-7 receptor alpha and CD62L. *J. Immunol.* **175,** 4686–4696 (2005).

48.   Huster, K. M. *et al.* Selective expression of IL-7 receptor on memory T cells identifies early CD40L-dependent generation of distinct CD8+ memory T cell subsets. **101,** 5610–5615 (2004).

49.   Hikono, H. *et al.* Activation phenotype, rather than central- or effector-memory phenotype, predicts the recall efficacy of memory CD8+ T cells. *J. Exp. Med.* **204,** 1625–1636 (2007).

50.   Jung, Y. W., Rutishauser, R. L., Joshi, N. S., Haberman, A. M. & Kaech, S. M. Differential localization of effector and memory CD8 T cell subsets in lymphoid organs during acute viral infection. *J. Immunol.* **185,** 5315–5325 (2010).

51.   Anderson, K. G. *et al.* Cutting Edge: Intravascular Staining Redefines Lung CD8 T Cell Responses. *J. Immunol.* **189,** 2702–2706 (2012).

52.   Sullivan, B. M. *et al.* Point mutation in the glycoprotein of lymphocytic choriomeningitis virus is necessary for receptor binding, dendritic cell infection, and long-term persistence. *Proc. Natl. Acad. Sci. U. S. A.* **108,** 2969–2974 (2011).

53.   Salvato, M., Borrow, P., Shimomaye, E. & Oldstone, M. B. Molecular basis of viral persistence: a single amino acid change in the glycoprotein of lymphocytic choriomeningitis virus is associated with suppression of the antiviral cytotoxic T-lymphocyte response and establishment of persistence. *J. Virol.* **65,** 1863–1869 (1991).

54.   Bergthaler, A. *et al*. Impaired antibody response causes persistence of prototypic T cell-contained virus. *PLoS Biol*. **7,** e1000080 (2009).

55.   Sevilla, N. *et al*. Immunosuppression and resultant viral persistence by specific viral targeting of dendritic cells. *J. Exp. Med*. **192,** 1249–1260 (2000).

56.   Kaech, S. M. & Ahmed, R. Memory CD8+ T cell differentiation: initial antigen encounter triggers a developmental program in naïve cells. *Nat. Immunol*. **2,** 415–422 (2001).

57.   Henrickson, S. E. *et al*. T cell sensing of antigen dose governs interactive behavior with dendritic cells and sets a threshold for T cell activation. *Nat. Immunol*. **9,** 282–291 (2008).

58.   Blair, D. A. *et al*. Duration of Antigen Availability Influences the Expansion and Memory Differentiation of T Cells. **187,** 2310–2321 (2017).

59.   Burchill, M. A. *et al*. T cell vaccinology : Exploring the known unknowns. *Vaccine* **31,** 297–305 (2013).

60.   Cui, W., Joshi, N. S., Jiang, A. & Kaech, S. M. Effects of Signal 3 during CD8 T cell priming: Bystander production of IL-12 enhances effector T cell expansion but promotes terminal differentiation. *Vaccine* **27,** 2177–2187 (2009).

61.   Intlekofer, A. M. *et al*. Requirement for T-bet in the aberrant differentiation of unhelped memory CD8+ T cells. *J. Exp. Med*. **204,** 2015–2021 (2007).

62.   Shedlock, D. J. & Shen, H. Requirement for CD4 T Cell Help in Generating Functional CD8 T Cell Memory. *Science* **300,** 337–339 (2003).

63.   Laidlaw, B. J., Craft, J. E. & Kaech, S. M. The multifaceted role of CD4+ T cells in CD8+ T cell memory. *Nat. Publ. Gr*. **16,** 102–111 (2016).

64.   Kim, J. *et al*. Memory programming in CD8+ T-cell differentiation is intrinsic and is not determined by CD4 help. *Nat. Commun*. **6,** 1–17 (2015).

65.   Barber, D. L. *et al*. Restoring function in exhausted CD8 T cells during chronic viral infection. *Nature* **439,** 682–687 (2006).

66.   Moskophidis, D., Lechner, F., Pircher, H. & Zinkernagel, R. M. Virus persistence in acutely infected immunocompetent mice by exhaustion of antiviral cytotoxic effector T cells. *Nature* **362,** 758–761 (1993).

67.   Matloubian, M., Concepcion, R. J. & Ahmed, R. CD4+ T cells are required to sustain CD8+ cytotoxic T-cell responses during chronic viral infection. *Microbiology* **68,** 8056–8063 (1994).

68.   Henson, S. M. & Akbar, A. N. KLRG1-more than a marker for T cell senescence. *Age* **31,** 285–291 (2009).

69.   Cush, S. S. & Flaño, E. KLRG1+NKG2A+ CD8 T cells mediate protection and participate in memory responses during γ-herpesvirus infection. *J. Immunol*. **186,** 4051–4058 (2011).

70.   Edwards, L. E., Haluszczak, C. & Kedl, R. M. Phenotype and function of protective, CD4-independent CD8 T cell memory. *Immunol. Res*. **55,** 135–145 (2013).

71.   Charlton, J. J. *et al*. Programmed death-1 shapes memory phenotype CD8 T cell subsets in a cell-intrinsic manner. *J. Immunol*. **190,** 6104–6114 (2013).

72.   Hokey, D. a *et al*. Activation drives PD-1 expression during vaccine-specific proliferation and following lentiviral infection in macaques. *Eur. J. Immunol*. **38,** 1435–1445 (2008).

73.   Mccausland, M. M. & Crotty, S. Quantitative PCR (QPCR) technique for detecting lymphocytic choriomeningitis virus (LCMV) in vivo. *J. Virol. methods* **147,** 167–176 (2008).

74.   Lutz, M. B. *et al*. An advanced culture method for generating large quantities of h

Different roles of Axl in cell entry of Lassa virus

Chiara Fedeli[1a], Giulia Torriani[1a], Clara Galan-Navarro[1, 2], Marie-Laurence Moraz[1], Hector Moreno[1], Gisa Gerold[3], and Stefan Kunz[1*]

[1] Institute of Microbiology, Lausanne University Hospital, Lausanne, Switzerland

[2] Laboratory of Lymphatic and Cancer Bioengineering, Institute of Bioengineering, École Polytechnique Féderale de Lausanne (EPFL) 1015 Lausanne, Switzerland

[3] TWINCORE -Center for Experimental and Clinical Infection Research, Institute for Experimental Virology, Hannover, Germany

[a] Contributed equally

* Corresponding author.

Mailing address: Institute of Microbiology, Lausanne University Hospital, Lausanne CH-1011, Switzerland. Phone: +41-21 314 7743, Fax: +41-21 314 4060, E-mail: Stefan.Kunz@chuv.ch.

Abstract: 250 words

Running title: Axl in Lassa virus entry

ABSTRACT

Fatal infection with the highly pathogenic Lassa virus (LASV) is characterized by extensive viral dissemination, indicating broad tissue tropism. Although the principal LASV receptor dystroglycan (DG) is ubiquitously expressed, virus binding critically depends on DG's post-translational modification with the unusual O-linked sugar polymer matriglycan. This functional glycosylation of DG is under tight tissue-specific control *in vivo* and does not always correlate with susceptibility. The broadly expressed phosphatidylserine (PS) receptors Axl and Tyro3 were recently identified as alternative LASV receptor candidates. However, their role in LASV entry is not entirely understood and published data seem conflicting. Here we examined LASV receptor candidates in primary human cells and found co-expression of Axl with differentially glycosylated DG. To study LASV entry in the context of productive arenavirus infection, we used recombinant lymphocytic choriomeningitis virus expressing LASV glycoprotein (rLCMV-LASVGP) as a validated BSL2 model. First, we confirm and extend previous work, showing that Axl can serve as an authentic LASV entry receptor in absence of functional DG using "apoptotic mimicry", similar to other enveloped virus. We show that Axl-dependent LASV entry requires receptor activation and involves a pathway resembling macropinocytosis. Axl-mediated LASV entry is facilitated by heparan sulfate and critically depends on the late endosomal protein LAMP-1 as intracellular entry factor. In endothelial cells expressing low levels of functional DG, both receptors are engaged by the virus and can contribute to productive entry. In sum, we characterize the role of Axl in LASV entry and provides a rationale to target Axl in anti-viral therapy.

IMPORTANCE

The highly pathogenic arenavirus Lassa (LASV) represents a serious public health problem in Africa. Although the principal LASV receptor dystroglycan (DG) is ubiquitously expressed, virus binding critically depends on DG's post-translational modification, which does not always correlate with tissue tropism. The broadly expressed phosphatidylserine receptor Axl was recently identified as alternative LASV receptor candidate, but its role in LASV entry is unclear. Here we investigated the exact role of Axl in LASV entry as a function of DG's post-translational modification. We found that in absence of functional DG, Axl can mediate LASV entry via "apoptotic mimicry". Productive entry requires virus-induced receptor activation, involves macropinocytosis, and critically depends on LAMP-1. In endothelial cells that express low levels of glycosylated DG, both receptors can promote LASV entry. In sum, our study defines the roles of Axl in LASV entry and provides a rationale to target Axl in anti-viral therapy.

INTRODUCTION

The Old World arenavirus Lassa (LASV) is the causative agent of a severe viral hemorrhagic fever with high mortality in humans **[1, 8]** and is currently considered as one of the most important emerging pathogens by WHO **[76]**. Carried in nature by persistent infection of reservoir rodent host of *Mastomys* species, LASV is endemic in large areas of Western Africa where it causes several hundred thousand infections per year with thousands of deaths. Transmission of LASV from rodents to humans occurs mainly via contaminated aerosolized rodent excreta and ingestion of contaminated food **[1]**. Human-to-human transmission has been reported in nosocomial settings **[77]**. Due to its transmissibility via aerosol **[10]** and high lethality, LASV is considered a Category A agent by the Centers of Disease Control **[11]**.

Following productive infection at the sites of entry, the virus enters the bloodstream and disseminates to lymph nodes, spleen, and liver. Severe LASV infection is characterized by extensive viral replication in many tissues, resulting in high viremia and progressive signs and symptoms of shock. Early targets of LASV during systemic dissemination are dendritic cells and macrophages, followed by infection of hepatocytes, endothelial cells, and epithelial cells of lung and kidney in severe disease **[71]**. A highly predictive factor for disease outcome is the viral load, indicating a close competition between viral spread and replication and the patient's immune system **[7]**. There is no licensed vaccine and treatment is limited to supportive care and ribavirin, which reduces mortality when delivered early in infection **[9]**. Drugs targeting early steps of the viral life cycle may delay viral spread providing the immune system a window of opportunity to develop an anti-viral immune response. An in-depth understanding of the molecular mechanisms underlying LASV cell entry into relevant target cells is therefore of great importance to develop novel and efficacious anti-viral strategies.

Arenaviruses are enveloped negative-strand RNA viruses, whose non-lytic life cycle is confined to the cytoplasm [2]. The arenavirus genome is comprised of two RNA segments that code for two proteins each, using an ambisense coding strategy. The small (S) RNA segment encodes the envelope glycoprotein precursor (GPC) and the nucleoprotein (NP), while the L segment encodes the matrix protein (Z) as well as the viral polymerase (L). GPC is synthesized as a single polypeptide and undergoes processing by signal peptidases and protease SKI-1/S1P yielding an unusually stable signal peptide (SSP), the N-terminal GP1, and the transmembrane GP2. The GP1 binds to cellular receptors, whereas GP2 mediates viral fusion and structurally resembles class I viral fusion proteins.

Expression of cellular receptors is a key determinant for transmission, tissue tropism, and disease potential of a virus. The first cellular receptor for LASV and other Old World arenaviruses was identified as dystroglycan (DG), a ubiquitously expressed and highly conserved receptor for extracellular matrix (ECM) proteins **[12]**. Dystroglycan is expressed in most developing and adult

tissues and provides a molecular link between the ECM and the actin-based cytoskeleton. Initially encoded as a single polypeptide, DG is cleaved into the extracellular α-DG and membrane anchored β-DG [14]. In mammals, α-DG is subject to complex post-translational modifications that are essential for its function as a receptor for ECM proteins and arenaviruses [15, 21, 22]. The unusual O-linked trisaccharide [O-Man-β1-4-GlcNAc-β1-3GalNAc] on α-DG undergoes phosphorylation at the O-mannosyl residue, followed by synthesis of [Xyl-α1-GlcA-3-β1-3] co-polymers by the dual-specific glycosyltransferase like-acetylglucosaminyltransferase (LARGE) [17, 18]. The LARGE-derived [Xyl-α1-GlcA-3-β1-3] polysaccharide, known as "matriglycan", is recognized by ECM proteins and arenavirus GP1 via a lectin-type binding [15, 19, 20]. A genetic screen revealed that LASV strikingly mimics the molecular mechanisms of receptor recognition of host-derived ECM proteins [23]. The recently solved high-resolution X-ray structure of the pre-fusion conformation of LASV GP indicates that multiple residues located at the trimeric interface engage the DG-derived matriglycan polymers with high avidity [78].

While the DG core protein is ubiquitously expressed in most mammalian cells, functional glycosylation by LARGE is under tight tissue-specific control [19], making DG a "tunable" receptor [19], whose virus-binding affinity greatly varies between tissues. Notably, the observed functional glycosylation of DG in human and animal tissues does not always correlate with susceptibility to LASV *in vivo* [70, 71, 79], suggesting the existence of alternative receptors. Using an expression cloning approach, the Tyro3/Axl/Mer (TAM) receptor tyrosine kinases Axl and Tyro3, as well as the C-type lectins DC-specific ICAM-3-grabbing nonintegrin (DC-SIGN) and LSECtin have been identified as candidate LASV receptors [34]. Based on their restricted expression patterns, DC-SIGN and LSECtin may contribute to LASV entry into specific cell types, such as particular dendritic cells, but their exact role is currently unclear [46]. The TAM kinases Axl and Tyro3 are conserved receptors for the phoshatidylserine (PS)-binding serum proteins Gas6 and protein S that are involved in removal of apoptotic cells [35, 36]. Over the past years, TAM kinases and other cellular PS receptors have been implicated in viral entry via "apoptotic mimicry", a mechanism initially described by Mercer and Helenius for poxviruses [42] that is characterized by recognition of PS displayed on the viral lipid envelope [37, 80]. Viral apoptotic mimicry is increasingly recognized as an entry strategy for a broad spectrum of enveloped viruses and some non-enveloped viruses, including important emerging pathogens such as Ebola virus, Dengue, West Nile, and Zika virus [37, 80]. Currently, the exact role of TAM receptors in LASV entry is not entirely clear and published data appear conflicting [34, 37, 43]. The initial report identifying TAM kinases as a candidate LASV receptors provided evidence for a role of Axl and Tyro3 in DG-independent entry of lentiviral LASV pseudotypes [34]. However, a subsequent systematic study covering a large panel of emerging viruses, using different pseudotype platforms, concluded that the PS receptors Axl and T cell immunoglobulin and mucin

(TIM)-1 were unable to mediate productive LASV entry **[43]**. Here we sought to resolve these apparent contradictions and investigated the exact role of Axl in LASV entry in the context of productive arenavirus infection using a validated BSL2 surrogate model. We further investigate the mechanism underlying Axl-mediated LASV entry and provide a rationale for targeting Axl in anti-viral therapy.

MATERIALS AND METHODS

Antibodies and reagents

Monoclonal antibody (mAb) IIH6 anti-✔-DG (mouse IgM) has been provided by Dr. Kevin Campbell (Howard Hughes Medical Institute, University of Iowa). Mouse mAb 8D5 anti-β-DG was purchased from Novocastra. Purified polyclonal goat IgG anti-human Axl, mAb 96201 anti-Dtk/Tyro3, and mAb 120507 anti-DC-SIGN were from R&D Systems and mouse mAb ab54803 anti-Axl from Abcam. Mouse mAb sc-20011 anti-LAMP1 was from Santa Cruz Biotechnology. MAb 83.6 to LASV GP2 has been described [81] as has been mAb113 anti-LCMV NP [82]. MAb cl14a to phospho-β-DG PY982 was from BD Bioscience and mAb 4G10 to phospho-tyrosine from St. Cruz Biotechnology. Antibody to clathrin heavy chain was purchased from BD Biosciences. Other mAbs included mouse mAb B-5-1-2 anti-α-tubulin and goat polyclonal antibody to human IgG Fc (Sigma Aldrich). Horseradish peroxidase (HRP) conjugated polyclonal goat anti-mouse IgG, goat anti-mouse IgM, and rabbit anti-goat IgG weres from Dako. FITC-conjugated goat anti-mouse IgG was from Jackson Immuno Research. The nuclear dye 4',6-diamidino-2-phenylindole (DAPI) and phalloidin-FITC was purchased from Molecular Probes (Eugene, OR). The full-length GPC of Tacaribe virus (TCRV) was kindly provided by Juan-Carlos de la Torre (Scripps Research Institute, La Jolla, CA). The Cell Titer Glo® assay system was obtained from Promega (Madison WI). Annexin-V from human placenta conjugated to biotin, heparin, and streptavidine-HRP were from Sigma. The DG fragment DGEKFc4 is comprised of amino acids 1 –485 of α-DG, followed by an enterokinase (EK) cleavage site and the Fc portion (hinge, CH2, and CH3) of human IgG1 and was produced and purified as described [83]. For optimal sensitivity of our assay, DGEKFc4 was produced in cells over-expressing LARGE, resulting efficient matriglycan modification, as described [21]. Inhibitors used in this study included R428 to Axl tyrosine kinase (Sellekchem), dynasore, dyngo-4a, pitstop-2 (Ascent Scientific), pirl1 (Chembridge), CT04, blebbistatin, cytochalasin D, 5-(N-ethyl-N-isopropyl)amiloride (EIPA), IPA-3, jasplakinolide, latrunculin A, ML7, ribavirin, and ammonium chloride (NH_4Cl) (Sigma).

Cell culture

Human lung carcinoma alveolar epithelial cells *A549, the* human fibrosarcoma cell line HT-1080, HeLa cells, and human embryonic kidney (HEK)-293H cells, were cultured in DMEM, 10 %

(vol/vol) FBS, supplemented with glutamine and penicillin/streptomycin. Primary human hepatocytes were isolated from liver specimens obtained after partial hepatectomy at Hannover Medical School and plated at a density of 1.3×10^6 cells on collagen-coated P6 dishes as described [84]. Cells were kept in hepatocyte culture medium (Lonza) for 1-3 days before cell lysis. Cultures were 90% confluent and cells showed typical hepatocyte morphology with multiple nuclei. Human umbilical vein endothelial cells (HUVEC) (CC-2517), primary human lung microvascular endothelial cells (HMVEC-L) (CC-2527), and primary human small airway epithelial cells (SAEC) (CC-2547) were purchased from Clonetics®/Lonza as cryopreserved specimens and cultured following the manufacturers protocol using endothelial cell growth medium EGM^{TM} BulletKit^{TM}, EGM^{TM} 2MV BulletKit^{TM}, and small airway epithelial cell growth medium (CC-3118), respectively. HMVEC-L are isolated from small vessels within normal lung tissue cultured to ≥90% purity and represent a mixed population of both blood and lymphatic endothelial cells. HUVEC and HMVEC-L were passed 5 times, corresponding to < 15 population doublings to assure preservation of the differentiated phenotype. Expression of the differentiation marker CD31/105 was verified by immunofluorescence staining using mAb 28364 to CD31 (Abcam). SAEC are isolated from normal human lung tissue the distal portion of the lung in the 1 mm bronchiole area. Cells were passed 5 times and differentiation verified by staining for cytokeratin 19 using mAb ab52625 (Abcam), as recommended by the manufacturer. For infection studies, cells were seeded in collagen- or poly-L-lysine-coated M96 tissue culture plates at 20'000 cells/cm^2 and experiments performed at a confluency of >90% after 2-3 days.

Viruses and virus purification

The generation, growth, and titration of recombinant LCMV expressing the envelope GP of LASV strain Josiah (rLCMV-LASVGP) and the G protein of vesicular stomatitis virus (rLCMV-VSVG) have been described elsewhere [48, 85]. According to the institutional biosafety guidelines of the Lausanne University Hospital, the chimera rLCMV-LASVGP has been classified as a BSL2 pathogen for use in cell culture. Inactivated LASV strain Josiah was provided by Dr. Christina Spiropoulou, Special Pathogens Branch of the Centers for Disease Control and Prevention (CDC, Atlanta, GA). Recombinant human adenovirus (AdV)-5 expressing GFP has been described [86] as has recombinant vesicular stomatitis virus (VSV) expressing GFP [87]. Recombinant VSV pseudotypes bearing the envelope GP of Tacaribe virus (TCRV) were generated as reported earlier [87]. To obtain serum-free rLCMV-LASVGP, virus was purified following a modified protocol from Dutko et al. [88]. Briefly, rLCMV-LASVGP was grown in BHK21 cells as described [48]. Conditioned cell culture supernatants were harvested after 72 h and virus precipitated from cleared supernatants by addition of 6.5 g per 100 ml polyethylene glycol (PEG)-8000 and stirring over night at 6 °C. After centrifugation at 8,000 rpm for 30 min at 4°C, the PEG pellet was dissolved in TNE/EGTA (10 mM Tris/HCl pH 7.5, 100 mM NaCl, 1

mM EDTA, 5 mM EGTA) using 1 ml of TNE/EGTA for 50 ml of original supernatant. After incubation for 2 h at 4 °C, virus was layered on a discontinuous renografin gradient and purified by ultracentrifugation as described [88]. After dialysis against PBS, infectious virus titers were determined by immunofocus assay on VeroE6 cells in complete medium containing 10% (wt/vol) FBS. Concentrated virus titers were 10^8 -10^9 PFU/ml. Inactivated LASV obtained as PEG precipitate from CDC was treated with TNE/EGTA for 2 h at 4 °C, followed by purification over a renografin gradient. A "mock-preparation" was prepared from conditioned supernatant of uninfected BHK21 cells subjected to PEG precipitation and purification over a renografin gradient analogous to the virus preparation.

Capture ELISA for rLCMV-LASVGP and inactivated authentic LASV

MAb 83.6 to LASV GP2 (10 μg/ml, 50 μl/well) was added to a 96-well microtiter plate (EIA/RIA) high-bond plates (Corning) and immobilization carried out at RT for 4 h. Wells were washed 3 times with PBS and non-specific binding blocked by adding 200 μl/well 1% (wt/vol) BSA/PBS for 1 h at RT. For capture of virus, serum-free preparations of rLCMV-LASVGP and inactivated authentic LASV were diluted to 10^7 PFU/ml and added (50 μl/well) in triplicates to immobilized mAb 86.3 for 16 h at 6°C. As a negative control, AdV5-GFP was included. Wells were washed 3 times with PBS. For detection of phosphatidylserine (PS) on bound virus, annexin-V (ANX-V) biotin conjugate from human placenta (1: 50 in 1% (wt/vol) BSA/PBS) was added overnight at 6 °C in presence and absence of 5 mM EGTA. LASV GP1 was probed with DGEKFc4 (10 µg/ml in 1% (wt/vol) BSA/PBS) overnight at 6 °C. Wells were washed 3 times with PBS. Bound ANX-V was detected with streptavidine HRP), 1:1000 in 1% (wt/vol) BSA/PBS for 2 h at 6 °C and DGEKFc4 with anti-human IgG Fc antibody conjugated to HRP, 1:1000 in 1% (wt/vol) BSA/PBS for 2 h in the cold. After incubation, plates were washed four times and developed using 50 μl of 3,3,5,5'-tetramethylbenzidine (eBiosciences, MA). The color reaction was stopped by adding 20 μl of 2 M H_2SO_4. Plates were analyzed using a plate reader spectrophotometer (Tecan, Mannedorf, Switzerland) by measuring the absorbance at 450 nm with correction at 570 nm. Background binding to wells without immobilized antibody was subtracted and the ratios of GP1/PS binding calculated.

Micro-scale isolation of DG using wheat germ agglutinin

Enrichment of DG by wheat germ agglutinin (WGA) affinity purification was carried out following a modified protocol reported earlier [89]. Briefly, two T150 flasks of A549, HT-1080 cells and HUVEC (>90% confluency) were washed twice with 20 mM Hepes, pH 7.5, 150 mM NaCl. Cells were solubilized in 2 ml of cold solubilization buffer per flask: 50 mM Hepes pH 7.5, 200 mM NaCl/ 1% (wt/vol) NP-40, 1.2 mM EDTA, protease

inhibitor cocktail complete (Roche), 1 mM PMSF for 45 min. in cold-room. Lysates were cleared by centrifugation for 10 min at 14, 000 krpm in a microfuge and 5 mM $MgCl_2$ and 10 mM sodium pyrophosphate (final concentration) added. The WGA matrix (20 μl/ml) was added and incubated on a head-over shaker over night at 6 °C. The WGA matrix was washed 4 times with 10 volumes of 50 mM Hepes pH 7.5, 200 mM NaCl/ 0.05% (wt/vol) NP-40, 1.2 mM EDTA, protease inhibitor cocktail, 1 mM PMSF, 5 mM $CaCl_2$, 5 mM $MgCl_2$. Elution of WGA-bound proteins was achieved by incubation of matrix with 5 x 5 volumes elution buffer: 10mM Tris (pH 8.0), 0.15 M NaCl, 0.2 M N-acetyl glucosamine for 15 min at RT. Individual fractions were probed for the presence of DG in Western blot using mAb 8D5 to β-DG and the most concentrated factions pooled, followed by dialysis against PBS.

Solid-phase virus binding assay

The WGA-purified DG fractions derived from A549, HT-1080 cells and HUVEC (above) were analyzed by Western blot and signals for β-DG quantified by densitometry to allow immobilization of normalized amounts of DG protein using the dilutions HT-1080 (1:1), HUVEC (1:1.32) and A459 (1:2.02) carried out overnight at 6°C. Wells are washed 3 times with PBS. Non-specific binding was blocked by adding 200 μl/well of 1% (wt/vol) BSA/PBS and incubation for 1 h at RT. Dilutions of rLCMV-LASVGP were prepared in 1% (wt/vol) BSA in PBS and virus (50 μl/well) added in triplicates for 16 h at 6 °C. Wells are washed 3 times with PBS and bound virus was detected with mAb 83.6 to LASV GP2 (20 μg/ml) in 1% (wt/vol) BSA in PBS for 6 h at 6 °C. After three washes, bound primary antibody was detected using biotinylated goat anti-mouse IgG combined with streptavidine as described [21]. Plates were developed as described in section "capture ELISA". Background binding to wells without immobilized DG was subtracted and binding curves plotted.

Virus infections

Cells were seeded in 96-well plates at 2 x 10^4 cells per well and grown into confluent monolayers for 16-20 h, unless stated otherwise. Cells were treated with drugs as detailed in the specific experiments, followed by infection with the indicated viruses at the defined multiplicity of infection (MOI) for 1 hour at 37 °C. Unbound virus was removed, cells washed twice with DMEM, and fresh medium added. Infection of rLCMV-LASVGP and rLCMV-VSVG were quantified by detection of LCMV NP in immunofluorescence assay (IFA) with mAb 113 as described [90]. VSV pseudotypes, AdV5-GFP, and rVSV-GFP were detected via the GFP reporter using direct fluorescence.

For the determination of serum-dependence of rLCMV-LASVGP infection in HT-1080 cells, serum-free virus was pre-treated with complete medium containing increasing

concentrations of FBS for 2 h at 4 °C. Virus was added to cells for another 2 h at 4 °C, followed by washing to remove unbound virus. Cells were shifted to 37 °C by adding 200 μl per well of warm complete medium containing 10% (vol/vol) FBS. After 1 h, 20 mM ammonium chloride was added and infection detected after 16 h as described above.

Blocking with ANX-V was achieved by pre-treating virus with the indicated concentrations of ANX-V in DMEM, 20 mM Hepes for 2 h at 4°C as described [39]. Kinetics of virus-cell attachment and endosomal escape were determined as described [55].

For perturbation with antibodies to Axl and DG, M96 plates were chilled on ice, medium removed, and cells washed three times with cold serum-free medium containing 2% (wt/vol) BSA, supplemented with 20 mM Hepes to remove serum proteins. Polyclonal Ab to Axl, mAb IIH6 to DG, and control Ab were diluted as indicated in serum-free medium containing 2% (wt/vol) BSA, supplemented with 20 mM Hepes and incubated with cells for 2 h at 4°C (50 μl/well). Viruses were prepared at 10-fold final concentration in serum-free medium containing 2% (wt/vol) BSA, supplemented with 20 mM Hepes. Five microlitees of virus inoculums were added to the Ab mixtures on cells, mixed carefully and incubated for another 2 h at 4°C. Inoculums were removed, cells washed three times with serum-free medium containing 2% (wt/vol) BSA, supplemented with 20 mM Hepes, and 200 μl/well complete medium added. Cells were cultured at 37°C, 5% CO_2 for the indicated time periods, fixed, and infection assessed as described above.

Immunoblotting

For immunoblotting, proteins were separated by SDS-PAGE and transferred to nitrocellulose. After blocking in 3% (wt/vol) skim milk in PBS, membranes were incubated with 1-10 μg/ml primary antibody in 3% (wt/vol) skim milk, PBS overnight at 4 ºC. After several washes in PBS, 0.1 % (wt/vol) Tween-20 (PBST), secondary antibodies coupled to HRP were applied 1: 5,000 in PBST for 1 h at room temperature. In Western blots detection tyrosine phosphorylated Axl and β-DG, membranes were rinsed three times in PBST containing 250 mM NaCl. Membranes were developed by chemiluminescence using LiteABlot kit (EuroClone). Signals were acquired by ImageQuant LAS 4000Mini (GE Healthcare Lifesciences) or by exposure to X-ray films. Quantification of Western Blots was performed with ImageQuant TL (GE Healthcare Lifesciences).

Generation of DG-deficient HT-1080 cells using lentivirus-delivered small hairpin (sh)RNA

To deplete DG core protein in HT-1080 cells, lentiviral vector expressing validated shRNA targeting human DG (sh-DG) (ID clone: TRCN0000056191, Thermo Scientific RHS3979-9623375) or a scrambled control shRNA (sh-sc) were generated as described by the ViraPower™ Lentiviral Expression System protocol from Invitrogen (UK). Briefly, a puromycin kill curve

determination was performed in HT-1080 cells where 2 μg/ml was the minimum puromycin concentration required to kill untransduced cells. For the production of lentiviruses, 3 x 10^6 HEK293T cells were cultured in 10 cm tissue culture dishes in serum-free 293 SFM II medium (Gibco™ , Cat. No. 11686-029). At 24 h post-seeding, fresh medium was added to cells 4 h before the transfection. $CaCl_2$ (250 mM $CaCl_2$, ultrapure H_2O) and HBS (50 mM Hepes, 1.5 mM Na_2HPO_4, 140 mM NaCl, ultrapure H_2O) solutions were used to co-transfect the four required DNA plasmids: pLP1 helper (gag/ pol), pLP2 helper (rev), pCAGGS/ VSVGP, with sh-DG 56191 (human pLKO.1) or with sh-sc (human pLKO.1) shRNA control. The transfected cells were incubated for16 h at 37°C. After 16 h, the transfection medium was replaced by fresh serum-free 293 SFM II medium and cells incubated for 24 h at 37°C, 5% CO_2. At 40 h post-transfection, cell supernatants were collected and centrifuged for 5 min at 500 x g to remove cellular debris. Each lentivirus was concentrated using the Amicon® Ultra-15 Centrifugal Filter Devices by ultra-centrifugation according to the manufacturer's instructions (Millipore, Ultracel® 100KREF. UFC910024). For infection, 5 x 10^5 HT-1080 cells/well were seeded in 6-well plates and cultured for 24 h at 37°C. The day after, cell medium was replaced by complete medium supplemented with 6 μg/ml polybrene® and 100 μl of each crude lentivirus stock. The cells were spinoculated at 2,600 rpm for 3 h at 23°C. Cells were then washed twice with medium. Transduced cells were incubated for 72 h at 37°C. After 72 h, cells were washed once with 1 x PBS and complete medium supplemented with 2 μg/ml puromycin added. After 48 h, cell death was checked and the selective medium replaced every two days during 2 weeks. Depletion of DG core protein from HT-1080 cells was verified by Western blot using mAb 8D5 as described above. DG-deficient cells were passed for a maximum of 10 times and the DG null phenotype verified for cells used for our experiments.

RNA interference

RNA interference (RNAi) was performed using validated small interfering RNAs (siRNAs) ONTARGETplus SMARTpool for Axl (L-003104-00-0005) and scrambled siRNA (D-001820-10-05) as control from Thermo Scientific Dharmacon (Lafayette, CO). For the depletion of clathrin heavy chain, siGENOME ON-TARGETplus SMARTpool duplex (J-004001-09) to human clathrin heavy chain and a control siRNA pool was obtained from Dharmacon Research (Lafayette, CO). A pool of the following siRNAs was used: siRNA #1: 5'-GAG AAU GGC UGU ACG UAA U-3', #2: 5'-UGA GAA AUG UAA UGC GAA U-3', #3: GCA GAA GAA UCA ACG UUA U-3', #4: 5'-CGU AAG AAG GCU CGA GAG U-3'. Briefly, 3 x 10^6 HT-1080 cells were reverse transfected with 0.72 μM siRNA using a10-cm-diameter dish and Lipofectamine RNAiMAX (Invitrogen, Paisley, United Kingdom) according to the manufacturer's recommendation. For LAMP-1 knock down, 3 x 10^5 cells were seeded over night and transfected using the Lipofectamine RNAiMAX Reagent (Invitrogen) with All Star scramble RNA or

LAMP-1 specific siRNA (Qiagen) at a final concentration of 50 nM   (siRNA 5'
CACGTAATGCATTGCCTGTAA 3') for 48 h.

Twenty-four hours after transfection, cells were replated in 96-well plate format, and 48 h post-transfection, cells were infected with rLCMV-LASVGP (MOI = 0.1) and rLCMV-VSVG (MOI = 0.02) or mock infected. Parallel specimens were lysed to confirm Axl knock-down by Western-blotting using goat pAb at Axl. To prevent secondary infection, 20 mM ammonium chloride was added to the cells 4 hours postinfection. Cells were fixed 16 hours post-infection and infected cells quantified by immunofluorescence assay (IFA) detection of LCMV NP using mAb 113 (anti- LCMVNP) and combined with fluorescence-labeled secondary antibody as described [91].

Virus-induced receptor signaling

Purified rLCMV-LASVGP (8.4×10^8 PFU/ml) and equivalent volumes of mock preparation were incubated in 10 ml HBSS with 10% (vol/vol) FBS for 2 h at 4°C, followed by layering a cushion of 20% (wt/vol) sucrose in PBS containing 1 mM $MgCl_2$ and 0.1 mM $CaCl_2$. After spinning at 35,000 rpm for 90 min in a SW41 swing-out rotor, supernatant was decanted completely. Pellets were resuspended in 250 μl of HBSS for 16 h at 4°C in a closed vial on a shaker. Concentrated virus was titrated by IFA on VeroE6 cells. HT-1080 cells, HMVEC-L, and SAEC were seeded at 4×10^5 cells per well in complete medium and cultured to obtain closed monolayers of >90% confluency. Cells were serum-starved for 16 h replacing FBS by 0.2% (vol/vol) horse serum. Cells were chilled on ice for 5 minutes. Medium was removed and 4×10^7 PFU virus was diluted in 1 ml of serum-free medium added, corresponding to an MOI of circa 50. Virus was added to the cells in the cold and incubated for 2 h on ice. To control wells, mock-prep was added. Cells were washed twice in cold serum-free DMEM, followed by addition of pre-warmed serum DMEM (4 ml/well). Cells are shifted to 37°C. At the indicated time points, medium was removed and cells lyzed in cold lysis buffer: 1% (wt/vol) NP-40, 50 mM Tris, pH 7.5, 150 mM NaCl, 2 mM EGTA, 0.2 mM EDTA, 50 mM NaF, protease inhibitor cocktail "Complete®" from Roche, and 1 mM PMSF. Cells were scraped off with a plastic cell scraper and passed 5 times through a blue tip, transferred to microtube and incubated on a head-over shaker in the cold-room for 30 minutes. Lysates were cleared by centrifugation at 14,000 rpm in a microcentrifuge for 10 minutes in the cold. For the detection of tyrosine phosphorylated β-DG PY982 and β-DG protein with mAbs cl14a and 8D5, respectively, total protein was extracted [92], separated by SDS-PAGE and Western blot performed as described above. For the detection of tyrosine phosphorylation of Axl, total Axl was isolated by immunoprecipation using a modified protocol reported by Meertens et al. [93]. For this purpose, purified polyclonal goat anti-IgG was immobilized on cyanogens bromide activated Sepharose 4B (Sigma) following the manufacturers recommendations. Anti-Axl matrix was mixed with cleared lysate (10 μl of matrix per ml of lysate), and incubated on a head-over shaker for 4 h or overnight in the cold room. After antibody binding over night, matrix

was washed four times with lysis buffer and once with lysis buffer without detergent. Immunocomplexes were eluted by boiling in non-reducing SDS-PAGE sample buffer for 5 minutes, followed by separation by SDS-PAGE using Tris/glycine running gels with 5.5% (wt/vol) polyacrylamide to achieve optimal separation of Axl from the IgG heavy chain. Axl protein was revealed in Western blot using a mouse mAb anti-Axl and tyrosine phosphorylation detected in anti-Axl IP using a mAb to tyrosine phosphate.

RESULTS

Human cells targeted by LASV co-express Axl and differentially glycosylated DG

Histological examination of mammalian tissues revealed that DG's functional glycosylation by LARGE is under tight tissue-specific control, resulting in considerable variation in the length of DG-associated matriglycan chains [94], affecting DG's function as LASV receptor. LARGE was originally discovered as a tumor-suppressor gene [95] and its expression is frequently altered in immortalized tumor cell lines [96]. In a first step, we therefore examined expression of functional DG and alternative LASV receptor candidates in a panel of primary human cells targeted by LASV *ex vivo*, including hepatocytes, endothelial cells, and epithelial cells [70]. Primary human hepatocytes were isolated from liver specimens obtained after partial hepatectomy and cultured as described in Materials and Methods [84]. As primary cell culture models for microvascular endothelial cells, human umbilical cord vascular endothelial cells (HUVEC) and human microvascular endothelial cells of the lung (HMVEC-L) were used. Primary human small airway epithelial cells (SAEC) served as model for primary respiratory epithelial cells. The extent of functional glycosylation of DG in these primary cells was assessed by Western blot combining mAb IIH6 specific for the α-DG-linked matriglycan epitope with mAb 8D5 directed to the β-DG core protein [97]. As controls, we included the human fibrosarcoma line HT-1080 that is deficient in LARGE expression [34] and the human alveolar epithelial cell line A549 expressing functional DG [22]. In line with *in vivo* data, primary hepatocytes expressed DG core protein without detectable matriglycan [94] (Fig. 1A). Both endothelial cell types expressed an under-glycosylated α-DG form migrating at an apparent molecular mass of 100-110 kDa, whereas α-DG from SAEC ran around 125-145 kDa, similar to the form detected in A549 cells and in adult lung epithelia *in vivo* [98] (Fig. 1A). Examination of the expression of the candidate receptors Axl, Tyro3, and DC-SIGN revealed the presence of Axl in all cell types, whereas Tyro3 and DC-SIGN seemed absent. Together, the data indicated co-expression of Axl with differentially glycosylated DG on primary human cells targeted by LASV.

Previous studies demonstrated that distinct apparent molecular masses of α-DG in SDS-PAGE are due to different lengths of the matriglycan chains [19, 97, 99]. Recent structural data on the pre-fusion conformation of mature LASV GP suggest an avidity-based binding mode of the GP1 trimers to DG-linked matriglycan chains [78]. To address this issue, we assessed virus binding affinity to differentially glycosylated DG employing a quantitative solid-phase binding assay [21]. Since LASV is a BSL4 pathogen, work with live virus is restricted. We therefore used a recombinant LCMV expressing the envelope GP of LASV strain Josiah (rLCMV-LASVGP). As viral entry is exclusively mediated by the viral envelope, this chimera represents a suitable BSL2 surrogate to study LASV entry and has been widely used for the characterization of LASV cell tropism *in vitro* [30, 32, 48, 49] and *in vivo* [100, 101]. Dystroglycan was enriched from A549, HUVEC, and HT-1080 cells by affinity purification using the lectin WGA that recognizes

generic N-glycans [99] (Fig. 1B). Equal amounts of DG protein were immobilized in microtiter plates and incubated with increasing concentrations of purified virus. Bound virus was detected with mAb 83.6 to LASV GP2 as described [21]. As shown in Fig. 1C, virus binding affinity indeed correlated with the apparent molecular mass of α-DG, consistent with the avidity-based binding mode proposed by the current structural model [78].

Axl can mediate productive LASV entry in absence of functional DG

In line with histological evidence, our examination of LASV candidate receptor expression on primary human cells revealed that Axl can be co-expressed with DG that either lacks functional glycosylation or bears matriglycan chains of different length. Considering the conflicting reports in the literature [34, 43], we sought to clarify the exact contribution of Axl in LASV cell entry as a function of DG's post-translational modification in the context of productive arenavirus infection, using our rLCMV-LASVG chimera. A large body of evidence supports the current model of TAM receptor-mediated viral entry by apoptotic mimicry, involving recognition of PS in the virion envelope by the high affinity ligands Gas6 and protein S [37] that are naturally present in serum [39, 102]. The exact ratio of LASV GP1 to PS in the viral envelope appears therefore critical to study receptor use. As a first step, we tried to validate our rLCMV-LASVGP chimera, comparing its GP1/PS ratio with authentic LASV using a capture ELISA (Fig. 2A). To remove serum-derived PS binding proteins that may interfere with our assay, viruses were treated with the Ca^{2+} chelator EGTA that efficiently dissociates Gas6 and pS [39], followed by purification over a renografin gradient, as detailed in Materials and Methods. Purified virus was added to microtiter plates coated with mAb 83.6 that recognizes a highly conserved epitope in GP2 [81] and does not interfere with virus-receptor binding [12] (Fig. 2A). After specific capture of virus for 16 h in the cold, plates were washed and PS displayed on the viral envelope detected with the PS-binding protein annexin(ANX)-V. LASV GP1 was detected using the recombinant virus-binding DG fragment DGEKFc4, which contains a C-terminal human IgG1 Fc moiety [83]. Across different preparations, the GP1/PS ratios of rLCMV-LASVGP were similar to the authentic virus (Fig. 2B), validating our chimera as a suitable BSL2 model to investigate receptor use.

As our primary hepatocytes turned out to be challenging to manipulate *in vitro*, we needed a suitable cell model to study Axl-mediated cell entry of rLCMV-LASVGP in absence of functional DG. After examination of a panel of cell lines, we opted for the fibrosarcoma cell line HT-1080 that lacks functional DG and expresses Axl, similar to primary hepatocytes (Fig. 1A). To exclude any contribution of the remaining DG core protein, we depleted DG from HT-1080 cells using specific shRNAs delivered by lentiviral vectors (Fig. 3A). Cells depleted for DG and controls were infected with rLCMV-LASVGP at low multiplicity (MOI = 0.01). After 16 h, cells were fixed and productive infection assessed by detection of LCMV NP using mAb 113 in immunofluorescence assay (IFA). Depletion of DG core protein by >98% did not affect infection with rLCMV-LASVGP, excluding a

significant contribution (Fig. 3B). In contrast, knock-down of Axl using validated siRNAs markedly reduced productive infection by rLCMV-LASVGP, but not recombinant LCMV expressing the G protein of VSV (rLCMV-VSVG), which enters independently of TAM receptors [39] (Fig. 3C, D). The RNAi data were confirmed by antibody perturbation using a polyclonal antibody to Axl (Fig. 3E). In sum, our results confirm that endogenous levels of Axl in HT-1080 cells can contribute to LASV entry in the context of productive arenavirus infection in absence of functional DG, in line with the original report [34].

Axl-mediated LASV entry is serum-dependent and requires PS of the viral envelope
A hallmark of Axl-mediated entry of most enveloped viruses via apoptotic mimicry is dependence on Gas6 that provides a molecular bridge between PS of the viral envelope and the TAM receptor [37, 39]. In a first step we assessed serum-dependence of Axl-mediated rLCMV-LASVGP attachment to HT-1080 cells. As a positive control, we used recombinant VSV pseudotypes bearing the envelope GP of the New World arenavirus Tacaribe (rVSVΔG-TCRVGP) that critically depend on PS receptors for cell entry [43]. As a negative control rLCMV-VSVG was included. Serum-starved HT-1080 cells were incubated with purified rLCMV-LASVGP, rVSVΔG-TCRVGP, and rLCMV-VSVG at low multiplicity (MOI = 0.01) in presence of increasing concentrations of serum in the cold to allow virus-cell attachment without internalization (Fig. 4A). After 2 h, unbound virus was removed, fresh complete medium containing serum added, and cells shifted to 37°C. After 1 h, the medium was supplemented with 20 mM of the lysosomotropic agent ammonium chloride. When added to cells, ammonium chloride raises the endosomal pH instantly and blocks low pH-dependent endosomal escape of viruses, without causing overall cytotoxicity [103, 104]. After 16 h cells were fixed and productive infection quantified by detection of LCMV NP in IFA, whereas rVSVΔG-TCRVGP was detected via its GFP reporter. The presence of serum during viral attachment increased infection with rLCMV-LASVGP and rVSVΔG-TCRVGP in a dose-dependent manner, but did not affect rLCMV-VSVG (Fig. 4B). In a complementary approach, we tried to mask PS displayed in the lipid bilayer of rLCMV-LASVGP with ANX-V. For this purpose, purified rLCMV-LASVGP and the rLCMV-VSVG control were pre-treated with increasing concentrations of ANX-V, followed by infection of HT-1080 cells in presence of serum. ANX-V blocked entry of rLCMV-LASVGP, but not rLCMV-VSVG in a dose-dependent manner, implicating PS in viral entry.

Kinetics of Axl-mediated viral attachment and viral endosomal escape
In a next step to characterize Axl-mediated infection of rLCMV-LASVGP, we assessed the kinetics of virus attachment. Specifically, we compared Axl-mediated binding of rLCMV-LASVGP to HT-1080 cells with viral attachment to HEK293H cells, which express highly glycosylated DG but lack Axl (Fig. 5A). Differential receptor use in HT-1080 cells (Axl) and HEK 293H cells (DG) was verified by antibody perturbation (Fig. 5B). To estimate the kinetics of virus-receptor attachment,

purified rLCMV-LASVGP was pre-treated with 10% serum and added to cells at low multiplicity (MOI = 0.01) in the cold, allowing receptor binding without internalization. At different time points, unbound virus was removed by washing, and cells rapidly shifted to 37 °C to allow entry. After one hour, ammonium chloride was added to prevent further entry, followed by detection of infection by IFA after 16 h. In line with previous studies, DG-mediated virus attachment to HEK293H cells was rapid with 50% binding reached after a few minutes (Fig. 5C) [22]. In contrast, Axl-mediated virus binding to HT-1080 cells occurred slower with half-maximal binding after 15-20 min, consistent with a different binding mode (Fig. 5C).

In productive infection, receptor-bound LASV is internalized by endocytosis, followed by delivery to late endosomes, where fusion occurs under low pH. We next compared the kinetics of late endosomal escape in HT-1080 and HEK293H cells, determining the time the virus required from receptor attachment to become resistant to ammonium chloride. Virus was added to cells in the cold to allow receptor binding without internalization. Temperature was rapidly shifted to 37°C and ammonium chloride added at the indicated time points and left throughout the experiment. Readout of productive infection revealed similar half-times for endosomal escape of 30-45 min in both cell types (Fig. 5D). The data suggest that once bound, both Axl and DG can mediate endocytosis followed by rapid delivery to late endosomes, where fusion occurs.

Heparan sulfate proteoglycans contribute to LASV entry via Axl, but not DG

A recent haploid screen for LASV entry factors in DG null cells uncovered several genes involved in the biosynthesis of heparan sulfate as candidates, suggesting a role of glycosaminoglycans in DG-independent LASV entry [64]. To address this issue experimentally in the context of Axl-mediated cell entry, we pre-incubated rLCMV-LASVGP and rLCMV-VSVG with increasing concentrations of heparin in the cold. Subsequent infection of HT-1080 cells revealed an incremental, but consistent, dose-dependent reduction of Axl-mediated rLCMV-LASVGP (Fig. 5E). In contrast, infection of HEK293H cells via DG seemed not affected by heparin (Fig. 5E). The data support the genetic studies [64] and suggest a contribution of heparan sulfate in DG-independent LASV cell entry in our system.

Virus-induced Axl tyrosine kinase activation is required for rLCMV-LASVGP entry

Engagement of cellular receptors by viruses frequently induces cellular signaling that can serve as a "knock on the door" to prime the host cell for further steps of infection [26, 53, 105]. In previous studies, recombinant full-length Axl over-expressed in otherwise refractory cell lines enhanced entry of LASV pseudotypes [34]. Deletion of the cytosolic tyrosine kinase domain or insertion of "kinase dead" mutations reduced LASV pseudotype infection, providing first evidence for a role of Axl signaling in LASV entry [34]. To confirm these findings with endogenous Axl in the context of productive arenavirus infection, we used the novel small molecule Axl tyrosine kinase inhibitor R428

144

that shows high selectivity and fast drug action [106, 107]. To minimize the duration of drug exposure and unwanted off-target effects, we performed a drug washout assay outlined in Fig. 6A. Briefly, HT-1080 cells were pre-treated for 30 min with the inhibitor, followed by infection with rLCMV-LASVGP at low multiplicity (MOI = 0.01) in presence of drug. As positive and negative controls, we included rVSVΔG-TCRVGP and the non-enveloped AdV5-GFP, respectively. After one hour, drug was washed out using medium containing ammonium chloride to block further entry. Productive infection was detected after 16 h by IFA. The Axl inhibitor R428 reduced rLCMV-LASVGP and rVSV-TCRVGP infection in a dose-dependent manner, whereas AdV5-GFP was not affected (Fig. 6B). While the inhibitor reduced the number of infected cells per well, residual infected cells still expressed high levels of LCMV NP (Fig. 6C), suggesting an effect of the drug on viral entry, rather than transcription or replication. To further validate cell entry as the main target of R428, we performed "time-of-addition experiments". As shown in Fig. 6D, the Axl inhibitor was highly active against rLCMV-LASVGP when added before or during infection, but had only a mild effect at later time points post-entry. The nucleoside analogue ribavirin that inhibits replication of the viral core was active at all time points during infection, as expected (Fig. 6D).

The observed inhibition of Axl-mediated entry by R428 confirmed that Axl tyrosine kinase activity was indeed required for rLCMV-LASVGP entry, in line with the original report [34]. Next, we addressed if engagement of cellular Axl by the virus could activate receptor signaling or whether Axl tyrosine kinase activity served merely as a "permissive signal". To this end, we pre-incubated purified rLCMV-LASVGP with 10% FBS, followed by ultracentrifugation through a sucrose cushion. Pelleted virus was washed, re-suspended in HBSS, and infectious titers verified by IFA. As control, we included a "mock preparation" produced from the supernatants of uninfected cells by the same procedure, as described in Materials and Methods. Serum-starved HT-1080 cells were incubated with rLCMV-LASVGP at high multiplicity (50 PFU/cell) and equivalent amounts of mock preparation in the cold to prevent membrane fluidity and signaling. After removal of unbound virus, cells were rapidly shifted to 37°C and lysed at the indicated time points. Total Axl was immunoprecipitated (IP) with polyclonal anti-Axl antibody. Receptor autophosphorylation was detected by Western blot using a mAb to tyrosine phosphate, as described [93]. As shown in Fig. 6E, engagement of rLCMV-LASVGP induced detectable Axl tyrosine phosphorylation above background within circa 10 min. In sum, the data suggest that virus-induced Axl tyrosine kinase activity is required for DG-independent rLCMV-LASVGP entry.

Axl-dependent LASV cell entry involves macropinocytosis and requires LAMP-1
Although TAM receptors have been implicated in viral entry via apoptotic mimicry for many viruses [37], the endocytotic pathway(s) underling TAM-mediated virus uptake remain largely unknown. Early studies on Ebola virus demonstrated that engagement of Axl by the virus can enhance macropinocytosis [108]. However, more recent work on Zika virus provided evidence

for clathrin-mediated endocytosis (CME) [93], suggesting important virus-specific differences. To characterize the Axl-dependent entry pathway used by rLCMV-LASVGP in HT-1080 cells, we employed a panel of well-described "diagnostic" inhibitors to known cellular factors implicated in clathrin-mediated entry and macropinocytosis proposed by Mercer and Helenius [57, 59] (Table 1).

To assess clathrin- and dynamin dependence of rLCMV-LASV entry via Axl, we used the inhibitor pitstop-2 that prevents ligand binding to the N-terminal domain of clathrin, and the dynamin inhibitors dynasore and dyngo4a, respectively. To target preferentially viral entry and minimize off-target effects, inhibitors were tested in the entry assay outlined in Fig. 6A. As a positive control, a recombinant VSV expressing GFP (rVSV-GFP) was used. Pitstop-2, dynasore, and dyngo4a only mildly affected rLCMV-LASVGP, but reduced infection with rVSV-GFP [109] (Fig. 7A). In a complementary approach, clathrin heavy chain was depleted by RNAi [48]. Knock-down of >95% of clathrin heavy chain (Fig. 7B) did not affect rLCMV-LASVGP entry (Fig. 7C), supporting a clathrin- and dynamin-independent pathway.

A conserved hallmark of viral entry via macropinocytosis is dependence on sodium proton exchangers (NHE) that are sensitive to amiloride drugs [57]. Inhibition with EIPA reduced rLCMV-LASVGP entry in a dose-dependent manner, but only mildly affected rLCMV-VSVG (Fig. 7D). A second conserved feature of macropinocytosis is actin-dependence [53, 54]. To address this issue, cells were treated with the inhibitors cytochalasin D and latrunculin A, that disrupt actin filaments, as well as jasplakinolide, a drug that stabilizes actin fibers and blocks actin dynamics. Pretreatment with all actin inhibitors markedly reduced infection with rLCMV-LASVGP, without affecting overall cell viability (Fig. 7E). The small GTPases Cdc42, Rac1, and RhoA represent important downstream effectors of NHE involved in actin regulation [110]. Using the well-characterized inhibitors Pirl1, NSC23766, and CT04, we addressed the role of Cdc42, Rac1, and RhoA in Axl-mediated LASV entry. Pirl1 and NSC23766, but not CT04 specifically reduced productive infection with rLCMV-LASVGP, pinpointing Cdc42 and Rac1, but not RhoA as entry factors (Fig. 7F). Infection of rLCMV-LASVGP was likewise reduced after inhibition of the Cdc42 downstream effector p21-activating kinase (PAK)-1 with IPA-3 (Fig. 7G). Productive entry of viruses via macropinocytosis frequently depends on non-muscle myosin II required for membrane fission during formation of early macropinosomes [54]. To address this issue, HT-1080 cells were treated with blebbistatin, an inhibitor of myosin II as well as the myosin light chain kinase inhibitor ML-7. As shown in Fig. 7G, both inhibitors specifically reduced entry of rLCMV-LASVGP, suggesting that Axl-mediated entry of rLCMV-LASVGP involves a pathway related to macropinocytosis.

Upon entry via DG, LASV is rapidly delivered to the late endosome, where the virus undergoes a "receptor switch" and engages the late endosomal/lysosomal resident protein LAMP-1 that is essential for efficient fusion [64, 65, 67]. Although most Old World arenaviruses can use

DG as a receptor, the ability to hijack LAMP-1 as a late endosomal entry factor is unique for LASV [111]. We therefore investigated if LAMP-1 was also needed for Axl-mediated LASV entry into HT-1080 cells. Depletion of LAMP-1 by specific siRNAs impaired rLCMV-LASVGP entry in HT-1080, suggesting an essential role for LAMP-1 as a late endosomal entry factor also for Axl-mediated entry (Fig. 7H, I).

Axl can contribute to LASV entry into endothelial cells

Endothelial cells represent important targets for LASV late in infection and functional perturbation of the vascular endothelium precedes shock and death in fatal Lassa fever [112]. Early studies revealed that microvascular endothelial cells are highly susceptible to LASV infection *in vitro* and can become prodigious sources of infectious virus [113]. Examination of LASV candidate receptor expression in HUVEC and HMVEC-L in our present study revealed co-expression of Axl with an underglycosylated form of DG with relatively low virus binding affinity (Fig. 1). To address the relative contribution of DG and Axl to LASV entry, HUVEC and HMVEC-L were blocked with specific antibodies to Axl and functional DG, either alone or in combination, followed by infection. Perturbation of individual receptors hardly affected rLCMV-LASVGP entry, whereas the antibody combination lowered infection significantly (Fig. 8A), suggesting that both Axl and DG may contribute to infection.

Previous studies revealed that engagement of cellular DG by LASV GP induces tyrosine phosphorylation of β-DG's cytosolic domain, resulting in dissociation from the cytoskeletal adaptor protein utrophin, which may facilitate internalization of the virus-receptor complex **[30]**. In a next step, we therefore assessed virus-induced tyrosine phosphorylation of Axl and DG in endothelial cells. Monolayers of HMVEC-L were exposed to rLCMV-LASVGP and mock preparation. After removal of unbound virus, cells were rapidly shifted to 37°C and lysed at the indicated time points. Activation of Axl was detected as described above (Fig. 6E). Virus-induced tyrosine phosphorylation of DG was examined in Western blot using a mAb that specifically recognizes β-DG phosphorylated at residue YP892 located in a C-terminal PPPY motif implicated in utropin binding **[30, 114]**. In HMVEC-L, rLCMV-LASVGP induced tyrosine phosphorylation of Axl and DG with similar kinetics, suggesting that both receptors are engaged (Fig. 8B).

DISCUSSION

Many important human pathogenic viruses evolved to use different receptors. However, the exact operational definition of a receptor, co-receptor, attachment- and entry factors is frequently not straightforward and critically depends on species and cell type [26, 115]. For LASV, the situation seems particularly complicated considering remarkably complex tissue-specific post-translational modification of its major receptor DG that results in a large spectrum of receptor variants with strikingly different virus binding affinities [116]. The specific function of DG as a LASV receptor in a particular cell type appears therefore as a complex function of the expression of >20 genes currently implicated in the biosynthesis of functional DG [15]. As for many other emerging enveloped viruses, the broadly specific cellular PS receptors Axl and Tyro3 have been proposed as candidate LASV receptors [37, 80]. However, the published data on their specific role in LASV appear conflicting [34, 43]. In the present study, we thought to clarify and characterize the roles of Axl in LASV entry.

Functional glycosylation of DG and expression of TAM receptors are frequently altered in tumor cells [96, 117]. In a first step of our study, we therefore examined the expression of LASV candidate receptors in relevant primary human cell types cultured *ex vivo*. In primary human hepatocytes derived from liver biopsies, we could not detect functional DG, in line with histological findings in adult liver tissue [79]. The detection of Axl in our primary liver cells was further consistent with the recently reported Axl expression in healthy human hepatic tissue [118]. Endothelial and epithelial cells are highly sensitive to LASV infection *in vitro* and *in vivo* [113, 119] and represent important targets for the virus late in disease [1, 71]. Our examination of LASV candidate receptors in primary microvascular endothelial cells and respiratory epithelial cells revealed differential glycosylation of DG that correlated with distinct virus binding affinity, emphasizing the current concept of DG as a "tunable receptor" [15, 19]. Both, endothelial and epithelial cells expressed Axl, in line with recent reports [40, 120]. In sum, our results obtained from primary human cells are consistent with existing histological and biochemical *in vivo* data and confirm that susceptible human cell types co-express Axl with differentially glycosylated DG.

The susceptibility of a given cell type to LASV at the level of entry is likely a complex function of DG glycoslation and the expression levels of alternative receptors like Axl. The specific contributions of DG and Axl to LASV attachment and entry further critically depend on the exact GP1/PS ratio in the virion particles. Using a capture-ELISA, we consistently found GP1/PS ratios in the envelopes of rLCMV-LASVGP that were comparable to authentic LASV, validating our chimera as a suitable BSL2 model for entry studies in the context of productive arenavirus infection.

In a first step, we confirmed the findings of the original report by Shimojima and colleagues [34], showing that Axl can indeed function as an authentic LASV entry receptor in the context of productive arenavirus infection in absence of functional DG. We then characterized Axl-mediated virus-cell attachment and found similarities to the model of "apoptotic mimicry" proposed for many viruses [37, 80]. However, compared to glycosylated DG that rapidly captures free virus via avidity-based lectin-type binding [55], virus attachment to Axl followed a slower kinetics, consistent with the proposed distinct binding mode involving lipid-protein (PS-Gas6) and protein-protein (Gas6-Axl) interactions [37]. Using our rLCMV-LASVGP chimera, we further provide first experimental evidence that heparan sulfate can facilitate DG-independent LASV entry via Axl, in line with a recent genetic screen [64].

Axl-mediated entry of several viruses requires receptor signaling through the receptor's cytosolic tyrosine kinase domain [40, 93, 121, 122]. Interestingly, in most cases studies so far, including the flaviviruses Dengue, West Nile, and Zika virus, Axl signaling seems not required for virus internalization, but promotes later steps of viral multiplication, increasing infectious virus production [40, 93, 121]. In addition to their role in removal of apoptotic cells, TAM receptors play a crucial role in the negative regulation of innate immune signaling, regulating the host cell's type interferon (IFN)-I response [36, 123, 124]. In a current model, engagement of Axl by enveloped viruses down-regulates innate immune signaling, blunting the IFN-I response thus promoting viral replication [37, 80, 121]. Similar to the situation with Zika virus [93] we found that engagement of cellular Axl by rLCMV-LASVGP induces rapid receptor signaling. However, a combination of drug wash-out and time-of-addition experiments, using the fast-acting Axl inhibitor R428, suggests a role for virus-induced Axl activation during rLCMV-LASVGP entry, but not at later steps of viral replication. Previous studies demonstrated that HT-1080 cells used in our study induce a robust IFN-I response when challenged with other RNA viruses [125], excluding an overall defect in innate anti-viral immunity. The observed difference to flaviviruses may rather be explained by the fact that infection of LCMV and LASV in many cell types, including HT-1080, fails to induce a robust IFN-I response [113, 125-128]. The ability of LASV and LCMV to evade innate immunity seems independent of receptor use and is based on the potent IFN antagonist function of the viral NP and Z proteins that efficiently block IFN-I induction, likely making attenuation via Axl obsolete [126, 129-132].

Previous studies on Axl-mediated viral entry pinpointed different endocytotic pathways, including macropinocytosis [108] and CME for Zika virus [93], suggesting virus-specific differences. Application of a panel of well characterized "diagnostic" inhibitors revealed that Axl-mediated entry of rLCMV-LASVGP occurs via an endocytotic pathway related to macropinocytosis, similar to filoviruses [133] and distinct from Zika virus [93]. The Axl-mediated LASV entry pathway uncovered in our present study shares similarities with the

recently characterized unusual macropinocytosis-related pathway linked to DG-mediated entry of LASV and LCMV into epithelial cells and fibroblasts [52, 55]. However, we also noted important differences. In contrast to DG-mediated viral entry, the pathway linked to Axl depends e.g. on non-muscle myosin II, required for early macropinosome formation [54], similar to the pathways used by poxviruses [42] and Ebola virus [108]. Despite differences in attachment kinetics, both DG and Axl mediated rapid internalization and delivery of the virus to endosomes. The similar kinetics of viral endosomal escape suggests convergence of the endocytotic pathways, likely at the level of late endosomes. This is supported by our observation that LASV entry via both receptors critically depends on LAMP-1, making this late endosomal entry factor an attractive target for anti-viral therapeutic intervention.
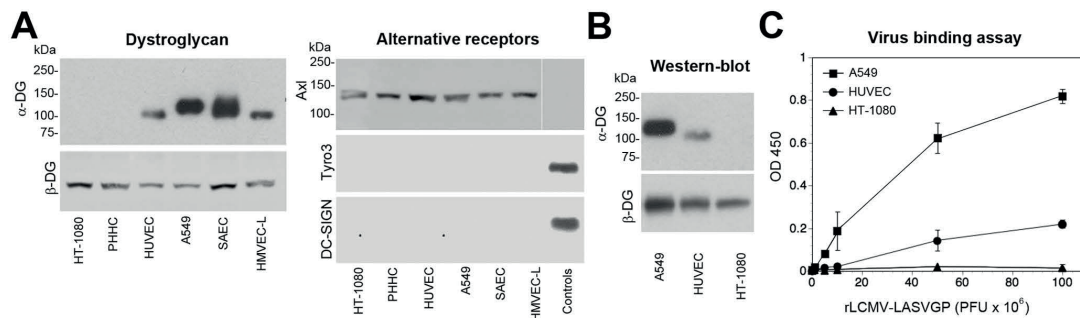
Examination of candidate receptors on endothelial cells revealed co-expression of Axl with an underglycosylated form of DG with relatively low virus binding affinity. Simultaneous blocking of both DG and Axl was required to affect rLCMV-LASVGP entry, whereas perturbation of the individual candidate receptors had only mild effects, suggesting some degree of redundancy. In line with this observation, viral attachment to endothelial cells was followed by rapid virus-induced tyrosine phosphorylation of both receptors, suggesting that DG and Axl may be engaged during productive viral entry. This seems distinct from Zika virus that uses Axl as a primary receptor in endothelial cells in a non-redundant manner [120].

In sum, our study confirms and extends previous work, supporting the notion that Axl can fulfill different functions in LASV entry in different cell types, depending on the extent of post-translational modification of DG. Based on the combined information available, we propose the following model for the specific functions of DG and Axl during LASV infection: During zoonotic transmission, highly glycosylated DG present in epithelial cells can rapidly catch and internalize the virus, acting as a primary entry receptor [55]. A role of DG glycosylation as a host determinant during virus-human co-evolution is indeed suggested by genome-wide association studies that uncovered positive selection for specific LARGE alleles in populations from regions of Western African where LASV is endemic [6, 24, 25]. In severe LASV infection, the virus rapidly spreads via the bloodstream, reaching, among other organs, the liver and the vascular endothelium. In human hepatocytes and other cells lacking functional DG, the Axl-dependent, DG-independent LASV entry pathway characterized here may be operational. Interestingly, chronic infection with hepatitis C virus (HCV) in humans markedly increases Axl expression in the liver [118]. Considering the high prevalence of HCV in many regions of Western Africa [134], chronic viral hepatitis may contribute to susceptibility of local populations to LASV infection. In endothelial cells, DG and Axl may both contribute to LASV entry, making this cell type highly susceptible and contributing to the endothelial dysfunction that precedes shock and death. Therapeutic strategies against LASV may therefore consider Axl as an additional drug target.

FIGURES

FIG1. Primary human cells LASV co-express Axl and differentially glycosylated DG. (A) Detection of candidate LASV receptors in primary human cells. Total cell protein was extracted from primary human hepatocytes (PHHC), HUVEC, HMVEC-L, and SAEC, separated by SDS-PAGE and blotted onto nitrocellulose. Functional DG was detected with mAb IIH6 recognizing the matriglycan sugar polymers on α-DG. Presence of the core protein was probed with mAb 8D5 to β-DG. A549 and HT-1080 cells were included as positive and negative controls, respectively. Axl, Tyro3, and DC-SIGN were detected with goat pAb anti-human Axl, mAb 96201 anti-human Tyro3, and mAb 120507 anti-DC-SIGN. Human THP-1 monocytes and THP-1-derived immature dendritic cells were used as positive controls for Tyro3 and DC-SIGN, respectively [46]. As a negative control for Axl, HEK293H cells were included. The negative control lane of the Axl blot was taken from the same membrane and moved, as indicated by the thin white line. Primary antibodies were detected with HRP-conjugated secondary antibodies using enhanced chemiluminescence (ECL) for development. The observed differences in the apparent molecular masses of Axl in different cells may be due to different glycosylation patterns. The expression levels of Axl in PHHC varied between donors and a representative example was selected. (B) Western blot of WGA-purified DG. Dystroglycan was purified from the indicated cells by WGA

affinity chromatography. Concentrated fractions were probed in Western blot for functional glycosylation of α-DG with mAb IIH6 and for β-DG with mAb 8D5 as in (A). (C) Solid-phase virus binding assay. Equal amounts of DG purified from the indicated cells were immobilized in microtiter plates and incubated with the indicated concentrations of purified rLCMV-LASVGP. Bound virus was detected with mAb 83.6 to LASV GP2 using a biotinylated secondary antibody and HRP-conjugated streptavidine for signal amplification in a color reaction. Data are means $\pm$ SD, n = 3.
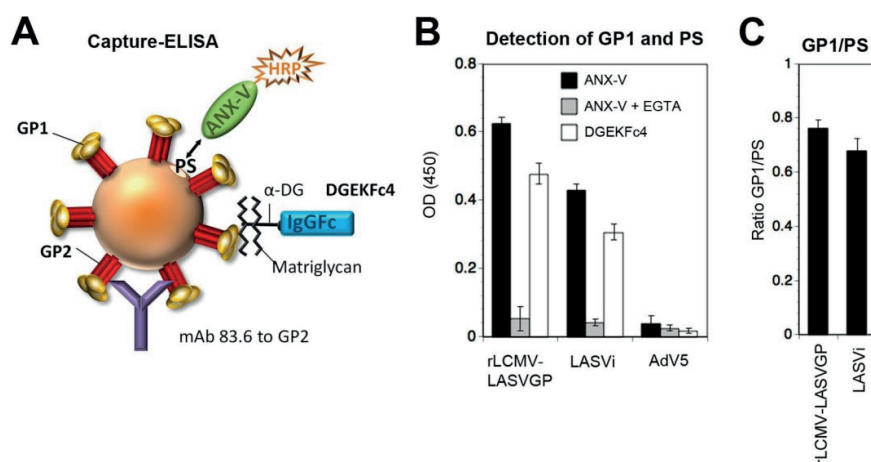

FIG2. Determination of GP1/Ps ratios in rLCMV-LASVGP and authentic LASV. (A) Schematic of the capture-ELISA. Virus is captured by immobilized mAb 86.3 that recognizes a conserved non-neutralizing epitope in GP2. After removal of unbound material, bound virus is probed with ANX-V to detect PS displayed in the lipid bilayer of the viral envelope and DGEKFc4 that binds to GP1. For details, please see text. (B) Detection of GP1 and PS. Purified rLCMV-LASVGP, authentic inactivated LASV, were incubated with immobilized mAb 83.6, using the non-enveloped AdV5-GFP as a negative control. After washing, bound virus was incubated with biotin-conjugated ANX-V in presence and absence of EGTA, as well as DGEKFc4. Bound biotinylated ANX-V and DGEKFc4 were detected by streptavidine HRP and HRP-conjugated anti-human Fc antibody in a color reaction. Please note the reduced ANX-V binding in presence of the Ca^{2+}-chelator EGTA. Data are means $\pm$ SD, n = 3. (C) The ratios of GP1/PS for the virus preparations tested in (B).
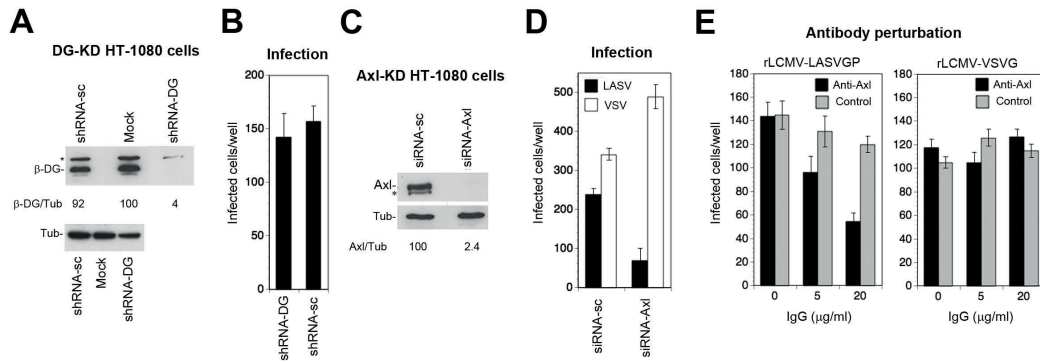
FIG. 3. Axl can mediate productive LASV entry in absence of functional DG. (A) Knock-down of DG in HT-1080 cells. HT-1080 cells were transduced with a lentiviral vector expressing a DG-specific shRNA (shRNA-DG) or scrambled shRNA (shRNA-sc), or mock transduced (mock), followed by selection with puromycin as detailed in Materials and Methods. Depletion of DG core protein was verified in Western-blot using mAb 8D5 to β-DG and α-tubulin (Tub) as a loading control. The asterisk (*) indicated an unspecific band. Efficiency of depletion was assessed by densitometric analysis, followed by calculation of the signal ratios of β-DG/α-tubulin (β-DG/Tub). (B) HT-1080 cells transduced with shRNA-DG or shRNA-sc (A) were seeded in 96 well plates and infected with rLCMV-LASVGP (300 PFU/well) for one hour. Cells were washed with medium supplemented with 20 mM ammonium chloride to prevent secondary infection. After 16 h incubation in presence of ammonium chloride, cells were fixed and infection detected by IFA using mAb 113 to LCMV NP, combined with a Alexa488-conjugated secondary antibody. Infection was quantified by counting infected cells per well considering cell doublets as single infection events. Data are means ± SD, n = 3. (C) Depletion of Axl from HT-1080 cells. HT-1080 cells were transfected with siRNAs to Axl (siRNA-Axl) and scrambled control siRNAs (siRNA-sc) as detailed in Materials and Methods. After 72 h, expression of Axl was detected in Western blot using α-tubulin (Tub) as a loading control. In some blots, a lower molecular mass band (*) was detected. However, this was not consistently observed. Efficiency of Axl depletion was assessed by densitometry, followed by calculation of the signal ratios of Axl/α-tubulin (Axl/Tub). (D) Infection on Axl-depleted HT-1080 cells. HT-1080 cells transfected with siRNA-Axl and siRNA-sc were infected with 300 PFU/well rLCMV-LASVGP (LASV) and rLCMV-VSVG (VSV) and infection detected as in (B). Data are means ± SD, n = 3. (E) Blocking of Axl-mediated infection by antibody perturbation. HT-1080 cells were chilled on ice, washed with cold serum-free medium, and blocked with goat pAb anti-Axl (20 μg/ml), and control goat IgG for 2 h in the cold in absence of serum. Cells were then incubated with 300 PFU/well of rLCMV-LASVGP (LASV) and 200 PFU/well of rLCMV-VSVG (VSV) in presence of antibody for 2 h in the cold. Unbound virus was removed by washing and cells cultures in complete medium at 37°C. After

45 min, 20 mM ammonium chloride was added and infection detected as in (B). Data are means ± SD, n = 3.
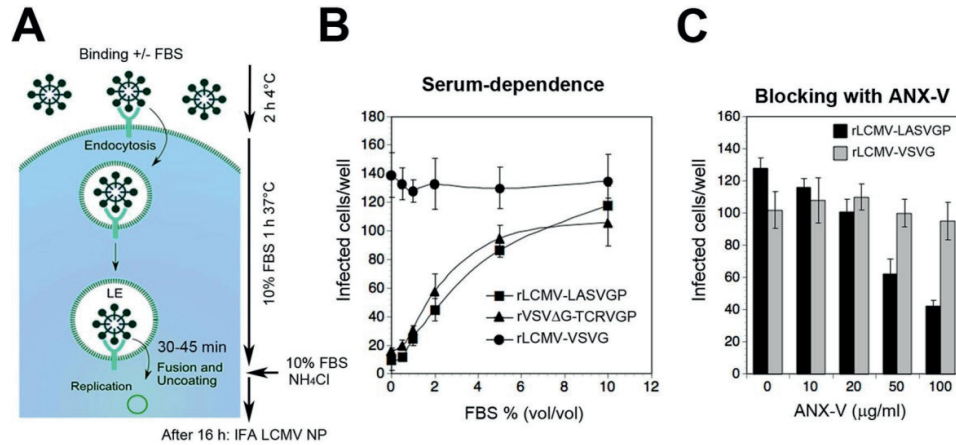
**FIG.4. Axl-mediated LASV entry is serum-dependent and requires PS of the viral envelope.** (A) Schema of the entry assay. For details, please see text, LE, late endosome. (B) Entry of rLCMV-LASVGP into HT-1080 cells serum-dependent. Purified rLCMV-LASVGP (300 PFU/ml), rLCMV-VSVG (200 PFU/well), and rVSVΔG-TCRVGP (100 PFU/well) were pre-treated with the increasing concentrations of serum and added toHT-1080 cells cultured in 96 well pates for 2 h in the cold. Cells were washed 3 times and incubated with complete medium containing 10% (wt/vol) FBS. After 1 h, complete medium containing 20 mM ammonium chloride was added, followed by 16 h incubation in presence of the lysosomotropic agent. Infection was detected by IFA as in (3B). Data are means ± SD, n = 3. (C) Blocking of infection of HT-1080 cells with ANX-V. Purified rLCMV-LASVGP and rLCMV-VSVG were diluted in DMEM and pre-treated with the indicated concentrations of ANX-V for 2 h in the cold. The virus/ANX-V mix was then diluted 1:10 in complete medium containing 10% (wt/vol) FBS, resulting in a virus concentration of 300 PFU/ml, and added to HT-1080 cells for 1 h at 37 °C. After 1 h, complete medium containing 20 mM ammonium chloride was added, followed by 16 h incubation and detection of infection by IFA as in (3B). Data are means ± SD, n = 3.
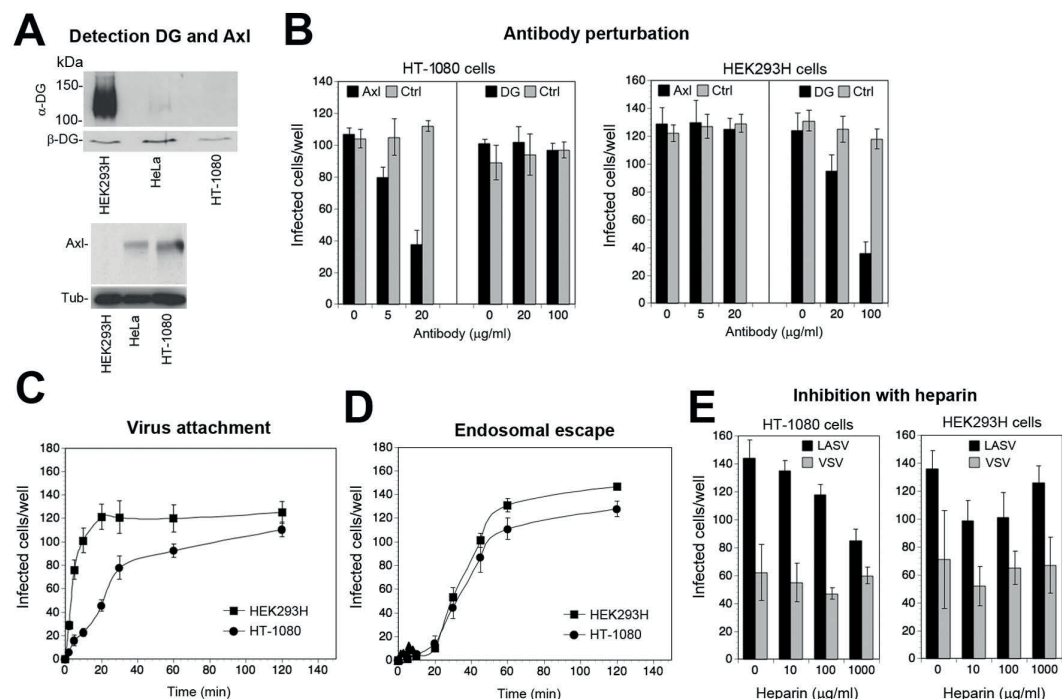
FIG.5. Kinetics of Axl-mediated viral attachment and viral endosomal escape. (A) Detection of functional DG and Axl in HEK293H and HT-1080 cells by Western blot as in (1A), including the LARGE-deficient cell line HeLa. Please note the residual signal for functionally glycosylated α-DG in HeLa cells that was absent in HT-1080. The double band for Axl in HT-1080 cells was not consistently observed. (B) Verification of DG and Axl-mediated entry of rLCMV-LASVGP into HT-1080 and HEK293H cells, respectively. The indicated cells were blocked with mAb IIH6 to glycosylated α-DG (100 µg/ml), goat pAb anti-Axl (20 µg/ml), and control antibodies (Ctrl) for 2 h in the cold as in (3E). Cells were then incubated with rLCMV-LASVGP at 100 PFU/well (HEK293H) and 300 PFU/well (HT-1080) for 2 h in the cold in presence of antibodies. Cells were washed, kept in complete medium for 45 min at 37°C, followed by addition of 20 mM ammonium chloride, cultured for 16 h, fixed, and infection detected as in (3B). Data are means ± SD, n = 3. (C) Virus attachment to HEK293H and HT-1080 cells. The indicated cell lines were chilled on ice, followed by incubation with rLCMV-LASVGP at 100 PFU/well (HEK293H) and 300 PFU/well (HT-1080). At the indicated time points, unbound virus was removed by washing with cold medium and cells rapidly shifted to 37°C. After 1 h at 37°C, 20 mM ammonium chloride was added to the medium and cells incubated for a total of 16 h. Virus infection was detected by IFA with mAb 113 to LCMV NP, combined with Rhodamine Red-X anti-mouse IgG and quantification performed as in (3B). Data are means ± SD, n = 3. (D) Endosomal escape of virus. rLCMV-LASVGP at 100 PFU/well (HEK293H) and 300 PFU/well (HT-1080) was attached to monolayers of the indicated cells in the cold for 2 h. Unbound virus was removed and cells rapidly

shifted to 37°C. At the indicated time points, 20 mM ammonium chloride was added and left throughout the experiment. After 16 h, infection was assessed by IFA as in (C). Given are means $\pm$ SD, n = 3. (E) Blocking of infection of HT-1080 and HEK293H cells with heparin. rLCMV-LASVGP (LASV) and rLCMV-VSVG (VSV) (300 PFU/ml) were diluted in complete medium and pre-treated with the indicated concentrations of heparin for 1 h in the cold, followed by infection of monolayers of HT-1080 cells for 1 h at 37 °C in presence of the inhibitor. After 1 h, complete medium containing 20 mM ammonium chloride was added, followed by 16 h incubation and detection of infection by IFA as in (3B). Data are means $\pm$ SD, n = 3.
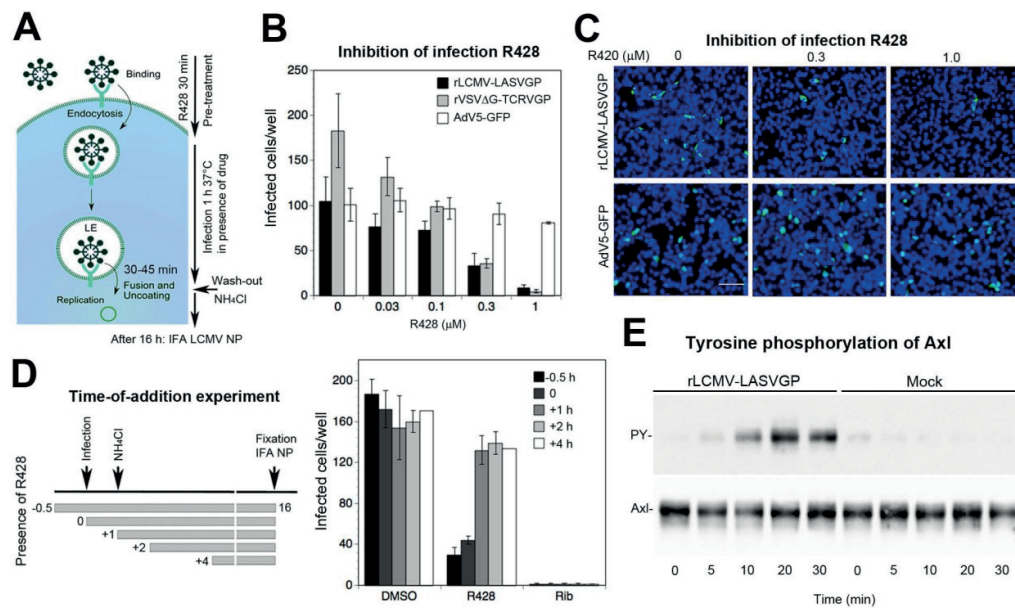
FIG.6. Virus-induced Axl tyrosine kinase activity is required for rLCMV-LASVGP entry. (A) Schema of the inhibitor experiment. For details, please see text, LE, late endosome. (B) Infection of rLCMV-LASVGP depends on the activity of Axl tyrosine kinase. HT-1080 cells were pre-treated with the Axl tyrosine kinase inhibitor R428 at increasing concentrations for 30 min, followed by infection with the indicated viruses at (200 PFU/well) in presence of drug. After 1 h, cells were washed 3 times with medium containing 20 mM ammonium chloride, followed by 16 h incubation in presence of the lysosomotropic agent. Infection was detected by IFA as in (3B). Data are means $\pm$ SD, n = 3. (C) Example of the inhibition of rLCMV-LASVGP infection by R428 revealed by IFA using mAb 113 to LCMV NP (green) and counter-staining of nuclei (DAPI, blue). Note the similar intensity of the NP staining with increasing inhibitor concentration. (bar = 50 µm). The lower panel shows AdV5-GFP used as a negative control. NP or GFP positive cells were scored, considering cell doublets as single infectious events. (D) Time-of-addition

experiment. HT-1080 cells were infected with rLCMV-LASVGP (300 PFU/well) with R428 added at the different time points pre- or post-infection at 1 μM. Virus was added at time point 0, followed by washing and addition of ammonium chloride after 1 h (+1). Ammonium chloride was kept throughout the experiment and cells subjected to IFA after 16 h. Data are means $\pm$ SD, n = 3. Examination of cell viability by Cell TiterGlo® assay recelaed no significant toxicity of R428 under our experimental conditions (data not shown). (E) Engagement rLCMV-LASVGP induces activation of Axl's tyrosine kinase. Serum-starved HT-1080 cells were incubated with rLCMV-LASVGP at 50 infectious particles/cell and equivalent amounts of mock preparation for 2 h in the cold. Unbound virus was removed and cells shifted to 37°C. At the indicated time points, cells were lysed and Axl isolated by IP with goat polyclonal Ab anti-Axl immobilized on Sepharose matrix. Immunocomplexes were eluted by non-reducing sample buffer, followed by SDS-PAGE using 5.5% (wt/vol) running gels. Total Axl protein in IP was revealed in Western blot using a mouse mAb anti-Axl (10% of sample) and tyrosine phosphorylation detected in by a mAb to tyrosine phosphate (90% of sample). For detection TrueBlot® HRP-conjugated anti-mouse IgG was used in ECL. Blots for tyrosine phosphate (PY) were exposed for 2 minutes and blots detecting total Axl for 10 seconds.
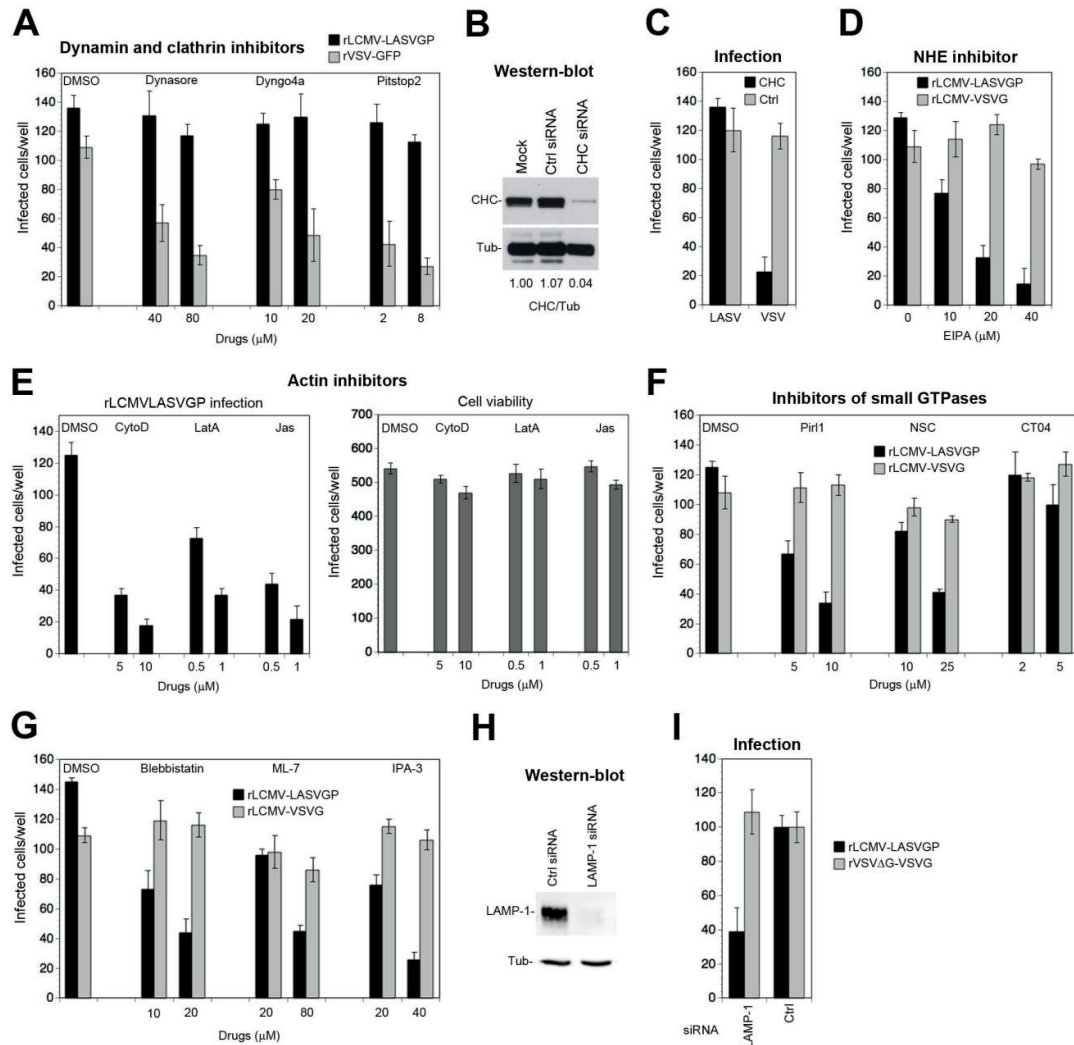
FIG.7. Axl-dependent LASV cell entry involves macropinocytosis and requires LAMP-1.
(A) Axl-mediated entry of rLCMV-LASVGP is independent of dynamin and clathrin. HT-1080
cells were pre-treated with inhibitors for dynamin-2 (dynasore, dyngo-4a) and clathrin (pitstop-
2) at the indicated concentrations for 30 min, followed by infection with rLCMV-LASVGP (300
PFU/well) and rVSV-GFP (100 PFU/well) in presence of drugs. After 1 h, cells were washed 3
times with medium containing 20 mM ammonium chloride, followed by incubation in presence
of the agent. After 16 h, cells were fixed and infection detected by IFA using mAb 113 to LCMV
NP as in (3B). Infection with rVSV-GFP was assessed after 8 h by detection of the EGFP reporter
in direct fluorescence microscopy. (B) Depletion of clathrin heavy chain (CHC) by RNAi. HT-
1080 cells were transfected with a pool of siRNAs specific for CHC, control scrambled siRNAs,
or mock transfected as in (3C). After 72 h, expression of CHC was detected in Western blot using
α-tubulin (Tub) as a loading control. Efficiency of CHC depletion was assessed by densitometry,
followed by calculation of the signal ratios of CHC/α-tubulin (CHC/Tub). (B) HT-1080 cells
subjected to RNAi for CHC (B) were infected with rLCMV-LASVGP (LASV) at 300 PFU/well

and rLCMV-VSVG (VSV) at 100 PFU/well for one hour. Infection was detected by IFA as in (A). Data represent means $\pm$ SD, n = 3. (D) The amiloride drug EIPA blocks Axl-mediated entry of rLCMV-LASVGP. HT-1080 cells were pre-treated with the indicated concentrations of EIPA for 30 min, followed by infection with rLCMV-LASVGP (300 PFU/well) and rLCMV-VSVG (100 PFU/well) in presence of drugs for 1 h and detection of infection by IFA as in (A). (E) Actin inhibitors block Axl-dependent rLCMV-LASVGP infection without causing cell toxicity. HT-1080 cells were pre-treated with the indicated concentrations of cytochalasin D (CytoD), latrunculin A (LatA), and jasplakinolide (Jas) for 30 min, followed by infection with rLCMV-LASVGP (300 PFU/well) as in (A). Data are means $\pm$ SD, n = 3. Cell viability was monitored by CellTiter Glo® assay as described in Materials and Methods measuring cellular ATP levels in a luminescence assay. Data are displayed in relative light units (RLU), means $\pm$ SD, n = 3. (F) Axl-mediated entry of rLCMV-LASVGP depends on Cdc42 and Rac1, but not RhoA. HT-1080 cells were pre-treated with DMSO vehicle control, or the inhibitors pirl1 (Cdc42), NSC23766 (Rac1), and CT04 (RhoA) at the indicated concentrations followed by infection with rLCMV-LASVGP (300PFU/well) and rLCMV-VSVG (100 PFU/well) for 1 h in presence of drugs, followed by detection of infection as in (A), means $\pm$ SD, n = 3. (G) Axl-dependent entry of rLCMV-LASVGP requires PAK1, non-muscle myosin II, and myosin light chain kinase. HT-1080 cells were treated with the indicated concentrations of IPA-3, blebbistatin, and ML7, followed by infection with rLCMV-LASVGP (300 PFU/well), and rLCMV-VSVG (100 PFU/well) as in (D). Data are means $\pm$ SD, n = 3. (H) Knock-down of LAMP-1 by RNAi. HT-1080 cells were transfected with a siRNAs specific for LAMP-1 and control scrambled siRNAs. After 48 h, depletion of LAMP-1 was verified in Western blot using α-tubulin (Tub) as a loading control. (I) Axl-dependent infection of rLCMV-LASVGP depends on LAMP-1. LAMP-1 depleted and control HT-1080 cells (H) were infected with rLCMV-LASVGP at 300 PFU/well and rLCMV-VSVG (100 PFU/well) for one hour. Infection was detected by IFA as in (A). Data are means $\pm$ SEM, n = 3 for rLCMV-LASVGP and n = 2 for rVSVΔG-VSVG.
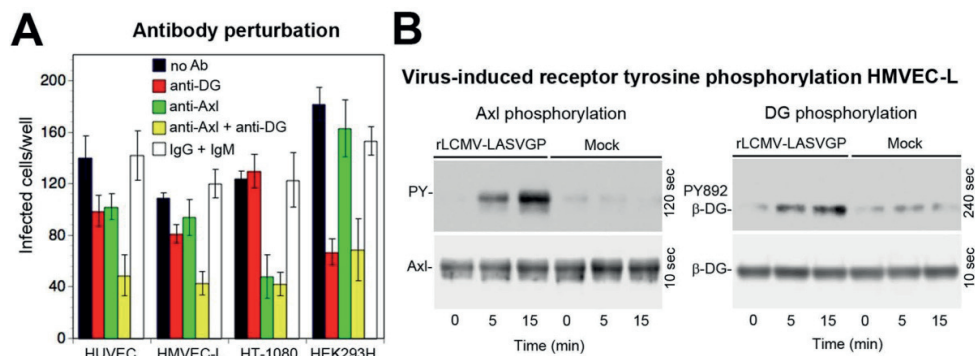
FIG.8. Axl contributes to LASV entry into endothelial but not epithelial cells. (A) Antibody perturbation of rLCMV-LASVGP entry in microvascular endothelial cells. Confluent monolayers of HUVEC and HMVEC-L were blocked with mAb IIH6 to glycosylated α-DG (Anti-DG, 100 μg/ml), goat pAb anti-Axl (Anti-Axl, 20 μg/ml), the combination of both antibodies (Anti-DG + Anti-Axl), a combination of control antibodies (IgG + IgM), and medium only (no Ab) in absence of serum for 2 h in the cold as in (5B). HT-1080 cells and HEK293H cells were included as positive controls for Axl- and DG-mediated viral entry, respectively. Cells were then incubated with rLCMV-LASVGP at 300 PFU/well (HUVEC and HMVEC-L), 100 PFU/well (HEK293H) and 300 PFU/well (HT-1080) for 2 h in the cold in presence of antibodies under serum-free conditions. Cells were washed, and incubated with complete medium. After 16 h incubation in presence of ammonium chloride, cells were fixed and infection detected as in (3B). Data are means $\pm$ SD, n = 3. (B) Entry of rLCMV-LASVGP to HMVEC-L cells induces tyrosine phosphorylation of Axl and DG. Monolayers of HMVEC-L cells were incubated with rLCMV-LASVGP (50 infectious particles/cell) and equivalent amounts of mock preparation for 2 h in the cold. Unbound virus was removed and cells shifted to 37°C. At the indicated time points, cells were lysed. Total protein was extracted from 10% of cleared lysate and probed in Western-blot with mAb cl14a (anti-β-DG PY892) and antibody 8D5 to β-DG. The positions of β-DG and β-DG PY892 are indicated. Blots for β-DG PY892 were exposed for 4 minutes and blots detecting total DG for 10 seconds. Axl was isolated by IP from 90% of the lysate and tyrosine phosphorylation of Axl detected as in (6E). Blots for tyrosine phosphate (PY, 90% of sample) were exposed for 2 minutes and blots detecting total Axl (10% of sample) for 10 seconds.

Table 1: Panel of "diagnostic" inhibitors used in the study

Inhibitor	target	concentrations (μM)
Dynasore	dynamin	40, 80
Dygo4a	dynamin	10, 20
Pitstop-2	clathrin	2, 8
EIPA	NHE	10, 20, 40
Cytochalasin D	actin	5, 10
Latrunculin A	actin	0.5, 1
Jasplakinoline	actin	0.5, 1
Pirl1	Cdc42	5, 10
NSC237766	Rac1	10, 25
CT04	RhoA	2, 5
IPA-3	PAK1	20, 40
ML7	Myosin light chain kinase	20, 80
Blebbistatin	Myosin kinase II	10, 20

REFERENCES

1. McCormick, J.B. and S.P. Fisher-Hoch, *Lassa fever.* Curr Top Microbiol Immunol, 2002. **262**: p. 75-109.
2. Buchmeier, M.J., J.C. de la Torre, and C.J. Peters, *Arenaviridae: the viruses and their replication*, in *Fields Virology*, D.L. Knipe and P.M. Howley, Editors. 2007, Lippincott-Raven: Philadelphia. p. p. 1791-1828.
3. Cosset, F.L., et al., *Characterization of Lassa virus cell entry and neutralization with Lassa virus pseudoparticles.* J Virol, 2009. **83**(7): p. 3228-37.
4. Klewitz, C., H.D. Klenk, and J. ter Meulen, *Amino acids from both N-terminal hydrophobic regions of the Lassa virus envelope glycoprotein GP-2 are critical for pH-dependent membrane fusion and infectivity.* J Gen Virol., 2007. **88**(Pt 8): p. 2320-8.
5. Nunberg, J.H. and J. York, *The curious case of arenavirus entry, and its inhibition.* Viruses, 2012. **4**(1): p. 83-101.
6. Andersen, K.G., et al., *Clinical Sequencing Uncovers Origins and Evolution of Lassa Virus.* Cell, 2015. **162**(4): p. 738-50.
7. McCormick, J.B., et al., *A case-control study of the clinical diagnosis and course of Lassa fever.* J Infect Dis, 1987. **155**(3): p. 445-55.
8. Geisbert, T.W. and P.B. Jahrling, *Exotic emerging viral diseases: progress and challenges.* Nat Med, 2004. **10**(12 Suppl): p. S110-21.
9. McCormick, J.B., et al., *Lassa fever. Effective therapy with ribavirin.* N Engl J Med, 1986. **314**(1): p. 20-6.
10. Stephenson, E.H., E.W. Larson, and J.W. Dominik, *Effect of environmental factors on aerosol-induced Lassa virus infection.* J Med Virol, 1984. **14**(4): p. 295-303.
11. Borio, L., et al., *Hemorrhagic fever viruses as biological weapons: medical and public health management.* Jama, 2002. **287**(18): p. 2391-405.
12. Cao, W., et al., *Identification of alpha-dystroglycan as a receptor for lymphocytic choriomeningitis virus and Lassa fever virus [see comments].* Science, 1998. **282**(5396): p. 2079-81.
13. Spiropoulou, C.F., et al., *New World arenavirus clade C, but not clade A and B viruses, utilizes alpha-dystroglycan as its major receptor.* J Virol, 2002. **76**(10): p. 5140-6.
14. Barresi, R. and K.P. Campbell, *Dystroglycan: from biosynthesis to pathogenesis of human disease.* J Cell Sci., 2006. **119**(Pt 2): p. 199-207.
15. Yoshida-Moriguchi, T. and K.P. Campbell, *Matriglycan: a novel polysaccharide that links dystroglycan to the basement membrane.* Glycobiology, 2015. **25**(7): p. 702-13.
16. Yoshida-Moriguchi, T., et al., *SGK196 is a glycosylation-specific O-mannose kinase required for dystroglycan function.* Science, 2013. **341**(6148): p. 896-9.
17. Inamori, K., et al., *Dystroglycan function requires xylosyl- and glucuronyltransferase activities of LARGE.* Science, 2012. **335**(6064): p. 93-6.
18. Praissman, J.L., et al., *The functional O-mannose glycan on alpha-dystroglycan contains a phospho-ribitol primed for matriglycan addition.* Elife, 2016. **5**.
19. Goddeeris, M.M., et al., *LARGE glycans on dystroglycan function as a tunable matrix scaffold to prevent dystrophy.* Nature, 2013. **503**(7474): p. 136-40.
20. Briggs, D.C., et al., *Structural basis of laminin binding to the LARGE glycans on dystroglycan.* Nat Chem Biol, 2016. **12**(10): p. 810-4.
21. Kunz, S., et al., *Posttranslational modification of alpha-dystroglycan, the cellular receptor for arenaviruses, by the glycosyltransferase LARGE is critical for virus binding.* J Virol, 2005. **79**(22): p. 14282-96.
22. Rojek, J.M., et al., *Old World and clade C New World arenaviruses mimic the molecular mechanism of receptor recognition used by alpha-dystroglycan's host-derived ligands.* J Virol, 2007. **81**(11): p. 5685-95.
23. Jae, L.T., et al., *Deciphering the glycosylome of dystroglycanopathies using haploid screens for lassa virus entry.* Science, 2013. **340**(6131): p. 479-83.
24. Sabeti, P.C., et al., *Genome-wide detection and characterization of positive selection in human populations.* Nature, 2007. **449**(7164): p. 913-8.
25. Andersen, K.G., et al., *Genome-wide scans provide evidence for positive selection of genes implicated in Lassa fever.* Philos Trans R Soc Lond B Biol Sci, 2012. **367**(1590): p. 868-77.
26. Grove, J. and M. Marsh, *The cell biology of receptor-mediated virus entry.* J Cell Biol, 2011. **195**(7): p. 1071-82.
27. Yang, B., et al., *SH3 domain-mediated interaction of dystroglycan and Grb2.* J Biol Chem, 1995. **270**(20): p. 11711-4.

28. Spence, H.J., et al., *Dystroglycan, a scaffold for the ERK-MAP kinase cascade.* EMBO Rep, 2004.
29. Cavaldesi, M., et al., *Association of the dystroglycan complex isolated from bovine brain synaptosomes with proteins involved in signal transduction.* J Neurochem, 1999. **72**(4): p. 1648-55.
30. Moraz, M.L., et al., *Cell entry of Lassa virus induces tyrosine phosphorylation of dystroglycan.* Cell Microbiol, 2013. **15**(5): p. 689-700.
31. Ferletta, M., et al., *Opposing roles of integrin alpha6Abeta1 and dystroglycan in laminin-mediated extracellular signal-regulated kinase activation.* Mol Biol Cell, 2003. **14**(5): p. 2088-103.
32. Rojek, J.M., et al., *Binding of Lassa virus perturbs extracellular matrix-induced signal transduction via dystroglycan.* Cell Microbiol, 2012. **14**(7): p. 1122-34.
33. Shimojima, M. and Y. Kawaoka, *Cell surface molecules involved in infection mediated by lymphocytic choriomeningitis virus glycoprotein.* J Vet Med Sci, 2012. **74**(10): p. 1363-6.
34. Shimojima, M., et al., *Identification of cell surface molecules involved in dystroglycan-independent lassa virus cell entry.* J Virol, 2012. **86**(4): p. 2067-78.
35. Lemke, G. and T. Burstyn-Cohen, *TAM receptors and the clearance of apoptotic cells.* Ann N Y Acad Sci, 2010. **1209**: p. 23-9.
36. Lemke, G. and C.V. Rothlin, *Immunobiology of the TAM receptors.* Nat Rev Immunol, 2008. **8**(5): p. 327-36.
37. Amara, A. and J. Mercer, *Viral apoptotic mimicry.* Nat Rev Microbiol, 2015. **13**(8): p. 461-9.
38. Morizono, K. and I.S. Chen, *Role of phosphatidylserine receptors in enveloped virus infection.* J Virol, 2014. **88**(8): p. 4275-90.
39. Morizono, K., et al., *The soluble serum protein Gas6 bridges virion envelope phosphatidylserine to the TAM receptor tyrosine kinase Axl to mediate viral entry.* Cell Host Microbe, 2011. **9**(4): p. 286-98.
40. Meertens, L., et al., *The TIM and TAM families of phosphatidylserine receptors mediate dengue virus entry.* Cell Host Microbe, 2012. **12**(4): p. 544-57.
41. Frei, A.P., et al., *Direct identification of ligand-receptor interactions on living cells and tissues.* Nat Biotechnol, 2012. **30**(10): p. 997-1001.
42. Mercer, J. and A. Helenius, *Vaccinia virus uses macropinocytosis and apoptotic mimicry to enter host cells.* Science, 2008. **320**(5875): p. 531-5.
43. Jemielity, S., et al., *TIM-family proteins promote infection of multiple enveloped viruses through virion-associated phosphatidylserine.* PLoS Pathog, 2013. **9**(3): p. e1003232.
44. Sullivan, B.M., et al., *Is the TAM receptor Axl a receptor for lymphocytic choriomeningitis virus?* J Virol, 2013. **87**(7): p. 4071-4.
45. Van Breedam, W., et al., *Bitter-sweet symphony: glycan-lectin interactions in virus biology.* FEMS Microbiol Rev, 2014. **38**(4): p. 598-632.
46. Goncalves, A.R., et al., *Role of DC-SIGN in Lassa Virus Entry into Human Dendritic Cells.* J Virol, 2013. **87**(21): p. 11504-15.
47. Lozach, P.Y., et al., *DC-SIGN as a receptor for phleboviruses.* Cell Host Microbe, 2011. **10**(1): p. 75-88.
48. Rojek, J.M., et al., *Different mechanisms of cell entry by human-pathogenic Old World and New World arenaviruses.* J Virol, 2008. **82**(15): p. 7677-87.
49. Pasqual, G., et al., *Old world arenaviruses enter the host cell via the multivesicular body and depend on the endosomal sorting complex required for transport.* PLoS Pathog, 2011. **7**(9): p. e1002232.
50. Quirin, K., et al., *Lymphocytic choriomeningitis virus uses a novel endocytic pathway for infectious entry via late endosomes.* Virology, 2008. **378**(1): p. 21-33.
51. Panda, D., et al., *RNAi screening reveals requirement for host cell secretory pathway in infection by diverse families of negative-strand RNA viruses.* Proc Natl Acad Sci U S A, 2011. **108**(47): p. 19036-41.
52. Iwasaki, M., N. Ngo, and J.C. de la Torre, *Sodium hydrogen exchangers contribute to arenavirus cell entry.* J Virol, 2014. **88**(1): p. 643-54.
53. Mercer, J., M. Schelhaas, and A. Helenius, *Virus entry by endocytosis.* Annu Rev Biochem, 2010. **79**: p. 803-33.
54. Mercer, J. and A. Helenius, *Gulping rather than sipping: macropinocytosis as a way of virus entry.* Curr Opin Microbiol, 2012. **15**(4): p. 490-9.
55. Oppliger, J., et al., *Lassa virus cell entry via dystroglycan involves an unusual pathway of macropinocytosis.* J Virol, 2016.
56. Mohr, E.L., et al., *Inhibitors of cellular kinases with broad-spectrum antiviral activity for hemorrhagic fever viruses.* Antiviral Res, 2015. **120**: p. 40-7.

57.   Mercer, J. and A. Helenius, *Virus entry by macropinocytosis.* Nat Cell Biol, 2009. **11**(5): p. 510-20.

58.   Krieger, S.E., et al., *Echovirus 1 entry into polarized Caco-2 cells depends on dynamin, cholesterol, and cellular factors associated with macropinocytosis.* J Virol, 2013. **87**(16): p. 8884-95.

59.   Krzyzaniak, M.A., et al., *Host cell entry of respiratory syncytial virus involves macropinocytosis followed by proteolytic activation of the F protein.* PLoS Pathog, 2013. **9**(4): p. e1003309.

60.   de Vries, E., et al., *Dissection of the influenza A virus endocytic routes reveals macropinocytosis as an alternative entry pathway.* PLoS Pathog, 2011. **7**(3): p. e1001329.

61.   Sanchez, E.G., et al., *African swine fever virus uses macropinocytosis to enter host cells.* PLoS Pathog, 2012. **8**(6): p. e1002754.

62.   Scott, C.C., F. Vacca, and J. Gruenberg, *Endosome maturation, transport and functions.* Semin Cell Dev Biol, 2014. **31**: p. 2-10.

63.   Rizopoulos, Z., et al., *Vaccinia Virus Infection Requires Maturation of Macropinosomes.* Traffic, 2015. **16**(8): p. 814-31.

64.   Jae, L.T., et al., *Virus entry. Lassa virus entry requires a trigger-induced receptor switch.* Science, 2014. **344**(6191): p. 1506-10.

65.   Cohen-Dvashi, H., et al., *Molecular Mechanism for LAMP1 Recognition by Lassa Virus.* J Virol, 2015. **89**(15): p. 7584-92.

66.   Li, S., et al., *Acidic pH-Induced Conformations and LAMP1 Binding of the Lassa Virus Glycoprotein Spike.* PLoS Pathog, 2016. **12**(2): p. e1005418.

67.   Cohen-Dvashi, H., et al., *Role of LAMP1 Binding and pH Sensing by the Spike Complex of Lassa Virus.* J Virol, 2016. **90**(22): p. 10329-10338.

68.   Jae, L.T. and T.R. Brummelkamp, *Emerging intracellular receptors for hemorrhagic fever viruses.* Trends Microbiol, 2015. **23**(7): p. 392-400.

69.   Fazakerley, J.K., et al., *High resolution in situ hybridization to determine the cellular distribution of lymphocytic choriomeningitis virus RNA in the tissues of persistently infected mice: relevance to arenavirus disease and mechanisms of viral persistence.* J Gen Virol, 1991. **72**(Pt 7): p. 1611-25.

70.   Walker, D.H., et al., *Pathologic and virologic study of fatal Lassa fever in man.* Am J Pathol, 1982. **107**(3): p. 349-56.

71.   Yun, N.E. and D.H. Walker, *Pathogenesis of Lassa fever.* Viruses, 2012. **4**(10): p. 2031-48.

72.   Iwasaki, M., et al., *Cell entry of lymphocytic choriomeningitis virus is restricted in myotubes.* Virology, 2014. **458-459**: p. 22-32.

73.   Gerold, G., et al., *Quantitative Proteomics Identifies Serum Response Factor Binding Protein 1 as a Host Factor for Hepatitis C Virus Entry.* Cell Rep, 2015. **12**(5): p. 864-78.

74.   Gerold, G., J. Bruening, and T. Pietschmann, *Decoding protein networks during virus entry by quantitative proteomics.* Virus Res, 2015.

75.   Wojcechowskyj, J.A., et al., *Quantitative phosphoproteomics reveals extensive cellular reprogramming during HIV-1 entry.* Cell Host Microbe, 2013. **13**(5): p. 613-23.

76.   Sweileh, W.M., *Global research trends of World Health Organization's top eight emerging pathogens.* Global Health, 2017. **13**(1): p. 9.

77.   Fisher-Hoch, S.P., et al., *Review of cases of nosocomial Lassa fever in Nigeria: the high price of poor medical practice.* Bmj, 1995. **311**(7009): p. 857-9.

78.   Hastie, K.M., et al., *Structural basis for antibody-mediated neutralization of Lassa virus.* Science, 2017. **356**(6341): p. 923-928.

79.   Dylla, D.E., et al., *Altering alpha-dystroglycan receptor affinity of LCMV pseudotyped lentivirus yields unique cell and tissue tropism.* Genet Vaccines Ther, 2011. **9**: p. 8.

80.   Moller-Tank, S. and W. Maury, *Phosphatidylserine receptors: enhancers of enveloped virus entry and infection.* Virology, 2014. **468-470**: p. 565-80.

81.   Weber, E.L. and M.J. Buchmeier, *Fine mapping of a peptide sequence containing an antigenic site conserved among arenaviruses.* Virology, 1988. **164**(1): p. 30-8.

82.   Buchmeier, M.J., et al., *Monoclonal antibodies to lymphocytic choriomeningitis and pichinde viruses: generation, characterization, and cross-reactivity with other arenaviruses.* Virology, 1981. **113**(1): p. 73-85.

83.   Kunz, S., L. Calder, and M.B. Oldstone, *Electron microscopy of an alpha-dystroglycan fragment containing receptor sites for lymphocytic choriomeningitis virus and laminin, and use of the receptoid body as a reagent to neutralize virus.* Virology, 2004. **325**(2): p. 207-15.

84.   Kleine, M., et al., *Explanted diseased livers - a possible source of metabolic competent primary human hepatocytes.* PLoS One, 2014. **9**(7): p. e101386.

85. Pinschewer, D.D., et al., *Recombinant lymphocytic choriomeningitis virus expressing vesicular stomatitis virus glycoprotein.* Proc Natl Acad Sci U S A, 2003. **100**(13): p. 7895-900.

86. Kunz, S., et al., *Molecular analysis of the interaction of LCMV with its cellular receptor [alpha]-dystroglycan.* J Cell Biol, 2001. **155**(2): p. 301-10.

87. Kunz, S., et al., *Characterization of the interaction of lassa fever virus with its cellular receptor alpha-dystroglycan.* J Virol, 2005. **79**(10): p. 5979-87.

88. Dutko, F.J. and M.B. Oldstone, *Genomic and biological variation among commonly used lymphocytic choriomeningitis virus strains.* J Gen Virol, 1983. **64 (Pt 8)**: p. 1689-98.

89. Michele, D.E., et al., *Post-translational disruption of dystroglycan-ligand interactions in congenital muscular dystrophies.* Nature, 2002. **418**(6896): p. 417-22.

90. Kunz, S., et al., *Use of alternative receptors different than alpha-dystroglycan by selected isolates of lymphocytic choriomeningitis virus.* Virology, 2004. **325**(2): p. 432-45.

91. Rojek, J.M., M. Perez, and S. Kunz, *Cellular entry of lymphocytic choriomeningitis virus.* J Virol, 2008. **82**(3): p. 1505-17.

92. Wessel, D. and U.I. Flugge, *A method for the quantitative recovery of protein in dilute solution in the presence of detergents and lipids.* Anal Biochem, 1984. **138**(1): p. 141-3.

93. Meertens, L., et al., *Axl Mediates ZIKA Virus Entry in Human Glial Cells and Modulates Innate Immune Responses.* Cell Rep, 2017. **18**(2): p. 324-333.

94. Durbeej, M., et al., *Distribution of dystroglycan in normal adult mouse tissues.* J Histochem Cytochem, 1998. **46**(4): p. 449-57.

95. Peyrard, M., et al., *The human LARGE gene from 22q12.3-q13.1 is a new, distinct member of the glycosyltransferase gene family.* Proc Natl Acad Sci U S A, 1999. **96**(2): p. 598-603.

96. de Bernabe, D.B., et al., *Loss of alpha-dystroglycan laminin binding in epithelium-derived cancers is caused by silencing of LARGE.* J Biol Chem, 2009. **284**(17): p. 11279-84.

97. Kanagawa, M., et al., *Molecular recognition by LARGE is essential for expression of functional dystroglycan.* Cell, 2004. **117**(7): p. 953-64.

98. Durbeej, M. and K.P. Campbell, *Biochemical characterization of the epithelial dystroglycan complex.* J Biol Chem, 1999. **274**(37): p. 26609-16.

99. Barresi, R., et al., *LARGE can functionally bypass alpha-dystrolycan glycosylation defects in distinct congential muscular dystrophy.* Nat. Med., 2004. **10**: p. 696-703.

100. Lee, A.M., et al., *Pathogenesis of Lassa fever virus infection: I. Susceptibility of mice to recombinant Lassa Gp/LCMV chimeric virus.* Virology, 2013.

101. Sommerstein, R., et al., *Evolution of recombinant lymphocytic choriomeningitis virus/Lassa virus in vivo highlights the importance of the GPC cytosolic tail in viral fitness.* J Virol, 2014. **88**(15): p. 8340-8.

102. Fernandez-Fernandez, L., L. Bellido-Martin, and P. Garcia de Frutos, *Growth arrest-specific gene 6 (GAS6). An outline of its role in haemostasis and inflammation.* Thromb Haemost, 2008. **100**(4): p. 604-10.

103. Ohkuma, S. and B. Poole, *Fluorescence probe measurement of the intralysosomal pH in living cells and the perturbation of pH by various agents.* Proceedings of the National Academy of Sciences of the United States of America, 1978. **75**(7): p. 3327-31.

104. Ohkuma, S. and B. Poole, *Cytoplasmic vacuolation of mouse peritoneal macrophages and the uptake into lysosomes of weakly basic substances.* The Journal of cell biology, 1981. **90**(3): p. 656-64.

105. Marsh, M. and A. Helenius, *Virus entry: open sesame.* Cell., 2006. **124**(4): p. 729-40.

106. Myers, S.H., V.G. Brunton, and A. Unciti-Broceta, *AXL Inhibitors in Cancer: A Medicinal Chemistry Perspective.* J Med Chem, 2016. **59**(8): p. 3593-608.

107. Holland, S.J., et al., *R428, a selective small molecule inhibitor of Axl kinase, blocks tumor spread and prolongs survival in models of metastatic breast cancer.* Cancer Res, 2010. **70**(4): p. 1544-54.

108. Hunt, C.L., et al., *The Tyro3 receptor kinase Axl enhances macropinocytosis of Zaire ebolavirus.* J Virol, 2011. **85**(1): p. 334-47.

109. Johannsdottir, H.K., et al., *Host cell factors and functions involved in vesicular stomatitis virus entry.* J Virol, 2009. **83**(1): p. 440-53.

110. Koivusalo, M., et al., *Amiloride inhibits macropinocytosis by lowering submembranous pH and preventing Rac1 and Cdc42 signaling.* J Cell Biol, 2010. **188**(4): p. 547-63.

111. Israeli, H., et al., *Mapping of the Lassa virus LAMP1 binding site reveals unique determinants not shared by other old world arenaviruses.* PLoS Pathog, 2017. **13**(4): p. e1006337.

112. Fisher-Hoch, S., et al., *Hematologic dysfunction in Lassa fever.* J Med Virol, 1988. **26**(2): p. 127-35.

113. Lukashevich, I.S., et al., *Lassa and Mopeia virus replication in human monocytes/macrophages and in endothelial cells: different effects on IL-8 and TNF-alpha gene expression.* J Med Virol, 1999. **59**(4): p. 552-60.

114. Sotgia, F., et al., *Localization of phospho-beta-dystroglycan (pY892) to an intracellular vesicular compartment in cultured cells and skeletal muscle fibers in vivo.* Biochemistry, 2003. **42**(23): p. 7110-23.

115. Yamauchi, Y. and A. Helenius, *Virus entry at a glance.* J Cell Sci, 2013. **126**(Pt 6): p. 1289-95.

116. Torriani, G., C. Galan-Navarro, and S. Kunz, *Lassa Virus Cell Entry Reveals New Aspects of Virus-Host Cell Interaction.* J Virol, 2017. **91**(4).

117. Gay, C.M., K. Balaji, and L.A. Byers, *Giving AXL the axe: targeting AXL in human malignancy.* Br J Cancer, 2017. **116**(4): p. 415-423.

118. Read, S.A., et al., *Hepatitis C Virus Driven AXL Expression Suppresses the Hepatic Type I Interferon Response.* PLoS One, 2015. **10**(8): p. e0136227.

119. Schlie, K., et al., *Viral protein determinants of Lassa virus entry and release from polarized epithelial cells.* Journal of virology, 2010. **84**(7): p. 3178-88.

120. Liu, S., et al., *AXL-Mediated Productive Infection of Human Endothelial Cells by Zika Virus.* Circ Res, 2016. **119**(11): p. 1183-1189.

121. Bhattacharyya, S., et al., *Enveloped viruses disable innate immune responses in dendritic cells by direct activation of TAM receptors.* Cell Host Microbe, 2013. **14**(2): p. 136-47.

122. Brindley, M.A., et al., *Tyrosine kinase receptor Axl enhances entry of Zaire ebolavirus without direct interactions with the viral glycoprotein.* Virology, 2011. **415**(2): p. 83-94.

123. Rothlin, C.V., et al., *TAM receptors are pleiotropic inhibitors of the innate immune response.* Cell, 2007. **131**(6): p. 1124-36.

124. Rothlin, C.V. and G. Lemke, *TAM receptor signaling and autoimmune disease.* Curr Opin Immunol, 2010. **22**(6): p. 740-6.

125. Pythoud, C., et al., *Lymphocytic Choriomeningitis Virus Differentially Affects the Virus-Induced Type I Interferon Response and Mitochondrial Apoptosis Mediated by RIG-I/MAVS.* J Virol, 2015. **89**(12): p. 6240-50.

126. Martinez-Sobrido, L., et al., *Inhibition of the type I interferon response by the nucleoprotein of the prototypic arenavirus lymphocytic choriomeningitis virus.* J Virol, 2006. **80**(18): p. 9192-9.

127. Martinez-Sobrido, L., et al., *Differential inhibition of type I interferon induction by arenavirus nucleoproteins.* J Virol, 2007. **81**(22): p. 12696-703.

128. Xing, J., H. Ly, and Y. Liang, *The Z proteins of pathogenic but not non-pathogenic arenaviruses inhibit the RIG-i-like receptor (RLR)-dependent interferon production.* J Virol, 2014.

129. Martinez-Sobrido, L., et al., *Identification of amino acid residues critical for the anti-interferon activity of the nucleoprotein of the prototypic arenavirus lymphocytic choriomeningitis virus.* J Virol, 2009. **83**(21): p. 11330-40.

130. Qi, X., et al., *Cap binding and immune evasion revealed by Lassa nucleoprotein structure.* Nature, 2010. **468**(7325): p. 779-83.

131. Xing, J., H. Ly, and Y. Liang, *The Z proteins of pathogenic but not nonpathogenic arenaviruses inhibit RIG-I-like receptor-dependent interferon production.* J Virol, 2015. **89**(5): p. 2944-55.

132. Russier, M., D. Pannetier, and S. Baize, *Immune responses and Lassa virus infection.* Viruses, 2012. **4**(11): p. 2766-85.

133. Hunt, C.L., N.J. Lennemann, and W. Maury, *Filovirus entry: a novelty in the viral fusion world.* Viruses, 2012. **4**(2): p. 258-75.

134. Mora, N., et al., *A Synthesis of Hepatitis C prevalence estimates in Sub-Saharan Africa: 2000-2013.* BMC Infect Dis, 2016. **16**: p. 283.

Clara Galan Navarro

Avenue Vinet 27, 1004 Lausanne
+41 763824532 | clara.galannavarro@epfl.ch
Skype: clara.galan.navarro | LinkedIn
Spanish (Swiss B Permit)
29 years old, single and willing to travel

Ph.D. in Bioengineering - Master in Business

· Dynamic young professional with solid scientific and technical foundations, complemented with business preparation and entrepreneurial mind-set.

· Leading interdisciplinary and international collaborative project provided with extensive *project management skills*, such as strengthened strategic planning, creative problem solving, negotiation skills, and a cooperative team disposition.

· Personality heavily marked by strong social and communications aptitudes, reflecting energetic and proactive attitude towards personal growth and the advancement of mankind.

· Very prominent international upbringing enabled seamless communication with people from different fields and backgrounds in professional and social environments.

CORE EDUCATION AND EXPERIENCE (BIOENGINEERING)

EDUCATION

· ***Ph.D. Thesis****. **Doctoral Program in Biotechnology and Bioengineering**   *Lausanne, Switzerland*

École Polytechnique Fédérale de Lausanne **EPFL**/ Lausanne University Hospital **CHUV**   *2014-Oct 2017*

"Engineering of nanoparticles as viral vaccine carriers and development of diagnostic tests and advanced serological detection systems"

Highlighted achievements: two high impact factor publications with great scientific value, which resulted in grant renewal, largely increasing the laboratory's annual budget and created a patentable system with potential economic implications.

Transferable skills obtained during PhD project: Information/data management, time management, project management, teamwork, legal and regulatory competency, leadership skills, communication skills, organizational skills, laboratory supplies management, strategic planning and creative problem solving.

· **Bachelor of Science in Biotechnology (Honours) and Master of Science in Biotechnology**   *Madrid, Spain*

Universidad Francisco de Vitoria   *2007-2012*

Specialisation in clinical and pharmaceutical biotechnology (licentiate)

EXPERIENCE AS RESEARCH ASISSTANT

· **The Scripps Research Institute (TSRI)**   *San Diego, CA, United States*

Structural studies of viral haemorrhagic fever pathogenesis   *Jan-April 2016*

· **CHUV Virology Department**   *Lausanne, Switzerland*

Enhancement of diagnostic analysis techniques for infectious diseases   *May 2013-Feb 2014*

· Institut Universitaire d'Hématologie (IUH) Université Paris Diderot   *Paris, France*

Investigation of cancer biology within HIV infection context   *Jan-April 2013*

Collaboration in diverse projects of specialised topics, quick adaptation and flexibility ensured the success of multiple projects. Use of different lab equipment and knowledge form various fields of science. Clinical work in different countries, work within different functioning standards and diverse working styles.

ADDITIONAL EDUCATION AND EXPERIENCE (BUSINESS)

EDUCATION

· Master of *Business Administration of Biotechnology Companies*   *Madrid, Spain*

Universidad Francisco de Vitoria   2012

Relevant interdisciplinary courses from the Technology Transfer Office and Technology Management Master at EPFL: Management of Innovation and Technology Transfer, Economics of Innovation in the Biomedical field and Project Risk Management.

EXPERIENCE

· Board member and Event Manager of the University Association of Spanish People (UASP)   *Lausanne*

Participating in the conception and execution of a successful association. Responsible for the organization of diverse events. Teamwork building and interpersonal skills, communication skills and diplomacy, interaction with people involved in non-scientific functional roles. Negotiation skills and being able to efficiently coordinate people was essential to the success of the association. Every year, I develop the association's financial plan and manage annual budgets attributed to the association by the university.

· Teaching assistant in Advance Laboratory Techniques Course of Life Sciences Bachelor and Biotechnology Lab in Chemical Engineering Master in EPFL

Representing complex information visually, public speaking to large groups, conveying complex information to non-expert audiences and evaluating and monitoring performance.

· Receptionist at the headquarters office of PepsiCo Inc.   *(Summer intern 2008, 2009)   Madrid, Spain*

Administrative skills, direct interaction with customers, strong client-facing skills.

LANGUAGES

Spanish	*Mother tongue*	**French**	*Proficient C2* Spoken and written
English	*Proficient C2* Spoken and written	**German**	*Beginner*

PERSONAL ACHIEVEMENTS

· Poster presentation and discussion at Negative Strand Viruses meeting (Sienna, Italy 2015) at Annual Novarits-EPFL Workshop (Basel, Switzerland 2015) and Life Science Switzerland (Zurich, Switzerland 2017)

· Participation in 2015 Swiss Romande edition of the public speaking contest "Your Thesis in 180 seconds"

· Scholarship from The African Medical and Research Foundation (AMREF) for 6 months of research abroad

· Volunteering in Minusvalidos en la Naturaleza (Handicaps in Nature) Summer 2010

· Passionate about scuba diving. Advanced Open Water Diver since 2005